Design and modelling of innovative machinery systems for large ships

Larsen, Ulrik; Haglind, Fredrik; Gabrielii, Cecilia; Elmegaard, Brian

Publication date:
2014

Document Version
Publisher's PDF, also known as Version of record

Design and modelling of innovative machinery systems for large ships

PhD Thesis

$$(EIv'')'' = q - \rho A\ddot{v}$$

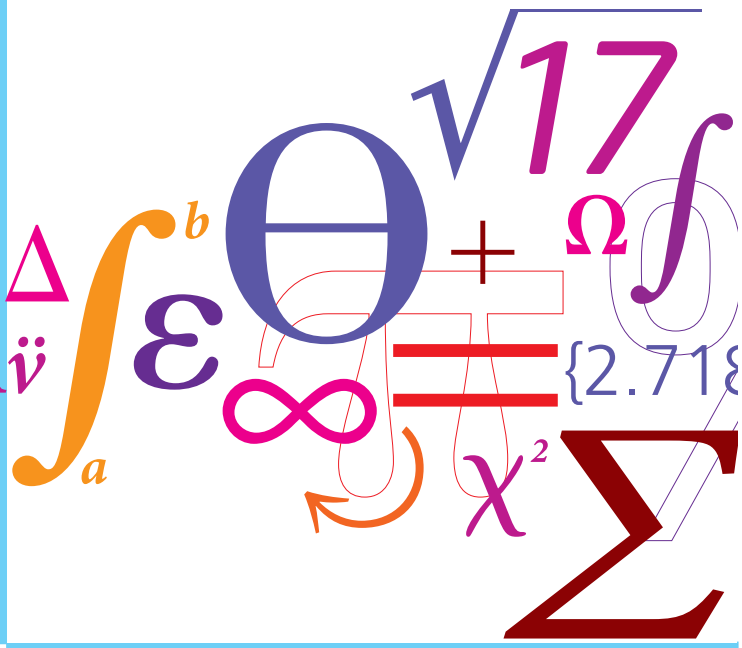

Ulrik Larsen
DCAMM Special Report No. S176
October 2014

DTU Mechanical Engineering
Department of Mechanical Engineering

Design and modelling of innovative machinery systems for large ships

A thesis for the partial fulfilment of the Doctor of Philosophy (Ph.D.) Degree at The Technical University of Denmark

A collaboration project between
Chalmers University of Technology
and
The Technical University of Denmark

Author
Ulrik Larsen

Supervisors
Fredrik Haglind, The Technical University of Denmark
Cecilia Gabrielii, Chalmers University of Technology
Brian Elmegaard, The Technical University of Denmark

Project period: December 2010 - May 2014

Preface

The studies presented in this thesis are prepared at the Thermal Energy Section, Department of Mechanical Engineering at the Technical University of Denmark (DTU), and at the Department of Shipping and Marine Technology, at Chalmers University of Technology, Gothenburg, Sweden.

The supervisors of the work are Fredrik Haglind and Brian Elmegaard from DTU and Cecilia Gabrielii from Chalmers. Some of the work is done in collaboration with MAN Diesel & Turbo through Anders Andreasen.

The project is financed by the maritime competence and research centre Lighthouse, located at Chalmers University of Technology in Gothenburg.

Acknowledgement is hereby given to a number of persons and organisations, reflecting the fact that not much of the work in the present thesis is done without involving co-workers. I would like to acknowledge Lighthouse for the financial support. I hereby thank you Fredrik, Cecilia and Karin for choosing me to carry out this project, it has meant a lot to me professionally and personally. Fredrik, Cecilia and Brian, you were always very competent and prompt in your support and supervision, I have enjoyed working with you all, and I can only highly recommend to study under your supervision, thanks.

Among co-workers you, Leonardo, stood out as always being an incredibly competent and giving person. Many others will testify to that, and I am proud to call you my friend now. I thank you Francesco for your contributions to this work and for the numerous interesting discussions. I am sure we have our best collaboration ahead of us. I thank you Tuong-Van for our excellent collaboration at just the right time. I also thank you, Thomas, Jorrit, Oskar, Anders I., Sigurdur and Rasmus, for your valuable contributions to this work. Thank you Anders Andreasen for the brief collaboration and to MAN Diesel & Turbo for providing the needed experimental data. Thank you Susan Canali for proof reading the publications, and thereby helping me to improve my English. Thanks to the remaining colleagues at Chalmers and DTU for being such good colleagues. Lastly, and by far most importantly, thank you Sree Gayathree for being an unbelievably supportive and wonderful wife.

Abstract: Design and modelling of innovative machinery systems for large ships

Eighty percent of the growing global merchandise trade is transported by sea. The shipping industry is required to reduce the pollution and increase the energy efficiency of ships in the near future. There is a relatively large potential for approaching these requirements by implementing waste heat recovery (WHR) systems. Studies of alternative WHR systems in other applications suggests that the Kalina cycle and the organic Rankine cycle (ORC) can provide significant advantages over the steam Rankine cycle, which is currently used for marine WHR.

This thesis aims at creating a better understanding of the Kalina cycle and the ORC in the application on board large ships; the thermodynamic performances of the mentioned power cycles are compared. Recommendations of suitable system layouts and working fluids for the marine applications are provided along with methodologies useful for the design and optimisation of the main engine and WHR system combined cycle.

Numerical models of a low-speed two-stroke diesel engine, turbochargers, and the mentioned types of WHR systems in various configurations, are used to achieve the mentioned objectives. The main engine is simulated using a zero-dimensional model consisting of a two-zone combustion and NOx emission model, a double Wiebe heat release model, the Redlich-Kwong equation of state and the Woschni heat loss correlation. A novel methodology is presented and used to determine the optimum organic Rankine cycle process layout, working fluid and process parameters for marine WHR. Using this mentioned methodology, regression models are derived for the prediction of the maximum obtainable thermal efficiency of ORCs. A unique configuration of the Kalina cycle, the Split-cycle, is analysed to evaluate the fullest potential of the Kalina cycle for the purpose. Integrated with three main engine waste heat streams, the Kalina cycle, the ORC and a dual-pressure steam cycle are compared with regards to the power outputs and other aspects. The part-load performances of four different WHR system configurations, including an exhaust gas recirculation system, are evaluated with regards to the fuel consumption and NOx emissions trade-off.

The results of the calibration and validation of the engine model suggest that the main performance parameters can be predicted with adequate accuracies for the overall purpose. The results of the ORC and the Kalina cycle optimisation efforts indicate that both cycles can achieve higher power outputs than the steam cycle; however, the results suggest that for the Kalina cycle to achieve such high power outputs, a relatively complex process layout and high working pressures are required. Conversely, the ORC can achieve superior power outputs with a much simpler process layout in comparison. The toxic ammonia-water working fluid of the Kalina cycle is problematic for the use in marine machinery rooms, and so are the highly flammable ORC working fluids.

Based on the analyses, no configuration of the Kalina cycle is recommended for marine WHR. An exhaust gas power turbine is recommended as an initial WHR system investment due its cost-effectiveness. For large ships, a dual-pressure steam cycle is recommended because it is well-known, proven, highly efficient and environmentally benign. The ORC is recommended for large and medium size ships and it is recommended to use the highly flammable working fluids and take the needed precautions. The main reasons are that the ORCs can achieve superior efficiencies with a simple process that can be operated fully automated. For the same reasons a WHR system consisting of a hybrid turbocharger and a recuperated ORC is recommended.

Abstrakt: Design og modellering af innovative maskinsystemer til store skibe

Firs procent af varerne i den stadigt stigende globale handel transporteres med skibe. Skibsfarten bliver i nær fremtid mødt af krav om reduceret forurening og øget energieffektivitet. Der er et betydeligt potentiale for at imødekomme disse krav ved at implementere varmegenvindingssystemer. Studier af alternative varmegenvindingssystemer i andre applikationer indikerer at Kalinaprocessen og den organiske Rankine process (ORC) kan være fordelagtige i forhold til dampkredsprocessen, som bruges i varmegenvindingssystemer på skibe i dag.

Denne afhandlings mål er at skabe en bedre forståelse af Kalinaprocessen og ORC-processen som varmegenvindingssystem på store skibe. Den termodynamiske ydelse af de nævnte systemer sammenlignes. Anbefalinger til valg af systemkonfigurationer og arbejdsmedier til samme brug præsenteres, sammen med metoder til design og optimering af hovedmotor og varmegenvindingssystem.

Numeriske modeller af en langsomtgående totakts dieselmotor, turbolader og de nævnte varmegenvindingssystemer, i forskellige konfigurationer, benyttes for at nå målene. Motoren simuleres med en nul-dimensionel model som består af en to-zone forbrændings- og NOx-emissionsmodel, en dobbelt Wiebe forbrændingsmodel, en Redlich-Kwong arbejdsmediemodel og en Woschni varmetabsmodel. En ny metode præsenteres og benyttes til at afgøre hvilken konfiguration, arbejdsmedie og procesparametre som er optimale til formålet. Ved hjælp af denne metode er udviklet regressionsmodeller som kan forudsige den maksimalt opnåelige termiske effektivitet for ORC processer. En unik konfiguration af Kalinaprocessen, kaldet Split-cycle, analyseres for at evaluere det fulde potentiale af Kalinaprocessen i den nævnte kontekst. De nævnte varmegenvindingssystemer integreres med tre spildvarmestrømme fra hovedmotoren og deres ydelse samt øvrige hensyn sammenlignes. Del-lastydelsen af fire forskellige varmegenvindingssystemkonfigurationer, heriblandt en konfiguration med recirkulation af udstødningsgas, evalueres mht. det trade-off som findes mellem brændstofforbrug og NOx emissioner.

Resultater fra kalibrering og validering af motormodellen indikerer at de vigtigste ydelsesparamtre kan forudses med tilstrækkelig nøjagtighed i fht. systemoptimering. Resultaterne fra design og optimering af varmegenvindingssystemerne viser, at både Kalinaprocessen og ORC-processen kan producere mere kraft end dampprocessen. Dog viser resultaterne også at Kalinaprocessen skal have et relativt komplekst processlayout for at kunne opnå den høje ydelse. Omvendt kan ORC-processen opnå den høje ydelse med et meget simplere processlayout. Det giftige ammoniak-vand arbejdsmedie i Kalinaprocessen er problematisk for brugen i maskinrum, og det er de meget brandfarlige ORC arbejdsmedier også.

Resultaterne indikerer at Kalinaprocessen ikke kan anbefales som varmegenvindingssystem på store skibe. En udstødsgasturbine anbefales som indledende investering i et varmegenvindingssys-

tem pga. dens gode omkostningseffektivitet. På store skibe anbefales det at benytte en to-tryks dampproces fordi den er velkendt, pålidelig, meget effektiv og miljøvenlig. ORC-processen anbefales til store og mellemstore skibe og det anbefales at benytte de meget brandfarlige medier samt at tage de nødvendige forholdsregler. De vigtigste grunde til denne anbefaling er at ORC-processen kan levere den højeste ydelse med en meget simpel process, som kan fuldautomatiseres. Med samme begrundelse anbefales det at benytte en hybrid-turbolader sammen med ORC-processen.

List of publications

Peer-reviewed journal articles

- Larsen U, Pierobon L, Haglind F, Gabrielii C. Design and optimisation of organic Rankine cycles for waste heat recovery in marine applications using the principles of natural selection [1]. Link to pdf
- Larsen U, Pierobon L, Wronski J, Haglind F. Multiple regression models for the prediction of the maximum obtainable thermal efficiency of organic Rankine cycles [2]. Link to pdf
- Larsen U, Nguyen TV, Knudsen T, Haglind F. System analysis and optimisation of a Kalina Split-cycle for waste heat recovery on large marine diesel engines [3]. Link to pdf
- Larsen U, Haglind F, Sigthorsson O. A comparison of advanced heat recovery power cycles in a combined cycle for large ships [4]. Link to pdf
- Larsen U, Pierobon L, Baldi F, Ivarsson A, Haglind F. Development of a model for the prediction of the fuel consumption and nitrogen oxides emission trade-off for large ships. [5].
- Scappin F, Stefansson SH, Haglind F, Andreasen A, Larsen U. Validation of a zero-dimensional model for prediction of NOx and engine performance for electronically controlled marine two-stroke diesel engines [6].
- Pierobon L, Rokni M, Larsen U, Haglind F. Thermodynamic analysis of an integrated gasification solid oxide fuel cell plant combined with an organic Rankine cycle [7]. Link to pdf
- Pierobon L, Nguyen TV, Larsen U, Haglind F, Elmegaard B. Multi-objective optimization of organic Rankine cycles for waste heat recovery: Application in an offshore platform [8]. Link to pdf
- Frimann Nielsen R, Haglind F, Larsen U. Design and modeling of an advanced marine machinery system including waste heat recovery and removal of sulphur oxides.[9]. Link to pdf
- Nguyen TV, Larsen U, Knudsen T, Haglind F. Thermodynamic evaluation of the Kalina Split-cycle concepts for waste heat recovery applications [10]. Link to pdf

- Andreasen JG, Larsen U, Knudsen T, Haglind F. Selection and optimization of pure and binary working fluids for low grade heat utilization using organic Rankine cycles [11]. Link to pdf

Peer-reviewed conference articles

- Larsen U, Nguyen TV, Haglind F. Development of a multi-level approach to model and optimise the Kalina split cycle [12]. Link to pdf
- Larsen U, Haglind F, Sigthorsson O. A comparison of advanced heat recovery power cycles in a combined cycle for large ships [13]. Link to pdf
- Frimann Nielsen R, Haglind F, Larsen U. Design and modeling of an advanced marine machinery system including waste heat recovery and removal of sulphur oxides [14]. Link to pdf
- Pierobon L, Larsen U, Nguyen TV, Haglind F. Optimization of Organic Rankine Cycles for Off-Shore Applications [15].
- Pierobon L, Larsen U, Haglind F. Part-load performance of a combined gas turbine - organic Rankine cycle for off-shore applications [16]. Link to pdf
- Baldi F, Larsen U, Gabrielii C, Andersson K. Analysis of the influence of the engine, propeller and auxiliary generation interaction on the energy efficiency of controllable pitch propeller ships [17]).

Contents

Preface i

Abstract iii

Danish abstract v

List of publications vii

Contents xv

Nomenclature xix

List of figures xxiii

List of tables xxvi

1 Introduction **1**

1.1 Background and motivation 1

1.1.1 Emissions and fuel economy 1

1.1.2 Current research 2

1.2 Thesis objectives 8

1.2.1 Research questions 8

1.2.2 Tasks 9

1.3 Scope and delimitations 10

1.3.1 Modelling 10

1.4 Numerical optimisation strategy 12

1.5 Thesis outline 15

2 The marine low-speed two-stroke diesel engine **17**

2.1 Introduction 17

2.1.1 Turbocharging 18

Turbocharger matching 19

Turbocharger efficiency . . . 19
Two-stage turbocharging . . . 20
Turbocharger cut-out . . . 20
2.1.2 Nitrogen oxides . . . 20
Nitrogen oxides reduction . . . 21
2.1.3 Choice of model type . . . 24
Examples in the literature . . . 26
2.2 Methodology . . . 28
2.2.1 Background . . . 28
2.2.2 Thermodynamic properties . . . 28
2.2.3 Working gas equation of state . . . 29
2.2.4 Heat losses . . . 31
The Woschni correlation . . . 32
2.2.5 Combustion . . . 34
Ignition delay model . . . 34
Heat release . . . 35
The two-zone combustion model . . . 36
Combustion species . . . 38
2.2.6 Exhaust temperature . . . 39
2.2.7 Nitrogen oxides formation and modelling . . . 40
Exhaust gas recirculation . . . 44
2.2.8 Friction . . . 45
2.2.9 Scavenging . . . 46
2.2.10 Modelling the turbocharger . . . 47
2.2.11 Calibration . . . 48
4T50ME-x . . . 48
7L70MC . . . 49

12K98ME 49
2.3 Results 50
2.3.1 Validation using the 4T50ME-x engine 50
2.3.2 Validation using the 7L70MC engine 53
2.3.3 Validation using the 12K98ME engine 56
Exhaust gas recirculation 58
2.3.4 Prediction deviations 60
2.4 Discussion 61
2.4.1 Model development 62
2.4.2 Uncertainties 63

3 Waste heat recovery power cycles **65**
3.1 Introduction 65
3.1.1 Available waste heat 66
3.1.2 The power gas turbine 67
Two thermodynamic alternatives 68
3.1.3 The state-of-the-art steam Rankine cycle waste heat recovery system . . 69
3.1.4 Design and optimisation of organic Rankine cycles for waste heat recovery in marine applications using the principles of natural selection 71
Fluid selection 72
Organic Rankine cycle expanders 75
3.1.5 Multiple regression models for the prediction of the maximum obtainable thermal efficiency of organic Rankine cycles 76
3.1.6 System analysis and optimisation of a Kalina Split-cycle for waste heat recovery on large marine diesel engines 78
Working media 79
Kalina plants currently in operation 82
The Kalina Split-cycle 82

3.2 Methodology 84
3.2.1 Design and optimisation of organic Rankine cycles for waste heat recovery in marine applications using the principles of natural selection 84
A flexible organic Rankine cycle model 84
3.2.2 Multiple regression models for the prediction of the maximum obtainable thermal efficiency of organic Rankine cycles 90
3.2.3 System analysis and optimisation of a Kalina Split-cycle for waste heat recovery on large marine diesel engines 92
Process descriptions 92
Modelling conditions 95
Modelling approach 95
Boiler and turbine sub-system model 96
Mixing sub-system model 97
Full process model 97
Cost analysis 99
3.2.4 Validation 101
3.3 Results and analyses 102
3.3.1 Design and optimisation of organic Rankine cycles for waste heat recovery in marine applications using the principles of natural selection 102
General influence of the heat source inlet temperature 102
Engine design point 104
Prediction of the thermal efficiency of organic Rankine cycles 106
3.3.2 Multiple regression models for the prediction of the maximum obtainable thermal efficiency of organic Rankine cycles 109
Statistical evaluation 110
Verification of model assumptions 111
Prediction ability 112
Extrapolation 114
Comparison with the theoretical maximum 114

Optimum working fluids 116

3.3.3 System analysis and optimisation of a Kalina Split-cycle for waste heat recovery on large marine diesel engines 117

Governing process mechanisms 117

Optimisation results 120

Cost analysis 122

3.4 Discussion 125

3.4.1 Design and optimisation of organic Rankine cycles for waste heat recovery in marine applications using the principles of natural selection 125

General influence of the heat source inlet temperature 125

Hazard levels and environmental impact 126

Thermal stability 127

3.4.2 Multiple regression models for the prediction of the maximum obtainable thermal efficiency of organic Rankine cycles 128

Limitations 128

Comparison with other studies 129

3.4.3 System analysis and optimisation of a Kalina Split-cycle for waste heat recovery on large marine diesel engines 131

4 Comparison of waste heat recovery systems **135**

4.1 Introduction 135

4.1.1 A comparison of advanced heat recovery power cycles in a combined cycle for large ships 135

4.1.2 Development of a model for the prediction of the fuel consumption and nitrogen oxides emission trade-off for large ships 137

4.2 Methodology 138

4.2.1 A comparison of advanced heat recovery power cycles in a combined cycle for large ships 138

An integrated steam cycle 138

An integrated Kalina cycle 138

An integrated organic Rankine cycle 141
Turbines 142
Optimisation 142
Modelling parameters and conditions 143
4.2.2 Development of a model for the prediction of the fuel consumption and nitrogen oxides emission trade-off for large ships 144
System configurations 144
Turbochargers and blowers 146
The hybrid turbocharger 146
The organic Rankine cycle 147
4.2.3 Optimisation 148
4.2.4 Modelling conditions 150
4.3 Results and analyses 150
4.3.1 A comparison of advanced heat recovery power cycles in a combined cycle for large ships 150
Engine model 151
Combined cycle performance 152
Qualitative comparison 155
4.3.2 Development of a model for the prediction of the fuel consumption and nitrogen oxides emission trade-off for large ships 157
Economical comparison 161
4.4 Discussion 161
4.4.1 A comparison of advanced heat recovery power cycles in a combined cycle for large ships 161
4.4.2 Development of a model for the prediction of the fuel consumption and nitrogen oxides emission trade-off for large ships 162

5 Conclusion **165**

5.1 Research questions 165

5.2 Contribution to current knowledge 170
5.3 Limitations 171
5.4 Recommendations for future research 172
5.5 Recommendations for a suitable waste heat recovery system 174
5.6 A final remark 176

References **176**

Appendix A Abstracts of co-authored journal publications **195**

A.1 Validation of a zero-dimensional model for prediction of NOx and engine performance for electronically controlled marine two-stroke diesel engines 195
A.2 Thermodynamic analysis of an integrated gasification solid oxide fuel cell plant combined with an organic Rankine cycle 195
A.3 Multi-objective optimization of organic Rankine cycles for waste heat recovery: Application in an offshore platform 196
A.4 Design and modeling of an advanced marine machinery system including waste heat recovery and removal of sulphur oxides 196
A.5 Thermodynamic evaluation of the Kalina Split-cycle concepts for waste heat recovery applications 197
A.6 Selection and optimization of pure and binary working fluids for low grade heat utilization using organic Rankine cycles 198

Appendix B Split-cycle state points **199**

Appendix C Fluids available in Refprop **203**

Nomenclature

Acronyms

AB	Auxiliary blower
ABDC	After bottom dead centre
AFR	Air-fuel ratio
BMEP	Brake mean effective pressure
BOI	Boiler
CAC	Charge air cooler
CAD	Crank angle degrees
CFD	Computational Fluid Dynamics
CN	Cetane number
CND	Condenser
EB	Exhaust gas recirculation blower
ECA	Emission control area
ECO	Economiser (preheater)
EEDI	The Energy Efficiency Design Index
EGR	Exhaust gas recirculation
EOI	End of injection
EOS	Equation of State
EVA	Evaporator
EVC	Exhaust valve close time
EVO	Exhaust valve opening
FMEP	Friction mean effective pressure
FOM	Figure of Merit
G	Generator
GA	Genetic Algorithm
GWP	Global Warming Potential
HMIS	Hazardous Materials Identification System
HP	High pressure
HTC	Hybrid turbocharger
IHX	Internal heat exchanger
IMO	International Maritime Organization
JWC	Jacket water cooler
LHV	Lower heating value
LP	Low pressure
MCR	Maximum continuous rating
MDT	MAN Diesel & Turbo
ME	Main engine
N/A	Not available
NIST	National Institute of Standards and Technology
ODP	Ozone Depletion Potential
ORC	Organic Rankine cycle
PP	Pinch point
PT	Power turbine
REC	Recuperator
RK	Redlich-Kwong equation of state
RMSD	Root mean square deviation
SAM	Scavenge air moisturisation
SC	Split-cycle
SCR	Selective catalytic reduction
SEP	Separator
SFOC	Specific fuel oil consumption
SH	Superheated state
SM	Shaft motor and generator
SOI	Start of injection
SOLAS	International Convention for the Safety of Life At Sea
SRC	Steam Rankine cycle

ST	Steam turbine
SUB	Subcooled state
SUP	Superheater
T/C	Turbocharger
TEU	Twenty foot equivalent units
TRF	Tillner-Roth and Friend
TUR	Turbine
USD	United States Dollars
WHR	Waste heat recovery
WIF	Water-in-fuel

Greek Symbols

α	Geometry scaling factor (-)
β	Regression coefficient (-)
Δ	Difference (-)
η	Efficiency (-)
γ	Ratio of specific heats (-)
λ	Air-fuel equivalence ratio (-)
ν	Characteristic velocity (-)
ω	Angular velocity (rad/s)
θ	Degrees of engine rotation ($^{\circ}CAD$)

Symbols

$\dot{m}$	Mass flow rate (kg/s)
$\dot{Q}$	Heat transfer rate (kJ/s)
$\dot{V}$	Volumetric flow rate (m^3/s)
$\dot{W}$	Power (kW or MW)
$\overline{U}$	Heat transfer coefficient ($W/m^2 \cdot K$)
$\overline{v}$	Mean piston speed (m/s)
A	Heat transfer area (m^2)
B	Bore (m)
C	Cost (USD)
c_p	Constant pressure specific heat ($kJ/kg-K$)
C_T	Turbine constant ($kgK^{0.5}s^{-1}bar^{-1}$)
c_v	Constant volume specific heat ($kJ/kg-K$)
e	Residual (Varying)
E_a	Activation energy ($kJ/mole$)
F	Electric loss (-)
f	Engine speed (rpm)
h	Specific enthalpy (kJ/kg)
Ja	Jacob number (-)
k	Rate constants (Varying)
l	Load (-)
M	Combustion shape parameter (-)
m	Mass (kg)
N	Turbine rotational speed (rpm)
P	Pressure (Bar or kPa)
Q	Heat (kJ)
q	Vapour quality (-)
R	Universal gas constant ($kJ/K-mole$)
S	Piston speed (m/s)
T	Temperature ($^{\circ}$C or K)
t	Time (s)
U	Internal energy (kJ)
V	Volume (m^3)
v	Specific volume (m^3/kg)
VH	Turbine size parameter (m)
W	Work (kJ)
y	Response variable (Varying)
z	Predictor variable (Varying)

Subscripts

0	Base or reference
a	Air
b	Bubble point
c	Cold stream

cl	Cylinder loss
co	Condensation
comp	Compression
cr	Critical point
cu	Copper
cyl	Cylinder
d	Dew point
dc	Diffusion controlled combustion
dp	Design point
e	Exhaust gas
el	Electrical
ev	Evaporation
ex	Expander
ext	External
f	Fuel
g	Gas
h	Hot stream
ha	Humid air
hr	Heat release
hx	Heat exchanger
i	Inlet condition
id	Ignition delay
int	Internal
j	Number of response
k	Number of predictor variables
l	Lean ammonia concentration
lm	Logarithmic mean
m	Maximum
max	Maximum
min	Minimum
mol	Molar basis
motor	Motoring
ms	Mass basis
o	Outlet condition
p	Pump
pc	Pre-mixed combustion
po	Polytropic
pp	Pinch point
r	Rich ammonia concentration
s	Isentropic
scav	Scavenging
sh	Superheater approach
src	Source
sw	Swept
t	Trilateral
th	Thermal
turb	Turbine or expander
w	Working fluid
whr	Waste heat recovery (inlet)

List of Figures

1.1 Pareto optimisation 14

2.1 Comparison of gas equations of state 31
2.2 Comparison of NOx emission when using different rate constants 43
2.3 Effect of maximum pressure 51
2.4 Effect of compression pressure 52
2.5 Effect of scavenge pressure 52
2.6 Model and experimental values for main performance parameters 55
2.7 Required turbocharger efficiencies 55
2.8 Model and experimental values for relative heat release per CAD 56
2.9 Model and experimental values for cylinder pressures 57
2.10 Model and experimental values for main performance parameters 57
2.11 Comparison of EGR effect on SFOC and NOx 59

3.1 Available waste heat from the main engine (MDT 12K90ME-C9.2 [18]) 67
3.2 Sketch of a temperature-entropy diagram 68
3.3 Steam Rankine process flow diagram 70
3.4 Temperature-entropy plot for the three fluid types 72
3.5 Sketch of a Kalina process with reheat 78
3.6 Temperature-concentration diagram for ammonia-water mixtures at 10 bar . . 80
3.7 Temperature-entropy diagram for a 70% ammonia in water mixture 81
3.8 Sketch of the flexible ORC model 85
3.9 Sketch of heat exchangers with numbering 87
3.10 Sketch of the Kalina Split-cycle process 93

3.11 Sketch of a Split-cycle boiler heat transfer diagram 93
3.12 Equilibrium conditions for Evaporator 1 outlet 94
3.13 Recuperator 2 calculation sketch 98
3.14 Optimum fluid and pressure (bar) at temperatures from 180-360°C with no constraints. 103
3.15 Optimum fluid and pressure (bar) at temperatures from 180-360°C with no recuperator. 103
3.16 Optimum fluid and pressure (bar) at temperatures from 180-360°C with limit of 20 bar on high pressure. 104
3.17 Effects of constraints and hazard levels 105
3.18 Thermal efficiency and. Figure of Merit at temperatures from 180-360°C 107
3.19 Thermal efficiency vs. heat source temperature 108
3.20 Normal probability plot 111
3.21 Plots of residuals 112
3.22 Prediction ability for the high temperature ORC model 113
3.23 Prediction ability for the low temperature ORC model 113
3.24 Extrapolation of the ORC regression models 114
3.25 Comparison with the Trilateral cycle efficiency 115
3.26 Working fluids for the ORC 116
3.27 Working fluids for the simple ORC 117
3.28 Trends for the separator outlet streams 118
3.29 Turbine inlet/outlet pressure ratio influence on turbine power 119
3.30 Rich stream composition effect on pinch point temperature difference 120
3.31 Heat transfer diagram 122

4.1 Steam cycle process flow diagram 139
4.2 Kalina cycle process flow diagram 139
4.3 Organic Rankine cycle process flow diagram 141

4.4 Sketch of configurations 1-3 145
4.5 Sketch of configurations 4 and 5 145
4.6 Sketch of the ORC process 145
4.7 Boiler heat transfer diagram for the three power cycle alternatives 154
4.8 Size parameter and volumetric flow ratio relative to the steam LP turbine . . . 155
4.9 Comparison of the condenser heat transfer-temperature profile 156
4.10 Fuel consumption and NOx trade-off 157
4.11 Fuel consumption and NOx trade-off using the main engine and ORC layout . 158
4.12 Fuel consumption and NOx trade-off using the main engine and HTC-ORC layout 159
4.13 Heat transfer-temperature diagrams (ME, HTC, ORC with i-hexane) 159
4.14 Fuel consumption for the main engine and HTC and ORC isohexane combined cycle 160

List of Tables

1.1 System hierarchy (inspired by the work of Chow et al. [19]) 4

1.2 Overview of the research and development efforts in Hercules 4

2.1 Rate constants for the Zeldovich reactions 42

2.2 4T50ME-x Main engine data 51

2.3 7L70MC mk6 Main engine characteristics 53

2.4 7L70MC mk6 Main engine performance data 54

2.5 Goldsworthy model output data 54

2.6 Prediction root-mean-square deviation 60

2.7 Maximum deviations in response trends 63

3.1 Indicated performance of WHR systems [18] 70

3.2 Modelling conditions 85

3.3 Genetic algorithm parameters 89

3.4 Parameters interval limits 90

3.5 Process parameters and conditions 95

3.6 Genetic algorithm parameters 99

3.7 Parameter limits 99

3.8 Engine parameters 105

3.9 Simulation results - hazard level 3 106

3.10 Simulation results - hazard level 2 107

3.11 Model coefficients and statistics for low-temperature heat sources 109

3.12 Model coefficients and statistics for high-temperature heat sources 109

3.13 Regression statistics 111

3.14 Optimum cycle performances 121
3.15 Optimised parameters 121
3.16 Estimated heat transfer areas 123
3.17 Estimated purchase cost (components cost in 1,000 USD) 123

4.1 Design and operation parameters 143
4.2 Weighting factors for NOx 148
4.3 Optimisation parameters and limits 149
4.4 Modelling conditions 151
4.5 Engine model outputs 152
4.6 Optimised performance 152
4.7 Optimised parameters 153
4.8 Comparative qualities 156
4.9 Optimised main engine performance parameters relative to the reference (75% load) 158
4.10 Optimised main engine operating parameters relative to the standard tuning (75% load) 160

B.1 State points, Kalina cycle. *SUB* and *SH* are subcooled and superheated. 199
B.2 State points, Kalina cycle, reheat 199
B.3 State points, Split-cycle 200
B.4 State points, Split-cycle, reheat 201

1 Introduction

This chapter describes the background and the motivation for the studies constituting the present thesis. The objectives and tasks for the work are presented, followed by a clarification of the thesis delimitations. Finally, a brief outline of the entire thesis is provided.

1.1 Background and motivation

According to a review of the maritime transport made by the United Nations Conference on Trade and Development [20], about 80% of the global merchandise trade is transported by sea. The resulting contribution to the man-made carbon dioxide emissions was estimated by the International Maritime Organisation (IMO) to be about 2.7% of the global total in 2007 [20]. Trade is growing still, induced by the growth of the general population and of the social middle-class [20], hence, even a small improvement in the transportation efficiency, for example quantified by the carbon dioxide emissions per ton goods transported one km, is important. Even though the marine engine fuel energy efficiencies can reach about 50%, a significant potential to utilise the remaining 50% still exists.

1.1.1 Emissions and fuel economy

The main emission factors being discussed in the literature on international shipping and marine propulsion systems, are carbon dioxide (CO_2), nitrogen oxides (NOx) and sulphur oxides (SOx).

CO_2 emissions are directly connected to the transportation fuel efficiency and there is therefore a straightforward economical incentive for CO_2 reduction. At the same time, (short-term) economics also provide reason for the continued use of diesel engines and fossil fuels. Perhaps therefore, the mandatory Energy Efficiency Design Index (EEDI), was introduced under the IMO MARPOL Annex VI. The EEDI is a measure for the CO_2 emissions of a ship relative to the transportation work done [21], and is gradually phased in with mandatory reductions reaching 30% by 2025.

There are a number of measures that can help to reduce the CO_2 emissions; important examples are: reduced vessel design speed, various hull and propeller improvements, alternative power production, such as sails and solar photovoltaic cells, and propulsion system optimisation. The application of a waste heat recovery (WHR) system is the technology

that can be applied to the main engine propulsion power plant, that has the largest potential for CO_2 reductions, with the exception of the use of alternative fuels. With the state-of-the art WHR systems, CO_2 reductions of about 5% can be achieved [18], depending on how the WHR system power is utilised.

NOx emissions are also connected to the main engine fuel consumption as long as an exhaust after treatment system is not applied. There is a general trade-off mechanism between fuel efficiency and NOx emissions, and this mechanism is studied in further detail in the present work (Ch. 4). There are several different strategies available for the reduction of NOx and these are to some extent treated in the present work also.

The IMO Annex VI mandatory NOx emission limits for new built ships are categorised in three tiers [22]. The limits depend on the engine type and for the low-speed two-stroke engine, which is the main focus in the present thesis, the limits are as follows: Tier I was mandatory in 2000 onwards and the limit was 17.0 g/kWh; from 2011 and onwards, the Tier II applies and the limit is now 14.4 g/kWh, a 15% reduction compared to Tier I. Tier III limits NOx emissions to 3.4 g/kWh and was originally scheduled to apply from 2016 in specified emission control areas (ECAs); however, at the time of writing, discussion within the IMO may result in a five year postponement of this application [23].

SOx and particulate matter emissions are mentioned in the same regulation because both are dependent on the amount of sulphur in the fuel. Measures to clean the exhaust gasses do exist, but are not used very widely. Before 2012, the fuel sulphur cap was 4.5% outside ECAs and 1.5% inside. After 2012, the cap is set to 3.5% and 1% respectively outside and inside the ECAs. A cap of 0.10% will apply from 2015 inside the ECAs, and it is to be decided whether or not a global cap of 0.5% is applied from 2020 onwards.

SOx emissions are not directly treated in the present work; however, the regulations on fuel sulphur has direct impact on the fuel prices which affect the overall shipping economy. The fuel expenses currently constitute about 30-55% of the total operating costs for large ships [24], and prices will likely increase with the need for decreased sulphur content; hence, the SOx regulations also motivate the use of advanced WHR systems to save fuel.

1.1.2 Current research

The present thesis builds on numerous relevant scientific studies and rather than presenting a major review in this section, each section provides the relevant aspects from the literature. In this section, a general introduction to the current research in the field and some examples of important studies are presented.

The most advanced propulsion power plants on board large container ships of today are almost comparable in complexity to large land based power plants. The current state-

of-the-art propulsion power plant is installed on the currently largest container ships, the Maersk Triple-E class vessels. They are powered by two identical two-stroke diesel engines with a WHR system which consists of a dual-pressure level steam Rankine cycle coupled with an additional exhaust gas driven gas turbine (also called a power turbine). The WHR system is co-generating propulsion power, steam and electricity from three different engine waste heat sources [25]. Moreover, adding to the complexity; with the ever stricter pollution regulations follows a demand for further expansion of the number of sub-systems in the machinery rooms.

The context in which these systems work poses important constraints; an example relevant to the present study is the required machinery room safety precautions, which can influence decisions about the type of alternative working fluid used in the WHR system. Another example is that the system operates as a stand-alone system, and a constant balance is thus required between the power production and the demand. To that regard, Baldi [26] points out the importance of including the auxiliary power production and demands in the evaluation of the feasibility of the WHR system; an aspect which is rarely considered in the literature though.

Perhaps due to these reasons, documentation of the knowledge about the interaction between the main engine design and operating parameters, and the turbocharger (T/C), WHR system and emission abatement systems, is relatively limited. For the same reasons, the design and optimisation process presents a significant challenge, particularly when considering these interactions.

On the other hand, the marine propulsion plant is then also a system with tremendous research and development possibilities; a fact which is reflected in the scientific literature. Table 1.1 provides an overview of the systems, sub-systems, components and models which constitutes the relatively narrow focus of the present thesis. The table also presents some of the main fields of research involved.

There is a fair amount of literature provided by the major industrial manufacturers, such as MAN Diesel & Turbo (MDT), Wärtsilä and ABB; however, this literature generally focusses on describing the results of the current research, and is in many cases not providing much details about the specific methodologies and conditions. This is understandable considering the commercial interests. Hence, to reach a deeper understanding, there is still a need for providing scientific documentation regarding the design and optimisation of the relevant technologies, even though some tasks have already been carried out by the leading companies.

The most significant current research and development programme for new technologies for marine engines is the Hercules programme [27]. The programme has run for ten years as of 2014 and has a budget of 76 million Euro so far. It is a collaboration project between the major European industrial stakeholders, shipping companies and a number of universities.

Table 1.1: System hierarchy (inspired by the work of Chow et al. [19])

System	Combined cycle			
Sub-systems	Diesel engine	Turbocharger	Power turbine	Rankine cycle
Components	Cylinder Piston Connecting rod Crankshaft Propeller Shaft motor	Turbine Compressor	Turbine Gearbox Generator	Turbines Generator Heat exchangers Pumps Separator Absorber
Models	Gas equation of state Media properties Ignition delay Combustion chemistry Heat release NOx Heat losses Friction Scavenging	Efficiency maps Media properties	Efficiency maps Media properties Electrical efficiency	Media properties Electrical efficiency Turbine constant Efficiency

Table 1.2: Overview of the research and development efforts in Hercules

Phase A (2004-2007)	Phase B (2008-2011)	Phase C (2012-2014)
Extreme engine design parameters	Extreme design parameters	
Advanced combustion concepts	Combustion	New combustion concepts Fuel injection models/experiments
Two-stage/intelligent turbocharging	Turbocharging	
Turbo-compound and hot engine	Overall power train optimization	
Emission reduction methods	Emission reduction methods	Nearzero emission technologies
Friction reduction	Adv. materials, friction and wear	New materials and tribology
Adaptive/intelligent engine control	Electronics and control	Adaptive engine control and reliability

Hence, it is reasonable to assume that the activities contained in the Hercules programme, can provide a good indication of the near future development. Table 1.2 presents an overview of the areas of innovation carried out or planned within the Hercules programme.

The table is divided into the three phases that the programme consists of so far. Each row, from left to right, represents a group of projects. From a closer study of the project descriptions, it appears that three of the project group activities have ceased, or merged with the other groups, while the combustion group activities have increased. The turbo-compound (WHR) activities, which are the most similar to the work in the present thesis, were discontinued after phase B [28]. In stead of further development of WHR technologies, the Phase C is focussed on the integration of the many systems, including the WHR and emissions reduction technologies.

Many interesting studies related to the Hercules projects, as well as other important projects, can be found in the important collection of CIMAC (The International Council On Combustion Engines at www.cimac.info) scientific conference articles, which is a forum where MAN, Wärtsilä and other major stakeholders publish scientific articles.

Kjemtrup et al. [29] report on the modelling efforts made by MDT aiming at exhaust gas emissions reductions. Mainly, two different types of models are used: a zero-dimensional model is used for cycle simulations with the inclusion of the turbochargers, fuel injection systems, auxiliary blowers, WHR system, emissions reduction systems and more; computational fluid dynamics (CFD) models are used for different studies of e.g., cylinder flow and combustion physics. The work also describes studies of scavenge air moisturisation (SAM) where the hot air exiting the compressor is used to evaporate water to saturate the intake air and thus reduce NOx emissions. Moreover, results from promising studies of using exhaust gas recirculation (EGR) are presented along with results from studies of the integration of both SAM and EGR into six different engine, turbocharger and WHR system layouts.

Kaltoft et al. [30] present the latest MDT efforts on a fully integrated EGR system installed on a 4,500 twenty-foot equivalent units (TEU) container vessel, which can comply with IMO Tier III. Different EGR operation modes are described, among those a fuel efficiency mode; by increasing the engine compression and maximum pressures, the brake specific fuel oil consumption (SFOC) can be reduced, though with a penalty of increased NOx emissions. By using low EGR rates (about 15%) the NOx can be controlled to comply with IMO Tier II, while at the same time achieve SFOC reductions of about 4-7 g/kWh. This technique is investigated in Sec. 4.1.2.

The most recent and detailed reporting on WHR systems by MDT [18] presents both (a few) thermodynamic and economical details of systems consisting of a power turbine and/or a single and dual-pressure steam Rankine cycle. A rule of thumb is provided for the type of WHR system that can be recommended for different rated engine power capacities: for engines below 15 MW an organic Rankine cycle (ORC), or a power turbine (PT) is recommended; for 15-25 MW engines a PT or a steam Rankine cycle is recommended, and for engines above 25 MW a combined system with a PT and a steam cycle is recommended. (An ORC is a Rankine cycle which utilises organic fluids as working media in stead of water/steam, see Sec. 3.1.4). Figures for the payback times of these WHR systems are presented for a 14,000 TEU container ship. The numbers are based on a typical ship operational profile and the resulting fuel expenses, and the WHR system cost including installation and commissioning. The presented payback times are 3.5 years for a PT system, 5.8 years for a steam Rankine cycle system and 4.3 years for a steam Rankine cycle and PT system. These numbers illustrate, among other things, the cost-effectiveness of the power turbine.

A number of authors present studies of the steam Rankine cycle (SRC) for marine application. In a recent study Theotokatos et al. [31] present a thermo-economical analysis of a single-pressure SRC WHR system for installation on a bulk carrier. System model details are provided and the economical study is based on a typical voyage pattern. A payback time of 2.4 years is reported for the WHR system; however, it is recommended to implement a more advanced WHR system for this application.

In two studies Dimopoulus et al. [32, 33] report on the thermo-economic modelling and optimisation of a dual-pressure SRC with a power turbine for a 4,500 TEU container vessel. The level of detail in the modelling of both the two-stroke diesel and the WHR system are among the highest publicly available at the present time. Validation of some of the main parameters of the main engine, turbocharger and WHR system is presented. The optimisation is done considering a typical operational profile for the vessel type and capital cost sensitivity analyses are presented. It is concluded that a payback time of about 8 years and an overall system thermal efficiency of 51.3% can be expected.

Also among the most detailed thermodynamic studies is a two part study by Danov et al. [34, 35]. What distinguishes this study is that the interactions between the two-stroke engine, turbochargers and WHR system are included. Moreover, the engine model is among the most advanced presented (for this context).

It is noted that Shu et al. [36] present a review of WHR systems for two-stroke engines on board large ships. Several WHR system types are reviewed, e.g., gas turbine systems, refrigeration systems, thermo-electric systems, Rankine cycle systems and desalination systems.

Automotive engine systems face similar challenges as the marine engines do, and the scientific literature about the same type of systems is more abundant for this application. Since marine and automotive engines are similar in many ways, the available knowledge on the automotive application is of value to the marine area; the majority of the correlations used to model the two-stroke marine engine in the present thesis are derived for automotive engines, e.g., the correlations used for estimating engine cylinder heat transfer losses and for modelling the combustion phenomena. It can, and should, however be discussed to what extent these correlations can be used also in the modelling of marine engines.

The automotive diesel engine and WHR system combined cycle have been studied for more than 30 years, i.e., since the energy crisis in the 1970s [37]; Srinivasan et al. [38] recently reviewed selected articles of various approaches including simulations, experimental work, analytical and theoretical studies.

It is not easy to generally state to which extent knowledge can be transferred; however, a number of important points separate the typical automotive application of the diesel engine (and WHR system), from the marine low-speed two-stroke diesel engine system

studied in the present work:

- The typical automotive diesel engine working principle is four-stroke. This means that:
  - the four-stroke engine exhaust is hotter, but has a lower mass flow rate for a given power rating [31].
  - the need for proper scavenging limits the expansion stroke of the two-stroke engine because there has to be time enough to obtain high enough scavenging efficiencies [39].
  - the two-stroke engine needs high T/C efficiencies to ensure proper scavenging [39].
- The scale of the marine system is much greater; hence, the following issues related to the scale applies:
  - relatively large investments can be made in the T/C and WHR system components because the relative cost (price per kW) is low; hence a higher level of technology can be applied.
  - the support systems for the large engine can be made more advanced, and so can the WHR system in general.
  - space and weight may be a relatively larger concern for the design in the automotive application.
- The automotive system changes load much more frequently, with the exception of long haul trucks which may have load patterns somewhat similar to those of large ships.
  - for this reason and due to the smaller scale, the expander component of the WHR system for an automotive application may preferably be a scroll, screw or piston type where a high-efficiency turbine is preferred for the marine system.
- The reliability of the engine is crucial for the safety of the (usually very costly) vessel it is powering; there is therefore a tradition to focus on well-proven technological solutions for ships.

1.2 Thesis objectives

The overall objective of the present thesis is to create a better understanding of the Kalina cycle and the organic Rankine cycle, in the application on board large ships, in order to provide recommendations regarding WHR systems that can lead to reductions of NOx and fuel consumption. Creating this understanding includes providing answers to the research questions defined below.

The overall motivational background is (besides the already described aspects) that the organic Rankine cycle and the Kalina cycle, which are Rankine cycles with alternative working fluids, are shown to posses significant advantages over the steam Rankine cycle in numerous studies of geo- and solar-thermal applications, when converting low- and medium temperature heat to power. Since the exhaust gas temperature, and the temperatures of the other waste heat sources of the marine low-speed diesel engine are at a similar level, these power cycles may well be suitable and advantageous for WHR on board ships.

The overall task is to identify suitable power cycle designs and working fluids for the specific application mentioned, using numerical models. Additionally, the thesis aims at providing methodologies for the design and optimisation of this type of innovative machinery systems.

1.2.1 Research questions

As a result of the completion of the tasks listed in the next section, the following research questions may be answered:

1. In terms of thermodynamic performance, what advantages and disadvantages are related to the use of the Kalina cycle and the ORC in marine WHR systems, compared to the proven and well-known steam Rankine cycle?

2. Which WHR system layouts and working fluids are suitable for the application in question?

3. What methodologies are useful for the design and optimisation of the low-speed two-stroke diesel engine and WHR system combined cycle?

1.2.2 Tasks

The overall objective is fulfilled by completing a number of tasks (boldface) which are hereby briefly described along with the applied methodologies:

1. **Complete and validate an existing zero-dimensional diesel engine model to be able to design and optimise the WHR systems as a combined cycle, aiming at estimating the potential for reducing SFOC and NOx emissions.** An existing model and a validation were made before the present project and the validation was based on experimental data obtained from the engine manufacturer. The data describes the results of extensive engine tests performed by the manufacturer on their research and development engine (4T50ME-x). The model was validated with regards to the SFOC and NOx emissions response to a number of operating parameter variations. The task is to further validate the part-load performance of the model. (See Ch. 2, Sec. 2.3.2 and 2.3.3).

2. **To be able to investigate the effects of EGR operation on SFOC and NOx, further develop and validate the model to this regard.** The model was already prepared for simulation of EGR operation, and since EGR is one of the main NOx reduction techniques [40] along with catalytic reduction methods (SCR), the task is to complete the model and validate for EGR simulations using suitable data available in the literature (see Sec. 2.3.3).

3. **Develop modelling software to enable simulations of WHR systems using alternative working fluids and including mixtures.** Calculation of the thermo-physical properties of multiple working fluids and their mixtures is required for cycle analyses; the selection of a methodology for the implementation of new working fluid models is to be based on a literature survey. (See Sec. 3.2.3 and 3.2.1). Moreover, the inclusion of new component models is needed to enable simulations of the Kalina cycle. Studies are performed to select the proper equations for these components. (See Sec. 3.2.3 and 3.2.1).

4. **To be able to create knowledge about the thermodynamic performances, develop and implement methodologies for the design and optimisation of the combined cycle consisting of a diesel engine and the WHR systems.** Optimisation algorithms can assist both the design and the optimisation. Software is to be developed for the same purpose. (See Ch. 3 and 4).

5. **To facilitate the estimation of the effect of using WHR systems, produce analytical equations that can be used to estimate the potential power output for a given WHR technology.** The equations are written on the basis of simulations and with inspiration from relevant literature. (See Sec. 3.1.5, 3.2.2 and 3.3.2).

6. **Produce a number of recommendations for a suitable WHR technology, including cycle layout and choice of working fluid.** The recommendations is based on the results of the above mentioned efforts. (See Sec. 5.5).

1.3 Scope and delimitations

The focus of the present work is on the design and optimisation of alternative and innovative WHR system solutions for marine low-speed two-stroke diesel engines, using numerical systems modelling methodologies. This means that all efforts can be made with the freedom of being able to design the system in any desired way, with the aim of achieving the optimum design for a given set of boundary conditions.

The scope of the main engine modelling is limited to four specific engine models: a research engine (4T50ME-x), a widely used engine type for large feeder class vessels (7L70MC), an advanced electronically controlled engine (12K98ME), which is the perhaps most studied low-speed two-stroke engine in the literature; and finally a four-stroke engine (20V32), which is included only indirectly.

To limit the work load, very important aspects such as economical and environmental costs, space and weight requirements, strict attention to rules and regulations, and other non-thermodynamic decision factors, are analysed to a limited degree. The careful consideration of all relevant aspects would limit the time available for efforts towards investigating innovative solutions.

1.3.1 Modelling

The general delimitations related to the present work are summarised in the following.

The energy system: The energy system boundaries are including only the thermodynamic cycles, except for the final study which includes the propeller indirectly; the thermodynamic cycles consist of the main engine, turbochargers and WHR system. The system boundaries are slightly different in each study, according to the focus in each of the presented studies. In general, auxiliaries, such as fuel pumps, cooling water systems and the like, are not included.

Co-generation: The generation of steam and heating for various purposes on board is not included in the studies presented. This is to some extent a weakness of the present work; however, the argumentation for this decision is summarised as follows: with the introduction of new built innovative WHR systems may also follow changes in the general conditions of operation, and a re-design of the systems creating the demands for heat and steam today. For example, heating of the fuel oil is not needed in future scenarios where the heavy fuel oil is replaced by an alternative fuel, liquid or gas. There may be implemented innovative solutions to fulfil or strongly reduce needs of the accommodation areas, such as recirculation of heat and better insulated cabin structures. Moreover, the

scope is narrowed because the aim is not to design a specific machinery system in detail, but rather to compare different technologies. In addition, it can be argued that in all of the presented studies, there is at least one heat source which is not fully utilised; a heat source is thus available for heat and steam generation. Finally, in the case of container ships, which is the main focus of the thesis, the steam demand is rather limited. A manufacturer describes for example a steam demand of around 5% of the total steam flow in the Rankine cycle [18]; hence, the impact of this factor in the comparison of different WHR systems is expected to be relatively small. It is noted that the financial investment into an additional steam boiler may not be insignificant.

The cooling system: It is in all cases assumed that cooling water can be supplied with as high a mass flow rate as needed to meet the specifications, and the power consumption of circulation pumps is neglected. The reason is that design and optimisation of the cooling system is not within the scope of the present work. Moreover, since the cooling water pump consumption is relatively small compared to the WHR system power output, it is assumed that the relative difference in condenser cooling water pump power consumption for the different WHR system solutions is insignificant.

Auxiliary components: The power consumption of all auxiliary systems and components, such as fuel and oil pumps, cooling fans, and others, is neglected in the analyses. It can, for the present purpose, be assumed that these systems are somewhat similar for all the WHR systems and that the consumption is relatively small in comparison with the WHR system power output, making the differences insignificant.

Steady-state: The simulations are all limited to steady-state conditions which is considered an appropriate starting point in the design process. The importance of dynamic behaviour should not be disregarded, mainly because a ship operates as an independent self sustaining energy system. Dynamics and control aspects are fields of science in themselves and are kept out of the scope.

Operating parameters: The limits of the variations of the operational parameters in the optimisations, e.g., the engine maximum pressure, are all kept at levels which can be considered realistic compared to the current technologies. Higher efficiencies can always be achieved with higher pressures and temperatures, but such measures require a more detailed approach, including for example the analyses of the thermal loading of components.

1.4 Numerical optimisation strategy

The numerical optimisation strategy applied in the present thesis work played an important and central role for the completion of the work. The main reason is that the optimisation strategy was an integrated part of the system design methodology, such that the design of the process layout and the optimisation were done simultaneously (See Sec. 3.2.3 and 3.2.1).

With the complexity of the machinery system as described, finding the optimum performance using parametric studies can be overly time consuming and may not lead to the identification of the actual optimum; in most cases, the number of parameters makes it infeasible. With the use of numerical optimisation techniques, the work can to some degree be delegated to systematic algorithms; however, the risk of using such algorithms is that the behaviour of the system is not understood by the researcher, because only the final optimum is provided.

Using such algorithms requires that the system models are built to be robust towards input values, because the optimisation algorithm provides any combinations of model inputs leading to model convergence issues.

The range of available numerical optimisation techniques is relatively large. New methods are being developed continuously as the optimisation problem complexity and computational power increase; however, considering the nature of the optimisation problems which must be solved to achieve the objectives just presented, the range of methods narrows down quickly.

The method should for the mentioned tasks preferably be able to handle challenging optimisation problems with the following features:

- Between 10-25 parameters.
- Non-linear equation systems. The studied systems consist of multiple levels of equation systems; mainly the overall system equations, such as energy balances, and the equation systems to resolve thermodynamic state functions.
- Multiple constraints of varying nature which are not always algebraic expressions; e.g., a constraint can be a maximum pressure rise of the engine, which is the result of the engine model input parameters.
- Multiple local optima exist for this type of systems; many traditional optimisation techniques find an optimum, but it depends on the problem whether this is the global or local optimum [41].

- Relatively high computational cost of model execution - the method should therefore preferably be able to work in parallel to speed up convergence.
- Multiple conflicting objectives. Most relevant in the present thesis is the fuel consumption and NOx emissions trade-off which exists in the tuning of the main engine.

Direct search methods may be able to fulfil most of the requirements listed above; however, the genetic algorithm [42] immediately proved to be able to meet all the listed requirements, so this algorithm was eventually used in all the presented optimisations. A brief outline of the principles of the algorithm is provided in the following.

As the name implies, the genetic algorithm (GA) emulates the functions known from genetics. The model optimisation parameters constitute the genes of a given individual which is part of a population (or several populations). The genes of the fittest individuals are more likely to produce offspring i.e., to have their genes be combined to form subsequent generations of individuals. The fitness of each individual is determined by an objective function, which is a function that evaluates the system model by for example the power output, fuel consumption or NOx emissions - based on the parameter values given by the genes of the given individual.

A stochastic approach is used to form the first generation of individuals and this generation evolves to achieve better performance as generations pass. It is therefore important to choose a suitable number of individuals such that the chance of finding the global optimum is large; from experience, the choice of number of generations and number of individuals needs to be balanced to get the lowest computational cost of the optimisation and find the global optimum. A large number of individuals is likely to provide the GA with a better starting point; however, a large number of individuals slows down convergence because the model has to be run many times for each generation. (The total number of model runs for an optimisation attempt is the number of individuals times the number of generations). On the other hand, the number of generations must be high enough to ensure that the good parameter values (genes) are spread to other individuals and evolve towards the global minimum.

No conclusive calculations available in the literature were found to suggests the optimal number of generations and individuals. In the present work different values are used based on tests of the reproducibility of the optimisation results.

Principles from the nature are implemented in the GA mainly to speed up convergence and to ensure that the global minimum is achieved; the individuals can be arranged into sub-populations between which individuals can migrate. Genetic inheritance, cross-over and mutation are the main mechanisms to create the next generation individuals and by these principles a (pre-defined) level of randomness is ensured. Further investigation of these GA settings was not made because the default values worked well.

Pareto optimality is used for the optimisation of more than one objective; a task which is not straightforward because of the relative importance of each objective. It is not uncommon that the optimisation of one objective conflicts with another; as for example the above mentioned main engine fuel consumption and NOx emissions trade-off.

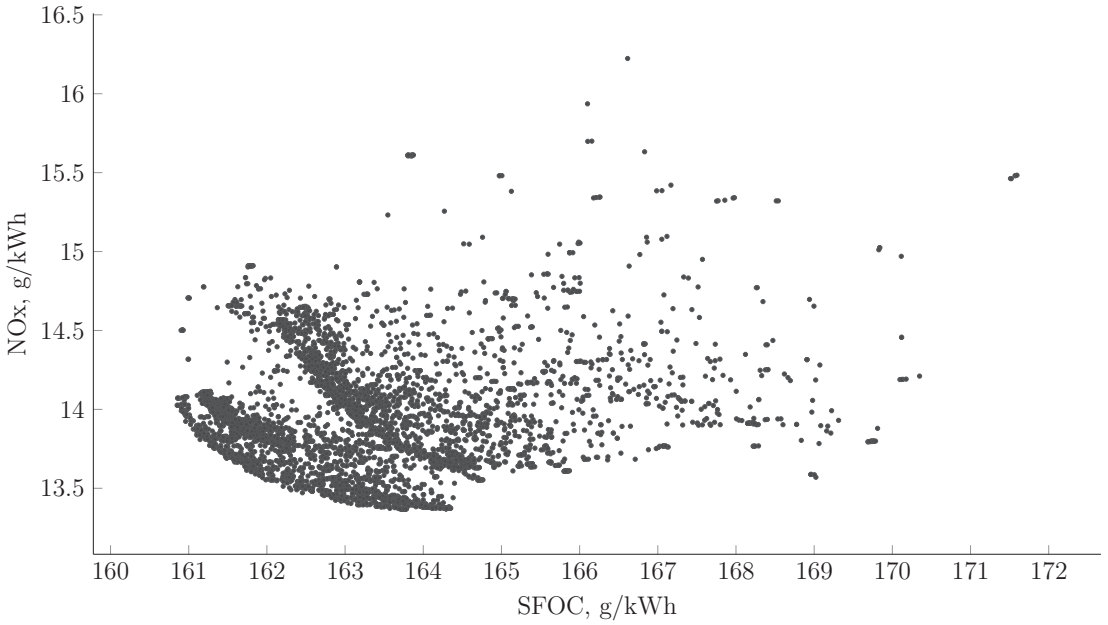

Figure 1.1: Pareto optimisation

A way to obtain a compromise optimum for multiple objectives is to average the objectives and turn the problem into a single value optimisation. Weights can be applied to emphasize the importance of each objective. It is then required to know the importance of each objective, and information for analysis of trade-off behaviour is in that case not provided by the result [43].

With true multi-objective optimisation there is no single solution but instead a set of optima, a curve. The Pareto front, named after the economist Vilfredo Pareto, describes such a set of optima for which it is true, that it is impossible to increase one objective function without decreasing another [44]. Figure 1.1 illustrates the results of running an optimisation using the GA multi-objective function to minimise both NOx and SFOC.

The Pareto front consists of the edge of the points facing towards the lower left corner of the figure. Many additional points are seen behind the front and those are all sub-optimal since these result in higher SFOC or NOx, or both, compared to the optima. It is evident that the algorithm found sub-optimal Pareto fronts, seen behind the final (lowest) Pareto front.

1.5 Thesis outline

The present thesis is structured into five chapters. Three chapters contain the five main scientific studies made for the fulfilment of the mentioned tasks and objectives. The chapters are structured in a general form with introduction, methodology, results and discussion sections.

Chapter 2 describes the background and methodologies applied to model the marine two-stroke diesel engines, used for further studies in this thesis. In the Results section, validation of the model is presented using three different engine types.

Chapter 3 contains three studies of WHR power cycles. Different process layouts of the organic Rankine cycle and the Kalina cycle are treated. The first study proposes and applies a novel methodology for the simultaneous process layout design, fluid selection and parameter optimisation of ORCs. An important finding in this study is that the maximum obtainable ORC thermal efficiency can be predicted accurately, without having to model and optimise the process.

This finding led to the second study of Ch. 3; based on a large number of randomised optimisation cases, four regression models are derived to enable the prediction of the maximum obtainable thermal efficiency of ORCs. These models can be used more generally for the estimation of the use of ORCs at various heat source and sink temperature levels, and takes into account the main process parameters.

The third study in Ch. 3 provides an analysis of a unique configuration of the Kalina cycle, the Split-cycle. Literature about the modelling and analysis of this cycle was not previously published. The main aim of this study is to investigate the full potential of the Kalina cycle in the context of WHR for large diesel engines, under the assumption that the Split-cycle can provide the highest efficiency, compared to any other Kalina cycle.

Chapter 4 presents two independent studies that include the adaptation of the main engine operating parameters to the WHR system. A direct comparison between a dual-pressure steam Rankine cycle, a Kalina cycle and an ORC is provided, looking at both the fuel consumption and NOx emissions, as well as important qualitative aspects. The three cycles are all integrated with the ship engine such that the utilisation of exhaust heat, charge air heat and jacket water heat is possible. An investigation of the trade-off mechanism between the fuel consumption and NOx emissions is also presented in this chapter. Five system layouts are optimised, taking into account the part-load performance, using a multi-objective genetic algorithm.

Chapter 5 contains the conclusion of the thesis with a number of recommendations related to the above mentioned studies of WHR systems for large ships.

2 The marine low-speed two-stroke diesel engine

This chapter describes the applied methodology for the modelling of the main engine and turbocharger. In the Introduction section a brief introduction to the two-stroke low-speed diesel engine is provided. An outline of the importance of the turbocharger is provided as well as introductions to NOx emissions and the general reduction techniques. Then follows an introduction to different engine model types, including a few important examples of relevant work in the literature. The Methodology section describes all the sub-models of which the engine model consists, and the background for choosing these. The Results section presents the calibration and validation results and the Discussion section treats the further development of the model, and the uncertainties related to the presented model type.

2.1 Introduction

It is in the following assumed that the reader is familiar with the diesel engine cycle in general; however, a few points are hereby mentioned about the special features of the low-speed two-stroke diesel engine.

The development of the marine low-speed two-stroke engine has lead to the common engine design of today, with the following features: scavenging air enters through ports at the bottom of the cylinders and exits through a single hydraulically controlled exhaust valve (uni-flow scavenging). The scavenging is driven by constant pressure turbochargers. The high stroke-to-bore ratio can be more than 4:1 and the brake mean effective pressures can exceed 20 bar. The maximum pressures are typically about 140 bar or more, at maximum power. The engines can have up to 14 cylinders and produce more than 80 MW [45].

A unique feature of the engine type is the low revolution speed which is typically from 55 to 250 rev/min. This enables a direct coupling between the engine crank shaft and the propeller shaft, which minimises conversion losses and increases propeller efficiency [45]. The propeller for this type of engine is most commonly of the fixed pitch type, mainly due to a lower price and a slightly higher efficiency, compared to the alternative, the controllable pitch propeller [46].

In the design and optimisation of the presently studied type of machinery systems, this coupling must be considered. This means that the engine should be designed under the constraint of the propeller law, which states that the engine brake power divided by the engine speed to the power of three is constant [46]; the constant value is related to the

characteristics and working conditions of the propeller. Thus, the propeller law poses an important constraint for the optimisation of the engine operational parameters when considering full- and part-load operation.

An important difference between the four-stroke and the two-stroke engine is that the four-stroke engine utilises an entire engine revolution to fill and empty the cylinder in a gas exchange process, while the two-stroke engine utilises a gas flow process where all the stages; intake, compression, combustions, expansion and scavenging; occur during a single engine revolution. As a consequence the two-stroke engine requires scavenging by blowing air through the cylinder. To ensure proper scavenging, a sufficiently large pressure drop must be present between the inlet and outlet ports and valves; consequently, the T/C will have a relatively low pressure available on the exhaust side to provide the work needed on the compressor side and this makes the requirement for highly efficient T/Cs on two-stroke engines more important [39].

2.1.1 Turbocharging

Turbochargers on marine two-stroke engines were first installed on a ship in 1952 [45] and have since become standard on marine engines. The main advantages of the T/C, leading to the success, can be summarised as follows [45, 47]:

- Engine power is increased for a given size and weight of engine with a given piston speed. The increase may be a factor four compared to a naturally aspirated engine of the same size [48].
- Significant specific fuel consumption reduction.
- Lower specific engine cost (price/power).
- Lower heat and friction losses for a given power output.
- Lower specific exhaust emissions.

The reason for this is that the T/C increases the air density and thereby the mass of air induced into the engine; thus enabling the combustion of more fuel compared to a naturally aspirated engine.

The T/C can be viewed as a simple WHR system that recovers energy from the exhaust gas and converts it into mechanical energy, which drives the compressor. The combined shaft power of the T/Cs is surprisingly large, and can reach a third of the engine power or more [39].

On large marine engines of the type studied here, each T/C supplies air for three to five cylinders and may typically consist of a radial flow compressor and a single stage axial- or a radial-flow turbine. They typically operate under constant pressure conditions as opposed to T/Cs which rely on the pulsation of gas arriving from the piston movement. Auxiliary blowers powered by electricity are used to supply scavenge air at loads typically lower than 30% [39].

Turbocharger matching

Two key factors govern the choice of T/C configuration for the marine low-speed engine: 1) the compressor operational line or steady-state working line, which should be drawn where the compressor efficiency is the highest, and 2) a safety margin (usually of 15% [39]) to the surge line must be ensured, for safe and reliable operation. Compressor surging is a situation where the operation occurs at too high pressure ratios for a given air mass or volume flow. Operation can thus only be maintained at reduced air pressures and/or flow rates resulting in reduced engine power [45].

Turbocharger efficiency

The currently available T/C efficiencies are at high engine loads more than adequate. Even though the turbine could produce more power from the available exhaust the compressor would not be able to utilise it. While higher compressor pressure ratios and flow ratios would lead to higher engine efficiencies, the marine one-stage compressors cannot deliver such due to physical limitations related to the Mach number at the compressor inlet [49].

To utilise the energy available in the exhaust that is not used in the T/Cs, a part of the exhaust gas can, as mentioned, be bypassed the T/Cs and the energy can be converted into electrical power using a dedicated power gas turbine. Alternatively, since less exhaust energy is required, the engine can, in theory, be allowed to have a longer expansion stroke, and thus a higher engine power output; a technique named the Low-port concept by Heim [39]. If an acceptable scavenging process can be maintained.

For the optimisation using numerical models, the efficiencies of the T/Cs pose a limit to how efficient the main engine can be tuned. When the exhaust temperature decreases with increased engine efficiency, the exhaust gasses are containing too little energy to drive the compressor; thus the T/Cs are in a symbiotic relationship with the engine, and should therefore not be neglected in main engine and WHR system optimisation efforts.

Two-stage turbocharging

As mentioned, the most efficient single stage compressors operate near to the limit of what can be achieved [39]. A mean to obtain even higher fuel efficiencies and lower NOx, is to implement a two-stage compressor. Inter-cooling between the two compressor stages reduces the compressor work, and the two stages enable very high scavenge pressures. The T/C manufacturer ABB recently presented a study of two-stage turbocharging, and compressor pressure ratios of up to 10 were investigated [49]. Results suggested that the two-stage T/C can achieve about 10% higher efficiencies than the single stage T/C. Moreover, results showed that such high pressure ratios can lead to reductions of NOx up to 40% and of SFOC up to 5%.

A drawback of two-stage turbocharging is the increased machinery complexity and additional space requirements. For the two-stroke engine application it appears to be a relatively new technology for which publicly available scientific studies are few.

Turbocharger cut-out

In order to increase the part-load efficiency of the turbochargers (and thus the engine), one or more T/Cs can be bypassed such that the flow rates of the remaining T/Cs increase; this can be achieved by simply blocking the compressor outlet and turbine inlet [50].

In a recent study presented by MDT [50], it is stated that the T/C cut-out technique is 'unbeatable' with regards to the return of investment, because it leads to lower fuel consumption at low loads for a low price. An alternative option to increase part-load efficiency described in the same work, is the variable turbine inlet area technology. The cut-out option does not provide as large improvements of the engine fuel efficiency at part-loads as the variable turbine area technology, except at loads lower than 30-40% where cut-out appears from the results to be a superior technology.

2.1.2 Nitrogen oxides

NOx emissions contribute to harmful environmental effects such as acidification, eutrophication and formation of ground level ozone [51]. Acidic rain damages trees and soils while the effect eutrophication can be observed as a greatly increased amount of plankton in the waters. Ground level ozone is generally harmful for the human health, but also to sensitive vegetation [52].

Compared to road vehicles, such as for example trucks powered by heavy-duty diesel engines, ship engines are allowed to emit much higher amounts of NOx per kWh of power

produced. The Euro VI emission standard (for road vehicles), which was effective as of 2013, sets a limit of just 0.40 g/kWh, and the Euro V limit of 2008 was 2.0 g/kWh; this makes it clear that the Tier III limit is far from strict in comparison with the limits for road vehicles. These numbers should be seen in relation to where the emissions occur. Studies [53] have estimated that about 70% of ship emissions occur closer than 400 km from land, and that these emissions therefore affect significantly the air quality on land, particularly in areas with heavy ship traffic .

Nitrogen oxides reduction

Depending on the degree of NOx reduction needed, a number of methodologies can be applied on the marine diesel engine. The most important methods are listed and ranked by the (immediate) potential for reduction, with the lowest potential first:

- Low NOx engine tuning
- Low NOx injection systems and strategies
- Use of water
- Exhaust gas recirculation (EGR)
- Selective catalytic reduction (SCR)

The NOx reduction achieved with the first four methods is based on creating a lower temperature and/or oxygen concentration in the combustion NOx formation zone [54]. Among the five alternatives, the most relevant technologies in the near future for marine low-speed engine use, i.e., which enables the achievement of Tier III emissions of 3.4 g/kWh, are by some believed to be EGR and SCR [40]; however, any one of the methods can be combined to achieve further reductions. An example is the WaCoReg concept described by Wärtsilä [55], where EGR and direct water injection is combined. Engine tuning is applied in any case.

Low NOx engine tuning include optimisation of valve and injection timings, fuel and air mass flow rates, as well as other engine operating parameters. The goal is in general to reduce the combustion temperatures and/or the duration time with high temperatures. The exponentially growing nature of the NO formation mechanisms with temperature, makes it particularly important to control the peak temperature, which usually occur early in the combustion process. Since pressure and temperature are related thermodynamically, important NOx reductions can be achieved simply by reducing the maximum pressure of the engine cycle. The all important downside of reducing the maximum pressure is the

increased fuel consumption and this constitutes a well known trade-off mechanism between NOx emission and fuel consumption (See Sec. 2.3.1).

Results from experimental tests are described by Holtbecker et al. [54] (Wärtsilä) and they show that when the excess air ratio was reduced from 2.2 to 1.9, a NOx emission reduction of 15% was achieved with an increase in SFOC of 2 g/kWh. The exhaust valve closing time was retarded and the compression ratio was increased while keeping the firing ratio (maximum pressure/compression pressure) constant.

Low-NOx injection nozzles and strategies are not addressed in the present work due to the limitations of the present model; however, the model could be modified to be able to consider injection strategies. Thus, for the sake of coherency this option is briefly described here. Injection strategies aim at reducing the peak combustion temperatures by utilising multiple injections over time. Kontoulis et al. [56] present a study on this technique applied on large two-stroke engines, and found that by using pilot fuel injections, the SFOC could potentially be reduced by 1.7% without increasing NOx emissions.

Effects of using low-NOx injection nozzles can not be predicted with the present model without major modifications, although this is an important technique as shown by for example Pedersen et al. [57] (MDT) and Holtebecker et al. [54] (Wärtsilä). Phenomena such as fuel evaporation, turbulence and mixing plays a role, suggesting that CFD models are better suited for this purpose.

Water in the combustion is not considered in detail in the present work; however, this technique is relevant and the model type used in the present work is, with some modifications, in theory suitable for the prediction of usage of water to reduce NOx.

The currently most important techniques to reduce NOx emissions using water are the following:

A) water can be added to the fuel forming an emulsion as described by MDT [58]. MDT name it water-in-fuel (WIF) and together with exhaust gas recirculation (EGR), it is able to provide very large NOx reductions [57]. Pedersen et al. [57] conclude that although EGR and WIF both cause increased SFOC, the engine can be tuned such that some of the NOx reduction caused by the EGR and WIF, is traded in for SFOC reductions by tuning the engine parameters; it was thus demonstrated that both NOx and SFOC can be reduced simultaneously. The study conclude that in extreme cases the NOx can be reduced by 98%.

B) a water mist can be added to the scavenge air, thus cooling and humidifying the intake air [58]. A modest NOx reduction potential seems to exist for this technique.

C) water can be injected directly into the cylinder during compression and combustion. Wärtsilä reports on a separate water injection system that can be controlled independently

of the fuel injection, with NOx reductions of more than 60% [54].

Exhaust gas recirculation is a technique that utilises redirection of a part of the exhaust gas back to the engine intake system, where it is mixed with the intake air. This technique is commonly applied on diesel engines in road vehicles, but rarely in ocean going vessels, even though MDT have been researching this option for decades [30]. A reason for this may be that the NOx limits until now have not provided the motivation for doing so. The present model was modified to be able to predict effects of EGR with only little additional modelling effort, because the prediction relies on NO formation mechanisms already modelled.

The oxygen concentration in the recirculated gas is naturally lower than that of the fresh air. The amount of fresh air mixed into the EGR stream determines the final oxygen-to-fuel ratio. In order to obtain an oxygen-to-fuel ratio similar to when running without EGR, the total amount of intake gas has to be relatively larger when using EGR. The effect is that the cylinder gas temperatures are lower given the same amount of heat is added (in each engine cycle) [30]. Alternatively, the total amount of intake gas can be chosen to be the same when running with or without EGR, and the result is then a lower oxygen-to-fuel ratio, which decreases NO formation during combustion [30, 59]. In addition to this, the recirculated exhaust gas has a higher specific heat value compared to air (due to the high amount of CO_2) and this also reduces the cylinder gas temperatures, (for a given fuel heat input). These two alternative strategies for the total intake gas amount and resulting exhaust temperature, also impact the design and operation of the turbochargers and WHR systems.

Generally, there is an SFOC penalty when using EGR. Kristensen [40] states that SFOC increases by 0.5 g/kWh for each 10% increase of EGR, which reduces NOx by about 20%. EGR can though also be used to lower the SFOC as discussed by Kaltoft et al. [30] who presented results of an SFOC reduction of 4-7 g/kWh while operating below the Tier II NOx limit. The basic principle is that the engine is tuned to provide the lowest possible SFOC, with the result that the NOx emissions are higher than the allowed limit. By using a small amount of EGR the NOx is reduced to the required limit. Is it noted that this seems only possibly when operating with the Tier II limit and not under the Tier III limit. In the latter case all measures seem to be needed to comply with this relatively strict limit.

The components needed for an EGR system are described in more detail by Kaltoft et al. [30] who present a study of an integrated EGR system from MDT. Additional components are various valves, scrubbers, water mist catchers, EGR cooler, EGR blower and mixing chambers.

The scrubber removes soot, particles and sulphur from the exhaust and it can also be used to cool the gas to some degree. The EGR blower, in the study of Kaltoft et al. [30], is a radial compressor type with variable guide vanes, with efficiencies up to about 80%. For

the 27 MW 6S80ME-c9.2 engine, the EGR blower consumption was shown to be about 50 kW for light EGR use (unspecified amount) and between 100 and 200 kW for Tier III heavy EGR use (30-40% EGR). This corresponds to about 0.2% and 0.75% of the engine power.

Selective catalytic reduction is also not analysed further in the present work, but a brief outline is provided here because of the relevance as a competing technology to EGR and water. Also, the present model methodology is well suited to also study SCR in a system with the two-stroke engine.

SCR is currently the most efficient NOx reduction technology and is well known from the use in large power plants, and more recently from the use in heavy duty road vehicles. For marine use it is estimated that SCR can reduce engine NOx emissions by 90-95% [40].

Ammonia, in the form of urea, is used together with a honeycomb material coated with a catalyst, to convert the nitrogen monoxide (NO) and nitrogen dioxide (NO_2) to nitrogen and water. The reactions need a relatively high temperature of the gasses and the catalytic material, and this impacts the operation of the engine and the design of the exhaust gas and intake air systems, particularly for the two-stroke engine considered here. The SCR needs to be placed before the T/C where the temperature is high. This is, however, not a major problem and examples of the use SCR on two-stroke engine exist, although it is not widespread at the time of writing [55].

The major drawbacks of the SCR technology is mentioned [54] to be the cost of the consumption of urea and the additional space required by the catalytic reactor.

In the same way as was explained with EGR, it is at least in theory an option to reduce SFOC, e.g., in Tier II areas, by tuning the engine for maximum fuel efficiency and letting the SCR remove the excessive amount of NOx produced.

2.1.3 Choice of model type

One of the advantages of numerical engine modelling is that it enables the evaluation of numerous design and operation scenarios. This is of particularly great importance when considering large marine engines because these engines consume significant amounts of fuel, and the experimental equipment is much more costly than for smaller engines; however, it seems at the current time to be a challenging task to construct a single model which can predict the results of the numerous imaginable designs and operating conditions for the engine process, and which at the same is time fast enough for systems analyses. A reasons for this may be that the diesel engine cycle includes so many phenomena which require complex description mathematically, some of which are not fully understood.

Various types of steady-state numerical engine models are proposed for different purposes. The model types can be categorised by their speed of execution, ranging from empirical correlations, over thermodynamic models to 3D CFD models. At the present moment, the available computing power determines in many cases, which is the most suitable type in a particular context; for example in a real-time application, such as the models in engine control algorithms used on board vehicles, only very fast models can be used. In the context of the present work, the time restraint is not as limited, and is determined by the overall time available for the optimisation of the whole energy system.

In the following, the main types of engine models found in the literature are introduced in order to provide a context for the present work.

Black box models are empirical models which are calibrated using experimental measurements, or alternatively, results from more advanced models; hence, execution occurs rapidly but the ability to (accurately) predict is usually limited to specific conditions, i.e., extrapolation is normally not an option. However, empirical models can in some cases be surprisingly useful, as was found in the present study (see Sec. 3.1.5).

Zero- and quasi-dimensional models is here included in the same category. Both types are based on mathematical descriptions of physical phenomena, but also employ empirical and semi-empirical correlations for some phenomena. The same sub-models can be implemented in the two types, as for example those accounting for friction, NO formation, cylinder heat losses, combustion chemistry, energy balances, the general cylinder mechanical behaviour and the equation of state for the working gas [60]. The main distinction between the two model types is how the fuel injection and heat release phenomena are accounted for.

The quasi-dimensional models are able to resolve the fuel spray in physical dimensions and let the ignition, combustion and NO formation occur in local zones. This type of phenomenologically based approaches bring the distinct advantage of having a higher level of detail of the most important phenomena, without significantly greater computational cost [61].

Models that are at the same time zero- and quasi-dimensional models are present in the literature [60]. The two-zone model, which is used in the present work, can be categorised as a hybrid type of model and so can the numerous multi-zone models which exist. One reason for developing a hybrid type is the desire to achieve relatively higher accuracy without much additional computational cost. In energy system design, analysis and optimisation, a difference in execution time between ten seconds and a minute, results in having the optimisation take one day or a week with for example 10,000 model evaluations. Moreover, the larger the energy system, the more optimisation variables are needed and the more individual model runs are needed for the optimisation to converge to the global optimum. For this reason, the most common model types used for energy system design and analysis

in the literature are the zero- and quasi-dimensional [62].

3D CFD models have the potential to be far more accurate than the other mentioned types. Local phenomena can be studied in detail using the laws of physics and chemistry and in ways which may not be possible even with experiments. CFD models can help to predict effects related to geometrical variations, which none of the mentioned types can. This aspect is relevant to the present work for example because the fuel injector geometries can affect the NOx emissions significantly [63]. Moreover, this type of model is not necessarily limited to making predictions within a certain range of conditions, as the other types are. The all important drawback for the CFD models is the amount of computational power required and this renders this type unsuitable for the present purpose.

Examples in the literature

In a recent publication, Kumar et al. [60] present a review of more than one hundred studies concerning diesel engine modelling.

A Ph.D. thesis by Weisser [64] compares the performance of a zero-dimensional and a CFD models. A conclusion is that at a specific set of operating conditions, the two models types can perform very similarly, in terms of combustion characteristics. Because the zero-dimensional model can be calibrated it is able to predict NOx emissions better than the CFD model, in the specific case. Another conclusion is that while zero-dimensional models can achieve high accuracies, accurate results are limited to variations of global operating conditions and a limited range of variation for injection parameters; moreover, Weisser concludes that complex phenomena related to for example injector geometries, number of injectors, cylinder wall interactions and more, require CFD modelling.

Wimmer et al. [65] compare performances of two zero-dimensional models and a CFD model against experimental data. They conclude that the heat release can be predicted well by all the models and the NOx emissions as well. They also conclude that the zero-dimensional models can deliver predictions that are in very good agreement with the experimental analysis of mixture formation and combustion.

Grimmelius and co-authors (mainly Stapersma) are authoring a number of articles concerning the marine propulsion power plant [66, 67]. The work is mainly focussed on the dynamic behaviour but not exclusively. A brief description follows here.

The main engine is modelled using a so-called *mean value first principle model* [66]. The T/C is modelled using component maps obtained from manufacturers. The cylinder process is modelled using a Seilinger process [68] which can be seen as an approximation of the Diesel process. The name mean value refers to the mean values used to model the compression and combustion processes. Using heat release data from test engines, the

mean value constants are used in a regression type empirical model, to predict effect of air/fuel ratio and maximum pressure level.

Detailed modelling of the engine heat losses is implemented; the cylinder heat loss is determined using the Woschni model [69]. Losses during the gas exchange process are divided into the stages of the cycle (induction, scavenging, expulsion and blow-down). The model output values are the lube oil, jacket water and charge air heat, detailing the low and high temperature cooling water circuits, and the exhaust gas.

A relatively detailed gas exchange model is implemented and some simple sub-models are used to determine the thermal loading of certain engine components, for example the exhaust valve. Friction is modelled using the model of Chen and Flynn [70].

The two major manufacturers Wärtsilä and MDT both use CFD and zero-dimensional models, each for specific purposes. Wärtsilä uses a two-zone model for process analysis and NOx emissions prediction [54]. Kjemtrup et al. [29] describe how MDT also utilises both types; the zero-dimensional model includes the entire engine with turbo, pipes, waste gates etc. CFD models are used for investigation of gas flows and for detailed combustion process analyses.

2.2 Methodology

This section describes the background and details of the engine and turbocharger models used in the present work. The applied sub-models are described and justified using the scientific literature. Finally, a description of the calibration procedures are provided.

2.2.1 Background

The starting point for the zero-dimensional two-stroke diesel engine model used in the present study was, that the model was developed to a first stage in a collaboration between Anders Andreasen from MDT and Fredrik Haglind, Spencer Sorenson and Fabio Scappin at the Technical University of Denmark. Initial validation efforts were made but no results were documented at the time.

Sigurdur Stefansson continued the development by including a scavenging model such that the trapped cylinder gas composition and state at the start of compression can be estimated by letting the model simulate a few cycle revolutions. Sigurdur also contributed with the important validation of the model outputs SFOC and NOx, considering variations of engine tuning parameters which control scavenging, compression and maximum pressures (see Sec. 2.3.1). This work involved also Anders Andreasen from MDT and it lead to a publication [6], which was edited and finalised by the present author, with the addition of the validation of a 7L70MC engine model at a single load point.

Due to reasons explained in the next sub-sections the model was further developed by updating the gas equation of state from an ideal gas to the Redlich-Kwong equation of state (EOS). The NOx model was also updated to include more formation reactions and a new ignition delay model was added. A friction model was added as well as models of the turbocharger and auxiliary blower. Finally, the model received a comprehensive revision with the aim of reducing the model execution time and several verification tests of intermediate results were also added.

Lastly, no documentation of a scientific evaluation or discussion of the chosen sub-models were presented with the model because it was at the time at the developmental stage; for this reason the most relevant parts of the model are described and discussed in the following sub-sections.

2.2.2 Thermodynamic properties

For each stage in the engine cycle, compression, combustion, expansion and blow-down, a set of differential equations are solved to resolve the thermodynamic states. Included are

an energy balance, a mass balance, an equation of state and heat loss and heat release correlations. The general energy balance is formulated as follows:

$$\frac{dU}{dt} = \frac{dW}{dt} + \frac{dQ_{hr}}{dt} - \frac{dQ_{cl}}{dt} + \dot{m}_i h_i - \dot{m}_o h_o \tag{2.1}$$

where U, W, Q, t and h are internal energy, work, heat, time and specific enthalpy. $\dot{m}$ is mass flow rate and subscripts hr, cl, i and o are short for heat release, cylinder loss, in and out.

Correlations described by Gyftopoulos and Baretta [71], that are valid at temperatures from 300-4000K thus covering the relevant range, are used for the estimation of internal energy, enthalpy and specific heats. The internal energy is found using the constant volume specific heat (c_v) which is found from the constant pressure specific heat (c_p) by subtracting the gas constant. The molar based c_p and specific enthalpy are found using the following correlations which assume ideal gas conditions:

$$c_{p,j,mol}(T) = a_j + b_j T^{1/4} + c_j T^{1/2} + d_j T^{3/4} \tag{2.2}$$

$$h_{j,mol}(T) = a_j T + 4/5 b_j T^{5/4} + 2/3 c_j T^{3/2} + 4/7 d_j T^{7/4} \tag{2.3}$$

where T is the gas temperature and a_j, b_j, c_j and d_j are constants for each relevant species j. The species included in the model are O_2, N_2, CO_2, H_2O, H, H_2, N, NO, O, OH and CO.

As described next, the ideal gas properties were since corrected by adding extra terms to account for the high pressures which occur in during the engine cycle.

2.2.3 Working gas equation of state

Due to the use of the ideal gas model, the original model under-estimates the compression pressures by about 5-10%, when using the detailed engine data from Goldsworthy [72]; these data are used for the calibration and validation of the model; hence, alternatives to the ideal gas equation of state (EOS) were investigated.

According to Zevenhoven [73], the pressures at which combustion occurs are at a level where the ideal gas equation is inadequate for modelling the engine cycle. This is mainly due to the fact that the species in the gas are at a super-critical state during the process, all except for the water. The conclusion of the study is that the use of the ideal gas

EOS results in higher temperatures during combustion (at the same pressure) compared to what was obtained experimentally, thereby affecting the NOx formation significantly. Zevenhoven also concludes that the van der Waals EOS is the best suitable for the purpose, when comparing the four EOS' investigated in the study.

The inadequacy of the ideal gas EOS is confirmed by Lapuerta et al. [74]. Calculations using four different cubic EOS' are compared to measurements of the diesel process and the conclusion is that the use of the ideal gas EOS results in higher temperatures compared to when using the cubic EOS'. Deviations are largest around the piston top dead centre, i.e., during the maximum pressures, and Lapuerta et al. conclude that the deviations might affect predictions of (NOx) pollutant formation. The investigated EOS' are van der Waals, Redlich-Kwong (RK), Soave and Peng-Robinson, and the Soave EOS provides the best predictions.

Danov et al. [75] propose a new mathematical model of the working media in large two-stroke engines. The study points out that the implementation of a real gas EOS necessitates mathematical dependencies between thermal parameters, i.e., pressure, temperature and volume, and caloric functions, i.e., internal energy, enthalpy and heat capacities. Danov et al. confirms that the use of the ideal gas EOS results in relatively lower pressures, when the pressure is above 80-90 bar, compared to experimental data and when using a real gas EOS, in this case the RK EOS. In a case with a maximum cycle pressure of 111.5 bar, the ideal gas under-predicts the pressure by 5.5 bar or 5%. A consequence is in that case an over-prediction of the fuel consumption by about 7%. Lastly, the ideal gas prediction error is found to exceed the experimental error margins, while the real gas EOS results are found to be within these margins.

The dependency between EOS and caloric functions is already implemented in the original ideal gas version of the present model since internal energy and enthalpy are found using specific heats calculated as ideal gas properties. Replacing the EOS thus requires replacement of the method for calculating specific heats as well. Since the RK EOS is shown to provide good predictions and since Danov et al. [75] already provide a thermodynamically consistent approach to ensure the mentioned dependency, this EOS is now implemented in the model.

A brief description of the implementation is provided here, for further information about the methodology the reader is referred to the publication by Danov et al. [75]. Generally, the approach introduces an additional term to any ideal gas calorific property, in order to make it dependent on both temperature and specific volume (and thereby pressure). The real gas specific heat (c_v) is thus estimated as follows:

$$c_v(v,T) = c_{v,0}(T) - \frac{3a}{4b}T^{(-3/2)}ln(v/(v+b)) \tag{2.4}$$

where v is the specific volume, 0 signifies the ideal gas formulation and a and b are RK constants calculated for the gas mixture. Similar expressions can be found for c_p, internal energy and enthalpy in the mentioned study [75]. Figure 2.1 presents calculated pressures around top dead centre using van der Waals, RK and ideal gas EOS' which are all implemented in the present model.

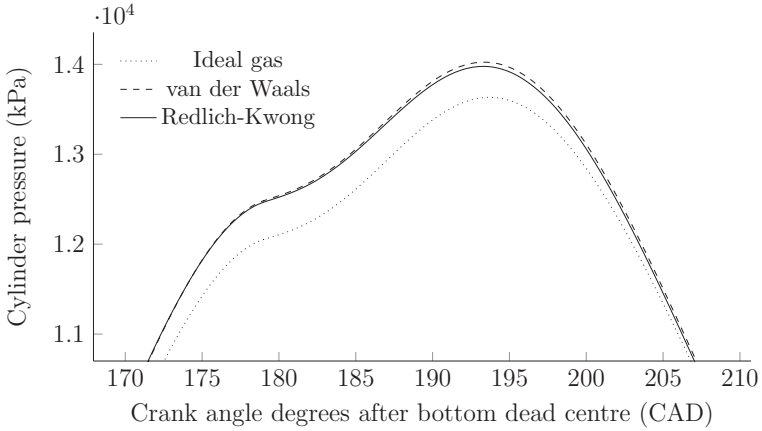

Figure 2.1: Comparison of gas equations of state

It is seen that the RK and van der Waals EOS' predict very similar pressure developments and that the ideal gas EOS predicts significantly lower pressures, which makes it less useful for the purpose of predicting NOx formation. In a later section (2.3.3) the results of using the RK EOS are compared to experimental data.

2.2.4 Heat losses

The heat transfer in internal combustion engines greatly influences the pressures and temperatures over the engine cycle and is therefore perhaps the second most important factor, after the combustion, for model predictions of engine performance.

The physical conditions which a cylinder heat transfer correlation must be able to take into account are immensely complex. There are considerable variations over space and time which are hard to predict accurately, especially when the calculation time is limited. Among other factors there are turbulence, specific volume variation, varying gas composition (clean air and exhaust gas), radiation and flame propagations. For these reasons, the

heat transfer rate varies locally and over time; hence the information needed to describe every instant and every location is too extensive for the fast prediction with today's personal computers. For example, the heat flux can vary from zero to ten MW/m^2 in ten milliseconds and two surface areas one cm apart can experience a difference of five MW/m^2 [76]. Moreover, the physical conditions varies from one engine cycle to another. Due to this high level of complexity, the literature about heat transfer in internal combustion engines is abundant [76].

As a starting point, the heat losses integrated over an engine cycle can be found by the following equation:

$$Q_w = \int_{cycle} \sum_i \overline{U} A_i (T - T_i) d\theta \tag{2.5}$$

where U is the average heat transfer coefficient, A_i and T_i are the area and temperature of the i'th surface while θ is the crank angle. Due to the above reasons, it is not surprising that heat transfer models in zero-dimensional models uses bulk averaged values for gas temperature and other properties; hence in the present engine model this equation is made global such that all surfaces are assumed to experience the same average heat flux.

In their comprehensive review of models, Borman and Nishiwaki [76] conclude that when using either one-zone global models or models which has the heat transfer in the cylinder divided into multiple zones, calibration of the heat transfer model is required to make it fit a specific engine geometry. In the case of marine engines, descriptions of the geometries are difficult to obtain due to confidentiality and no approaches for the simplified description of such geometries is found in the literature. Hence, the motivation for using simplified calibrated models is present and the engine model literature is not surprisingly dominated by this type.

The Woschni correlation

Where previous efforts were based on measurements of heat transfer in combustion bombs, Woschni formulated in 1967 [69] a method for determining the heat transfer coefficient in internal combustion engines, based on measurements on a test engine. Woschni motivated the necessity of using a test engine for the development of a suitable correlation, and his model aims at including a variety of physical phenomena. The model is based on steady turbulent convective heat transfer, but includes radiation heat transfer in a lumped form implicitly [77].

The Woschni correlation is among the most widely used and has proven its validity many

times [77]. Boulouchos and Brunner (of Sulzer) [78] compare the performances of the Woschni correlation and of two more recently developed correlations, the New Sulzer Diesel model and the ETH model. The Sulzer model is developed for modelling large bore low-speed marine engines. Due to inaccuracies in the measurements, the study focuses on relative trends only and the authors conclude that the new models are slightly more accurate than the Woschni correlation, but a need for a more accurate model exist. There seems to be consensus about this need, still, at the time of writing the present work.

The Woschni heat transfer rate model implemented in the present engine model is described as follows:

$$\frac{dQ}{dt} = A_{cyl}\left[\alpha B^{-0.2} P(t)^{0.8} T(t)^{-0.55} \nu(t)^{0.8}\right](T(t) - T_{cyl}) \tag{2.6}$$

$$\nu(t) = c_1 S + c_2 \frac{V_{sw} T_0}{P_0 V_0}(P(t) - P_{motor}) \tag{2.7}$$

$$P_{motor} = P_0 (V_0/V(t))^{\gamma} \tag{2.8}$$

where α is a scaling factor used to match a specific engine geometry. A_{cyl} is the heat transfer surface area in the cylinder, B is the bore, and P and T the bulk gas pressure and temperature. ν is the characteristic velocity and T_{cyl} the average cylinder and piston surface temperature. For the present model, a bulk temperature is to be provided as an input parameter. V is volume and subscripts sw and 0 designates swept and reference, where the reference is the time when compression starts. P_{motor} is the motoring pressure and γ is the ratio of specific heats. The constants c_1 and c_2 are specific for each phase in the engine cycle with the values: 6.18 and 0 during compression, 2.28 and 0 during combustion and 2.28 and 3.24e-3 during expansion [6]. S is the instantaneous piston speed.

Several models are proposed in attempt to improve the Woschni correlation by incorporating terms for radiation directly; among those the mentioned New Sulzer Diesel model. The lack of a dedicated radiation term is considered a shortcoming of the Woschni correlation [76], which is therefore generally expected to under-predict the heat transfer especially during combustion.

In the present studies the effects of using other heat transfer correlations were also investigated, among those the correlation by Annand [79] and different versions of the Woschni correlation. While the presented version of the Woschni model (Eq. 2.6) under-predicts the heat losses (see Sec. 2.3.2 and 2.3.3), the other alternatives did even more so.

2.2.5 Combustion

Diesel combustion is usually divided into three phases [80]: 1) a pre-mixed phase where the injected fuel accumulated before ignition starts, burns rapidly because the fuel has had time to be mixed with the air, in a similar fashion as in a spark-ignition engine. During this phase the pressure increases the fastest and the maximum pressure of the cycle is likely to occur during this phase (though this also depends on the injection timing). 2) a diffusion phase where the combustion rate is limited by the time it takes to mix fuel and air sufficiently. This phase constitutes the main part of the combustion. 3) a post-combustion phase which happens at relatively low pressures and temperatures. Reaction kinetics control the rate of combustion and the remaining unburned fuel and the not fully oxidised species are burned in this phase.

Ignition delay model

The ignition delay is here defined as the time between the start of fuel injection (SOI) and the start of combustion. The ignition delay model of the original engine model, is an Arrhenius type expression which is used often in the literature; however, the ignition delay model was changed because the delay time was found to be too short, both compared to what is stated by Heywood [59] and compared to the experimental heat release data provided by MDT (for a 12K98 engine type).

Alternative models are present in the work of Poulsen [81], who investigate the low-speed two-stroke diesel engine and various ignition delay models in comparison with experimental data. The most suitable model is a semi-empirical model presented by Hardenberg and Hase [59], a model which is also used in Danov et al. [34]:

$$\Delta\theta_{id} = (0.36 + 0.22\overline{v})exp\Big[E_a\Big(\frac{1}{RT_{comp}} - \frac{1}{17,900}\Big)\Big(\frac{21.2}{P_{comp} - 12.4}\Big)^{0.63}\Big] \tag{2.9}$$

Δ is a difference, in this case between the start of injection angle and the combustion start angle, $\overline{v}$ is the mean piston speed, E_a is the activation energy and R is the universal gas constant. Subscripts *id* and *comp* are short for ignition delay and compression. The activation energy is based on the cetane number (CN) of the fuel, which is assumed to be 45 [82]:

$$E_a = \frac{618,000}{CN + 25} \tag{2.10}$$

With the introduction of this new model, the cetane number enables the present model to take the fuel type into account (to a limited degree).

The new model provides better agreement with the ignition delay durations presented by Poulsen and also data presented by Kjemtrup et al. [29], i.e., the original model resulted in delays in the order of $10^{-6} - 10^{-7}$ s. where the updated model results in delays of around 1-4 ms (see also Sec. 2.3.4).

Heat release

Combustion engine heat release is very commonly modelled using the Wiebe function, which is derived from one or more normal distribution functions [83]. The function was derived by Ivan Wiebe as early as 1962 and it describes the heat release with no spacial resolution. As explained by Ghojel [83], the Wiebe function is derived in a variety of forms, for example presenting the burn rate or the burn fraction as functions of time or degrees. While the original single Wiebe function may be sufficient to model the heat release of spark ignition engines and indirect injection diesel engines, it is not suitable for the diesel combustion due to the two distinct combustion stages [83]. Miyamoto et al. [84] presented a double Wiebe function derived to model the heat release taking into account the heat released during the premixed (Q_{pc}) and the diffusion controlled (Q_{dc}) phases:

$$\begin{aligned}\frac{dQ}{\omega dt} = 6.9\frac{Q_{pc}}{\Delta\theta_{pc}}(M_{pc}+1)\Big(\frac{\theta}{\Delta\theta_{pc}}\Big)^{M_{pc}} exp\Big[-6.9\Big(\frac{\theta}{\Delta\theta_{pc}}\Big)^{M_{pc}+1}\Big] \\ +6.9\frac{Q_{dc}}{\Delta\theta_{dc}}(M_{dc}+1)\Big(\frac{\theta}{\Delta\theta_{dc}}\Big)^{M_{dc}} exp\Big[-6.9\Big(\frac{\theta}{\Delta\theta_{dc}}\Big)^{M_{dc}+1}\Big]\end{aligned} \tag{2.11}$$

$\Delta\theta$ is combustion duration in crank angle degrees (CAD), ω is angular velocity, M is the combustion shape parameter and subscripts pc and dc are short for premixed and diffusion combustion phases.

Miyamoto et al. [84] state that the six parameters Q_{pc}, Q_{dc}, $\Delta\theta_{pc}$, $\Delta\theta_{dc}$, M_{pc} and M_{dc} are adjustable and are used to fit the heat release curve to match a realistic one; however, Miyamoto conclude, after a range of experiments on diesel engines, that the values of M_{pc}, $\Delta\theta_{pc}$ and M_{dc} can be assumed constant across varying brake mean effective pressures (BMEP) for direct injection diesel engines, with the values 3, 7° and 0.9 respectively. Despite this, these values vary in works of other authors and are subjected to parametric studies and optimisation, by for example Egnell [85] and Yu et al. [86]. Loganathan et al. [87] propose a correlation between the engine load and the Wiebe parameters. In the present work, the same parameters were adjusted to match measured heat release data (see Sec.2.3.3)

Other useful functions can be used to model the heat release in a combustion engine model, as for example the Seiliger process which Yu et al. [86] compare with the Wiebe function. They conclude that, for their mean value model, the Seiliger process can be adjusted to perform as well as the Wiebe function while being simpler.

In the present work the choice of heat release model was already made by the original developers. The present author has throughout the work found the flexibility of the Wiebe model to be adequate for the purpose, and also, validation of this model can be found in numerous studies in the literature as Loganathan et al. [87] point out; hence, no further investigation of alternatives was made.

The two-zone combustion model

Combustion modelling is generally at the centre of interest in the engine model literature and the reasons are likely that it is the most complex phenomena occurring during the engine cycle, it is not yet fully understood, and it is of the highest importance to the prediction of the engine performance. For combustion models restrained by the requirement of fast execution, it is commonly accepted that the validity is confined to a limited parameter range, and that it relies on measurements and calibration.

When considering the combustion as it takes place in the cylinder, it is advantageous to construct the diesel combustion model to have at least two control volumes or zones, i.e., one zone containing the combustion (reaction zone) and one zone containing the remaining fuel and gasses (unburned gas zone). The reason is that each zone has distinctly different properties in terms of chemical species and temperature [88]. The reaction zone may be resolved into numerous zones over time and these zones may be mixed with the unburned gas zone to some degree or not at all, depending on the assumptions.

The majority of zero-dimensional models in the literature are two-zone models. There are efforts aiming at providing theoretical explanations and sound justifications for choosing the various methodologies concerning the reaction and unburned gas zones [88]; the aim is generally to improve the prediction ability of SFOC and NOx emissions, under varying injection parameters [88]. The time dependent development of the reaction zone(s) after combustion, i.e., descriptions of how the temperature, volume, pressure, mass and composition develop; and how they are mixed with the unburned gas zone, has received significant attention; however, no consensus seems to exist, except that all the models require at least one calibration parameter, which is most often the local air-fuel ratio (AFR) in the reaction zone [88]. Moreover, the agreement in the literature is that the value of the local AFR should be near to stoichiometric (for diesel engines).

The present model uses a two-zone combustion model, and the purpose of the two zones

is mainly to provide inputs to the NOx model. The combustion event is divided over time into a user defined number of equal time steps or packages. This number was in the present work set to 30 for the best compromise between accuracy and computational cost.

The time duration of the combustion is determined by the ignition start time, the injection end time and by a constant b which has the value of 24.5 as according to Heywood [59]. The parameter b determines the remaining combustion period when injection has ended. This value was confirmed to be suitable to match the experimental data used for validation (see Sec. 2.3.3).

The mixing of the two mentioned zones is such that after the combustion reaction in each reaction zone is calculated, the resulting gas products are mixed with the other zone. When a reaction zone is made, the gas composition is the same as that of the unburned gas zone, plus fuel. The mass (m) of the gas in the burn zone (excluding fuel), is found using the local AFR:

$$m_{g,j} = AFR[O_2]_{ha,ms}\frac{m_{f,j}}{[O_2]_{ms}} \tag{2.12}$$

Subscripts ha and ms are short for humid air and mass basis. The mass of fuel ($m_{f,j}$) in the j'th interval is determined by the j'th fraction of the total heat release, which is determined by the Wiebe function.

This approach keeps the mass ratio of oxygen to fuel constant in the burn zone in all the steps of the combustion event. It can be discussed whether this is the optimum way to model the combustion, because the ratio is the same in all cases, also during the use of EGR, for example.

The general assumptions for the present two-zone model are:

- No transfer of mass or heat occurs between the reaction and unburned gas zones
- The two zones are both at the same (bulk) cylinder pressure
- The reaction zone temperature is the adiabatic flame temperature
- The unburned zone temperature is the (bulk) cylinder gas temperature
- The thermodynamic states are constant in the time frame of each reaction zone
- The volume of the reaction zone is constant in the time frame of each reaction zone
- NO is formed in the reaction zone only

- The AFR in the reaction zones is constant

The assumption that the volume of the reaction zone is constant in the individual reaction zone time intervals is not an accurate assumption. The volume changes with up to 6% from start to end time in the interval, with division of 30 intervals, but only up to 2% with 90 intervals. Similar arguments can be made for some of the other assumptions; hence, using a high number of intervals will make the time interval small and negate these arguments. This example shows how the realism of the model is compromised in order to reduce computational costs, such that the model can be used for systems analysis.

Models that take into account the volume change of the reaction zone are presented by Wilhelmsson et al. [89] and Goldsworthy [72]. Wilhelmsson et al. [89] claim that the original Zeldovich mechanism in the common form, is not valid when the burning zone volume changes, and they propose a new modified version. The implementation of this new version, is hereby suggested as future work.

Combustion species

The composition of the working gas is important because it influences the thermodynamic states and the NOx formation, both with regards to the (adiabatic) flame temperature and to the Zeldovich mechanisms (see Sec. 2.2.7). The present model resolves the working gas composition at every instant during combustion (as the composition only changes during this phase).

The combustion phenomenon is modelled as an incomplete combustion. As mentioned, the 11 species considered in the model are: O_2, N_2, CO_2, H_2O, H, H_2, N, NO, O, OH and CO; however, unburned hydrocarbons and particulate matter are constituents which would be useful to add to the model, because the minimisation of some pollutants, as for example NOx, may easily cause increased amounts of other pollutants, as for example particulate matter. Fuel-bound impurities, such as for example sulphur, are not considered even though particularly sulphur is of relevance in the present context.

The combustion products are found using the algorithm described by Rakopoulus [90]. The algorithm considers the chemical equilibrium of the mentioned 11 species. Seven equilibrium equations are considered as well as four mass (atom) balance equations. These 11 equations are manipulated mathematically into a system of four non-linear equations, which are then solved with the $fsolve$ function in Matlab. The equilibrium reactions are:

$$\tfrac{1}{2}\,H_2 \longleftrightarrow H \tag{2.13}$$
$$\tfrac{1}{2}\,N_2 \longleftrightarrow N \tag{2.14}$$
$$\tfrac{1}{2}\,O_2 \longleftrightarrow O \tag{2.15}$$
$$2\,H_2O \longleftrightarrow 2\,H_2 + O_2 \tag{2.16}$$
$$H_2O \longleftrightarrow OH + \tfrac{1}{2}\,H_2 \tag{2.17}$$
$$H_2 + CO_2 \longleftrightarrow H_2O + CO \tag{2.18}$$
$$H_2O + \tfrac{1}{2}\,N_2 \longleftrightarrow H_2 + NO \tag{2.19}$$

The resulting NO concentrations are disregarded because NO formation should not be assumed to occur under equilibrium conditions (see Sec. 2.2.7).

This algorithm is a good compromise between more advanced and accurate, but slower models, and simpler, faster but more inaccurate models. The validation of the combustion model is made with experimental data using n-dodecane fuel ($C_{12}H_{26}$) [90], which is similar to the fuel used in the present work.

2.2.6 Exhaust temperature

In the original version of the model the exhaust gas temperature is calculated using an overall energy balance of one engine revolution:

$$T_e = \frac{\dot{m}_a c_{p,a} T_i + \dot{m}_f h_f + \dot{m}_f LHV - \dot{W} - \dot{Q}_{cyl}}{\dot{m}_e c_{p,e}} \tag{2.20}$$

where LHV is the fuel lower heating value (42,700 kJ/kg) and subscript e is short for exhaust gas and a is short for air.

This formulation does not take into account the temperature of the cylinder gas after the expansion stroke when the exhaust valve opens. It can thus occur that the expansion stroke is so long that the calculated exhaust gas temperature is higher than the cylinder gasses at valve opening.

To counter this inconsistency problem, which can occur during parameter variations when optimising the engine, a new formulation is implemented. The trapped cylinder gas, which is the amount of gas contained in the cylinder at the time of exhaust valve opening, is mixed with the scavenging air. These two flows add up to the total mass flow rate of

the engine, which is a known (input) value. The enthalpies are calculated and an energy balance provides the mixed gas (exhaust) temperature. The final pressure drop, and the resulting temperature drop, from opening the valve is accounted for using an equation derived by Scappin et al. [6].

The results are very similar when using the original and the new approach; however, the new approach is preferred because it removes the mentioned risk of inconsistency.

2.2.7 Nitrogen oxides formation and modelling

Nitrogen oxides emission prediction models applied in engine modelling are common and convincing results are presented repeatedly. Numerous articles propose NO formation models while including different formation reactions [91]; however the perhaps most advanced work within the field available at the time of writing [92, 93] conclude that further efforts (within the field of NO formation modelling) are still needed. A general conclusion, which may be drawn, is that the prediction of NOx emission trends and comparisons are feasible, but the accurate prediction of the absolute emissions are barely within reach with the presently available NOx models, even the most advanced ones. It is therefore noted that calibration generally have to be applied for the models to be able predict satisfactorily, and this also applies to the present model.

The combustion engine produces mainly nitrogen monoxide (NO) which after some time under conditions closer to ambient, for example in the exhaust manifold system, oxidises to nitrogen dioxide. NOx is the term that covers these two species. Therefore, the chemical reactions considered in the engine modelling literature is focussed solely on the NO product. Studies by Zabetta et al. [94] and Kilpinen et al. [92] show how complex NO formation during combustion can be described, considering 353 elementary gas-phase reactions and 57 species; however, it is far more common in the engine model literature, that NO is considered to be formed as either fuel NO, prompt NO, thermal NO and through N_2O (nitrous oxide) [51].

NO is produced in the flame front and in the gasses produced immediately after the flame front has passed. Since the combustion occur under high pressure, the flame front is thin and relatively fast moving. The cylinder pressure rises due to the heat of the combustion, at least in the majority of the combustion duration, and this means that the temperature of the gasses also increases and NO is produced at even faster rates [59]. The combustion gas species are all formed very rapidly and quickly reach what can be assumed to be an equilibrium state, except for NO which is formed more than ten times slower [95]. For these reasons it is sufficient and reasonable to separate the combustion products calculation from the NO formation calculations [59], as it is done in the present work. The same argument makes it reasonable to use equilibrium concentrations when resolving the chemical reaction

equations, as described in the following [95].

Fuel bound nitrogen normally occur in insignificant amounts in motor fuels. An exception is the residual fuels, such as HFO, where 50-100% of any fuel bound nitrogen is converted to NO [54]. The contribution of fuel NO can reach up to about 10% of the total engine NOx when running on residual fuels, which may contain up to 0.5% nitrogen [54]. Assuming the nitrogen content is known, this contribution can be accounted for, and some researchers have simply assumed that all the fuel bound nitrogen is converted into NO, without considering any detailed modelling [96]. In general, it seems that this topic is not very well documented and that detailed modelling may not be worth the effort in cases such as the present. Instead, it may be sufficient to simply add an additional 10% to the calculated NOx emissions, when HFO is used (although this depends on the conditions, e.g., whether or not EGR is used).

Prompt NO is produced from ambient nitrogen in fuel rich areas of the flame front during the combustion. This mechanism is also referred to as the Fenimore mechanism and the reactions involved can be described, though with a significant level of complexity [80]; however, according to Goldsworhty [96], several authors conclude that prompt NO is negligible in the context of diesel engine combustion. Goldsworthy [97] state two reasons: the pre-mixed flame in diesel engines is fuel lean and the residence times (when fuel rich conditions occur) are very short in diffusion flames. Due to these reasons prompt NO is not considered in the present work.

Thermal NO is by far the most important mechanism and it is most commonly the only mechanism included in engine models. As the name implies, the NO is formed under high temperatures, and it is formed from the atmospheric nitrogen and oxygen in the working gas.

The thermal NO formation mechanism is in engine models very commonly modelled using the Zeldovich mechanism (or the extended version), which Zeldovich presented in 1946 and Bauch et al. presented an extended version in 1991 [80]. The extended version is used in the present model and the included reactions are as follows:

$$N_2 + O \longleftrightarrow NO + N \tag{2.21}$$

$$N + O_2 \longleftrightarrow NO + O \tag{2.22}$$

$$N + OH \longleftrightarrow NO + H \tag{2.23}$$

The equations are generally accepted as being valid for near-stoichiometric combustion scenarios [59]. It is noted that the NO formation via the second and third reactions (Eqs. 2.22 and 2.23) depends on the presence of available nitrogen (N); hence, the first step

Table 2.1: Rate constants for the Zeldovich reactions

	Heywood [59]	Spencer [95]	Kilpinen [92]
k_{1+}	$7.6 \cdot 10^{13} e^{-38000/T}$	$2.0 \cdot 10^{14} e^{-23650/T}$	$3.3 \cdot 10^{-60} T^{17.994}$
k_{1-}	$1.6 \cdot 10^{13}$	$1.55 \cdot 10^{13}$	$3.3 \cdot 10^{6} T^{0.3}$
k_{2+}	$6.4 \cdot 10^{9} T e^{-3150/T}$	$1.33 \cdot 10^{10} T e^{-3600/T}$	$6.4 \cdot 10^{3} T e^{-3161/T}$
k_{2-}	$1.5 \cdot 10^{9} T e^{-19500/T}$	$3.2 \cdot 10^{9} T e^{-19700/T}$	$6.4 \cdot 10^{-26} T^{8.52} e^{-3161/T}$
k_{3+}	$4.1 \cdot 10^{13}$	$7.1 \cdot 10^{13} e^{-450/T}$	$3.8 \cdot 10^{7}$
k_{3-}	$2.0 \cdot 10^{14} e^{-23650/T}$	$1.7 \cdot 10^{14} e^{-24560/T}$	$6.3 \cdot 10^{-35} T^{11.2}$

limits the rates of the two others. The third reaction was found, through experiments, to contribute to a net reduction of the total NO formation [92].

The three reactions have rate constants for the forward and backward reactions which are dependent on the flame temperature. The forward and backward reaction rate constants for each of the reactions are not of the same value and the system is not assumed to be in a state of chemical equilibrium [80]. As shown by Spencer [95] there is a significant difference between the NO formation rates when assuming chemical equilibrium and when not. Instead, the NO formation is controlled by reaction kinetics and various values of the rate constants for the Zeldovich reactions are proposed. In the literature it is often not clearly justified why different values are assumed. The rate constants are generally derived through experimental studies [59] and from the commonly known Arrhenius equation:

$$k = Ae^{-E_a/(RT)} \tag{2.24}$$

where A is a constant (sometimes called the frequency factor), R is the gas constant and T is the adiabatic flame temperature. Table 2.1 presents constants found in a few different studies and the resulting NOx emissions when using these are shown for comparison in Fig. 2.2. It is noteworthy that the constants used by Kilpinen are described quite differently from the others. Figure 2.2 shows how the Heywood rate constants lead to significantly lower NOx emissions compared to the two other alternatives.

The NO formation rate is described using the equilibrium concentrations of the relevant combustion products together with the rate constants:

$$\frac{d[NO]}{dt} = k_{1+}[N_2][O] - k_{1-}[NO][N] + k_{2+}[N][O_2] - k_{2-}[NO][O] + k_{3+}[N][OH] - k_{3-}[NO][H] \tag{2.25}$$

where the square brackets signify equilibrium concentrations (mol/cm^3) of the specified species. k are rate constants, subscripts 1-3 are reaction numbers and subscripts + and

– signify the forward and backward direction of the reactions. The concentrations of the species are those included in the burning zone.

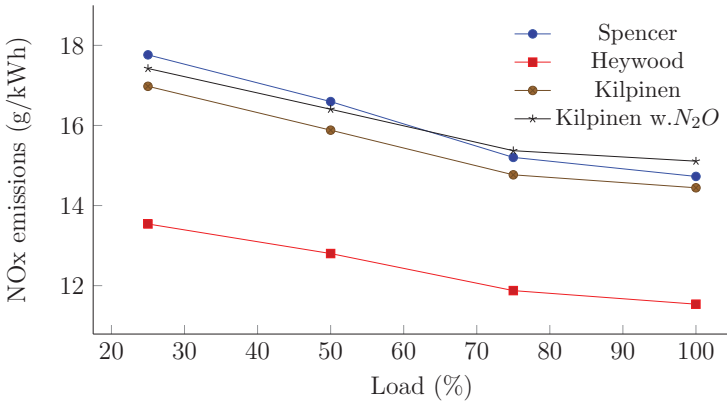

Figure 2.2: Comparison of NOx emission when using different rate constants

The nitrous oxide mechanisms are, among others, studied by Goldsworthy [96] who compare five different reaction schemes using a model of a low-speed marine two-stroke diesel engine. The extended Zeldovich reactions are included in all the schemes and each scheme includes additional reactions to enable the evaluation of their individual importance. It is concluded that two schemes, besides the Zeldovich mechanisms, are of significant importance to the low-speed marine diesel engine modelling: the N_2O intermediate and the N_2O extension schemes. The N_2O intermediate scheme is shown to be the most important one, when considering near stoichiometric combustion.

Intermediate reactions were presented for use in CFD models of low- and medium-speed diesel engines by Zabetta and Kilpinen [93] and earlier by Mellor [98]. In recent work [92] Kilpinen revises the earlier work of Zabetta and Kilpinen [93] because important errors, that are leading to over-predictions, is found in the original work. It is concluded that the models in the original work are not recommended for use. Hence, the now revised intermediate reaction scheme by Kilpinen [92] is implemented in the present engine model (in addition to the Zeldovich reactions), to include the following reactions:

$$N_2O(+M) \longleftrightarrow N_2 + O(+M) \tag{2.26}$$
$$N_2O + O \longleftrightarrow NO + NO \tag{2.27}$$
$$N_2O + H \longleftrightarrow N_2 + OH \tag{2.28}$$
$$N_2O + O \longleftrightarrow N_2 + O_2 \tag{2.29}$$

where M is simply described as a third body molecule which affects the reactions, and its concentration is found from concentrations of other species as follows:

$$[M] = 1.7[N_2] + 1.4[O_2] + 3.0[CO_2] + 12.0[H_2O] + [fuel] + [CO] + [H2] \tag{2.30}$$

The proposed reaction rate constants and the equation used to calculate the N_2O concentration can be found in the work of Kilpinen [92].

An example of the influence of adding the N_2O intermediate mechanism can be seen Fig. 2.2 where an increase of 3-5% NOx can be observed; however, it is not always given that the N_2O mechanism leads to higher emissions. Rao et al. [98] found lower predicted NOx emissions, and better predictions, when using the N_2O mechanism together with the Zeldovich mechanism.

According to Haglind [51], a number of authors points to the importance of including the N_2O mechanism in the case of low-speed diesel engines; however, it is worth noting that while the results of the work of Goldsworthy [96] shows excellent agreement with measured data, the applied reaction schemes are, as mentioned, erroneous. This example illustrates the issues associated with NOx modelling in diesel engines and how calibration can provide the desired results even though the model is not entirely consistent.

Moreover, it is noteworthy in relation to the present work that Seykens [99] states that the N_2O (intermediate) mechanism is of high importance when modelling the combustion and NOx under high EGR rates, because of the lower combustion temperatures.

In can thus be concluded that calibration is required in order to be able predict absolute NOx emissions correctly. To calibrate the model, the rate coefficients can be used, as done by Kilpinen [92], or the local AFR ratio, as done by Goldsworthy [96], Egnell [88] and also in the present model. Wilhelmsson et al. [89] points out that it is important that the model has as few parameters used for calibration as possible, because this benefits the validity of the model. Egnell [88] shows how it is possible to correlate the local AFR in a zero-dimensional model with experimental measurements. He conclude that the local AFR for the NOx model remains constant for a given injection system, even when varying the injection parameters. In case this conclusion can be generalised, it supports the validity of the predicted NOx emissions of the present model, across injection parameter variations and confirms the usefulness of the local AFR as a calibration parameter.

Exhaust gas recirculation

The exhaust gas recirculation technique is modelled simply by letting the engine inlet gas composition and temperature correspond to mixing a specified amount of exhaust gas into the fresh inlet air. The recirculated exhaust gas composition changes due to the changed

inlet gas composition from the first engine revolution to the next, iteration is therefore required until the composition of the exhaust gas or the NOx emissions converge.

2.2.8 Friction

Engine friction is an area under constant study because the amendment of friction losses holds significant potential for improvements that lead directly to increased efficiency and reduced wear. The mechanical loss in engines is estimated to be 4-15% [100]; however, it is still a challenge to set up experiments for exact determination because the losses are distributed throughout the engine.

Friction models with different levels of complexity are implemented in engine models in the literature [101]; the simplest model is to use a constant value for the friction loss as suggested by MAN B&W in an instruction book [102]. It is here stated that the friction mean effective pressure (FMEP) is practically independent of the engine load and is by experience approximately 1 bar.

An example of a study proposing a model with a very detailed accounting of the loss contributions is Livanos et al. [103]. It is given that the increase in complexity of the friction model may lead to higher accuracy, but the downside is that detailed knowledge about the engine to be modelled must first be acquired.

For the present task, two models were evaluated: a model by Chen and Flynn and a model by Winterbone. Both are simple and rely only on the engine (piston or rotational) speed and the maximum pressure (P_m). Few studies, using marine low-speed engine models, consider friction modelling; an exception is the work of Grimmelius et al. [104] in which the friction model by Chen and Flynn [70] is applied:

$$FMEP = 0.137 + \frac{P_m}{200} + 0.162\overline{v} \tag{2.31}$$

where $\overline{v}$ is the mean piston speed (m/s).

A recent example of the use of the Winterbone model is Yun et al. [105] who present a model tool for combined heat and power production, using an internal combustion engine; the engine model performance results show very good agreement with experimental data. The friction mean effective pressure is as according to the Winterbone correlation:

$$FMEP = 0.061 + 1.167P_m + 4.9 \cdot 10^{-6} f/60 \tag{2.32}$$

where f is the engine speed in revolutions per minute.

The evaluation of these two models suggests that the Winterbone model results in friction losses of about 5-10% of the engine indicative power, for one engine model (of a 12K98ME engine, see Sec. 2.3.3). For the engine parameters to make sense compared to the model output, this loss is excessive and renders the model unable to match the measured data. The Chen model results in friction losses in the order of 5% of the brake power, or about 1 bar FMEP. For another engine model (7L70MC, see Sec. 2.3.2), the Winterbone model results in the best results and the Chen model seems to under-estimate the friction. Therefore, the two models use different friction models.

Livanos et al. [103] present a detailed study of the friction losses in a four-stroke marine engine and conclude that the FMEP is not constant across loads, with an increasing trend as the load increases. This finding is in accordance with the results from using other friction models. Livanos et al. [103] state that the FMEP is 0.4-1.4 bar at loads from 26-86%, corresponding to about 5.8-13.6% of the engine brake power.

The significance of the deviation in results from different friction models is debatable. Friction is not always considered in engine models; a recent example of a presentation of a zero-dimensional model (entitled a complete model) by Payri et al. [106], lacks any such consideration. Adjustments of the parameters of the engine model can compensate for the omission of a friction model as the results of the validation of the 4T50ME-x model presented later in the present work shows (see Sec. 2.3.1). The modelled SFOC and NOx emissions show agreement within a 5% tolerance, which is the stated tolerance for the measurements. This is achieved with no friction model at all.

Though such results can be achieved by fitting the model, it is an unnecessary simplification not considering friction, because the implementation is simple and friction losses do affect the brake power output of a real engine. For the two other validation cases presented later (see Secs. 2.3.2 and 2.3.3), the friction model turned out to be the missing piece for the calibration and validation of the models. Due to the more detailed input information, the lack of a friction model made it impossible to calibrate the models to the measured values.

2.2.9 Scavenging

A scavenging model was before the start of the present project implemented in the model by Sigurdur Stefansson. The model provides better estimation of the temperature of the cylinder gasses at the start of the compression because residual gasses are considered with this addition. Moreover, the scavenging model improves the estimate of the composition of the gasses which is important when modelling the effects of the use of EGR.

The model simply estimates the scavenging efficiency (η_{scav}) using a numerical fit obtained

from experimental data; it uses the scavenging ratio (r_{scav}) defined as the ratio between the charge air volume and the cylinder volume [6]:

$$\eta_{scav} = 1 - exp(c_0 + c_1 r_{scav} + c_2 r_{scav}^2) \tag{2.33}$$

Typically between two and four revolutions of the engine cycle is needed for the estimated gas composition and temperatures to converge.

2.2.10 Modelling the turbocharger

The procedure used in the present study to estimate the T/C and bypass flows is summarised in the following. As this procedure is developed for fast estimation in system optimisation, the procedure is designed to avoid iteration of the engine model.

1. Given the scavenge air volume flow rate and compressor inlet and outlet pressures, the power required by the compressor is estimated using the isentropic efficiency found using a compressor map provided by ABB. Since ABB asked for it to be confidential the map is not provided here. The map was entered into the mathematical model as a scatter plot and efficiencies were found using linear three-dimensional interpolation (using the Matlab *scatteredInterpolant* function).

2. The inlet pressure of the turbine, mass flow rate and power output was found using an iterative procedure ($fsolve$), involving the Stodola turbine constant (see Sec. 4.2.2) and the isentropic efficiency from a turbine map. The map was provided by ABB and is also kept confidential. At any load, a part of the exhaust gas mass flow is bypassed the turbine and throttled to the turbine exhaust pressure before being mixed with the turbine exhaust stream.

At 25% load the T/C is assumed not to contribute to the scavenge air flow and pressure, and the auxiliary blower power consumption is calculated using the inlet and outlet pressures and the volumetric flow.

Two methods for the estimation of the thermodynamic properties of the air and exhaust gas in the T/C calculations were investigated: an ideal gas calculation methodology presented by Sorenson [95] and a method using the NIST Refprop software [107]. The Refprop method uses the calculated exhaust gas composition as opposed to the ideal gas equations which uses an average heat capacity of the exhaust gas. Data from a case for the 12K98ME

engine running at 100% maximum continuous rating (MCR) with a turbine inlet temperature of 409°C and a compressor inlet temperature of 25°C was used for comparison. The data was found in the MDT CEAS software available online [108].

Results suggest that the ideal gas equations and Refprop results in very similar figures for the turbine, and these figures are also close to the reference data. The compressor outlet temperature is over-estimated by about 7% with the ideal gas equations and predicted 0.5% too low with Refprop. More importantly, the two models deviates by about 5% with regards to the T/C power estimation. Results of an investigation of the T/C power using calibration data for an engine (7L70MC), suggest that the Refprop method is the more accurate and this method is therefore used in the present work. It is noted that no validation of turbochargers are made.

2.2.11 Calibration

Calibration and validation of the engine model is done using three engine types and corresponding sets of data:

1. A 4T50ME-x electronically controlled engine which is located in Copenhagen, Denmark, and is used for research by MAN Diesel & Turbo. Through direct collaboration with MDT important data was obtained, which showed information about the engine response on NOx and SFOC, caused by changes in key tuning parameters, i.e., injection and valve timing and scavenge air pressure.

2. A 7L70MC mechanically controlled engine for which detailed information regarding performance data and engine parameters is available in the work of Goldsworthy [72]. This engine is one of the most commonly used engine type in the current container ship fleet of the world.

3. A 12K98ME electronically controlled engine for which information about heat release and pressure curves at loads 25-100% were available. This engine type is so large that complex WHR systems are feasible.

4T50ME-x

The calibration methodology used on the model of this engine is not described in detail here as no details are documented by Sigurdur H. Stefansson, who did the calibration. The efforts resulted in the publication of a scientific article, which provides additional details [6]. Regarding the validation results as shown in the section 2.3.1, the present author

was not able replicate them. Sigurdur explained that specific engine operating conditions were used to calibrate the model, but information about these conditions could not be recovered. The reason for including the validation figures for this engine model in the present thesis, is that they document how well the engine model predicts the mentioned important experimental results.

7L70MC

The genetic algorithm was used to calibrate this model as a number of parameters thus can be adjusted simultaneously to produce results best matching with experimental data. For this, the root-mean-square deviation (RMSD) was used to calibrate the exhaust valve opening time (EVO), the end of injection time (EOI) and α constant of the Woschni heat transfer correlation (Eq. 2.6), at the four loads (subscript l) 25 to 100% as follows:

$$RMSD_l = \sqrt{\frac{\sum_{i=1}^{n} \left(\frac{\hat{y}_i - y_i}{y_i}\right)^2}{n}} \tag{2.34}$$

Here y_i is the i'th experimentally obtained output parameter value, for example the engine brake power, and $\hat{y}_i$ is the predicted value. n is the number of parameters. The deviation of each of the parameter was converted to the relative value in percent, in order to assign equal weight to each parameter. The sum of the RMSD of the four loads was used as the objective value in the genetic algorithm optimisation/calibration.

Since this engine controls the exhaust valve timing using a camshaft, the EVO time is the same value at any load. The remaining input data for the model was found either in the article by Goldsworthy [72] or through the online engine room tool CEAS by MDT [108].

12K98ME

For this engine model, experimentally obtained heat release and pressure curves for four loads were available as provided by the manufacturer, see Figs. 2.8 and 2.9. The heat release of the model was thus adjusted to match the measured data using Q_p, M_p, $\Delta\theta_p$ and M_d in the Wiebe heat release equation (Eq. 2.11) and the SOI and EOI. The EVO was adjusted to match the power outputs and since this engine is electronically controlled, the EVO can be adjusted to different values for each load.

The remaining input data for the model was found in documents provided by MDT, which are also kept confidential, or through the online engine room tool CEAS by MDT [108].

2.3 Results

In this section the validation results for the three mentioned engine models are presented. For each of the three models the available input and output parameters are of different character. The three model validations complement each other in showing how the model predicts the low-speed two-stroke engine behaviour as well as can reasonably be expected:

1. The 4T50ME-x model: Validation shows that the effects on NOx and SFOC from variations in the main engine tuning parameters, injection timing, valve timing and scavenge pressure, are within the tolerance of 5% given for the available measurements for the same engine. Data is provided for a single load point only. Further detail is provided in Scappin et al. [6].

2. The 7L70MC model: In this case only few parameters are available for calibration because the set of input parameters is nearly complete. At the same time the set of output parameters is also nearly complete and the model is therefore constrained to a high degree. Data is available for four load points.

3. The 12K98ME model: The most valuable input to an engine model may well be the measured heat release, since the combustion event is so decisive for the engine performance. In this case both the heat release and the resulting pressure trace curves are available by courtesy of MAN Diesel & Turbo. Because the model responds so well to the input information, only few parameters are adjusted to match the available output parameters. Data is available for four load points.

It is noted that the same measurements are used both to calibrate and to validate the engine models and that this an issue and a weakness in the validation. Considerable efforts were made to obtain more information because with more available information, some input/output data sets could be used for calibration and others for validation. This lack of information is not uncommonly seen in the literature, for example in the work of Dimopoulus et al [32].

2.3.1 Validation using the 4T50ME-x engine

Table 2.2 lists the engine specifications and model input parameters. The reference point injection timing and combustion shape parameters are calibrated using heat release data obtained from then engine manufacturer. It is concluded that the deviation between the modelled and the experimental heat release is acceptable and the modelled cumulative heat release is in good agreement with the experimental data [6].

Table 2.2: 4T50ME-x Main engine data

Cylinders (-)	5
Load (%MCR)	75
Speed (rpm)	111.8
Bore x stroke (mm)	500 x 2200
Compression volume (m^3)	0.0252
Compression ratio (-)	18.14
Fuel LHV (kJ/kg)	42700
Specific humidity of the charge air (ISO)	0.0107
Maximum pressure (MPa)	16
Compression pressure (MPa)	14.1
Scavenge pressure (MPa)	0.29
Fuel per cylinder (kg/s)	0.06199
Air per cylinder (kg/s)	3.26
Scavenge temperature (°C)	30.6

The effect on SFOC due to changes in the maximum pressure is shown in Fig. 2.3 in the left figure. The variation of P_m is made by varying the injection timing. The model results are within the measurements uncertainties, and they are also within a 95% confidence interval of the measurements. The validation of the modelled effect on NOx due to variations in P_m is seen in the right figure. As with SFOC, the model response is within the uncertainty margins of the experiments.

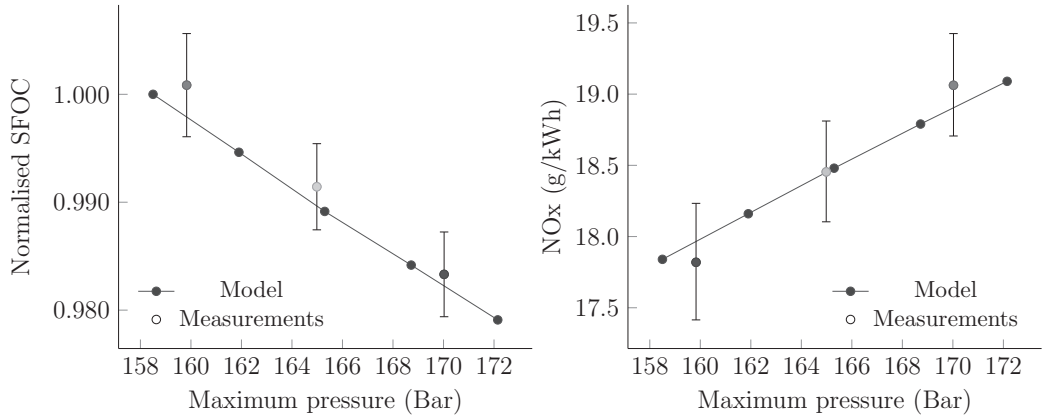

Figure 2.3: Effect of maximum pressure

The slope of the SFOC response is very similar for the model and measurements (left), while the slope of the NOx response (right) is steeper for the experimental data compared to the modelled results. Therefore it should be expected that the NOx results of engine tuning optimisation efforts show a too modest response.

Figure 2.4 depicts the model and experimental SFOC and NOx responses arriving from variations in the compression pressure (P_{comp}). P_m is kept constant while P_{comp} is varied using the EVC timing.

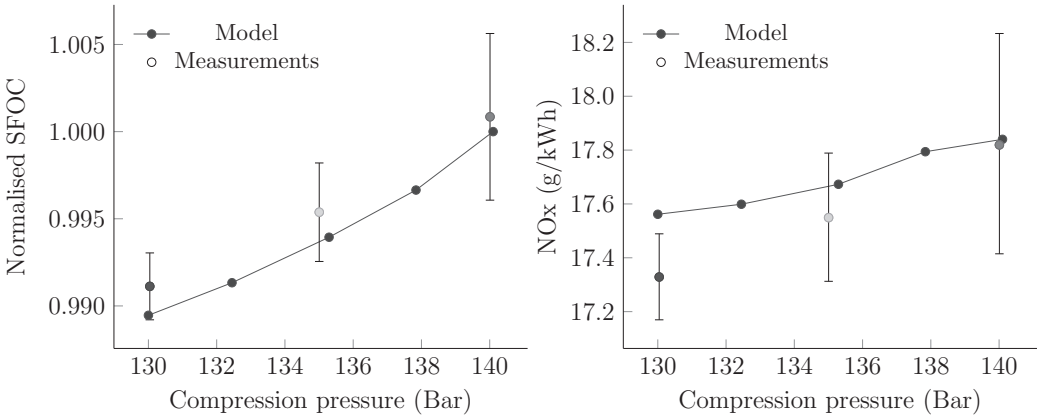

Figure 2.4: Effect of compression pressure

The left figure suggests that the model predicts the SFOC response well. The slope is very similar and the absolute values are within the uncertainty margins of the experiments. From Fig. 2.4 to the right it is evident that the model predicts the absolute values quite well; however, the slope is again steeper for the experimental results.

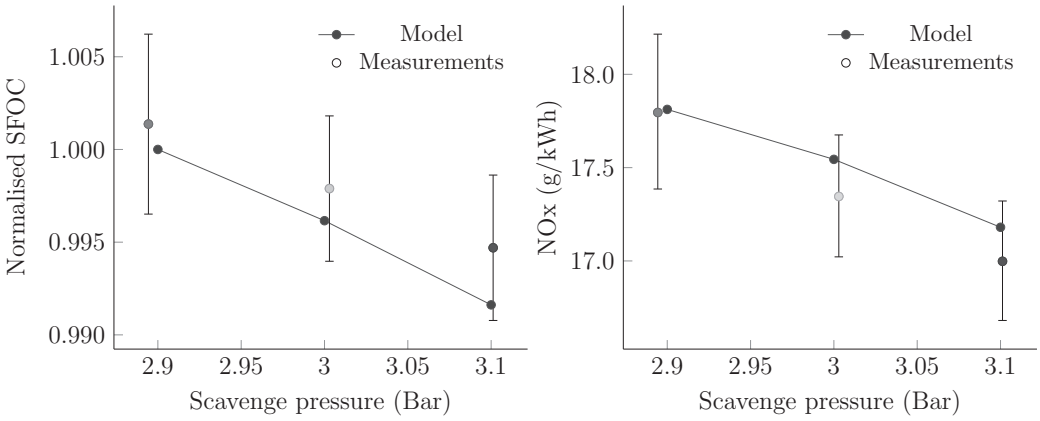

Figure 2.5: Effect of scavenge pressure

Figure 2.5 shows how the model predicts the effects on SFOC (left) and NOx (right) due to variations in the scavenge pressure. The same trends as in the previous figures (2.3 and 2.4) are present. The effects are predicted within the margins of error and the slope of the NOx is steeper for the experimental data compared to the model results.

As mentioned, a reproduction of the data in Figs. 2.3-2.5 could not be made by the present author due to missing information; particularly the NOx response due to variations of the maximum pressure. Many combinations of input parameters were investigated, except the manipulation of the heat release curve parameters. Such manipulation can in reality

provide almost any desired results and the simulation thus risks being speculative; hence the lacking information may well be information regarding the heat release.

2.3.2 Validation using the 7L70MC engine

Also presented in the work of Scappin et al. [6] is a validation of the camshaft engine model 7L70MC; however, the model is validated at one load point (75% MCR) only. In the following, validation of the four load points 25, 50 75 and 100% is presented. The data from Goldsworthy et al. [72] provides an extensive data set which in the following is referred to as experimental data, although the data was not obtained experimentally by Goldsworthy directly, but in stead collected and derived in different ways.

The data presented by Goldsworthy et al. [72] is the most detailed data found available during the project period, and it includes all the essential performance parameters along with a range of model input parameters. By having such an almost complete set of input and output parameters, there are not many parameters left to calibrate the model. Therefore this set of parameters play a key role in the validation of the engine model.

The fuel used is a test bed fuel with a LHV of 42,700 kJ/kg and a carbon-to-hydrogen ratio of 7. The engine has direct injection and variable injection timing. The provided main engine characteristics are shown in Table 2.3 and indicative data, supplied by MAN B&W for the Goldsworthy study, are shown in Table 2.4.

Table 2.3: 7L70MC mk6 Main engine characteristics

Cylinders (-)	7
Bore x stroke (m)	0.70 x 2.268
Effective compression ratio (-)	12.6
Connecting rod length / stroke ratio (-)	1.2037

The start of injection time, i.e., the injection angle with the unit °CAD after bottom dead centre (ABDC), is inferred by Goldsworthy using the model, design data and shop trial data of the same engine, while assuming a fixed ignition delay of 2.3 ms or 1.5 CAD. The Goldsworthy model results are shown to be very similar to the data shown in Table 2.4 and additional model outputs are seen in Table 2.5.

Figure 2.6 presents the Goldsworthy data and the (presently) modelled results. The fully drawn lines show the outputs resulting from the given inputs parameters. The dotted lines show the results when the fuel flow rate is allowed to be up to 5% higher than specified; in this case 4.32% more fuel is added. This amount corresponds to the tolerance normally specified by the manufacturer. The tolerances for the fuel flow rate and the exhaust gas temperature are shown also. The reason for showing this information is that

Table 2.4: 7L70MC mk6 Main engine performance data

Load (%)	100	75	50	25
Speed (rpm)	108.0	98.1	85.7	68.0
Scavenge pressure (bar)	3.60	2.80	2.00	1.38
Exhaust pressure (bar)	3.27	2.53	1.81	1.25
Fuel flow/cylinder (kg/s)	0.13678	0.10088	0.06839	0.0360
Air flow/cylinder (kg/s)	7.3095	5.885	4.190	2.164
Scavenge temperature, (°C)	41	34	29	34
Power (MW)	19.810	14.858	9.905	4.953
Compression pressure (bar)	131	101	75	51
Maximum pressure (bar)	141	126	99	70
Cylinder cooling load (kW)	3,000	2,400	1,890	1,335
Injection angle (°CAD ABDC)	179.0	178.5	179.5	179.5
Specific fuel oil consumption (g/kWh)	174.0	171.1	174.0	183.2
Measured NOx (g/kWh)	13.6	17.6	19.1	16.5

Table 2.5: Goldsworthy model output data

Load (%)	100	75	50	25
Air temperature at injection (°C)	559	544	535	545
Maximum pressure rise (bar/CAD)	3.1	4.9	5.2	3.8
Exhaust temperature before turbine (°C)	333	284	257	259
Time of peak pressure (°CAD ABDC)	188.8	189.9	190.9	189.9

an investigation of the conditions for the T/C proved that possibly unrealistically high T/C efficiencies are required to match this set of input/output data.

Figure 2.6 suggests that there is good agreement between the present engine model and the Goldsworthy data on all the important performance parameters. The cylinder cooling is under-estimated and the NOx emissions does not show the same trend across load variations, but they are within the same range as the experimental values. It is noted that the local AFR has the same value at all loads, in accordance with the findings of Egnell [88], a that value corresponds to an air-fuel equivalence ratio (λ) of 1.10. Fitting of the local AFR for each individual load allows the trend to be replicated much better; however, justification for doing was not found in the literature (See also Sec. 2.2.7).

When calculating the T/C efficiency by the definition provided by MAN Diesel & Turbo [109], the resulting efficiency is excessively high, i.e., about 77.5-79%. This indicates that the performance data from Goldsworthy are not entirely accurate, although the model results presented by Goldsworthy are in good accordance with the experimental results. There is no mention of the T/C in the article by Goldsworthy [72].

To obtain more reasonable T/C efficiencies, i.e., within 70-75% (as shown in a turbocharger guide [109]), the model is calibrated while allowing the fuel and exhaust to vary with the mentioned tolerances; i.e., ± 15% for the exhaust gas temperature and ± 5% for the SFOC; this case is designated *Model**. Figure 2.7 shows how the T/C efficiency is affected by the

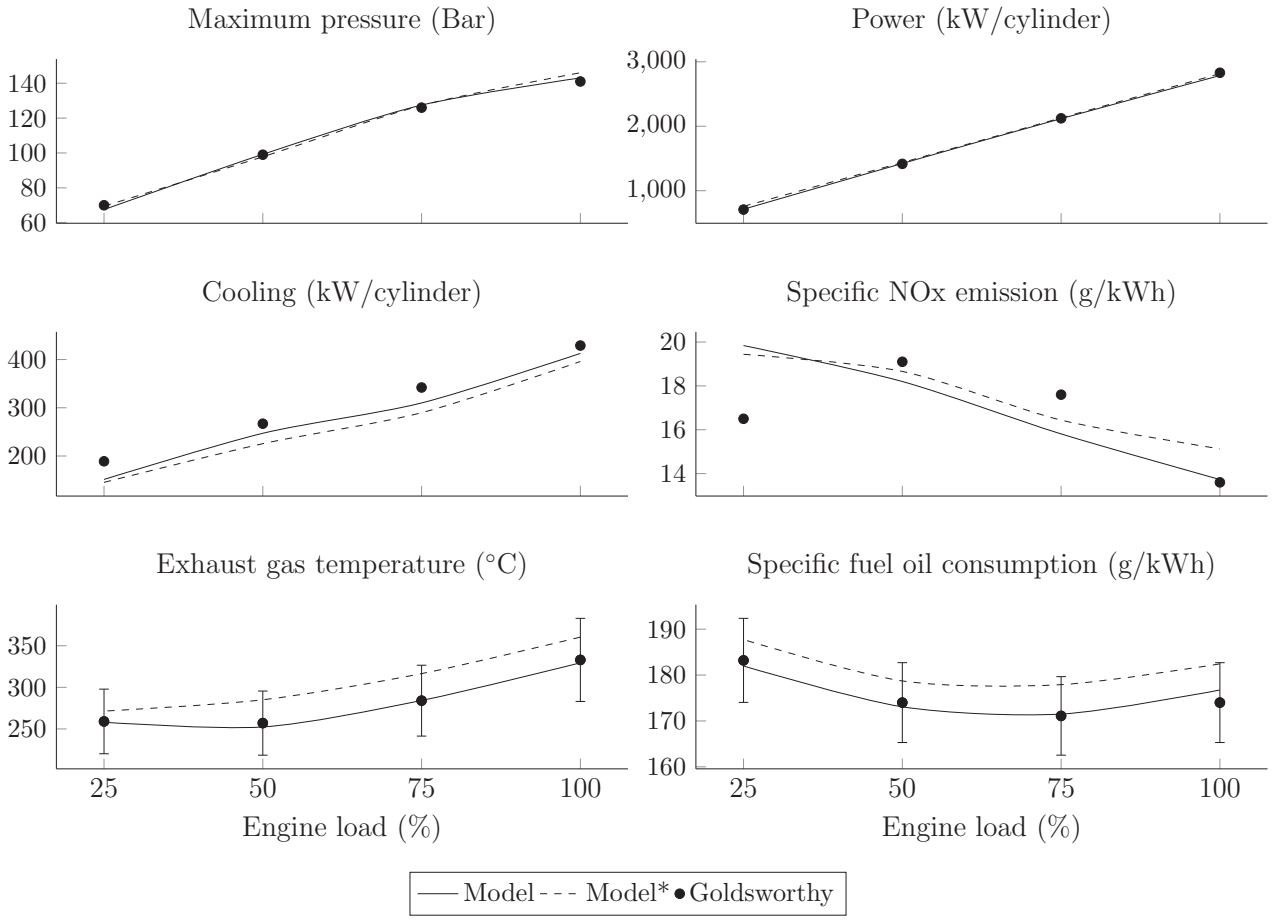

Figure 2.6: Model and experimental values for main performance parameters

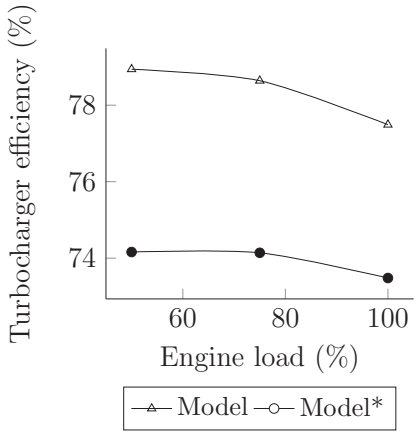

Figure 2.7: Required turbocharger efficiencies

additional fuel input and how the efficiency is more reasonable although still quite high. (To obtain a T/C efficiency of 75% the compressor and turbine efficiencies must both be around 85%).

2.3.3 Validation using the 12K98ME engine

Measured heat release curves at loads 25, 50, 75 and 100% MCR are used as inputs to the model. The heat release in percent (of the total heat release) per CAD for the four loads is shown in Fig. 2.8. The resulting predicted pressure development for the four load points can be seen in Fig. 2.9, along with the measured pressure development for validation.

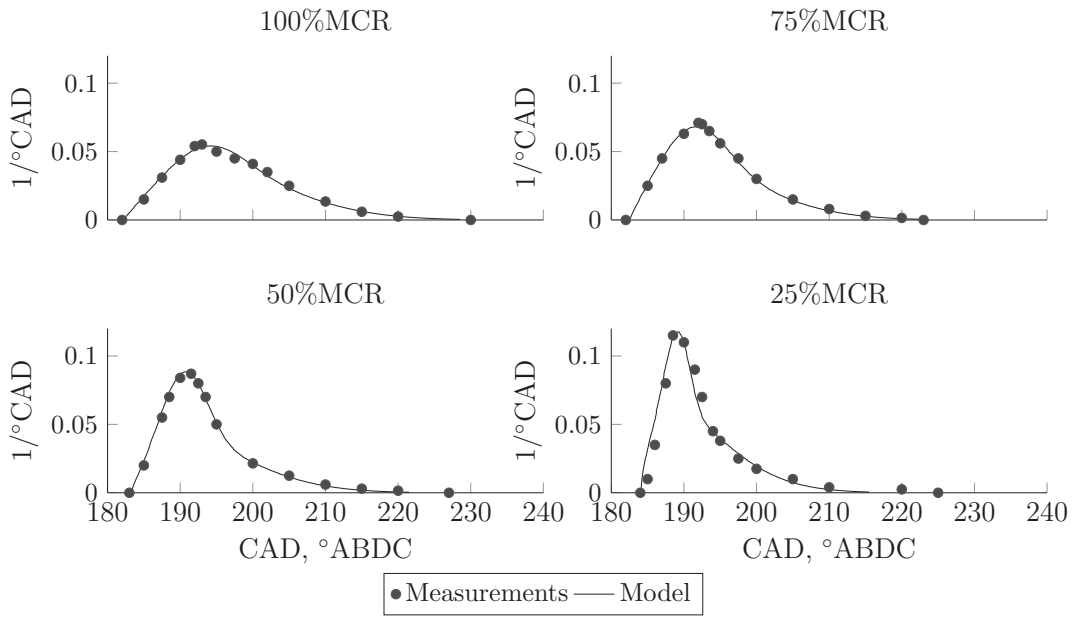

Figure 2.8: Model and experimental values for relative heat release per CAD

Figure 2.10 presents the results for the main performance parameters. There is good agreement with regards to power, maximum pressure, exhaust temperature and SFOC, while the cooling load is greatly under-estimated. Apparently the Woschni heat loss model is a part of the explanation for this under-estimation.

The figure shows how the SFOC is approaching the tolerance of 5% given by the manufacturer. The model can be tuned to better match the cooling load by adjusting the α parameter in the Woschni heat transfer correlation; however, the result is that the exhaust gas approaches the lower tolerance limit. In that case the required T/C efficiency will be higher than the currently available, according to calculations.

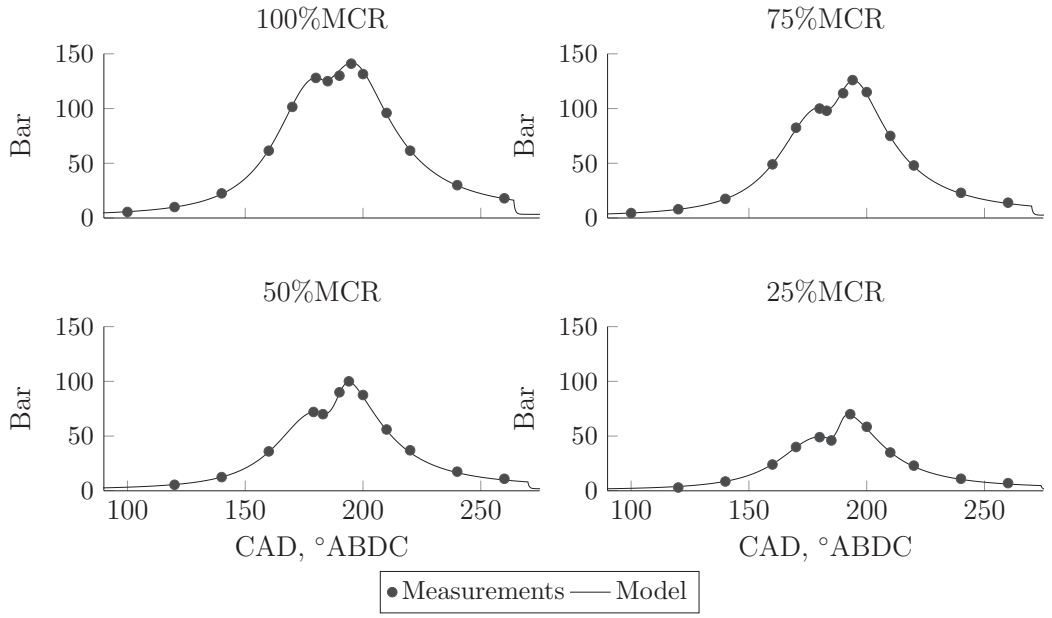

Figure 2.9: Model and experimental values for cylinder pressures

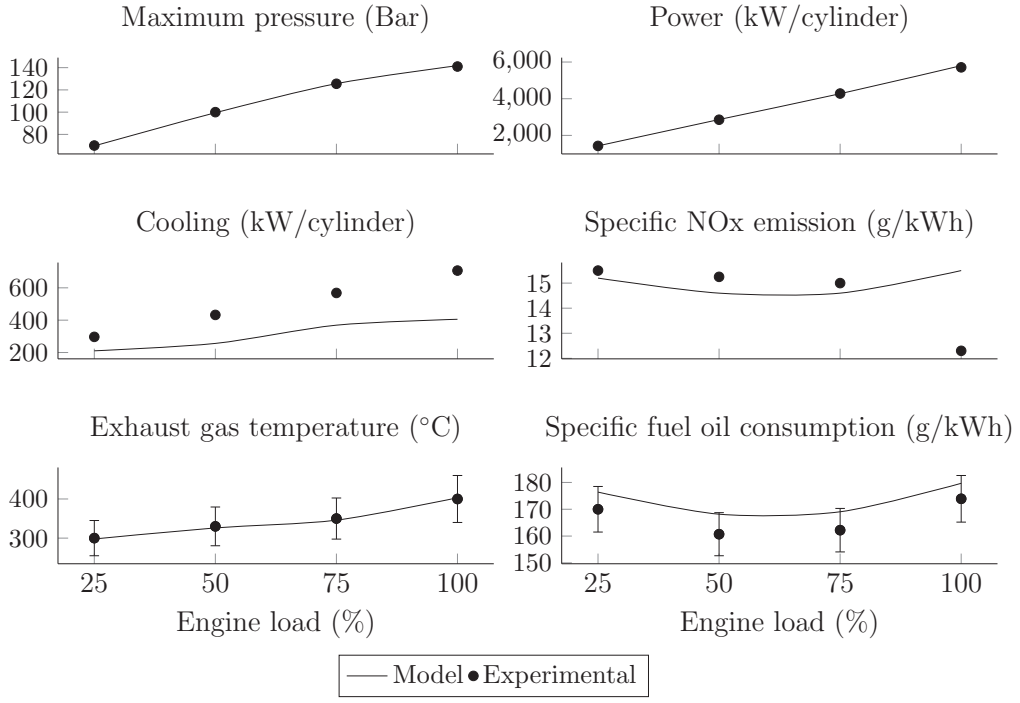

Figure 2.10: Model and experimental values for main performance parameters

No measured NOx values is found in the literature or elsewhere for the 12K98ME engine; however, the engine is stated to be certified for IMO Tier I NOx compliance so the IMO weighted NOx must be below 17.0 g/kWh. The IMO weights are 20, 50, 15 and 15% for the emissions at loads 100, 75, 50 and 25 as according to ISO 8178 [110]. Kjemtrup et al. [29] presented figures for a K98MC engine (the mechanically controlled counterpart), and the emissions are near to the Tier II compliance level (14.4 g/kWh). Egeberg et al. [111] presents figures for the 12K98MC engine and these are shown in Fig. 2.10 as experimental values since they are the closest available data. There is good agreement although the trend across loads does not match. It is noted that the engine can be tuned in various ways, so it is difficult to precisely explain this deviation; it may be attributed to the fact that the engine 12K98ME engine is electronically controlled and is thus tuned differently.

The available data for the validation of the 12K98ME-C6 engine model is summarised as follows:

- Pressure curves at loads 25, 50, 75, 90 and 100%.
- Heat release curves at loads 25, 50, 75, 90 and 100% .
- Injection pressure vs. engine rotation.
- Cylinder liner temperature at 100% load.
- Scavenge and exhaust pressures at loads 25, 50, 75, 90 and 100%.
- Bore and stroke.
- Connecting rod length.
- Compression volume.
- Performance parameters for loads 25, 50, 75 and 100%, i.e., power, SFOC, compression and maximum pressures, exhaust temperatures and cooling loads.
- Exhaust valve timing at loads 25, 50, 75, 90 and 100%.

Exhaust gas recirculation

Available measurements of the effects of EGR on marine two-stroke engines are limited and more so the specific conditions of the measurements. Fig. 2.11 presents model results and measured data from initial tests of a MAN two-stroke engine fitted with EGR [58]. The model is run at 75% load, and the only parameter varied to obtain the shown results

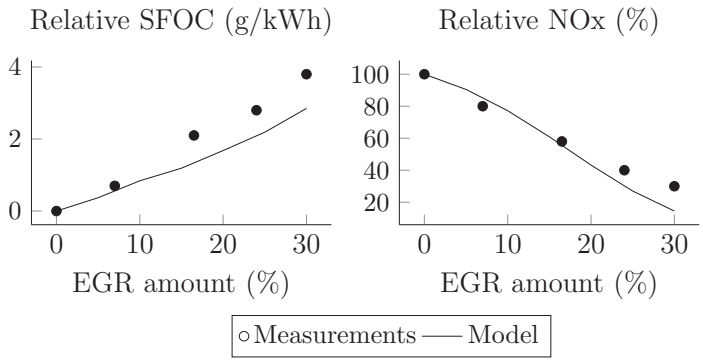

Figure 2.11: Comparison of EGR effect on SFOC and NOx

is the EGR ratio; defined as the recirculated mass flow rate divided by the total inlet mass flow rate.

While the results in figure above does not validate the model regarding the ability to predict effects of EGR, it suggests good agreement between model and measurements. The model over-estimates the NOx reduction at high EGR rates and under-estimates the SFOC increase. A similar over-estimation trend was found by Yamamoto et al. [112] and also by Kim et al. [113].

An explanation for the NOx under-estimation may be that the applied NO formation reactions (Zeldovich and N_2O schemes) are not entirely adequate when using high amounts of EGR. The simplified combustion model may also play an important role. Regarding the SFOC predictions, the experimental results in Fig. 2.11 are presented with limited specific information [58], e.g., the engine model type is not specified. A range of engine tuning parameters can influence the results; e.g., it is unknown whether or not the maximum pressure is kept constant at all EGR amounts by adjusting the operation parameters.

The applied NO formation mechanisms have proved, throughout the literature and over many years, to be useful for the prediction of effects of EGR under a large variation of circumstances. The model NO formation depends on the temperature, pressure and concentration of species at any given time. Therefore it is reasonable to assume that the ability to predict EGR effects depends on the ability to predict the conditions in the cylinder, especially during the combustion event.

The literature presents several examples of studies of EGR, mainly in road vehicle applications. Hountalas et al. [114] predicts measured NOx emissions on a heavy-duty diesel engine with relatively good accuracy using the Zeldovich mechanism. Yamamoto et al. [112] describe how the NO formation is under-estimated with the extended Zeldovich mechanism under high EGR rates, even though the heat release and pressures of the analysed engine cycle are accurately simulated. Kim et al. [113] use the extended Zeldovich

mechanism and predict NO formation well; however, for EGR rates greater than 30%, the NO emissions are under-predicted, i.e., the effect of EGR is over-estimated. This trend is general in a number of publications.

2.3.4 Prediction deviations

Table 2.6 presents the model prediction root-mean-square deviations from the experimental data (see Figs. 2.6 and 2.10). Large deviations are seen for the cooling load, particularly in the 12K98ME case. The SFOC prediction deviations for the 12K98ME engine are also significant; however, predictions are within the mentioned tolerance of 5% and the SFOC trend across loads is correctly predicted.

The NOx prediction deviations are significant for the 7L70MC engine (see Fig. 2.6); though noting that Kjemtrup et al. [29], who reviewed engine emissions modelling, conclude that exact predictions cannot be expected from the present type of model. Moreover, Kilpinin [92] conclude that the present NOx model needs further development and validation to be able to make absolute predictions, while trends can be predicted well.

The exhaust temperatures are predicted with root-mean-square deviations of about 1% which is particularly important for the present analysis of WHR systems.

Table 2.6: Prediction root-mean-square deviation

	7L70MC	12K98ME
Maximum pressure (%)	2.0	0.5
Power (%)	0.9	0.8
Cooling (%)	11.8	37.3
Exhaust temperature (%)	1.1	1.0
NOx (%)	11.6	N/A
SFOC (%)	0.9	4.0

2.4 Discussion

Kjemtrup et al. [29] conclude that engine models at the present stage rely at least partly on empirical models and that exact predictions cannot be expected. Moreover, Kjemtrup et al. [29] point out the that high accuracy cannot be achieved without the cost of computational power and that different types of models must be used for different types of tasks. Lastly, Kjemtrup et al. [29] explain how model tuning/calibration against experimental data is always required and that the expected accuracy depends on the validation.

These arguments apply also to the present engine modelling work which would undoubtedly benefit from more available experimental data (which is again expensive to obtain and hard to obtain due to confidentiality reasons). The lack of experimental data leads to the questioning about the discrepancies between model predictions and measured data, which may arise from either model errors or experimental uncertainties, or more likely from a combination of the two. The arguments of Kjemtrup et al. [29] should serve as a reminder of what can be expected, and it is the impression of the present author that the objectives of the present work, particularly concerning NOx predictions, is near to the limit of what can be expected from a model which has to be fast enough for systems analysis.

The combined validation using the three models suggest much more strongly than each individual validation, that the overall physical behaviour of the low-speed two-stroke engine is correctly predicted. In modelling it is desirable to have very detailed experimental results, and the validity of the somewhat limited validation just presented can be debated; however, engine models are generally able to produce useful predictions as shown in years of scientific publications, and the sub-models used in the present model are most of them recognised as trustworthy through the use in many studies. It is noted that the sub-models are derived for the use in models of much smaller engines.

The greatest potential for improvement of the presented model is likely the addition of a detailed fuel injection spray based combustion model and a thereby dependent NOx formation model. Several scientific articles document the effect on NOx due to varying injection spray characteristics, e.g., Mayer et al. [63]. Improvements of the combustion model might as previously discussed not add significantly to the computational cost of the model.

Moreover, the addition of a fuel injection based combustion model may help enabling the prediction other emission factors than NOx and CO_2, such as for example unburned hydrocarbons, carbon monoxide and particulate matter. The latter would make an interesting addition to the analyses made, because of the trade-off mechanism which exist between NOx and particulate emissions.

A more detailed heat loss model may also present an important opportunity for improve-

ments. The estimation of heat losses are of particular interest when modelling advanced WHR systems that utilise all the waste heat sources from the engine. A desirable improvement is a model of the oil cooling system, because the temperatures of the oil, which is cooling the piston, can reach relatively high temperatures and is thus interesting for WHR purposes.

Investigation of new concepts, such as the 'hot engine' (Hercules project [27]), require a more coherent model that can combine the convection and radiation heat losses, wall temperatures and piston cooling. Generally, the prediction of the thermal loading of the engine components could play an important role in further investigations of the potential of diesel engine-WHR systems. Interactions between the different phenomena in the engine model is not rarely overlooked in the engine modelling literature; however, an example of such effort is the study of Nanda et al. [115] who proposed an approach to correlate the thermal loading of the combustion chamber and piston as a function of the combustion air-fuel ratio.

Though it is desirable to increase the level of detail and the number of the sub-models of the engine model, and thereby take into account more of the many phenomena, it is noted that all sub-models must also be validated experimentally. More calibration is then needed and each sub-model brings some degree of uncertainty in the prediction. Besides the additional computational cost, which may or may not be insignificant, validation, calibration and knowledge about uncertainty require detailed knowledge which may be specific only to a certain engine type and geometry. Hence, deciding on the level of detail suitable for the task is not straightforward.

2.4.1 Model development

As mentioned, updates to the engine model are made after the initial validation of the model NOx and SFOC responses to variations in compression, maximum and scavenge pressures. Consequently, the effects of the updates are investigated for verification. The parameters are varied as described in Scappin et al. [6], i.e., the compression pressure is varied 10 bar while keeping the maximum pressure constant, the maximum pressure is varied 10 bar while keeping the compression pressure constant and the scavenge pressure is varied from 2.9 to 3.1 bar while keeping the compression and maximum pressures constant. The variations are made using the EVC, SOI and EOI [6].

The main results of the investigation are shown in Table 2.7. The largest deviation is about 0.34% for the NOx emissions when assuming ideal gas conditions. A similar deviation of about 0.3% is found for the SFOC when assuming that no friction exists.

The results of the investigation suggests that the new sub-models lead to insignificant

Table 2.7: Maximum deviations in response trends

	Varied P_{comp} (%)		Varied P_m (%)		Varied P_{scav} (%)	
	NOx	SFOC	NOx	SFOC	NOx	SFOC
Ideal gas	0.34	0.06	0.27	0.12	0.05	0.06
No friction	0.13	0.12	0.23	0.28	0.07	0.07
No N_2O mechanisms	0.20	0.06	0.02	0.02	0.01	0.04

changes in the qualitative prediction ability of the NOx and SFOC trends, while improving the quantitative predictions of the absolute NOx and SFOC; at the same time the model parameters are closer to engine operating parameter settings provided by the manufacturer.

2.4.2 Uncertainties

There are numerous sources contributing to the overall numerical uncertainty of the model. Moreover, an investigation leading to an account of each source would require information which is hardly available. Uncertainties are present both in the model inputs provided by the engine manufacturer and are also inherent in each sub-model. Payri et al. [116] present a study on the uncertainties of diesel engine models and conclude that the most important uncertainties are those related to the estimated heat losses and the consequent effects on the heat release rate.

The best measure for the uncertainties of the present model are the results of the 4T50ME-x validation case; based on those it can be concluded that the SFOC can be predicted with sufficient accuracy. The NOx predictions are quite good qualitatively, but the prediction of the absolute emissions are highly dependent on the local AFR; however, using the same local AFR for both the 7L70MC and 12K98ME cases did provide credible results. The 7L70MC case can thus be seen as a calibration case and the 12K98ME case is then a validation of the prediction ability regarding the quantitative NOx emissions. Further validation still seems needed though.

3 Waste heat recovery power cycles

Large parts of this chapter consist of reprints of three studies previously published as scientific articles [1–3]. First, these studies are briefly outlined and then the waste heat recovery system types under study are introduced. Though modelling and studies of the steam Rankine cycle and the power turbine are first described in the next chapter, they are briefly described here together with the ORC and the Kalina cycle, to give a reference and to have all the studied WHR system types described in the same chapter. Following the introduction, the methodologies are described and finally, results are presented and then discussed.

3.1 Introduction

First in this section the general contents and the aims of the three mentioned studies are described. It is noted that the studies are not based on the same conditions and can therefore not be used to directly compare the treated processes. The reason is that the studies are made in different research teams and contexts; however, the direct comparison of a steam cycle, an ORC and a Kalina cycle is presented in the next chapter, and a general discussion of the findings is provided in Ch. 5.

Design and optimisation of organic Rankine cycles for waste heat recovery in marine applications using the principles of natural selection is a study which proposes a generally applicable methodology for the simultaneous optimisation of process layout, choice of working fluid and operation parameters for organic Rankine cycles. Noting that the ORC is a Rankine cycle, usually with a simple process layout, that uses an organic fluid as working fluid in stead of water/steam, the selection of the working fluids is of key importance for the performance and therefore also in the design and optimisation process. The aim of the study is to identify suitable process layouts and working fluids for ORCs in marine applications. The study also presents the application of the methodology in a case study using exhaust properties from the 12K98ME engine. The general results led to the interesting finding that the maximum obtainable thermal efficiency of any (simple) ORC can be predicted using a simple regression model. This finding motivated the second study presented in this chapter.

Multiple regression models for the prediction of the maximum obtainable thermal efficiency of organic Rankine cycles is a statistically based study of how well regression models can provide said predictions. Hundreds of random cases are optimised

to provide the observations needed for statistical evaluation. Four models, covering the heat source temperature range relevant to the waste heat sources from the two-stroke diesel engines (80-360°C), are presented. Determining the optimum process, working fluid and operational parameters is a non-trivial and labour intensive task. Therefore, the aim of this study is provide models to enable the immediate and accurate estimation of the maximum obtainable thermal efficiency for the application of an ORC system. The models can be used in for example combined cycle simulations or assist decision makers with limited technical knowledge.

System analysis and optimisation of a Kalina split-cycle for waste heat recovery on large marine diesel engines is a study that introduces and analyses the Kalina Split-cycle, a cycle not previously studied in the literature. The Kalina cycle is a Rankine cycle which uses ammonia-water mixtures as working fluid and the Split-cycle is a variation which is able to achieve higher thermal efficiencies than the regular Kalina cycle. The study analyses the governing mechanisms of the process and results of an optimisation of the process used for WHR of marine diesel engines are presented. The overall aim is to determine the highest potential, in terms of thermal efficiency or net power production, of Kalina cycles, under the assumption that the increased complexity of the Split-cycle process layout results in the highest efficiency.

3.1.1 Available waste heat

Figure 3.1 illustrates temperatures and amounts of heat of the available waste heat streams of a low-speed two-stroke diesel engine; the values are frequently used as representative figures by MAN Diesel & Turbo [18]. The available heat is shown as percentage of the fuel input energy. Though the figure is representative, the numbers can vary depending on the engine type and operation parameters; e.g., the study of the Kalina cycle (Sec. 3.2.3) is based on heat from two four-stroke engines for which the exhaust temperatures are 346°C. Moreover, as will be shown in Sec. 4.3.2, the altered waste heat temperatures and amounts of energy caused by tuning of the engine, are important in relation the WHR system performance.

Four major sources are shown and the engine is in this example assumed to have an efficiency of 49.3% [18]. The figure shows the estimated temperature window for each source to be utilised. It is evident that not all of the energy is available for WHR; most importantly the exhaust gas which has a lower temperature limit of around 160°C to avoid acid condensation on heat exchanger surfaces when running on high sulphur fuels.

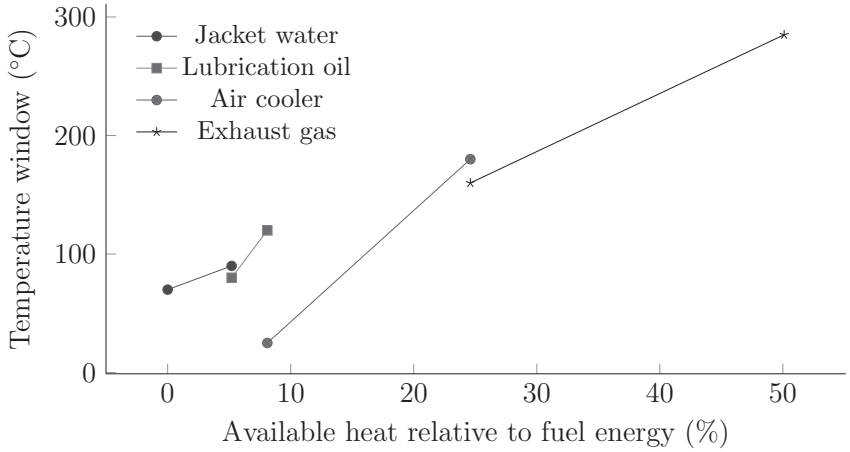

Figure 3.1: Available waste heat from the main engine (MDT 12K90ME-C9.2 [18])

3.1.2 The power gas turbine

With increasing turbocharger efficiencies, some of the exhaust gas can be bypassed the turbochargers. The great potential related to the utilisation of this surplus of exhaust gas energy was shown already in 1987 by Tsalapatis et al. [117]. The turbo compounding system consists of an additional power gas turbine (PT) driven by a flow which is typically about 10% of the total exhaust mass flow [18]. The mechanical energy created is transferred to either, a) a gearbox which transfers the energy back to the main engine; this is labelled a Power-take-in system; or b) to the electrical grid of the ship with the use of an asynchronous generator.

An alternative use of the excess exhaust energy, called the The Integrated Charge Air System, is described by Tsalapatis et al. [117]. Running at very low loads with the auxiliary engines was at the time not possible due to a too low difference between the scavenge air and exhaust gas pressures. A small part of the scavenge air from the main engine is directed to the auxiliary engines, and this enables the auxiliary engines to run with higher efficiencies at part-load conditions, and to run at loads down to less than 4% MCR, without affecting the main engine operation.

Hou et al. [118] analyse the influence of the power turbine efficiency on the potential for WHR performance. A comparison is made between the use of a regular PT and a variable geometry PT in combination with a steam Rankine cycle (SRC). The variable geometry PT is estimated to be able to produce 1-2% more power in the combined cycle. This result illustrates the very large potential for increasing the energy efficiency with a relatively simple additional system.

A study by Dimopoulus et al. [33] provides an exergy analysis of the option of utilising

the bypassed exhaust gas first in a high pressure (HP) superheater in a SRC. After the superheater the exhaust energy is further utilised in a PT and is then mixed with the T/C exhaust to be directed back to the SRC. Dimopoulus et al. [33] conclude that the overall system efficiency is very sensitive to the turbocharger performance.

Two thermodynamic alternatives

As described, the PT can be an integral part of the diesel engine and WHR system combined cycle. Because of the relatively high temperature energy available in the hot bypassed gas, it is of particular interest to utilise the energy optimally. Woodward [119] provides a thermodynamic analysis which clearly illustrates the advantage of the using a PT, and it is summarised as follows.

Figure 3.2 is a sketch of a temperature-entropy diagram of the exhaust gasses for illustration. T_e, P_e represents the pressure and temperature of the bypassed exhaust when entering the system and T_0, P_0 are the conditions of the surroundings. $Path\ a$ and b are two alternative reversible paths by which reversible work can be produced from the waste heat. Since both paths start (T_e, P_e) and end (T_0, P_0) at the same states and the processes are reversible, they provide the same reversible work from the same heat source and sink.

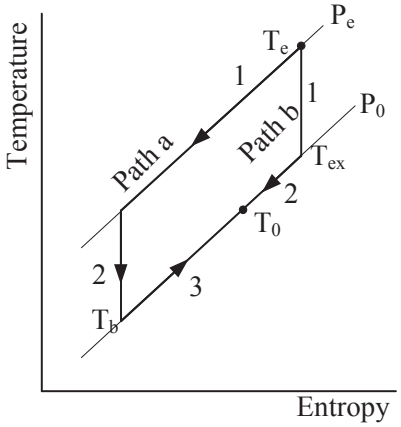

Figure 3.2: Sketch of a temperature-entropy diagram

The reversible processes of $Path\ a$ are: 1) an isobaric cooling to T_0 where work is produced using Carnot engines, 2) an adiabatic expansion to P_0 and a temperature, T_b, which is below the temperature of the surroundings, and 3) an isobaric heating to T_0 where heat is added from the surroundings to the gas, passing through Carnot engines that produce work. Process 1 is in practice a Rankine cycle with the heat source at an elevated pressure.

Process 2 is in practice a gas turbine expansion and process 3 is also a Rankine cycle in practice.

The reversible processes of *Path b* are: 1) an adiabatic expansion to P_0 and 2) an isobaric cooling to T_0. In practice, process 1 is here a gas turbine and process 2 is a Rankine cycle.

Woodward concludes that for process 3 on *Path a*, the added complexity of a Rankine cycle and the fact that the recoverable energy is relatively small, make it unlikely that this process will be feasible in practice. Moreover, for the processes of *Path b*, less heat transfer is required, thus less exergy destruction is likely to occur.

In theory, the thermodynamics do not provide a conclusive answer to which path is advantageous, but in practice Woodward provides strong arguments. When also considering the space requirement and cost [18], the PT is a good first choice for WHR and in combination with a Rankine cycle WHR system, the PT is still beneficial due to its ability to utilise the pressure component of the waste heat energy.

3.1.3 The state-of-the-art steam Rankine cycle waste heat recovery system

An advanced dual-pressure level steam Rankine cycle WHR system is proposed by MDT [18], utilising all the sources shown in Fig. 3.1, except the lubrication oil heat. This WHR system uses the jacket water and charge air cooler heat to allow the low pressure feedwater to reach its evaporation temperature or to partially evaporate the feedwater. It is claimed that the output from this WHR system increases the combined cycle efficiency by 5.5% points, compared to not having a WHR system, resulting in a thermal efficiency of 54.8%.

Figure 3.3 is a schematic representation of the process and this configuration is modelled for comparison in the next chapter (see Sec 4.1.1), though without the power turbine. A brief description of the process is hereby provided.

Starting from (1) the working fluid (water) is at a low pressure. Running through an engine jacket water cooler heat exchanger (JWC) and then a charge air cooler heat exchanger (CAC), the water is preheated to the bubble point (3). The water stream is then split into two streams that run through a low-pressure circuit (4) and a high-pressure circuit (7) in the boiler. Hot exhaust gasses from the engine are running through the boiler from point (30) to (35). The low-pressure stream is evaporated and superheated before entering the steam turbine (ST). The high-pressure stream (7) is pumped to a high pressure, preheated, evaporated and superheated before entering the turbine. After the turbine (12), the stream is condensed.

The turbocharger (TC) is coupled to the process such that the exhaust gas from the engine

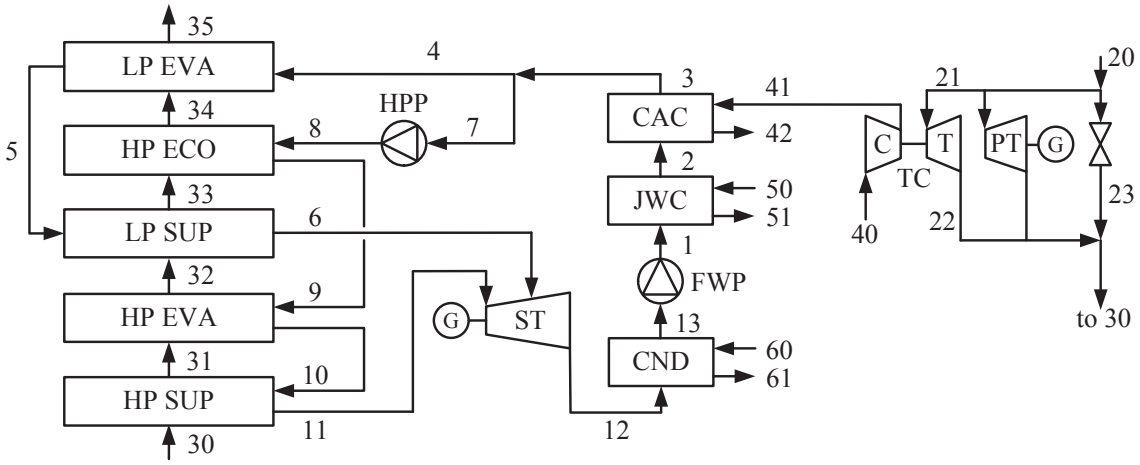

Figure 3.3: Steam Rankine process flow diagram

is entering at (20) into a splitter which allows gas to be bypassed the T/C turbine (T) and the PT. The mass flow rate needed for the turbine to drive the compressor is led through the turbine at (21). The PT mass flow is about 10 % of the total exhaust flow and the rest is bypassed and mixed with the gas exiting the turbines. Charge air for the engine is compressed in the T/C compressor (C) and then rejects heat to the WHR process via the CAC at (40) to (42).

A single-pressure level SRC is also presented by MDT [18] and the resulting gain in combined cycle efficiency is stated to be 4.9%-points (compared to not having a WHR system). The stated WHR system recovery efficiencies for four configurations are shown for reference in Table 3.1. Note that the efficiency is given as a percentage of the main engine power.

Table 3.1: Indicated performance of WHR systems [18]

System	Percent of main engine power (%)
Power turbine	3-5
Single pressure SRC	4-7
Dual pressure SRC	5-8
Dual pressure SRC with power turbine	8-11

3.1.4 Design and optimisation of organic Rankine cycles for waste heat recovery in marine applications using the principles of natural selection

It appears that already in 1826 Thomas Howard discovered that a higher efficiency could be reached when using other working fluids than water. This was long before William Rankine presented his complete theory of the steam engine in 1859 [120]. In 1886 it was reported that United States naval engineers were using methyl alcohol-water mixtures in a heat engine which proved to have a higher efficiency than when using steam, although no explanation could be provided at the time. There are several other examples dating back to that time [120]. The modern era of the ORC started in the 1960s and intensified in the 1980s with a strong contribution from Italian engineers. Hence, the ORC can be viewed as a relatively old and well studied technology, both in practice and in theory.

Among the most accomplished engineers in the field are Angelino, Gaia and Macchi. In a 1984 review [121] they list some important advantages of the ORC compared to steam cycles, which can be attributed to the fluid properties. In summary the advantages of ORCs are [122]:

- ORC fluids can be operated as super-critical cycles at low temperatures. This means, among other things, that the heat transfer can occur with a lower heat transfer entropy generation, thus enabling a higher thermodynamic performance.
- Simple cycles with a single stage expander can achieve (relatively) high efficiencies because of the thermodynamic properties of the organic fluids; fluids that are heavier than water.
- The ORC turbine can have relatively low peripheral speeds and volume flows but high expansion ratios and supersonic flows are common [120].
- Fluid condensation during expansion is easily avoidable.
- For given source and sink temperatures, the pressure levels can be chosen to suit a specific application, by choosing a suitable fluid.
- Low turbine mechanical stress.
- Simple start-up and automatic operation/ no operator needed.
- Low maintenance and long service life.

Fluid selection

There is a great number of working fluid candidates, especially when including fluid mixtures, and these are commonly categorised according to the state after expansion. Figure 3.4 illustrates the saturation curves of three different types of fluids, a wet, an isentropic and a dry fluid. It is seen that toluene, representing a dry fluid, will normally reach a state of superheated vapour after expansion. Ethanol, representing a wet fluid, may, similarly to water, easily expand to a state in the two-phase region. Acetone, representing an isentropic fluid, is seen to have an almost vertical (isentropic) vapour saturation curve slope.

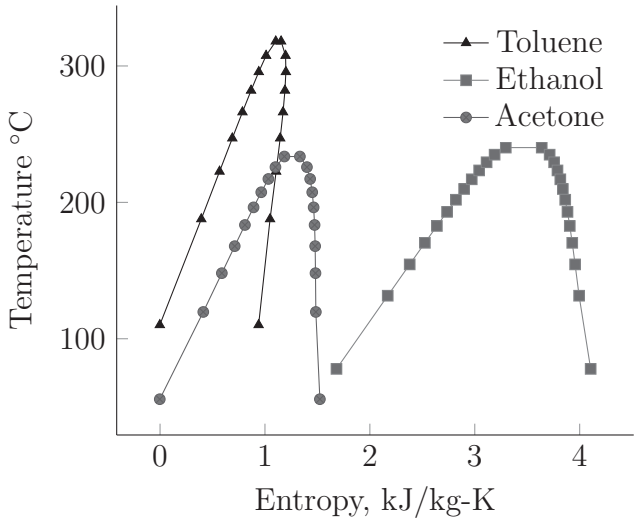

Figure 3.4: Temperature-entropy plot for the three fluid types

The most relevant fluids for the ORC are [123]: linear, branched and aromatic hydrocarbons, perflourocarbons, siloxanes (silicon oils), partially flouro-substituted straight-chained hydrocarbons, ethers (fluorinated), alcohols and inorganics. Among the most commonly investigated fluids are the refrigerants R123, R134a, R141b, R236ea and R245fa/ca, the aromatic hydrocarbons toluene and benzene, the alkanes propane, butane, pentane and hexane, the alcohols methanol and ethanol and the siloxanes MM (hexamethyldisiloxane) and MDM (octamethyltrisiloxane).

Selecting the optimum working fluid of the ORC is a laborious and non-trivial task and the topic has received significant attention in the scientific literature. Some are of the opinion that the literature on this topic is over-abundant [124]. Recent examples are, Wang et al. [125] who presen a method for selection among 13 fluids based on a multi-objective optimisation model. Wang et al. [126] present a study on fluid selection for a small scale ORC plant applied for waste heat recovery from a combustion engine. A comprehensive review made by Bao et al. 2103 [123] presents an overview of studies and which fluids the

authors conclude to be suitable.

However, seemingly no single fluid can fully meet the numerous requirements for the ideal working fluid in an ORC process [127, 128]. Naturally, the fluid should be thermodynamically suitable, such as having appropriate evaporation and condensation properties. Among non-thermodynamic concerns are environmental measures such as global warming potential (GWP) and ozone depletion potential (ODP), corrosiveness, chemical stability over the relevant temperature range, toxicity, flammability, explosiveness, general industrial acceptance, lubrication properties and cost. Furthermore, the fluid properties should be advantageous to the component design, not least importantly the expander. Therefore the fluid evaluation process is a matter of finding the candidate that best meets multiple requirements, weighted according to their (subjective) importance in the application. Ideally, the optimisation process should include the simultaneous design and optimisation of components, thermodynamic performance, cost and environmental and hazards risk assessment. An effort in this regard was made by the present author in a collaboration project [8] (see a brief description in Sec. A.3, p. 196).

Other important fluid properties for the design of the ORC plant are [129]:

- To reduce the cost and pressure drops of the heat exchangers, the vapour density should be high to yield low volume flow rates.
- The liquid and vapour phases in the cycle should preferably have a high conductivity and a low viscosity to increase the heat transfer coefficients and reduce friction losses in the heat exchangers.
- A low evaporation pressure generally reduces the cost of the components.
- A condensing pressure higher than the ambient pressure ensures that ambient air will not be entering the system.

In the literature, guidelines on fluid selection based on thermodynamic properties are proposed. A recurring focus is the slope of the saturated vapour line in a temperature-entropy fluid property plot. In order to avoid a low vapour quality in the expander, wet fluids require superheating in the process, whereas isentropic and dry fluids do not [130]. It seems to be common practice to superheat the dry fluids by two degrees (K) in saturated vapour processes in order to reduce erosion wear on the expander occurring from accidental droplets [131]. Siddiqi et al. [132] studied the use of various alkane working fluids and found that increasing the degree of superheating resulted in lower efficiencies. While no supeheating somewhat simplifies the cycle layout, the dry fluids require an internal heat exchanger (recuperator) in order to avoid wasting the energy contained in the superheated fluid at the outlet of the expander [128].

The perhaps most consistently discussed property of ORC fluids is the critical point. A general rule of thumb is that the evaporation temperature should be close to the critical temperature, which again should be close to the heat source inlet temperature [129]. A study by Vaja et al. [133] presents the trends for the thermal efficiency as a function of evaporator pressure for a simple ORC cycle. They show that the efficiency increases continually, but asymptotically, towards the critical pressure. The same trend was found by Mago et al. [134] using other working fluids.

As mentioned, operating at super-critical pressures provides the benefit that the heat uptake is non-isothermal, thus potentially raising the average temperature during heat uptake, resulting in a higher thermal efficiency [135]. The same effect can be achieved when using fluid mixtures and the advantage for the mixtures is that excessively high pressures are not required. Another potential advantage of using mixtures is the non-isothermal condensing temperatures, which the supercritical cycle does not exhibit.

With the ongoing research within formulation of equations of state and the successive development of available EOS software packages, the number of fluids accessible for theoretical calculations is increasing. A need thus arises for a systematic methodology to evaluate a large number of fluids and an even larger number of mixtures of two or more fluids systematically. Drescher et al. [136] presents a method used for a screening of about 700 fluids based on the plant thermal efficiency. The results from thermodynamic screening of 30+ fluids is presented by Saleh et al. [137] and Chen et al. [128]. Tchanche et al. [138] presents a methodology using a qualitative evaluation by awarding each candidate fluid either a plus or a minus sign to signify whether or not the fluid is favoured regarding a number of criteria: pressure levels, expander volume, thermal and second law efficiencies, irreversibilities, toxicity, flammability, ODP and GWP. Twenty fluids are evaluated in a ORC process with no superheating or recuperator. Dai et al. [139] use the genetic algorithm in a parametric study to determine the optimum fluid among ten in a sub-critical ORC process. Papadopoulos et al. [140] use an unconventional multi-objective approach which aims at designing the molecule of ORC working fluids by looking at the resulting heat exchanger area, cost, toxicity, flammability, environmental and thermodynamic performances of a sub-critical ORC process.

In contribution to the previous work in this field, Section 3.2.1 presents a generally applicable methodology for determining the optimum Rankine process layout, working fluid and process parameters, based on given boundary conditions and requirements. The methodology is also presented by the present author in a scientific article [1].

The method builds on the principles of natural selection using the genetic algorithm, and compared with previous work, this methodology is pioneering in the sense that it includes at the same time both the process layout and working fluid selection. The evaluation is based on a number of rules which penalise solutions in order to remove thermodynami-

cally inconsistent results. The method determines the optimal fluid among any number of working fluids (and also mixtures of fluids though this is not included in this work), while optimising the process layout to the thermodynamic properties of the fluid. Fluids are evaluated across a chosen pressure range including super-critical states. All possible solutions are included in the solution domain, i.e., wet, isentropic and dry fluids with the enabling of superheating and recuperation when thermodynamically feasible. Also included in the evaluation are requirements for physical, fire and health hazard levels.

Organic Rankine cycle expanders

The efficiency of the expander is naturally important for the final power output of the ORC. Small scale ORC systems usually uses piston, screw or scroll type expanders, and large scale ORCs use axial or radial turbines [129]. Quoilin et al. [129] present a figure illustrating that turbines are most relevant for WHR applications with a power output of above 100 kW. In the following, only turbine characteristics are considered as it is expected to be the best choice for marine applications, considering the scale of application.

The working fluid properties are, as mentioned, very relevant in the turbine design and therefore the efficiency which can be obtained in a cost-effective scenario. Invernizzi [120] mentions the size of the enthalpy drop across the turbine, the high molar mass and the outlet to inlet volumetric flow ratio, as important parameters leading to relatively simple turbine designs with only a single stage with low peripheral speeds and stresses. Angelino et al. [121] emphasise that for a simple turbine design, the expansion pressure ratio, the size parameter, which is a function of volume flow rate and isenthalpic drop over the turbine, and the volumetric expansion ratio are parameters to be optimised by choosing the optimum fluid. In addition, Bao et al. [123] state that since the densities of organic fluids are higher than that of water, the turbine dimensions can in general be smaller in comparison.

Quoilin et al. [129] point to the fact that organic fluids have low speeds of sound, which impacts the turbine negatively because high Mach numbers are related to higher irreversibilities and low efficiencies. Shock losses can occur if the flow is supersonic at the nozzle outlet [123].

The design of radial inflow turbines is receiving significant attention at the time of writing. Compared to axial turbines, they have more robust characteristics; i.e., high pressure ratios, higher peripheral speeds and higher enthalpy drops can be allowed, due to the design [129]. The part-load performance is better than the axial type [123, 129], the strength is higher and possibly also easier to manufacture [123].

3.1.5 Multiple regression models for the prediction of the maximum obtainable thermal efficiency of organic Rankine cycles

Correlations are proposed for the prediction of ORC process efficiencies; Liu et al. [141] propose an equation for the prediction of the thermal efficiency of an ORC plant using isentropic fluids, based on the evaporation, condensing and critical temperatures of the working fluid. The equation is shown to be in reasonable agreement with a limited number of model results. Teng et al. [142] derived a very similar relation [142]. Recently, Wang et al. [143] also describe a similar correlation. Kuo et al. [144] present a thorough study of the Jacob number which is shown to be very useful for the prediction of thermal efficiency. Additionally, a new figure of merit (FOM), based on the ratio of the sensible and latent heat, is shown to be able to extend the use of the Jacob number, to make predictions at various condensation and evaporation temperatures. Wang et al. [145] later include the Jacob number in two prediction models: one for thermal efficiency and one for exergetic efficiency.

Common for the mentioned correlations is that the prediction of the efficiency is based on fluid properties, which are specific for a given fluid candidate. While being very useful, the correlations do not provide the knowledge of what could maximally be obtained from a given heat source when using the best fluid. The Carnot efficiency can provide the idealistic maximum for a constant temperature heat source, and the Trilateral cycle efficiency equation can be used for a non-isothermal heat source [146]. The Trilateral efficiency is derived from the Carnot cycle efficiency and provides an idealistic estimate where the heat source is utilised fully; however, in many cases not all the heat available can be used. An example, relevant to the present context, is when the heat is supplied by exhaust gas where condensation of sulphuric acid in heat exchangers must be avoided; another example is when the cooler part of a heat source is needed for heating purposes.

Using the methodology introduced above and further explained in Sec. 3.2.1, it is possible to determine the maximum obtainable thermal efficiency, given the heat source and other process parameters, while considering a wide range of working fluids, pressures and process layouts. As is shown later in Fig. 3.19 (Sec. 3.3.1), the maximum thermal efficiency obtainable across the solution domain, is very strongly correlated with the heat source inlet temperature. Furthermore, it is, in the same section, concluded that the optimum working fluid depends upon the heat source inlet temperature, a finding which is confirmed by Wang et al. 2013 [145] among others.

Based on this, four correlations which can be used as models to predict with good accuracy the maximum obtainable thermal efficiency of simple and recuperated ORCs are derived. The simple ORC is hereby defined as a cycle which consists of a pump, a boiler, an expander

and a condenser. The recuperated ORC includes a heat exchanger which is used to transfer heat from the expander exhaust stream to the pump outlet stream (See Fig. 3.8, p. 85). The maximum potential performance of many waste heat recovery systems can thus be predicted using only a few key design parameters and without the need of knowledge of working fluid properties and their use in ORCs. Furthermore, the influence of each of the design parameters can be straightforward evaluated using the proposed models.

The correlations are based on multiple regression analyses of the results in a large number of optimisation cases. They cover a heat source temperature range from 80-360°C. The parameters in the models are the heat source inlet and outlet temperatures, the expander efficiency, the condensation temperature and the minimum allowed temperature difference in the boiler and recuperator.

It is the aim that the models can help increase the accessibility of the ORC technology by significantly reducing the resources needed to evaluate the potential of its implementation. As an example, the models can be used in preliminary studies of combined cycles and other integrated energy systems.

3.1.6 System analysis and optimisation of a Kalina Split-cycle for waste heat recovery on large marine diesel engines

With the growing attention towards waste heat recovery power cycles, the patented Kalina cycle is among the most studied alternatives. The cycle is named from its inventor Alexander Kalina and was first publicised in 1983 [147]. The main feature of the Kalina cycle is the working fluid which is a mixture of water and ammonia; being a mixture, the working fluid evaporates and condensates non-isothermally. Figure 3.5 is a sketch of a one of the most commonly proposed configurations of the process used for recovery of heat at temperatures from 300-500°C [148, 149].

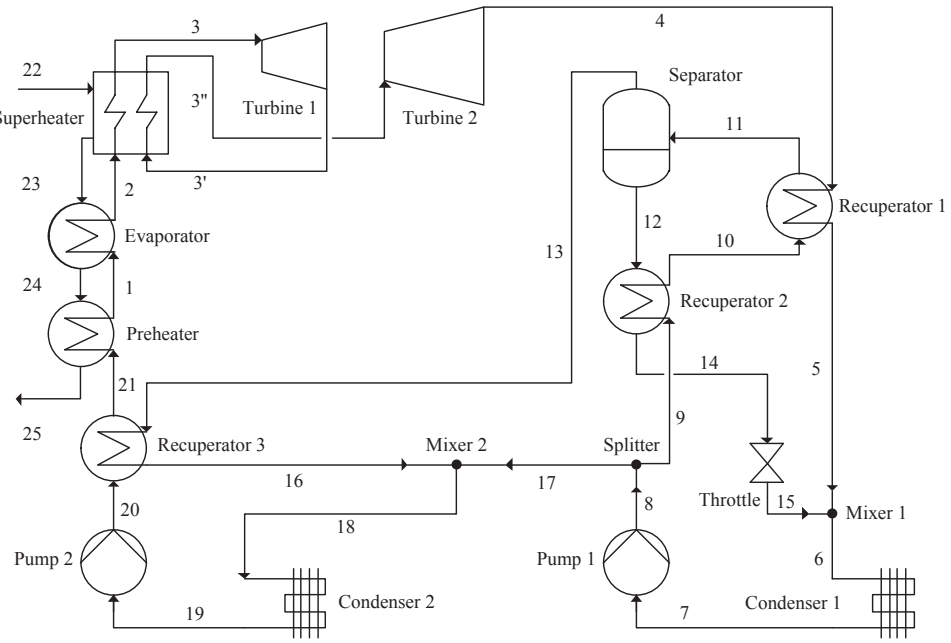

Figure 3.5: Sketch of a Kalina process with reheat

The process can be described as follows. Starting from (21) to (1), the preheated working fluid is evaporated and superheated in the boiler before it enters the turbine (3). The heat source enters in (22) and exits in (25). The outlet stream from the turbine (3') is heated in the boiler before entering (3") a second turbine. Reheat is not always included in the process and in case it is not, stream (3) runs directly from the turbine outlet (4) to Recuperator 1. From the stream (4) heat is transferred to the stream (10) in Recuperator 1. The stream (5) is then mixed with stream (15) from the separator, which is a weak ammonia solution (hereafter called lean) to form a leaner solution. This solution is condensed (7) and after being pumped to an intermediate pressure level, the stream (8) is divided into

two streams (9) and (17). The stream (9) is heated in Recuperator 2 and in Recuperator 1 to a partially evaporated state. It then enters the separator which separates the stream into a lean liquid (12) and a very strong solution of ammonia rich vapour (13). Heat from stream (13) is used to preheat stream (20) in Recuperator 3, and the stream (16) is then mixed with a leaner solution (17) to form the stream (18). This stream is finally condensed and pumped to the boiler pressure. The solution concentration of the stream which runs through the boiler (18)-(5), is called the working solution.

The Kalina cycle is intended for waste heat recovery in three main fields of application: geothermics at temperatures from 100-200°C [150–157], integrated combustion engine heat recovery, mainly at temperatures around 300°C [148, 158–161] and for gas turbines at even higher temperatures [149, 162–165]. The Canoga plant (USA) [151, 166–168] is a well-documented and tested Kalina cycle pilot plant converting heat from a gas furnace, at relatively high temperatures (450-550°C).

For the scale and heat source temperature level of application considered in the present work, both the ORC and the Kalina cycles are studied using thermodynamic models. Bombarda et al. [169] compare the two processes applied for WHR on large marine engines and conclude that both cycles, when optimised, produce equal power outputs. Jonsson et al. [170] study the Kalina cycle and two steam Rankine cycles in WHR systems for large diesel engines. They predict that the Kalina cycle can produce about 45% and 25% more power than a single- and a dual-pressure steam cycle. More recently, but utilising a heat source with a lower temperature, the economical performances of a Kalina cycle and an ORC are compared by Wang et al. [171]. The Kalina cycle is predicted to deliver power at a 15% lower cost than the ORC.

Research on the Kalina cycle is currently ongoing. A recent study by Li et al. [172] proposes to substitute the traditional throttle valve with an ejector for improved efficiency. Wang et al. [171] optimise the thermodynamic and economical performance of a Kalina cycle using a multi-objective algorithm and present a Pareto front useful for making decisions about the final process layout.

Working media

The mixture of ammonia and water is zeotropic; this means that the vapour and liquid phases at equilibrium never have both identical temperatures and compositions (see Fig. 3.6). In practice this means that it is possible at any concentration to change the liquid and vapour concentrations, unlike for example ethanol-water mixtures which are azeotrope.

During the evaporation and condensation processes, the liquid and vapour compositions of zeotropic mixtures continually change, and the saturation temperatures of these two

phases vary in consequence. This feature enables the possibility of affecting the thermophysical properties of the Kalina working fluid, either by changing the operating pressure or by varying the ammonia concentration of the mixture; hence, the Kalina cycle provides an extra degree of freedom thermodynamically compared to steam cycles and pure fluid ORCs.

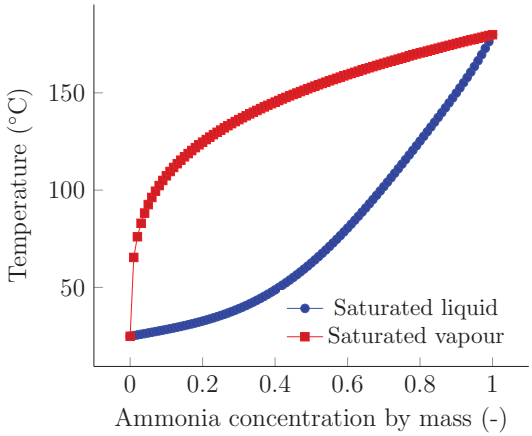

Figure 3.6: Temperature-concentration diagram for ammonia-water mixtures at 10 bar

Since ammonia is the more volatile fluid in the mixture it is the first component to evaporate. The ammonia concentration in the liquid phase progressively decreases, causing a continual rise of the boiling temperature. The Kalina cycle is designed to take advantage of this temperature glide which improves the match between the temperature profiles of the heat source and the working fluid, reducing the internal irreversibilities of the heat recovery process (see an example in Fig. 4.7 on p. 154).

Figure 3.7 shows a temperature-entropy plot of a 70% ammonia-water mixture (concentrations are all by mass in the present work). The temperature changes along the isobars in the two-phase area. Generally, the temperature glide of ammonia-water mixtures is relatively large compared to other mixtures, and this is likely one of the main reasons for choosing ammonia and water.

While the non-isothermal phase change property is an advantage during evaporation, this property can also be viewed as a disadvantage when aiming at having the lowest possible condensing pressure. In the case where the amount of cooling media can be considered practically unlimited, the cooling media temperature will change insignificantly during condensation of the working media. In this case the minimum entropy generation in the condenser occurs if the working media condensates isothermally due to the better match between the temperatures of the hot and cold sides. Conversely, if the mass flow rate of cooling media is rather limited, the condensation glide of ammonia-water results in a better temperature profile match compared to when using pure fluids (see also Fig. 4.9 on

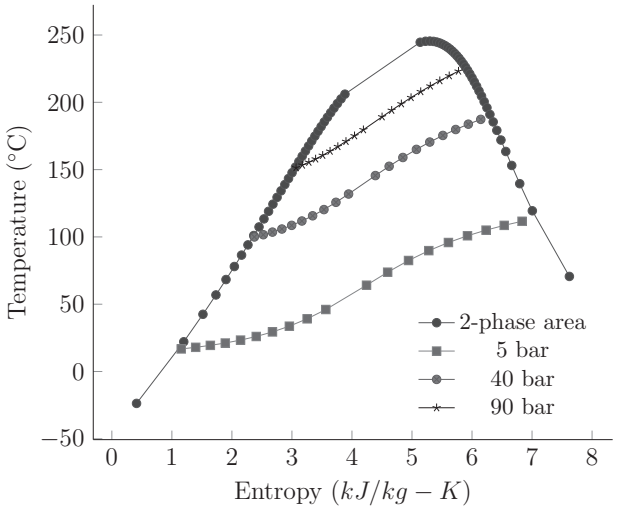

Figure 3.7: Temperature-entropy diagram for a 70% ammonia in water mixture

p. 156).

Equations of state correlations for the prediction of the properties of ammonia-water mixtures are numerous and more than 40 versions are developed. Among those are cubic functions, simple polynomials, virial EOS' and EOS' based on Helmholtz and Gibbs free energy; however most of these are developed for other purposes than for modelling the Kalina cycle, i.e., for lower pressure levels and temperatures. Moreover, there is limited experimental data available showing the properties near to and above the critical pressure [36].

Tillner-Roth and Friend (TRF) presented their model of the ammonia-water system in 1998 [173]. Their motivation was the rising interest in modelling the Kalina cycle and thus the arising need for an accurate model for this working fluid mixture over a wide range of concentrations, temperatures and pressures. At the time, there was no model covering both the liquid, two-phase and vapour domains with satisfying accuracy [173]. Based on a thorough survey [174] of the publicly available experimentally obtained properties for the system, a fundamental equation of state which is claimed to be accurate up to 40 MPa was derived.

Thorin et al. [175] compare the Tillner-Roth and Friend model with both experimental data and two other EOS' derived for the ammonia-water system (Stecco-Desideri and Ibrahim and Klein). Their analysis shows that the TRF EOS is generally more accurate than the two other EOS because of an additional correction factor. Additionally the TRF EOS is valid up to higher pressures than the two others, which are valid up to 11.5 and 20 MPa respectively. Thorin et al. [175] also compare the thermal efficiency of a Kalina cycle

using boiler pressures between 10-18 MPa and conclude that the choice of EOS influences the efficiency up to 1.5% points. This model is generally considered the most accurate available [176].

For the above mentioned reasons and since the TRF EOS can be integrated with Matlab using the Refprop [107] software, this EOS was chosen for the models. A disadvantage of using this property model is its complexity. Except when the phase is specified, the model needs first to determine if the fluid is in the liquid, vapour or two-phase domain. As experienced by the author and as also confirmed by personal communication with the main author of Refprop (Eric Lemmon), the TRF model in Refprop has occasional non-convergence issues (at certain random points in the thermodynamic domain).

When compared to the Peng-Robinson EOS, the TRF EOS may be more accurate in the prediction of the states and the performance of the Kalina cycle [177]; however, an advantage of the Peng-Robinson EOS is that it is simpler and converges easily, a benefit traded in this work in order to obtain better accuracy.

Kalina plants currently in operation

Mirolli [178] provides an overview of the current (as of 2012) Kalina cycle plants in operation; a list of only eight plants. Two are very small with an output of 0.05 MW and the six others are outputting between 0.6 MW and 4 MW. The operational experiences are generally described as positive; i.e., the plants are highly reliable and encounters only minor challenges. Corrosion and erosion issues are among the challenges and measures to counter such problems are to maintain a high purity of the working fluid and to use appropriate materials.

Recently, the Copenhagen based global engineering company FLSmidth acquired license to build Kalina cycles for WHR in cement plants and two plants are possibly built at the time of writing [179].

Nguyen et al. [180] mention that difficulties with control of the boiler evaporation ratio and with controlling the separator, mixers and splitters present an insurmountable challenge; however, no such challenge is mentioned by either Mirolli [178] or FLSmidth [179].

The Kalina Split-cycle

Among the many variations of the Kalina cycle, Kalina proposed in 1985 a unique and innovative type of cycle layout that enables the further improvement of the match between the temperatures of the heat source and the ammonia-water working fluid. The improvement is enabled using a system of mixers and splitters to form two streams of working

fluid with different mixture compositions that enter the boiler separately. With this configuration the cycle was named the Split-cycle (SC) [181], and while the conceptual idea is described in the literature [181], no thermodynamic analyses or modelling efforts are presented (before the present author and co-workers did so). The process is furthermore described in a patent petition from 1985 [182].

In the present work a system analysis is provided (See Sec. 3.3.3), with the objective of identifying the governing mechanisms of the process. Moreover, the potential of the Split-cycle process, in terms of conversion efficiency, is investigated in the context of the marine diesel engine WHR using a genetic algorithm optimisation methodology. The performance of a reference Kalina process is compared to that of the Split-cycle process, and the potential effect of implementing reheat in both cycles is studied. Furthermore, a simplified cost analysis is presented such that the cost of the additional process complexity can be evaluated against the efficiency.

3.2 Methodology

This section presents the methodologies applied in the design and optimisation of the ORCs and the Kalina cycles. The methodology used for the mentioned multiple regression analysis is also presented here. The steam Rankine cycle is treated in the next chapter where it is compared with the two alternatives described in current chapter. A simplified cost analysis methodology is outlined for the Kalina cycle and a Split-cycle.

3.2.1 Design and optimisation of organic Rankine cycles for waste heat recovery in marine applications using the principles of natural selection

The objectives, features and details of the ORC optimisation methodology are described in the following. As the aim is to find the optimum process layout and fluid under varying constraints and for as wide a solution domain as possible, the methodology includes processes featuring: a) sub- and super-critical pressures, b) any degree of superheating, c) with or without internal recuperator, and d) with and without preheater. The methodology can be divided into three parts: a flexible ORC process model, a set of weights to confine the solutions, and a genetic algorithm to find the optimum solutions.

A flexible organic Rankine cycle model

Modelling the ORC is done with Matlab R2010b, using systems of equations representing each component in the cycle, while using equations of state procedures from Refprop 9.0 [107] to obtain thermodynamic states. All fluid candidates and their full chemical names can be found in the appendix (see p. 203). A sketch of the process is shown in Fig. 3.8. As mentioned, the recuperator, preheater and superheater are optional components depending on the fluid properties.

Heat is delivered to the boiler with a heat transfer fluid called DOWthermQ, which is heated by exhaust gas from a large marine engine. This precaution is taken to avoid fire hazards in the boiler. DOWthermQ was modelled using a polynomial function which reproduces the properties of the fluid as in Ref. [183]. The working fluid is (possibly) preheated, evaporated and (possibly) superheated in the boiler at high pressure and is then injected in the expander. After the expander the hot low pressure fluid enters an internal heat exchanger (Recuperator) to heat up the cooler fluid from the pump. In the case the recuperator can heat the working fluid to reach a two-phase state, there is an elimination of the preheater heat exchanger. This is inherent in the equation systems.

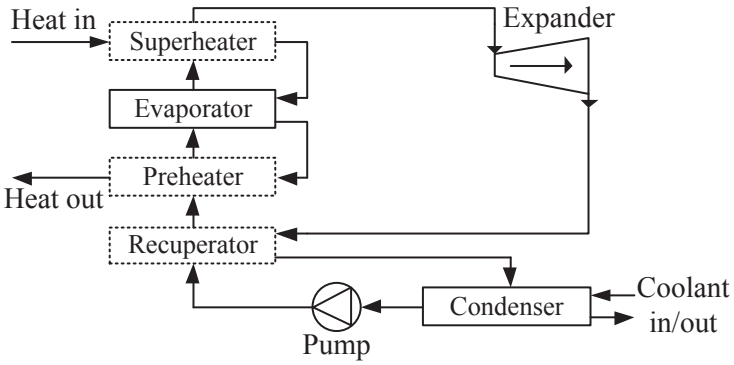

Figure 3.8: Sketch of the flexible ORC model

After the recuperator, the fluid is condensed in the condenser before entering the pump.

Table 3.2 lists the process conditions used. The heat source outlet temperature was defined to prevent condensation of sulphuric acid in the exhaust gas to heat transfer fluid heat exchanger. A temperature of 129°C of the heat transfer fluid is adequate to cool the exhaust gas down to 160°C. No liquid was allowed in the expander, to ensure long life and low service requirements of this component. It is stated by Chen et al. [128] that some liquid can be allowed in the expander hence investigations were also made where vapour qualities down to 85% were allowed. Allowing this lower limit did not however lead to higher efficiencies or other significantly changed results in general, likely because the best fluids are of the dry type.

Table 3.2: Modelling conditions

Heat source outlet temperature (°C)	129
Polytropic efficiency, expander (-)	0.80
Isentropic efficiency, pump (-)	0.80
Evaporator min. temperature difference (°C)	10
Minimum superheater approach (°C)	20
Recuperator min. temperature difference (°C)	15
Condenser outlet temperature (°C)	25
Minimum vapour quality, expander (-)	1.00

In order to optimise the process layout for the individual fluids, a degree of freedom for the superheater approach (ΔT_{sh}) is included. The ΔT_{sh} is defined as the difference between the temperature of the heat source at the inlet to the boiler and the working fluid at the outlet (before the expander). This enables the optimisation of the pinch points temperature difference (PP) in the boiler with four possible outcomes in terms of the limiting factor in the optimisation of the cycle: A) the PP is at evaporator inlet being at the minimum allowable temperature difference, B) the minimum allowable superheater approach is reached, C) the

recuperator minimum temperature difference is met, or D) none of the above in which case it is the minimum expander vapour quality which limits further optimisation.

By investigating the net power output of the process versus the pinch point temperature difference, it is concluded that the optimum power output is not synonymous with having the lowest allowable ΔT_{pp}. Thus an optimisation of the ΔT_{pp} for each individual case is justified to find the true optimum in the large solution domain.

The main equation systems applied in the methodology are described in the following for the sake of coherency. The expander is modelled using the assumed *polytropic* efficiency, expander inlet enthalpy (h_i) and pressure at inlet (P_i) and outlet (P_o).

The polytropic efficiency is generally introduced as an efficiency of a very small (imagined) stage in a turbine or a compressor. The turbine isentropic and polytropic efficiencies are related such that the isentropic efficiency converges as number of imagined turbine stages increases, and the pressure difference between inlet and outlet of each of the stages thereby decreases. Using this approach enables a search over wide range of expander pressure ratios while ensuring a comparable level of cost and technology of the expander, because polytropic efficiency is the same at all times. An adequate number of stages in the present work was found to be 500 for the convergence of the isentropic efficiency across the large range of fluids and pressures.

In order to make sure that solutions are limited to ones with acceptable vapour quality in the expander, the quality (q) is tested at all stages in the expander using EOS calls of the type $q = q(h, p)$. The pump is modelled using an assumed isentropic efficiency.

The recuperator is modelled with the mentioned flexibility as follows. In the recuperator there are two temperature differences which may limit the heat transfer from the stream entering from the expander to the cold stream entering from the pump: firstly, the internal difference (ΔT_{int}) between the entering cold stream ($T_{c,i}$) and the exiting hot stream ($T_{h,o}$), and secondly, the external difference (ΔT_{ext}) that allows the heat transfer fluid to be cooled down to a specific temperature; thereby limiting the inlet temperature of working fluid to the boiler. The inlet conditions to the recuperator are known from the pump and expander equations, and with no pressure loss applied, the recuperator is described by the following system:

$$T_{h,i} = T(P_{h,i}, h_{h,i}) \tag{3.1}$$
$$T_{c,i} = T(P_{c,i}, h_{c,i}) \tag{3.2}$$
$$T_{h,o} = T_{c,i} + \Delta T_{int} \tag{3.3}$$
$$h_{h,o} = h(P_{h,o}, T_{h,o}) \tag{3.4}$$
$$\Delta h_{max} = h_{h,i} - h_{h,o} \tag{3.5}$$
$$h_{c,o} = h_{c,i} + \Delta h_{max} \tag{3.6}$$
$$T_{c,o} = T(P_{c,o}, h_{c,o}) \tag{3.7}$$
$$\textbf{if } T_{c,o} > T_{h,i} - \Delta T_{int} \tag{3.8}$$
$$\textbf{then } T_{c,o} = T_{h,i} - \Delta T_{int} \tag{3.9}$$
$$\textbf{if } T_{c,o} > T_{h,o} - \Delta T_{ext} \tag{3.10}$$
$$\textbf{then } T_{c,o} = T_{h,o} - \Delta T_{ext} \tag{3.11}$$

Depending on the conditions, $h_{c,o}$ is updated according to the temperature $T_{c,o}$. Following this procedure, the second law of thermodynamics is not violated and the recuperator provides the maximum amount of preheating possible.

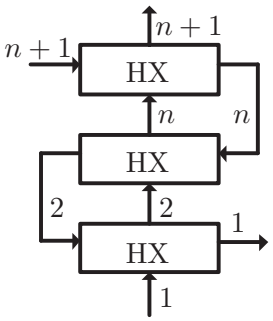

Figure 3.9: Sketch of heat exchangers with numbering

Modelling the boiler preheater, evaporator and superheater components is done as one heat exchanger divided into 30 divisions. The number of 30 is found to be a reasonable compromise between accuracy in the determination of the pinch point temperature difference and the computational time for the optimisation. Figure 3.9 is a sketch of the boiler heat exchangers with numbering. The heat source enters at the upper left and exits at the lower right, while the working fluid enters at the bottom and leaves at the top. With $j = 2, 3, ..., n + 1$:

$$h_{c,1} = h_{p,o} \tag{3.12}$$
$$T_{c,o} = T_{h,i} - \Delta T_{sh} \tag{3.13}$$
$$h_{c,n+1} = h(P_{c,i}, T_{c,o}) \tag{3.14}$$
$$h_{h,n+1} = h(P_{h,i}, T_{h,i}) \tag{3.15}$$
$$\Delta h_{step} = (h_{c,n+1} - h_{c,1})/n \tag{3.16}$$
$$h_{c,j} = h_{c,1} + (j-1)\Delta h_{step} \tag{3.17}$$
$$T_{c,j} = T(P_{c,i}, h_{c,j}) \tag{3.18}$$
$$h_{h,j} = h_{h,j+1} - (\dot{m}_c/\dot{m}_h)(h_{c,j+1} - h_{c,j}) \tag{3.19}$$
$$T_{h,j} = T(P_{h,i}, h_{h,j}) \tag{3.20}$$
$$T_{h,1} = T(P_{h,i}, h_{h,1}) \tag{3.21}$$
$$T_{c,1} = T(P_{c,i}, h_{c,1}) \tag{3.22}$$
$$\Delta T_j = T_{h,j} - T_{c,j} \tag{3.23}$$
$$\Delta T_{min} = fMin(\Delta T_j) \tag{3.24}$$
$$\dot{m}_c(h_{c,n+1} - h_{c,1}) - \dot{m}_h(h_{h,n+1} - h_{h,1}) = 0 \tag{3.25}$$

where *fMin* is a Matlab function that finds the minimum value in an array of values. Subscript c is cold stream, h is hot stream, and min means minimum. Subscript p is the stream from the pump. To find the optimum superheater approach, a Matlab $fminbnd$ optimisation algorithm is applied, using the *Golden section search* and *Parabolic interpolation* methods [184].

This approach is essential for the methodology because it accommodates all types of process scenarios. In sub-critical cases the ΔT_{pp} between the hot and cold sides will be at the start of evaporation; in super-critical cases and when using mixtures, the location of the pinch point cannot be as easily predicted (to the authors' knowledge). Additionally, the approach does not distinguish between cases with or without preheater and with or without superheater, and this provides the freedom to test processes and fluids without committing to a specific scenario (which is usually what is the case in the literature).

As the approach presented here aims at providing a generic approach not dependent on the physical design of the heat exchangers, the optimisation is simplified by assuming zero pressure losses in the cycles.

The approach potentially allows weights to be defined for the optimisation process to provide a weighted compromise solution enabling multiple objectives. Alternatively, a Pareto front may be the desired result of an optimisation using two objectives, an example of this was presented by Pierobon et al. [8]. In the present work, weights are applied simply to discard inconsistent or unwanted solutions. The following weights are implemented:

Table 3.3: Genetic algorithm parameters

Generations (-)	15
Sub-populations (-)	15
Individuals (-)	Pre-scan
Cross-over rate (-)	1
Generation gap (-)	0.8
Mutation rate (-)	0.5
Insertion rate (-)	0.9
Migration rate (-)	0.2
Generations between migration (-)	2

- The physical, health and fire hazard levels of the fluid must meet requirements of the process design.
- The expander vapour quality is checked to be above the specified minimum.
- Super-critical pressure solutions are optional and so is the internal recuperator.

The effects on thermal efficiency of imposing requirements on health, fire and physical hazards are studied by using the HMIS (Hazardous Materials Identification System) framework [185]. At hazard level four the fluid is life threatening in case of exposure(s); the fluid may ignite spontaneously when exposed to air and the fluid is able to chemically react in an explosive manner. At hazard level one the fluid may only cause irritation upon exposure; it will only burn if preheated and is chemically stable under normal conditions.

The optimisation in this study is made such that the genetic algorithm *genes* are the fluid and boiler pressure to be evaluated. The objective function is the net power output. The number of individuals is chosen as a balance between low computing time and high accuracy, and because there are 109 different possible working fluids to evaluate, a large number of individuals is required.

Table 3.3 lists the GA parameters used [42]. To reduce the number of individuals and speed up convergence, a preliminary scanning is applied to discard fluids for which the condensation pressure cannot be determined (by the EOS), as well as those fluids where the condensation pressure is higher than the maximum pressure of the cycle. Also discarded are fluid candidates which are unable to comply with the required hazard levels, as well as fluids banned or about to be banned in the near future (those are R115, R124, R141B, R142B, R11, R12, R21, R22, R113, R114 and R123 [128]).

3.2.2 Multiple regression models for the prediction of the maximum obtainable thermal efficiency of organic Rankine cycles

As mentioned in Sec. 3.1.5 the regression models are based on hundreds of cases where the methodology just described (Sec. 3.2.1) is used to optimise process, fluid and parameters to obtain the highest thermal efficiency.

In order to obtain reasonable accuracies for the models, two low-temperature models are derived covering the heat source inlet temperature range 80-180°C; one for simple (no recuperation) ORCs and one for recuperated (whenever advantageous) ORCs; and similarly, two high-temperature models covering the heat source inlet temperature range 180-360°C.

The input parameters are varied randomly within the intervals shown in Table 3.4, and for each case the maximum thermal efficiency is found. There seems to be a general consensus within the relevant literature that the varied parameters are the key process parameters, which are investigated most recently by Wang et al. [186]. η is efficiency, subscripts h, i, o, po, ex, co and pp are short for the hot (representing the heat source), inlet, outlet, polytropic, expander, condensation and pinch point, respectively. The condensing temperature and pinch point temperature difference were kept constant for the low-temperature models because the resulting equations were otherwise to inaccurate to be useful.

Table 3.4: Parameters interval limits

Model	Low	High
$T_{h,i}$ (°C)	80 to 180	180 to 360
$T_{h,o}$ (°C)	50 to 80	60 to 160
$\eta_{po,ex}$ (%)	60 to 80	60 to 80
T_{co} (°C)	25 (fixed)	15 to 50
ΔT_{pp} (°C)	5 (fixed)	5 to 20

A linear multiple regression model may be represented by the following equation:

$$y_j = \beta_0 + \beta_1 z_{j1} + \beta_2 z_{j2} + ... + \beta_r z_{jk} + e_j \tag{3.26}$$

where y_j is the jth response to be predicted using the (predictor) variables, z_{j1} to z_{jk} given as input. k is the number of predictor variables and β the regression coefficients. e_j is the jth residual or error between the predicted response and the observation. The observations are the optimised thermal efficiencies.

The least squares principle is used to determine the regression coefficients. The method determines the coefficients that produce the minimum sum of squared residual values, i.e., the best fitted regression line. Non-linear models were also investigated, but the linear model showed to provide the best fit with the observed data in all four cases.

In order to evaluate the regression models statistically, the following assumptions regarding the residuals (or standardised residuals) are verified as according to Larsen et al. [187]:

1. The mean value of residuals (e_j) is equal to zero.
2. The residuals can be plotted as a normal distribution.
3. The residuals have constant variance (homoscedasticity).
4. The residuals are independent (or random), i.e., there is no correlation with the regression coefficients or the response.

The first assumption is easily verified, while the remaining are checked using plots of the standardised residuals. If assumption (2) is correct, a normal probability plot of the standardized residuals should produce a straight line. Scatter plots showing the relationship between the standardised residuals and the predicted values can be used to evaluate assumptions (3) and (4). If the residuals are evenly and randomly distributed around zero, then the assumptions hold true. These four points are verified in Sec. 3.3.2.

3.2.3 System analysis and optimisation of a Kalina Split-cycle for waste heat recovery on large marine diesel engines

For a comparison with the Split-cycle, a reference Kalina process layout is used. To also be able to compare with an ORC studied in the work of Bombarda et al. [169], the conditions are chosen to the same as in that study. The Kalina process layout is chosen on the background of the studies by Bombarda et al. [169] and Jonsson et al. [170], who both find this particular design suitable for the marine diesel engine WHR. Both the reference cycle and the Split-cycle are evaluated with and without using reheat in the turbine, in order to determine the influence of this technique on the processes.

Process descriptions

In the following, the solution concentration running through the turbine is referred to as the *working solution*, and the terms *lean* and *rich* refer to a low and a high concentration of ammonia in the solution.

The reference Kalina cycle is described and illustrated in Fig. 3.5 in Sec. 3.1.6 (p. 78). Figure 3.10 illustrates the flow diagram of the Split-cycle process. To maintain focus on the special split stream boiler, the Split-cycle configuration modelled in this work is designed to have a minimum number of components needed for evaluating the concept. Hence, the Split-cycle presented here is based on the same principles as the reference Kalina cycle with some important differences.

In the Split-cycle, two streams of different ammonia concentration enter the boiler, a rich stream (25) and a lean stream (31) (Fig. 3.10). Before being mixed (Mixer 4), the rich stream is fully evaporated, and the lean stream is heated to the bubble point state. The aim of this arrangement is be able to modify the pinch point temperature difference in the overall process going from liquid (25,31) to vapour (2). To be able to produce these two streams with the desired concentrations and mass flow rates, an additional mixing subsystem, is needed. It consists of three splitters and two mixers, and the three splitters divide the inlet streams (11, 12 and 18) as needed. In general, a range of combinations of the splitting fractions can provide the right flow rates and concentrations of the streams, yet there are also conditions where the streams cannot be produced as desired.

The gradient of the evaporation temperature curve can to some degree be adjusted to the temperature profile of the heat source by selecting the optimal composition of each of the two streams, as illustrated in Fig. 3.11. The line from (25,31) to the point ($T_{r,b}$) represents the preheat stage. From ($T_{r,b}$) through points (1), (2) and (3), the fully drawn line represents the heat transfer when using the Split-cycle configuration. The upper dashed line represents how the heat transfer would be if the two streams were combined into a

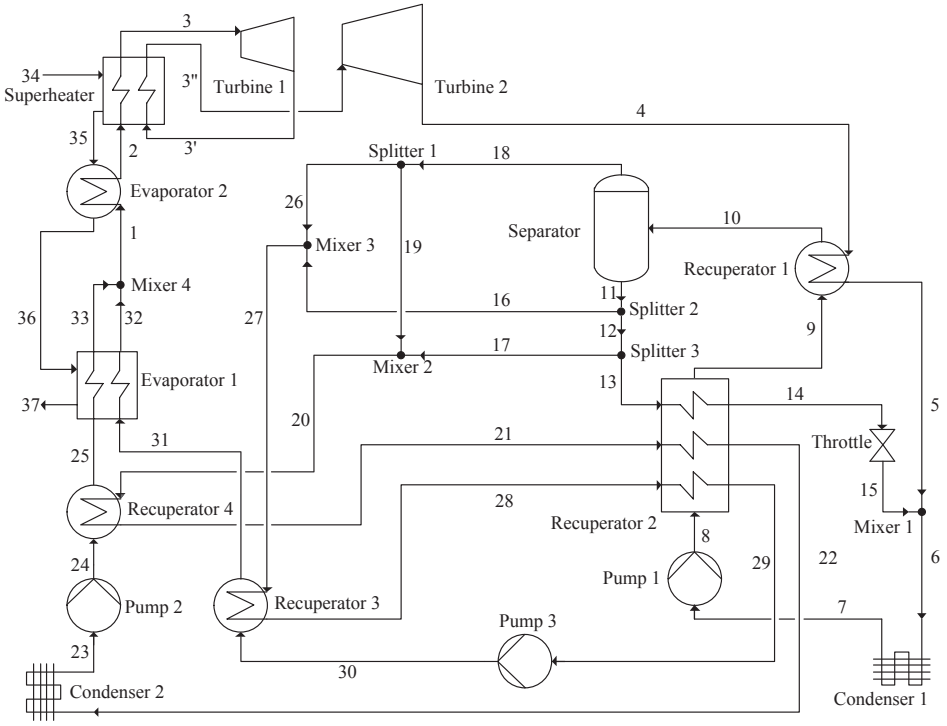

Figure 3.10: Sketch of the Kalina Split-cycle process

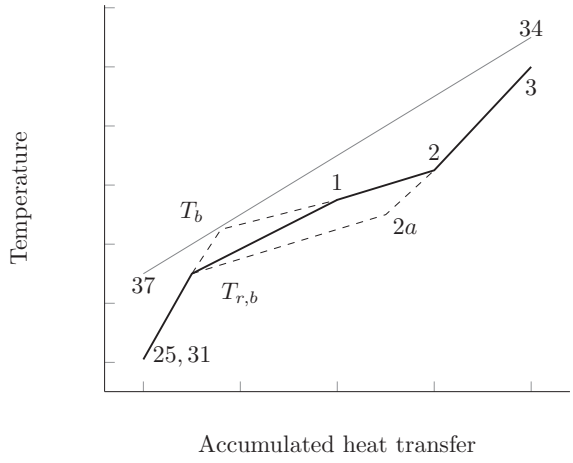

Figure 3.11: Sketch of a Split-cycle boiler heat transfer diagram

single mixed stream. The point (T_b) signifies the bubble point of the combined stream, and it is clear that the temperature difference at the pinch point is much smaller and possibly violated in this case. The lower dashed line from ($T_{r,b}$) through (2a) to (2), shows how the heat transfer would occur if only the rich stream concentration is used. Evaporation will then take place at lower temperatures possibly leading to a lower thermal efficiency of the overall process.

Kalina argued [181] that the state of the rich stream at point (33) (Fig. 3.10) should ideally be at the dew point and that the lean stream at point (32) should be at the bubble point, before the mixing of the two streams. The two streams should also have similar temperatures and pressures in order to minimise the entropy generation in this section of the boiler. These constraints are adopted without further analysis to focus on the full process analysis. By respecting these constraints the two streams are each in a state of equilibrium before they are mixed, and the resulting mixed stream is also in equilibrium; thus no exergy destruction occurs due to the mixing process. In the following, these conditions are referred to as the SC boiler constraints.

A direct consequence of the SC boiler constraints is that, once the ammonia concentration of one of the streams, (25) or (31), is chosen, the concentration of the other is fixed in order to satisfy the equilibrium conditions. Additionally, when the boiler pressure and the concentration in one stream are chosen, the temperature of the working fluid streams out of evaporator 1 is fixed. Both are illustrated in the example shown in Fig. 3.12 where it is evident that the mixing temperature decreases and the lean stream concentration increases, as the rich stream concentration increases.

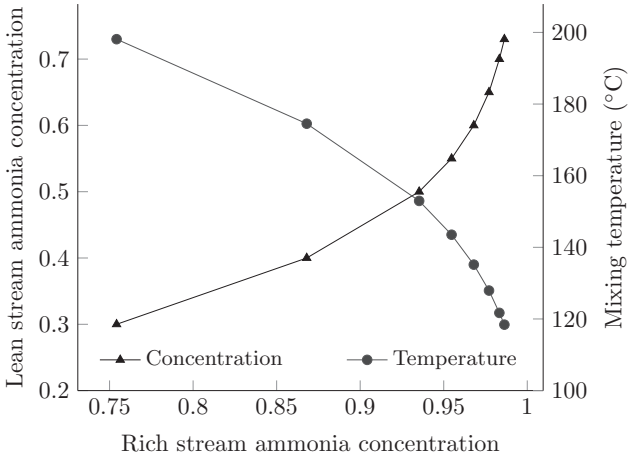

Figure 3.12: Equilibrium conditions for Evaporator 1 outlet

Modelling conditions

Table 3.5 presents the modelling conditions used for the comparison of the reference Kalina cycle with the Split-cycle. The heat source data are adopted from Bombarda et al. [169], being an exhaust gas stream from two marine diesel engines, with the molar composition 74.6% N_2, 11.7% O_2, 6.7% H_2O, 5.9% CO_2 and 1.1% Ar, and a total mass flow rate of 35 kg/s.

Pressure and heat losses are neglected in the models, to investigate the full potential of the cycles. All flows are considered homogeneous in terms of temperature, pressure and solution concentration, and the models are developed for steady-state conditions. An upper pressure limit of 130 bar is chosen for the optimisation cases to avoid near critical pressures in the simulations, because the EOS is particularly unstable in the critical region. Other studies investigate maximum pressures up to 180 bar [175], while Bombarda et al. [169] chose 100 bar. It is noted that this high boiler pressures may lead to excessive equipment costs and cause unwanted safety issues.

The risk of sulphuric acid condensation in the boiler limits the minimum exhaust gas temperature when the fuel contains sulphur. The value of 127.7°C is chosen to be able to compare results with the results of Bombarda et al. [169] directly. While providing higher thermal efficiencies, all optimisation efforts with higher exhaust temperatures resulted in lower power outputs. The discharge temperature is therefore kept fixed at 127.7°C in all cases.

Table 3.5: Process parameters and conditions

Heat source inlet temperature (°C)	346
Heat source outlet temperature (°C)	127.7
Turbine polytropic efficiency (%)	70.5
Turbine mechanical efficiency (%)	96
Pump isentropic efficiency (%)	70
Pump mechanical efficiency (%)	95
ΔT_{pp} evaporators (°C)	21.9
Superheater approach (°C)	16
ΔT_{pp} recuperators (°C)	5.0
Cooling water inlet temperature (°C)	25
ΔT_{pp} condenser (°C)	5.0

Modelling approach

Initial modelling was made using the existing software platforms DNA (Dynamic Network Analysis software [188]) and Aspen Plus [189]. Excessive convergence times of more than a minute were experienced even with relatively simple models. It became clear that attempts to optimise these models would require much faster model execution; hence, a new

modelling approach was derived.

Initial Kalina Split-cycle models were derived in Matlab [184] using Refprop to resolve thermodynamic properties and the detailed description of these efforts can be found in a scientific article by the present author [12]. A hypothesis for the study was that the cycle could be optimised by simulating parts of the system, i.e., two sub-system models: a sub-system consisting of the separator, splitters and mixers, and a subsystem consisting of the boiler and turbine components. While positive results were obtained, this approach was later proven insufficient mainly because the turbine outlet pressure cannot be optimised without modelling the rest of the process.

Since the process was already modelled in Aspen for validation purposes, attempts using this model were made to optimise the process further. The mentioned sub-system models were used to provide parameters for the (Aspen) full process model. Persistent attempts were made to optimise the process using parametric investigations; however, due to the complexity of the process, it was concluded that the genetic algorithm would be a better tool for the optimisation. Furthermore, the potential for optimising the process layout and the parameters simultaneously was also discovered, as explained next. For these reasons, a full process model was derived, building on the initial sub-system models.

Boiler and turbine sub-system model

The boiler consists of two evaporators, a mixer and a superheater (with reheater). In order to find the minimum allowed temperature difference (ΔT_{pp}) and prevent violation of the second law of thermodynamics in the boiler, each heat exchanger is discretised into 20 parts with equal temperature steps, a number found to provide sufficient accuracy while being computationally efficient. This approach is useful because the evaporation process is non-isothermal and the location of the pinch point is not easily predicted a priori when varying the parameters during the optimisation.

The heat source inlet and outlet temperatures, and pressure are kept constant throughout. The working fluid turbine inlet temperature is also kept as constant, allowing the boiler pinch point temperature difference and working fluid mass flow rate to be determined. The working fluid boiler inlet temperature and the boiler pressure are variables set by the optimisation algorithm.

The turbine is modelled using a constant polytropic efficiency in order to ensure a comparable level of technology, while investigating a wide range of boiler pressures. The polytropic efficiency is determined such to produce the same isentropic efficiency as was used in the work of Bombarda et al. [169], in order to compare the works on an even basis.

Mixing sub-system model

The mixing system consists of a separator, three splitters and two mixers. By modelling these components and using as inputs the compositions of the streams (25) and (31) found from the boiler model, the mass flow fractions of the three splitters and the separator feed mass flow rate (10) are calculated. Temperature, pressure and solution concentration of the separator feed stream as well as the working solution concentration are inputs for the mixing system model provided by the optimisation algorithm. The separator is modelled using the equation of state to find the vapour and liquid equilibrium concentrations of the two-phase mixture feed. Mass balance equations are used to determine the separator outlet mass flow rates (18) and (11) and also to determine the mass flow rate fractions of the splitters.

Full process model

The two sub-system models are used as a basis for a full process model. All recuperators are modelled using a suitable number of steps between inlet and outlet. This is required because the recuperator streams in the process are mixtures of two fluids which change phase non-isothermally; hence, the location of the pinch point is not known beforehand. The pumps are modelled using an isentropic efficiency.

The approach chosen to model and optimise the two cycles can be described as a combination of a sequential non-iterative procedure and an iterative equation system oriented approach. An algorithm by Barkley and Motta [190] is the inspiration to decompose (or tear) the cycle. The underlying idea is to solve those equations that can be solved in a straight-forward manner without iterations, and iterate as few equations as possible.

An advantage of this approach is that the solving procedure can be stopped early, if for example a thermodynamic inconsistency or an unwanted state occurs. An example is that a high liquid content is not tolerated in the turbine; because the turbine takes relatively long time to solve, the turbine states are resolved relatively early in the model solving sequence, such that the model calculation can be stopped if such conditions occur. Another example is to stop the model execution as soon as a temperature pinch point is violated. The experience is that this approach leads to significantly shortened optimisation times. When using the genetic algorithm, the optimisation requires thousands of simulation runs; hence, an approach that shortens execution time is mandatory to avoid the optimisation taking weeks or months, with the currently available computing power.

Interestingly, by using the mentioned strategy it is possible to simultaneously optimise both process parameters and process/component layout. The procedure of calculating and solving the Recuperator 2 (see Fig. 3.10) is described in the following to illustrate this.

Figure 3.13 is a sketch of how the Recuperator 2 is divided into three sections. As seen in Fig. 3.10 three hot streams enter the recuperator, (13), (21) and (28). The individual temperatures of these streams depends on the model input parameters and are thus not known in advance. In the model, the algorithm will let T_1 be the hottest of the three streams (13, 21 or 28), T_2 the next hottest and T_3 the coldest of the three. Seen from the hot side, T_1 is first cooled down to the temperature of T_2. T_1 and T_2 is then be cooled down to the temperature of T_3 in equal temperature steps; finally, the three streams are cooled, in equal temperature steps, down to the same outlet temperature T_4.

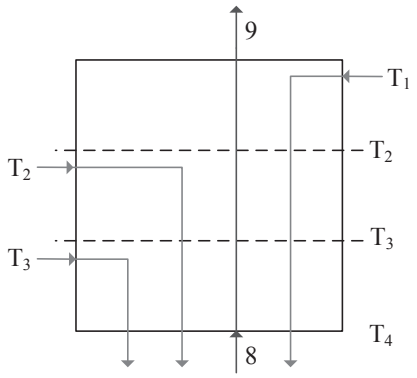

Figure 3.13: Recuperator 2 calculation sketch

Seen from the cold side, stream (8) is heated first to the boiling point in the first section ($T_4 - T_3$), because the temperature pinch point always occurs at this point. Then stream (8) is heated further in the next two sections of the heat recuperator. The terminal temperature of the hot streams (14), (22) and (29) is therefore not always the lowest possible, due to the mentioned pinch point limitation; however, following this approach, the pinch point will limit the heat transfer much less than if the three hot streams are all entering at the same point of the recuperator. In practice, the hottest stream is always stream (13); however, it can not be known a priori which is the next hottest. This approach is particularly important because having a high temperature of the separator feed is of key importance to the cycle efficiency, as will be discussed later (see Sec. 3.3.3).

The present study use the genetic algorithm parameters shown in Table 3.6 and the values are chosen based on experiences and tests with the process model and algorithm. Optimisations are done in two steps, using a first step to narrow the parameter limits for the second step.

Table 3.7 lists the optimisation parameters and the ranges allowed for the optimisation. In general the limits are chosen such that the optimisation is not limited by the parameter limits, except for the turbine inlet pressure. The boiler approach here refers to the minimum temperature difference between the hot and cold streams in the recuperator which preheats

Table 3.6: Genetic algorithm parameters

Generations (-)	30
Sub-populations (-)	4
Individuals (-)	100-200
Cross-over rate (-)	1
Generation gap (-)	0.8
Mutation rate (-)	0.5
Insertion rate (-)	0.9
Migration rate (-)	0.2
Generations between migration (-)	2

the stream(s) before entering the boiler. The working fluid boiler inlet temperature is therefore equal to the separator feed temperature minus the boiler approach.

Table 3.7: Parameter limits

Separator feed temperature (°C)	75-125
Separator feed pressure (bar)	6-14
Separator feed concentration (by mass)	0.30-0.70
Working solution concentration (by mass)	0.55-0.85
Turbine outlet pressure (bar)	2-7
Reheat pressure (bar)	20-60
Turbine inlet pressure (bar)	50-130
Boiler approach (°C)	5-50
Rich stream concentration (by mass)	0.60-0.96

Cost analysis

For the purpose of evaluating the additional cost resulting from an increased process complexity, a simplified equipment purchase cost estimation of the studied cycle configurations is made, using the methodology described by Rodriguez et al. [191]. No operational and maintenance expenses are considered in the analysis under the assumption that the purchase cost is the largest contributor to the total expenses, and that the marginal differences between the operational and maintenance costs in each of the cases are negligible. The heat transfer areas are estimated using the following correlation:

$$A = \frac{\dot{Q}}{\overline{U} \cdot \Delta T_{lm}} \tag{3.27}$$

where $\overline{U}$ is the heat exchanger overall heat transfer coefficient, $\dot{Q}$ is the heat transfer rate, A is the heat transfer area and ΔT_{lm} is the logarithmic mean temperature difference:

$$\Delta T_{lm} = \frac{T_{h,i} - T_{c,o} - (T_{h,o} - T_{c,i})}{ln((T_{h,i} - T_{c,o})/(T_{h,o} - T_{c,i}))} \tag{3.28}$$

Since the above equation assumes a linear heat transfer-temperature profile, it is, for zeotropic mixture fluids, necessary to discretise the heat exchangers into a number of steps. Here is used 20 as a good compromise between execution speed and accuracy.

The assumed overall heat transfer coefficients are shown in Table 3.16 (Sec. 3.3.3, p. 122). For the condensers, the $\overline{U}$ values are adopted from Rodriguez et al. [191], who provide an analysis of a low temperature Kalina cycle; however, since the heat source is hot water in the case studied by Rodriguez et al., the $\overline{U}$ values for the boiler components are derived by combining the information in two studies by Thorin et al. [175, 192], who analyse the heat transfer areas of a similar Kalina cycle driven by exhaust gas. The values found using Thorin et al. are in good agreement with what can be found elsewhere in the literature e.g., in Roetzel et al. [193].

The $\overline{U}$ values for each of the recuperators are unique because the phases on each side of the heat exchanger are different in each recuperator. In the present cycles all combinations occur: liquid/liquid, two-phase/liquid, two-phase/gas, two-phase/two-phase and gas/liquid; however, to simplify the analysis, an average value based on the values derived from Thorin et al. [175, 192], is used. All the heat exchangers are assumed to be of the shell and tube type.

The overall heat transfer coefficients are in practice highly dependent on heat exchanger geometries and materials, and the fluid flow conditions. It is a comprehensive task to predict these values accurately and furthermore, the currently available transport property models and heat exchanger coefficient models for ammonia-water mixtures may not be very accurate [192]. Therefore, the results can only be used as a first approximation of the heat transfer areas.

The base cost (C_0) for the components, also adopted from Rodriguez et al. [194], are 4,405 United States Dollars (USD) per kW for the turbines, 1,120 USD/kW for the pumps and 588 USD/m^2 for the heat exchangers. The cost (C) of the turbines (ex), pumps (p) and heat exchangers (hx) are found using:

$$C_{ex} = C_0 \cdot Power^{0.7} \tag{3.29}$$

$$C_p = C_0 \cdot Power^{0.8} \tag{3.30}$$

$$C_{hx} = C_0 \cdot A^{0.8} \tag{3.31}$$

In order to calculate a simplified payback period (as described in an example by MAN Diesel and Turbo [195]), it is assumed that the average number of days in operation per year is 280, the main engine fuel consumption is 180 g/kWh [196], the power is 2 times 8900 kW [169] and the fuel price is 438 USD/metric ton [197]. The fuel price is a July 2010 Rotterdam average high-sulphur heavy fuel (380) price. It is furthermore assumed that all electricity produced by the WHR system can be utilised on board the ship, where it is assumed to be installed.

3.2.4 Validation

The Kalina cycle models are validated using experimental data from the Canoga Park Kalina cycle plant [166] and also using the model results presented by Bombarda et al. [177]. The model of the Canoga park produce practically identical results, with deviations of less than one percent; however, the model results versus the results of the Bombarda study show deviations of up to a few percent on the state function values and about the same for the work output. The reason is that Bombarda use a Peng-Robinson EOS to model the ammonia-water working fluid.

The ORC model results were compared with the results in several (model) studies with practically no deviation (i.e., less than one percent). Moreover, model results are compared with results from using the commercial software Aspen Plus also with deviations of less than one percent.

All components models were validated against the mentioned software DNA and Aspen, with no deviations to report.

The results of the simulations depend on the fluid property models. Different methodologies are used for the different types of fluids in the Refprop software, and the prediction accuracies depend on the temperature and pressure (or density etc.). It therefore requires a lengthy description to account for the deviations; in summary the average deviation is below 1% according to the documentation of the individual Refprop fluids (which comes with the software package).

3.3 Results and analyses

The results from investigations using the previously described methodologies are presented in this section. First, the results from applying the flexible design and optimisation algorithm for ORCs are presented. Then follow the results from the multiple regression analyses presenting four correlations, which can be used to predict the maximum obtainable thermal efficiency of ORCs. Finally, is presented the results of an analysis of the thermodynamics and the cost of a Kalina Split-cycle compared to a reference cycle.

3.3.1 Design and optimisation of organic Rankine cycles for waste heat recovery in marine applications using the principles of natural selection

General influence of the heat source inlet temperature

Results from optimisation of the ORC process, fluid and pressure are presented here. A temperature range relevant to the heat recovery of large marine diesel engines in general, is investigated. Figure 3.14 presents the three fluid candidates which result in the highest cycle efficiency, at their respective optimum processes and pressures versus the heat source inlet temperature. The boiler pressure is the optimum in the range of 5-120 bar, an upper limit which is adequate to not limit the optimisation results, and which can be considered the maximum feasible for this type of application.

It is clear that the optimum pressures do not approach the upper limit of 120 bar in any of the cases. All the fluids in Fig. 3.14 are fluids of the dry organic type, i.e., hydrocarbons with five to seven carbon atoms and a molecular weight of 70-100 g/mol; except for R365mfc which contains fluor and weighs 148 g/mol.

An investigation is made of the effects on process, fluid type and pressure, and resulting efficiency caused by simplifying the cycle by removing the recuperator. In Fig. 3.15 results show that the maximum efficiency is about 6% lower at 180°C and ranging up to 12% lower at 360°C, in comparison with the recuperated cycles. Regarding the second and third best options, the decrease is larger. With the simple process layout the best fluids are not of the dry type exclusively, but instead wet (ethanol) and isentropic (acetone) while c2-butene is vaguely dry. This indicates that dry fluids are dependent on a recuperator to achieve superior efficiency; however, the difference in efficiency between the best fluid and the two other (dry) alternatives is relatively small (3-5%).

Several sources mention the importance of having a reduced boiler pressure. Drescher et

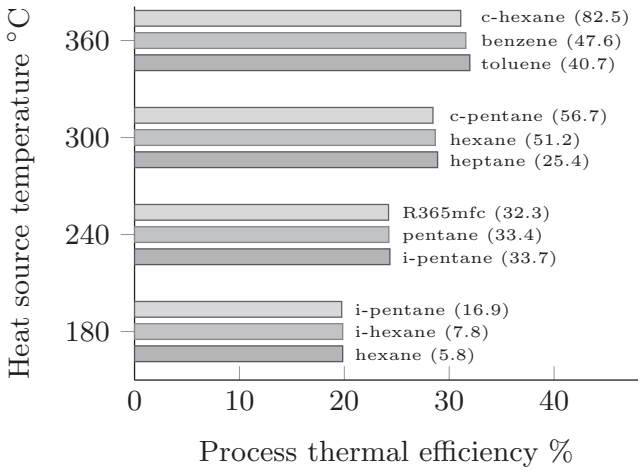

Figure 3.14: Optimum fluid and pressure (bar) at temperatures from 180-360°C with no constraints.

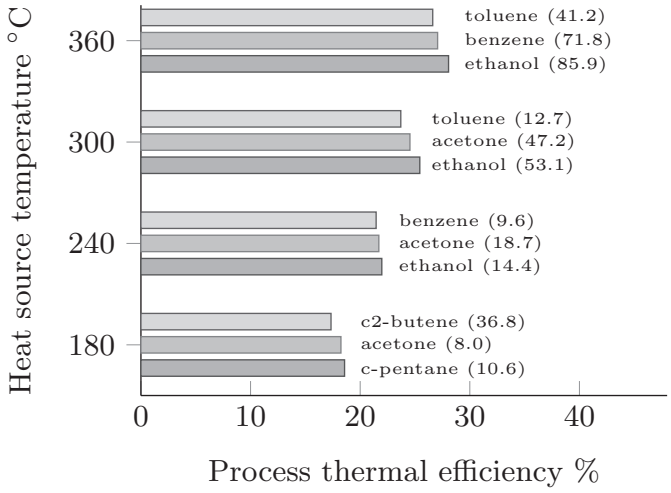

Figure 3.15: Optimum fluid and pressure (bar) at temperatures from 180-360°C with no recuperator.

al. [136] mention 20 bar due to safety and cost concerns. Lai et al. [198] mention that the 20 bar limit has come from legal prescriptions in certain countries. Kuo et al. [144] argue for a limit of 25 bar in order to keep material costs down (for small scale systems). The consequences of a 20 bar limit on the cycle are up to 2.5% lower efficiency for the best fluids and up to 6% for the third best fluids compared to when the limit is 120 bar; see Fig. 3.16. The largest decreases are seen at higher source temperatures. All the optimum fluids

for this low-pressure scenario are of the dry type, and pressures are below their respective critical pressures.

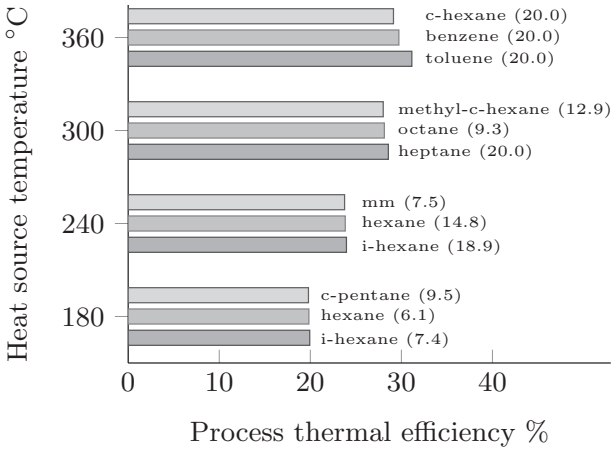

Figure 3.16: Optimum fluid and pressure (bar) at temperatures from 180-360°C with a limit of 20 bar on high pressure.

Engine design point

An optimisation of the process at the expected design point conditions for a low-speed two-stroke diesel engine is presented in the following case. The heat source is 284°C hot exhaust gas which leaves the system at 160°C to prevent excessive corrosion in heat exchangers. As mentioned an intermediate heat transfer fluid is utilised and the resulting heat transfer fluid temperatures are 255°C at the inlet and 129°C at the outlet of the boiler. The engine data shown in Table 3.8 are acquired from the MAN engine room dimensioning software [108] and the corresponding engine project guide [199]. The exhaust gas composition is found using the presented engine model (see Ch. 2).

Next, fluid candidates are discarded from the solution domain if either one of the hazard types is at a higher level than a specified maximum. Figure 3.17 shows the optimum cycle thermal efficiency for each of the hazard levels under the following constraints: NO) a high pressure limit of 120 bar with recuperator, LP) a high pressure limit of 20 bar with recuperator, SI) a simple plant layout without recuperator and a pressure limit of 120 bar, and LP+SI) the simple plant is limited to 20 bar.

As shown in the figure, the thermal efficiencies, across constraints, are generally decreasing as the allowed maximum hazard level (of any of the hazard categories) is decreasing. In general, no significant decreases are observed when moving from hazard level 4 to 3. At

Table 3.8: Engine parameters

Engine type (-)	12K98ME-C7
Engine tuning method (-)	Part load
Load (-)	(%MCR) 100
Cylinders (-)	12
Bore (m)	0.98
Stroke (m)	2.40
Turbocharger type (-)	High efficiency
Mean effective pressure (bar)	19.2
Nominal engine speed (rpm)	104
Maximum continuous rating (kW)	72,240
Maximum pressure (bar)	151
Mean effective pressure (bar)	19.2
Fuel lower heating value (kJ/kg)	42,700
Air flow rate (kg/s)	169.6
Scavenge air pressure (bar)	4.10
Scavenge air temperature (°C)	37.0
Exhaust flow rate (kg/s)	173.1
Fuel flow rate (kg/s)	3.5
Exhaust temperature after turbocharger (°C)	284
Cylinder cooling load (kW)	8,570

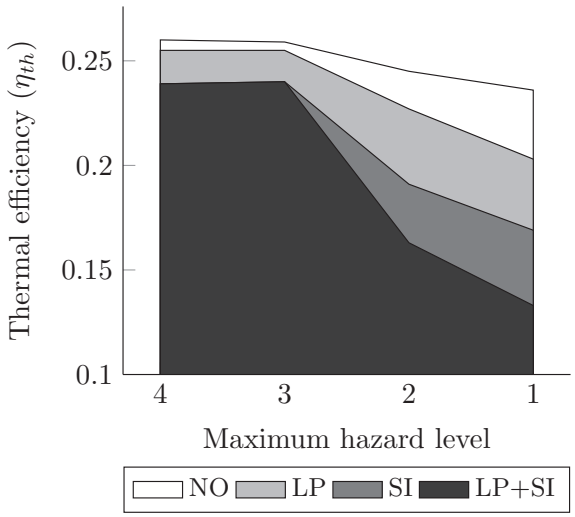

Figure 3.17: Effects of constraints and hazard levels

hazard level 2 the thermal efficiencies are markedly lower under all constraints and the same pattern is seen when moving to hazard level 1.

Requiring a limited maximum pressure of 20 bar is seen to cause modestly reduced efficiencies compared to the SI constraint. At levels 4 and 3, the LP constraint reduces efficiency by about 2%, while at levels 2 and 1 reductions of 7% and 14%, respectively, are seen. Under the SI constraint, the reduction is about 8% at levels 4 and 3; while at levels 2 and 1, 22% and 28% are found, respectively. With the LP and SI constraints combined, an

Table 3.9: Simulation results - hazard level 3

	Fluid (pressure in bar)	Fire hazard	Health hazard	Physical hazard	η_{th}
NO	I-hexane (29.4)	3	2	0	25.9
	Hexane (20.8)	3	2	0	25.1
	MM (9.9)	3	2	1	25.4
LP	I-hexane (20.0)	3	2	0	25.5
	Hexane (18.9)	3	2	0	25.5
	MM (9.9)	3	2	1	25.4
SI	Ethanol (19.0)	3	2	0	24.0
	Acetone (23.1)	3	2	0	23.5
	Benzene (12.0)	3	2	0	23.1
LP+SI	Ethanol (19.2)	3	2	0	24.0
	Benzene (12.0)	3	2	0	23.2
	Acetone (20.0)	3	2	0	23.2

cumulative effect is found only at hazard levels 2 and 1, where the reductions in efficiencies are 34% and 44%, respectively.

Results of the optimisation with allowed hazard levels up to 3 are shown in Table 3.9. Fluids at level 4 are not considered since they do not offer markedly higher efficiencies and are extremely hazardous. The best three fluids under each of the constraints are shown in order to present alternatives with similar net power output. Again the fluid type is notably different when comparing the process with and without recuperator. The range of efficiencies among the optimised processes and fluids at hazard level 3 is seen to be within about 11%.

Results from imposing hazard level 2 as the maximum are presented in Table 3.10. All the fluids in the table except cyclo-propane are compounds containing fluor atoms and are associated with a high global warming potential [200]. The efficiencies are strongly influenced by the constraints. It is seen that there are relatively large differences between the best fluids and the second and the third best (within the same constraints).

For cases at hazard level 1 the fluids are of the same type as for hazard level 2, with similar pressure levels, although efficiencies are lower in general.

Prediction of the thermal efficiency of organic Rankine cycles

As argued by Kuo et al. [144] no single fluid property seems to allow the prediction of the fluid performance in the Rankine process; however, Kuo et al. found that the ratio of sensible heat transfer to latent heat of evaporation, called the Jacob number, $Ja = \overline{c}_p \Delta T / h_{ev}$, is a good indicator of the performance of the fluid in an ORC process. $\overline{c}_p$ is the average specific heat at constant pressure, ΔT is the temperature difference

Table 3.10: Simulation results - hazard level 2

	Fluid (pressure in bar)	Fire hazard	Health hazard	Physical hazard	η_{th}
NO	R245ca (37.0)	1	2	0	24.5
	R236ea (57.7)	0	1	1	23.6
	RC318 (97.2)	0	1	2	23.4
LP	R245ca (20.0)	1	2	0	22.7
	C5F12 (20.0)	2	?	?	20.8
	R236ea (19.9)	0	1	1	20.3
SI	C-Propane (99.7)	2	2	0	19.1
	R245ca (37.1)	1	2	0	18.3
	R245fa (39.6)	0	2	1	17.0
LP+SI	R245ca (20)	1	2	0	16.3
	R245fa (20)	0	2	1	14.9
	R236ea (19.9)	0	1	1	13.3

during heating and h_{ev} is the latent heat of evaporation [144]. In order to generalize the prediction ability, Kuo et al. proposed the Figure of Merit (FOM) using the condensation and evaporation temperatures (T_ev): $FOM = Ja^{0.1}(T_{co}/T_{ev})^{0.8}$.

Figure 3.18 shows the calculated FOM for the optimised results shown in Figs. 3.14, 3.15 and 3.16. Excluded are results with super-critical pressures since FOM cannot be calculated in those cases.

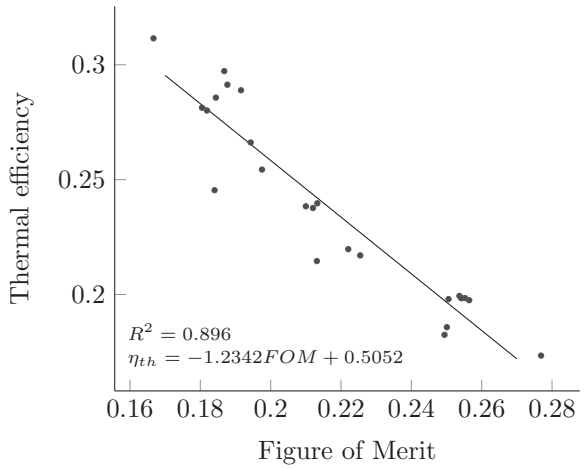

Figure 3.18: Thermal efficiency and. Figure of Merit at temperatures from 180-360°C

It is seen from the figure that a linear trend can be made with very good approximation having an R^2 value (the coefficient of determination) of about 0.90. This is remarkable because the optimised cases are of very different fluids, with a relatively large range of pressures and different process configurations (with or without preheating, superheating

and recuperation).

The optimum thermal efficiencies across all the types of processes, fluids and pressures treated in the present work, are shown in Fig. 3.19 along with results obtained at additional temperature levels.

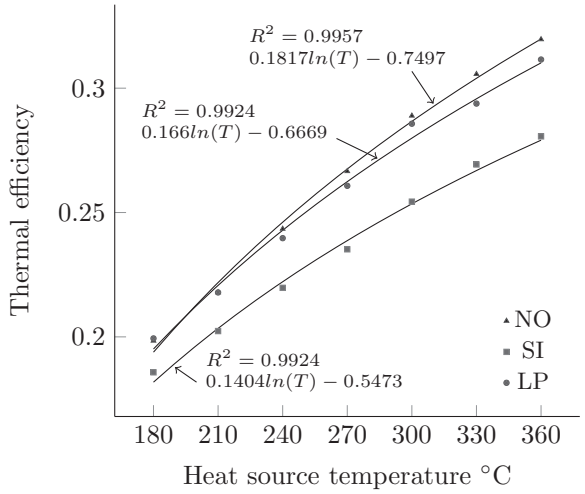

Figure 3.19: Thermal efficiency vs. heat source temperature

The graphs present strong correlations between the efficiencies and the temperatures for each of the treated constraints (NO, SI and LP). Thus the results strongly suggest that the maximum obtainable efficiency can be predicted from the temperature alone, with the given boundary conditions.

3.3.2 Multiple regression models for the prediction of the maximum obtainable thermal efficiency of organic Rankine cycles

Expanding on the findings in the previous section, Table 3.11 presents the regression coefficients and standard errors for both the low-temperature models. Each of the coefficients indicate the influence of each predictor variable ($T_{hs,i}$, $T_{hs,o}$ and $\eta_{po,ex}$) on the thermal efficiency. For example, the coefficient for the heat source inlet temperature is lower for the simple ORC, indicating that the benefit of increasing the heat source inlet temperature is relatively smaller compared to the ORC. The standard errors of each of the coefficients are the margins for the model output to remain within a 95% confidence interval of the observed (simulated) values. They are all seen to be minor compared to the coefficients.

Table 3.11: Model coefficients and statistics for low-temperature heat sources

	ORC		Simple ORC	
	Coefficient	Std. error	Coefficient	Std. error
Constant (β_0)	-16.32	0.5056	-14.92	0.9034
$T_{hs,i}$	0.08402	0.00129	0.07339	0.001718
$T_{hs,o}$	0.08349	0.0043	0.08363	0.006474
$\eta_{p,e}$	0.1583	0.00536	0.1464	0.009767

Table 3.12 presents the regression model coefficients and the associated statistics for the high-temperature models. It is seen that the influence of $T_{hs,i}$ on the model output (thermal efficiency) is again smaller for the simple ORC model. This is also the case for the other variables $T_{hs,o}$, T_{co} and ΔT_{pp}, but not the expander efficiency. This suggests that the expander efficiency is more important for the efficiency in the simple ORC case.

Table 3.12: Model coefficients and statistics for high-temperature heat sources

	ORC		Simple ORC	
	Coefficient.	Std. error	Coefficient	Std. error
Constant (β_0)	-12.76	0.5377	-12.33	1.100
$T_{hs,i}$	0.06428	0.0007	0.05858	0.001458
$T_{hs,o}$	0.05897	0.0012	0.03350	0.00259
$\eta_{p,e}$	0.2576	0.00604	0.2666	0.0130
T_c	-0.1727	0.0033	-0.1552	0.00790
ΔT_{pp}	-0.1556	0.0081	-0.0810	0.01832

Consequently, the regression models for predicting the maximum obtainable thermal effi-

ciencies of the ORC are Eq. 3.32-3.35:

$$\eta_{th,m} = -16.32 + 0.08402T_{hs,i} + 0.08349T_{hs,o} + 0.1583\eta_{po,ex} \quad (3.32)$$

$$\eta_{th,m} = -14.92 + 0.07339T_{hs,i} + 0.08363T_{hs,o} + 0.1464\eta_{po,ex} \quad (3.33)$$

$$\eta_{th,m} = -12.76 + 0.06428T_{hs,i} + 0.05897T_{hs,o} + 0.2576\eta_{po,ex} - 0.1727T_{co} - 0.1556\Delta T_{pp} \quad (3.34)$$

$$\eta_{th,m} = -12.33 + 0.05858T_{hs,i} + 0.03350T_{hs,o} + 0.2666\eta_{po,ex} - 0.1552T_{co} - 0.0810\Delta T_{pp} \quad (3.35)$$

where Eq. 3.32 is for ORCs with heat sources with an inlet temperature of 80-180°C, and Eq. 3.33 predicts the maximum performance of simple ORCs within the same temperature range. Temperatures are given in degrees Celsius and the efficiencies in percent. Subscripts th and m are short for thermal and maximum, respectively. Equations 3.34 and 3.35 yield predictions for heat sources from 180-360°C for ORCs and simple ORCs, respectively.

In addition, the same analysis for the ORC with a limit of 20 bar on the cycle maximum pressure results in the regression model below, which is valid for the 180-360°C temperature range:

$$\eta_{th,m} = -14.19 + 0.06398T_{hs,i} + 0.07535T_{hs,o} + 0.2455\eta_{po,ex} - 0.2069T_{co} - 0.1164\Delta T_{pp} \quad (3.36)$$

In order to obtain reasonable prediction accuracies, the number of parameters in the low temperature models is limited to the three shown in Eqs. 3.32 and 3.33. It should thus be noted that the low-temperature cases are only valid for a condensing temperature of 25°C and a ΔT_{pp} of 5°C; however, the high temperature models can maintain better prediction accuracies and the models thus include the condensing temperature and ΔT_{pp} parameters as well. The statistical evaluation is not including Eq. 3.36 because the results are so similar to the results shown for the other models.

Statistical evaluation

The regression statistics are listed in Table 3.13. The adjusted R^2 value (coefficient of determination) takes into account the size of the data set and the number of predictor variables [201], and for all the models it is seen to approach unity. The statistically strongest model, measured by the adjusted R^2 value, is the high temperature ORC; however, all the models are statistically strong judging from the F-significances.

Additionally, the P-values (not listed) for each of the coefficients represent the probability of each of the predictor variables being insignificant for the model result. For all the coefficients in the four models, the P-values are in the range of 10^{-30} to 10^{-100}, i.e., it is certain that the variables are important for the predicted maximum thermal efficiency, as should be expected. One exception is the ΔT_{pp} variable in the high temperature simple ORC model which has a P-significance of $3{\cdot}10^{-5}$. Similar statistics are found for Eq. 3.36.

Table 3.13: Regression statistics

	Adjusted R^2	Std. error	F-significance
ORC, low	0.961	0.343	$6.4{\cdot}10^{-91}$
Simple ORC, low	0.966	0.500	$9.0{\cdot}10^{-58}$
ORC, high	0.994	0.353	$3.5{\cdot}10^{-104}$
Simple ORC, high	0.965	0.694	$3.6{\cdot}10^{-57}$

Verification of model assumptions

Since the results are very similar, verification is omitted for models other than the high temperature ORC model; however, a brief discussion illustrates the outcome of these additional verifications.

For all the models, the mean value of the residuals is about 10^{-15}, i.e., very close to zero; hence, this first assumption is verified (see p. 91). The second assumption to be verified is that the residuals present a normal distribution. It can be shown that they do so when the residuals plotted versus the normal scores form a straight line as shown in Fig. 3.20 (see Larsen [187] for further details). It is evident that this is true to a relatively high degree, since the residuals form a fairly straight line, as the linear trend line also drawn has a R^2 value of 98.5%. Similarly, when plotting the residuals of the data for the other models, the R^2 values are 99.1% and 98.3% for the low temperature ORC and simple ORC models, respectively, and 97.3% for the simple ORC high temperature model.

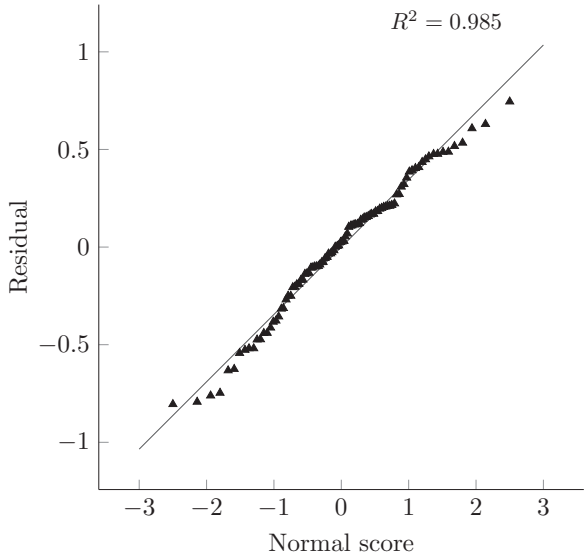

Figure 3.20: Normal probability plot

Figure 3.21 (a-f) depicts the residuals plotted against each of the five predictor variables

and the predicted thermal efficiency. The figure shows how all five variables are properly varied within their respective ranges. No specific pattern formed by the residuals can be observed, thus verifying the assumptions of constant variance and independence of the residuals. When examining the residuals for the other three models very similar pictures are seen.

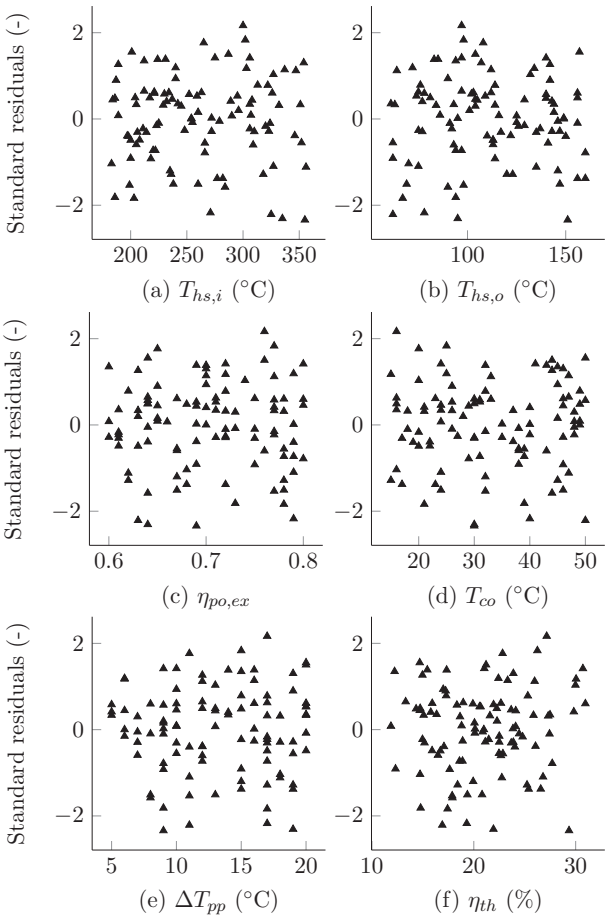

Figure 3.21: Plots of residuals

Prediction ability

As was seen in Table 3.13, the standard errors for the models are relatively small compared to the ranges of thermal efficiencies. This is illustrated in Fig. 3.22, where the predicted values for the high temperature ORC model are plotted against the observed (simulated). It is evident that the predicted maximum obtainable thermal efficiencies are very close to the simulated and optimised values.

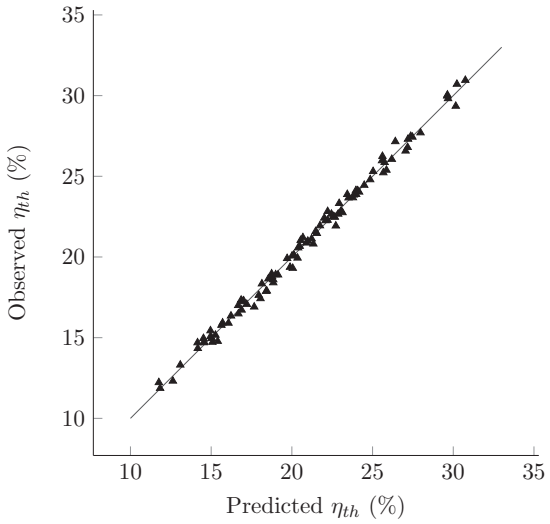

Figure 3.22: Prediction ability for the high temperature ORC model

Similarly, Fig. 3.23 presents the predicted against the observed values for the low temperature ORC model. The prediction is seen to be not as good with this model compared to the high temperature model. For the simple ORC models, the predictions show a very similar picture as in Fig. 3.23.

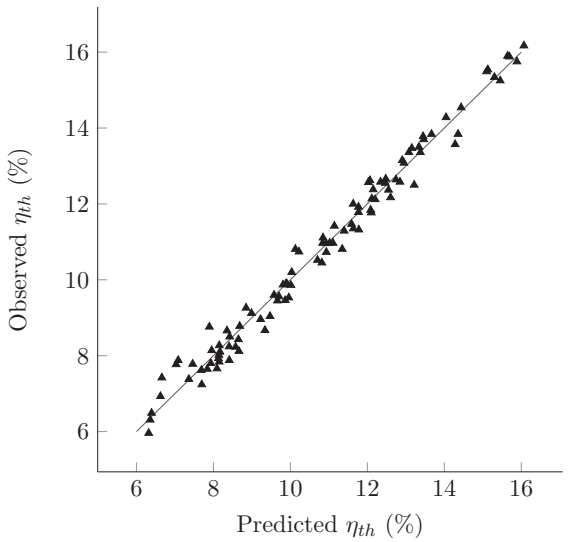

Figure 3.23: Prediction ability for the low temperature ORC model

Extrapolation

Model extrapolation outside the scope of the observed values (see Table 3.4) will result in predictions which are increasingly inaccurate. Figure 3.24 presents predictions using the low and high temperature models with extrapolations. In both cases shown, the heat source outlet temperature is kept at 60°C, the expander efficiency at 70%, the condensation temperature at 25°C and the ΔT_{pp} at 5°C. The figure illustrates how the two models diverge from each other when varying the heat source inlet temperature beyond the observation data ranges. The divergence is seen to be significant compared to the predicted values. Similar trends are present when extrapolating the other predictor variables.

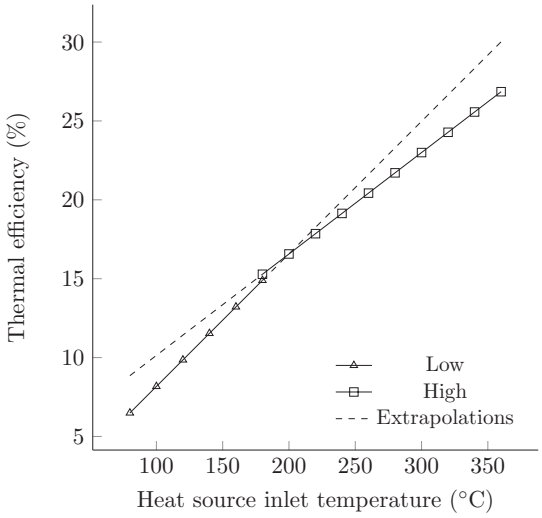

Figure 3.24: Extrapolation of the ORC regression models

Comparison with the theoretical maximum

The Trilateral cycle efficiency, which is derived from the Carnot cycle efficiency, can be used as a measure of the maximum obtainable efficiency for a non-isothermal heat source which is cooled to the condensing temperature [146]. In cases where the heat source is not cooled to that extent, the efficiency is higher due to the higher average temperature of the heat added to the process. Assuming that the heat source is cooled by the working fluid while describing a linear function, the Trilateral efficiency (η_t) can be described by the following equation:

$$\eta_t = 1 - \frac{T_{co} ln(T_{hs}/T_{co})}{T_{hs} - T_{co}} \tag{3.37}$$

where T_{co} is the sink or condensation temperature. Figure 3.25 presents a comparison of the maximum obtainable thermal efficiencies for the ORC, the simple ORC and the Trilateral cycle. The four regression models are combined to cover the temperature range from 80 to 360°C. The heat source outlet temperature is kept at 60°C, the expander efficiency at 70%, the condensation temperature at 25°C and the ΔT_{pp} at 5°C, in order to be able to connect the low and high temperature models for each process.

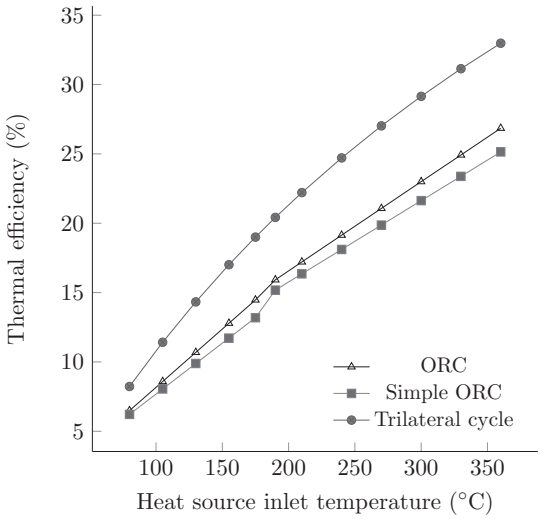

Figure 3.25: Comparison with the Trilateral cycle efficiency

It is seen that the difference between the predicted performances of the ORC and the simple ORC is relatively small. The Trilateral efficiency is seen to be non-linear as expected. The figure illustrates how the gradients for the low temperature models are slightly steeper than the high temperature models, indicating a similar behaviour as the Trilateral cycle efficiency. It should be noted that with values of $T_{hs,o}$ higher than the 60°C used for the figure, the predicted efficiency can easily exceed the Trilateral efficiency for any given heat source inlet temperature.

A sudden change at around 180°C is seen in the figure for the simple ORC model. This is where the low and high temperature models meet, and as seen, it is not given that the two models coincide at their respective end points. This sudden change can be regarded as an indicator of the size of the inaccuracy of the models.

Optimum working fluids

For coherence reasons Figs. 3.26 and 3.27 provide information on the working fluids leading to the results on which the regression analyses are made. The figures are made with inspiration from the work of Wang et al. [145]. The working fluids are the ones leading to the maximum efficiency from the ORC given the input parameters. The fluids are aligned from left to right with increasing heat source inlet temperature, within the intervals shown. The other parameters ($T_{hs,o}$, $\eta_{po,ex}$, T_{co} and T_{pp}) are randomly distributed within the intervals as shown in Fig. 3.21.

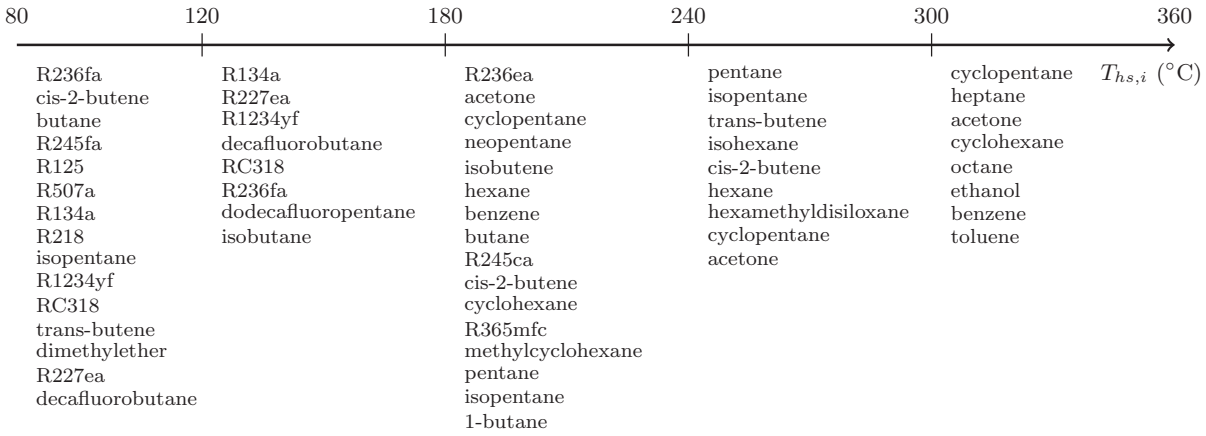

Figure 3.26: Working fluids for the ORC

The fluids are also aligned in the columns from the top down with increasing $T_{hs,i}$. For example, Fig. 3.26 shows that with the lowest value of $T_{hs,i}$ (80°C), the optimum working fluid is R236fa. As $T_{hs,i}$ gets closer to 120°C, the optimum working fluids are cis-2-butene, butane, R245fa, etc. It is noted, however, that many of the fluids are optimum at more than one heat source inlet temperature. This is because the optimum fluid is also dependent on the other parameters.

Figure 3.27 presents the optimum working fluids for the simple ORC. It is seen that the fluids are not the same as in Fig. 3.26. Moreover, the number of fluids in each column is smaller in comparison. This means that for the simple ORC fewer fluids dominate as the optimum fluids, across the temperature range.

In both Figs. 3.26 and 3.27 acetone is present in the temperature range 180 to 360°C. For the ORC, the refrigerants and alkanes (dry fluids) dominate the figure, while ammonia and ethanol (wet fluids) are frequently the optimum fluid for the simple ORC.

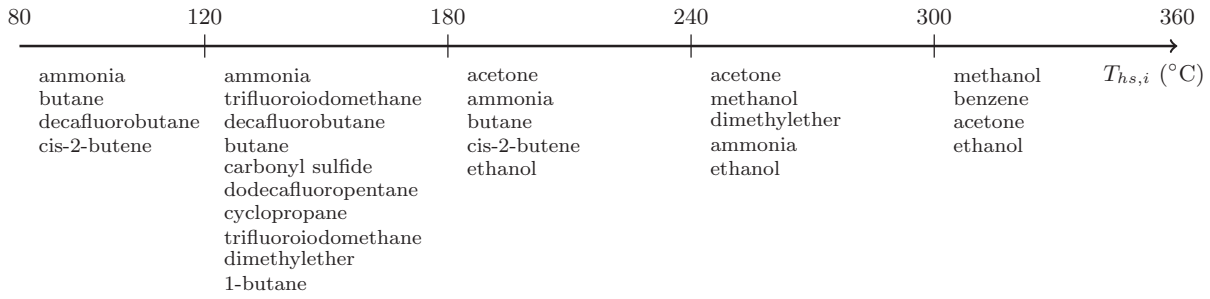

Figure 3.27: Working fluids for the simple ORC

3.3.3 System analysis and optimisation of a Kalina Split-cycle for waste heat recovery on large marine diesel engines

Governing process mechanisms

This section provides an analysis of the Kalina cycle in order to identify the governing mechanisms relevant for the process and its optimisation. The components that are of major influence on the process efficiency are identified to be the separator, the recuperators, the boiler and the turbine(s).

The separator is the characteristic component of the Kalina cycle separating it from the Rankine cycles. The condensing pressure of ammonia-water mixtures is directly dependent on the ammonia concentration; i.e., ammonia-rich mixtures have, at a given temperature level, a relatively higher condensing pressure. For example, an ammonia-water mixture of 75% by mass at 25°C condenses at a 7.3 bar while pure water condenses at 0.03 bar.

The outlet pressure of the turbine, and therefore the turbine power and thermal efficiency of this power cycle (see Fig. 3.10), is limited by (i) the ammonia concentration at the inlet of the condenser, and (ii) the cooling water temperature. The ammonia concentration at the inlet of the condenser (6) depends on the proportion between the lean stream exiting the separation system (15), and the stream exiting the turbine (5). The main function of the separator is therefore to minimise the condensing temperature by diluting the working solution prior to the condenser (6), allowing for a lower condensation pressure and a greater turbine power output for a given cooling water temperature.

The separator must also be able to restore the working solution concentration and mass flow by supplying an ammonia-rich vapour stream, which is mixed to form the streams that enter the boiler. How the balance of these two functions strongly influences the process net power output is described further below.

The phase equilibrium and the flow rate of the solution feeding the separator govern the concentrations and mass flow rates of the output streams. The decisive parameters are the ammonia concentration, the feed pressure and the temperature. Figure 3.28 illustrates how the ammonia concentrations and mass flow rates of the two separator outlet streams are affected by changes in the feed stream pressure and temperature.

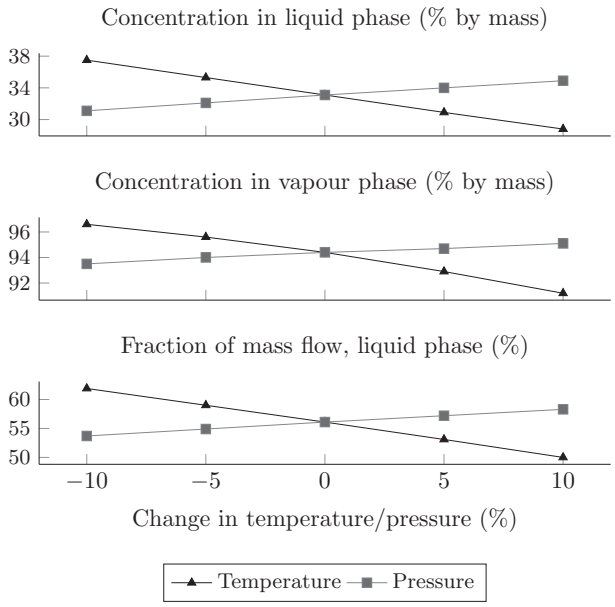

Figure 3.28: Trends for the separator outlet streams

The ammonia concentration at the inlet of the condenser can be regulated by adjusting the mass flow rate and/or the concentration of the lean stream exiting the separator. As Fig. 3.28 shows, a low concentration liquid stream can be obtained by having a combination of low pressure and high temperature. A high liquid mass flow rate can be obtained if the feed stream has a low temperature and a high pressure. Alternatively, an increased liquid outlet stream mass flow rate can be obtained by decreasing the feed stream concentration.

In theory, the highest power output is achieved for the minimum allowable condensing pressure, which is reached by diluting fully the working solution with the lean separator stream; however, the amount of lean liquid from the separator is limited by the amount of heat available for the feed stream to be heated sufficiently to reach the two-phase state required to support the second function of the separator, i.e., the restoration of the working solution. Therefore, the temperature and the amount of heat available from the outlet of the turbine determines how big a difference there can be between the ammonia concentrations of the condensing stream (15) (Fig. 3.10) and the working solution stream.

The turbine power per kg/s of working fluid mass flow rate is illustrated in Fig. 3.29, for ammonia concentrations from 0.72 to 0.84 and inlet/outlet pressure ratios of 100/6, 110/5, 120/4 and 130/3 (bar); these are the ranges where the optimum power output of the cycle is expected to be. High turbine power outputs can be obtained by increasing the working solution ammonia concentration and also the turbine pressure ratio, for a given turbine inlet temperature (330°C), and increased pressure ratios are relatively more beneficial for the turbine power output compared to changes in the solution concentration.

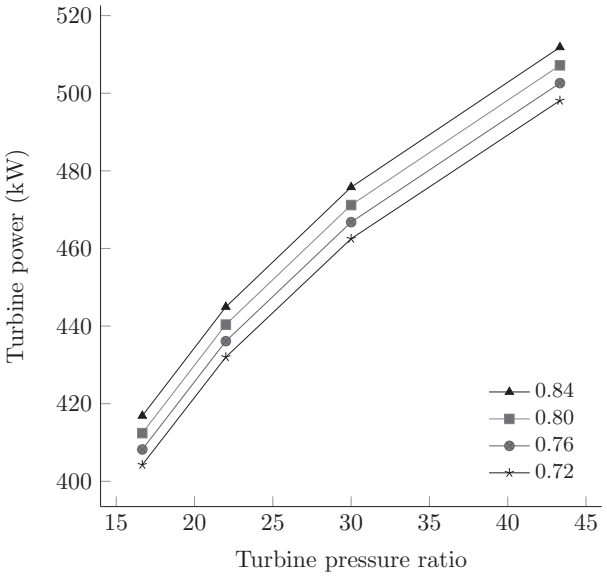

Figure 3.29: Turbine inlet/outlet pressure ratio influence on turbine power

Even though high turbine power outputs may be achieved by increasing the working solution concentration, this also increases the need for dilution of the condensing stream. Conversely, reducing the working solution concentration also reduces the need for dilution and/or enables lower turbine outlet pressures; hence, there is a trade-off mechanism inherent in the process, making optimisation less straightforward.

The Split-cycle boiler configuration with the two separate streams of different concentrations, enable the manipulation of the minimum pinch point temperature difference in the boiler, as illustrated in Fig. 3.30. The figure presents an example case where the working solution concentration is 0.75 and the rich stream solution concentration is varied from 0.76 to 0.92. The rich stream ammonia concentration can in this case not exceed 92% (by mass) at the given cooling water temperature and condensing pressure.

The minimum temperature difference in the first evaporator is affected by varying the concentrations of the two streams and increases with increasing rich stream concentrations;

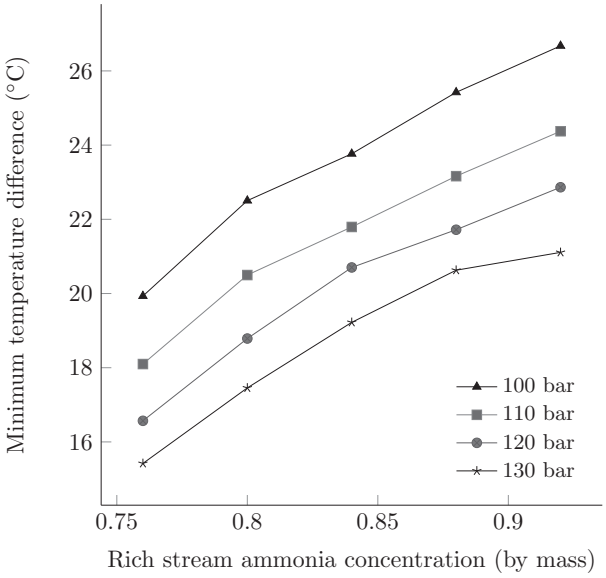

Figure 3.30: Rich stream composition effect on pinch point temperature difference

a trend which is general for a wide range of cases. Thus, for a given pressure and working solution concentration, the pinch point temperature difference can be enlarged, enabling optimisation of the process by changing one or a combination of the parameters, as follows: (i) lowering the ammonia concentration causes higher boiling temperatures but may enable a lower turbine expansion pressure which in turn increase the net power output (Fig. 3.29), or (ii) the boiler pressure can be increased thus increasing turbine power output, and (iii) the boiler inlet temperature of the working fluid can be increased to get a higher average heat uptake temperature and a higher mass flow rate of the working fluid, and thus increased net power output. Alternatively, the temperature difference at the pinch point is higher, and the required heat transfer area of the boiler can (at least in theory) be decreased.

Optimisation results

In the following, the results from applying the genetic algorithm for the optimisation of the mentioned processes are presented. Table 3.14 presents the respective net power outputs and thermal efficiencies. The relative gain from using reheat is more significant for the Split-cycle compared to the reference Kalina cycle. The Split-cycle without reheat has a higher efficiency than the Kalina cycle with reheat, and the Split-cycle with reheat has a significantly increased power output (+11.4%) compared to the reference Kalina cycle.

Table 3.14: Optimum cycle performances

	Power (kW)	Thermal efficiency (%)
Kalina cycle	1,753	20.8
Kalina cycle, reheat	1,813	21.5
Split-cycle	1,858	22.1
Split-cycle, reheat	1,953	23.2

The additional net power gained by using reheat is about 3.4% and 5.1% for the Kalina cycle and the Split-cycle. In relation to the results obtained by Bombarda et al. [169] for ORC and Kalina cycles (both with about 1,600 kW net power), the optimised SC process with reheat produces about 22% more power from the same amount of heat and process boundary conditions.

Using the derived multiple regression models (Sec. 3.3.2) to estimate the maximum obtainable efficiency of a recuperated ORC, with the same heat source temperatures, turbine polytropic efficiency, a condensing temperature of 30°C, and a pinch point temperature difference of 22°C, results in a thermal efficiency of 26.5%. It is noted that the generator and pump electrical efficiencies are not accounted for in this estimation. It is also noted that the recuperator pinch point for the ORC is also 22°C while it is only 5°C for the Kalina cycles.

Table 3.15: Optimised parameters

	Kalina cycle	Kalina, reheat	Split-cycle	Split-cycle, reheat
Separator feed temperature (°C)	86.5	86.5	81.2	85.8
Separator feed pressure (bar)	7.57	8.30	9.64	10.10
Separator feed concentration (-)	0.473	0.500	0.512	0.478
Working solution concentration (-)	0.692	0.735	0.683	0.677
Turbine outlet pressure (bar)	3.34	3.84	3.42	2.88
Reheat pressure (bar)	-	47.3	-	36.6
Turbine inlet pressure (bar)	110.7	102.1	127.1	101.7
Boiler approach (°C)	28.1	26.8	7.6	5.0
Rich stream concentration (-)	-	-	0.827	0.867

All thermodynamic states of the optimised modelled cases can be found in the appendix (p. 199), while Table 3.15 presents the optimised parameters for each investigated cycle. In the two cases with reheat, the optimum boiler pressures are lower than their counterparts without reheat. Table 3.15 also shows that the boiler temperature approach is lower for the Split-cycle cases, leading to higher boiler inlet temperatures compared to the regular Kalina cycle cases. The relatively higher temperatures suggest that the internal recuperation can be more effective in the Split-cycle processes, thus reducing the amount of heat rejected in the condensers.

No other clear trends is found when comparing the remaining optimised parameters, neither when comparing the Kalina cycles and the Split-cycles, nor when comparing the cases

with or without reheat. The parameters do indicate for each case the respective optimum balances between the two functions of the separator. For the Kalina cycle without reheat and the Split-cycle with reheat, the separator enables a relatively low turbine outlet pressure. This is made possible by having low concentrations of ammonia in the working solution and the separator feed streams.

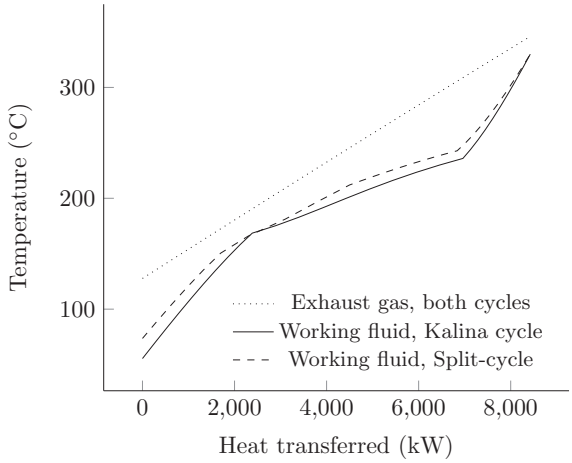

Figure 3.31: Heat transfer diagram

Figure 3.31 illustrates the boiler heat transfer process in the optimised cases of the reference Kalina cycle and the Split-cycle processes with no reheat. The boiler inlet temperature of the Split-cycle is higher than that of the Kalina cycle. It is evident that the Split-cycle heat transfer occurs at a higher average temperature, and a higher working fluid mass flow rate is enabled due to the smaller enthalpy difference between inlet and outlet. This would not be possible without the pinch point alteration made by the Split-cycle boiler configuration as explained with Fig. 3.11 (p. 93). The higher output of the Split-cycle compared to the Kalina cycle can in this case be attributed to the higher inlet pressure of the turbine and the mass flow, since the outlet pressures and working solutions are similar.

In the two cases with reheat, the turbine mass flow rates and the turbine inlet pressures are similar; however, the turbine exhaust pressure is markedly lower in the Split-cycle case. Hence, the overall turbine pressure ratio is in this case the reason for the improved efficiency, in spite of a significantly lower working solution concentration in the SC case.

Cost analysis

The resulting heat transfer areas in all the four cycles are shown in Table 3.16. The largest areas are in the boiler components due to the low heat transfer coefficients on the gas side.

An increase in heat transfer areas as a result of both reheat and the Split-cycle boiler is seen.

Table 3.16: Estimated heat transfer areas

Component	$\overline{U}$ $(W/(m^2 \cdot K))$	Kalina (m^2)	Kalina, reheat (m^2)	Split-cycle (m^2)	Split-cycle, reheat (m^2)
Recuperator 1	500	458	417	451	498
Recuperator 2	500	257	213	438	424
Recuperator 3	500	34	38	34	48
Recuperator 4	500	-	-	55	62
Preheater	37.5	1,663	1,346	-	-
Evaporator 1	34 (36 for SC)	2,968	3,186	4,945	4,083
Evaporator 2	28	-	-	1,829	2,849
Super-/re-heater	21	972	1,912	2,026	3,429
Condenser 1	1,100	347	327	383	390
Condenser 2	1,100	223	246	213	203
Total		6,922	7,685	10,374	11,986

The estimated purchase costs of the cycles are shown in Table 3.17. The boiler heat exchangers and the turbines represent in all cases about 85% of the total cycle cost. While only considering the expenses for the main components and not including piping, generators, cooling system, installation and maintenance, plus (possibly) the cost of the extra fuel added when the engine is tuned for WHR operation, the payback periods must be considered optimistic.

Table 3.17: Estimated purchase cost (components cost in 1,000 USD)

Component	Kalina cycle	Kalina, reheat	Split-cycle	Split-cycle, reheat
Recuperator 1	79	73	78	85
Recuperator 2	50	43	76	74
Recuperator 3	10	11	10	13
Recuperator 4			15	16
Preheater	222	187		
Evaporator 1	353	373	531	455
Evaporator 2			239	341
Superheater/reheater	144	248	260	396
Condenser 1	63	60	69	70
Condenser 2	45	48	43	41
Pump 1	6	6	7	9
Pump 2	39	34	30	20
Pump 3			24	18
Turbine 1	850	322	888	382
Turbine 2		713		718
Total cost (million USD)	1.86	2.12	2.27	2.64
Specific cost (USD/kW)	1,062	1,168	1,221	1,351
Savings (million USD/year)	0.93	0.96	0.98	1.04
Payback time (years)	2.0	2.2	2.3	2.5

In addition, in the calculation of the cycle power outputs, heat and pressure losses are not considered; however, the results in Table 3.17 suggest that the Split-cycle without reheat

and the Kalina cycle with reheat may present very similar costs and payback times. In comparison, the specific plant cost of an ORC with a similar nominal power capacity ranges from about 1,300 to 2,300 USD [129]. Considering a ship lifetime of 20 years, the potential economical and environmental gains of the Split-cycle, even with reheat, is considerable.

3.4 Discussion

This section discusses the methodologies and results of the previous sections, starting with the design and optimisation method for ORCs and the results provided. Then the methodology and results of the regression analysis are discussed, and finally the analysis of the Kalina Split-cycle.

3.4.1 Design and optimisation of organic Rankine cycles for waste heat recovery in marine applications using the principles of natural selection

This section discusses the results of the ORC optimisation across the relevant heat source temperature range. Discussions about the fluid hazard levels and the thermal stability of ORC working fluids are also presented.

General influence of the heat source inlet temperature

The 36 optimised cases shown in Figs. 3.14, 3.15 and 3.16 (p. 103) are discussed next. The trend for the dry fluids is that the optimisation of the net power is limited by the evaporator pinch point temperature difference; this is the case in 20 of 36 cases. In 13 of the 36 cases, the evaporator pinch point temperature difference is larger than the minimum allowable, and the limit for the superheater approach limits further optimisation; in those cases the fluids are mostly wet or isentropic type fluids. The recuperator pinch point temperature difference is in three cases the limiting factor, and the evaporator pinch point temperature difference and the superheater approach are larger than the minimum allowable. Generally for the optimised cases, the evaporator pinch point temperature differences are within a few degrees of the limit for sub-critical cases; for some of the optimised super-critical cases the optimum efficiency is found while having an evaporator temperature difference of up to 10 degrees larger than the minimum allowed.

In the ORC process with no constraints (Figure 3.14), the trend is that the optimum pressures are found at lower pressures when the heat source temperature is lower. The same trend is found in the constrained scenarios. At a heat source temperature of 180°C, pressures are all sub-critical; while at 240°C and above, pressures are in all cases very near to the critical pressure or above. This indicates that super-critical processes are not beneficial when the heat source is cooler than about 240°C, for this extensive group of fluid candidates, and conversely that super-critical processes are more efficient at this temperature and above. This is not the case when looking at the ORC process without

recuperator (Fig. 3.15). Here, all of the cases below 360°C except one, have their optimum pressures below the respective critical points. Overall, the optimum pressures are slightly lower; the results therefore suggest that super-critical pressures do not benefit the simple ORC process when the heat source is below 360°C.

Further analysis of the large body of simulations suggests that the consequence of not allowing the pressure to exceed the critical pressure is about one percentage point lower maximum net power output in comparison.

The results presented in Figs. 3.14, 3.15 and 3.16 may represent a relatively wide range of power outputs, and thus a difference in the scale of the ORC plant. Accordingly, the typology and efficiency of the expander (in a final process design) may be different at each end of this scale. For the application and scale in the present work, a suitable expander may be a highly efficient axial turbine. Kang et al. [202] estimate isentropic efficiencies of around 80% from small scale, low temperature ORC experimental data. Colonna et al. [203] state that a typical isentropic efficiency design value is 87%, for ORC turbines operating at the high end of the temperature range investigated in the present work. The assumed polytropic efficiency of 80% is therefore a reasonable value for the comparison within the temperature range investigated, since this value results in isentropic efficiencies of 80-82% depending on fluid and pressure ratio.

Hazard levels and environmental impact

Regarding minimizing the hazard levels, perhaps most importantly the fire hazard in the marine application, there is a clear trend in the results (see Fig. 3.17, p. 105). The results suggest that there is no single fluid that can satisfy the demand for safety and high efficiency; however, the means to obtaining the best compromise of both objectives is to allow relatively high pressures and design the ORC process with a recuperator.

The IMO SOLAS regulations state that the flash point of a fluid in a machinery space may not be lower than 60°C, without proper safety measures, such as double piping. All the hydrocarbons falls under this category and the need for additional safety equipment, and the increased hazard risk, may be regarded as a significant drawback for these fluids.

RC318, R245fa and R236ea are all non-flammable and can as such be used without additional fire hazard precautions; however, they have a relatively high GWP, especially RC318 with a value of 10,900 on a 100-years time horizon (CO_2-equivalent). R245fa and R236ea have GWP values of 1,020 and 1,350 respectively [204]. In a recent study, Domingues et al. [205] investigate R245fa as ORC working fluid applied to recover heat from a combustion engine. They conclude that the properties of R245fa lead to high heat exchanger effectiveness and that the fluid is suitable for the application.

Other non-flammable fluids among the tested are: decafluorobutane with a GWP_{100} of 7,000, sulfur fluoride with a GWP_{100} of 23,900 (among the highest for all substances) and nitrous oxide with a relatively low GWP_{100} of 310 [200]; however, these fluids are not recommended in this context. CO_2 is another non-flammable alternative with a low GWP. This fluid requires very high pressures to be efficient though, with an optimum of 18.1% efficiency at 210 bar (using the engine design point heat source, Sec. 3.3.1). No other non-flammable fluids suitable for ORC are found.

Further analysis of the simulations suggests that with the acceptance of a fluid fire hazard level of 3, a simplified process layout without superheater can achieve efficiencies as high as the highest found in this study. Within this group the siloxane fluid MM is likely a good candidate with a high efficiency at a low maximum pressure and low GWP. A drawback is the relatively low condensing pressure (0.06 bar at 25°C). Bombarda et al. [169] state that MM is proposed in the literature and is in use currently as working fluid for ORCs recovering heat from combustion engines. One of the leading ORC companies uses siloxanes in the same type of application [206]. This indicates that the durability and usefulness of the fluid in this context is proven.

Another fluid worth emphasizing is ethanol, which the results suggest is superior within a large temperature range. Possibly mixed with water to increase the flash point (55°C), ethanol may be a good candidate as working fluid in a low pressure Rankine process with no recuperator. The maximum efficiency is nearly as good as the highest in this investigation, and the environmental profile also is good with low GWP and ODP, as well as low ecotoxicity.

Thermal stability

Toluene is already in use in the industry by a Dutch company in high-temperature applications. It was selected due to its high chemical stability at elevated temperatures [207]. The stability is a key point, while information on these characteristics is only available for a few of the fluids considered in this work. Andersen et al. [208] tested the decomposition rate of normal-pentane, iso-pentane, neo-pentane, toulene and benzene under conditions relevant to high temperature ORC processes, i.e., up to 315°C and 41 bar. Benzene is found to be the most stable fluid, but decomposition is found after only a few days, though in small amounts. (As in the present study, benzene is also found to be the best among candidates in a recent study by Vaja et al. [133] investigating a combustion engine and high temperature ORC combined cycle.) A 50% loss of the fluids is predicted to be in a time frame within the order of years for all of the fluids. The study [208] highlights the need for further studies on fluid stability, as the long term consequences of using many of the ORC fluids are not described adequately.

3.4.2 Multiple regression models for the prediction of the maximum obtainable thermal efficiency of organic Rankine cycles

In this section the limitations associated with the proposed regression models is discussed and comparison with recent literature is provided.

Limitations

While the proposed models are useful, it is important to note the following limitations. The work presented relies on the accuracy of the thermodynamic states provided by the NIST Refprop software; in the process of constructing the equations of state, the goal is to produce the best fit, i.e., the model has the least average deviation from measured data. Hence, it can be assumed that the errors are randomly distributed, and consequently the effects of the errors may be somewhat balanced out. Thorin et al. [175] investigate, as mentioned, the effect of using different equations of state in power cycles and conclude that the results are somewhat different depending on the EOS; further studies are still needed. Using the genetic algorithm may on the other hand also result in the identification of the states with deviation errors favouring the efficiency.

It is required in the linear regression analysis that the errors of the models are evenly and randomly distributed as shown in Fig. 3.21 (p. 112). Consequently, the relative errors increase with decreasing predicted efficiency; this is particularly relevant for the low-temperature models, and consequently in this work, the models are limited by having constant condensing temperature and pinch point temperature differences. Initial attempts included these two variables also for the low-temperature models; however, the resulting models were very inaccurate with relative errors of more than 50%.

Due to the above, the efficiency of small-scale ORC plants for utilising low temperature heat sources is not predicted very accurately. Additionally, for this application type, factors other than the proposed ($T_{hs,i}$, $T_{hs,o}$ and $\eta_{po,ex}$) influence the process, as for example, the pump efficiency. Thus the low temperature models may be considered too simplified, and further studies dedicated to low temperature heat sources are therefore hereby proposed for future work.

Another important limitation is that the models are valid only for heat sources with a relatively constant specific heat over the temperatures of the heat source from inlet to outlet. Condensing heat sources can thus not be considered and neither can combinations of more than one heat source (at different temperature levels).

The upper limit of 120 bar in the optimisation of the boiler pressure does in practice not

limit the efficiency in the model results used for the regression analyses. The average optimum boiler pressure is about 40 bar; however, in the simple ORC high temperature model cases, the optimum boiler pressure is generally very high (nearly 100 bar) when ammonia is found to be the optimum fluid. Cis-2-butene, methanol and ethanol also require relatively high pressures to obtain optimum efficiencies. Due to the many available fluid alternatives, it is not expected that a significant decrease in efficiency will occur when substituting the optimum fluid with fluids having a lower optimum pressure, as the results presented in Sec. 3.3.1 also suggest.

More important are the many other requirements for a suitable ORC working fluid. There is a consensus in the literature that the following aspects are important: Global Warming Potential, Ozone Depletion Potential, chemical/thermal stability, cost, heat transfer properties, corrosiveness and levels of toxicity and fire hazards. For these reasons the proposed regression models should be seen as idealistic in the sense that they can only predict the thermodynamically calculated maximum obtainable efficiency. Despite the many requirements, the fluids found as optimum in the present study are commonly found in the relevant literature, as is discussed next.

Comparison with other studies

In a recent study Bao et al. [123] provide a comprehensive literature review on ORC working fluids where the recommended fluids of various authors are listed. Among those are a number of refrigerants, which are disregarded in the present work, since they will be banned in the near future; however, fluids matching with the presently found optimum fluids and temperature levels (Figs. 3.26, 3.27) are benzene, R236ea, butane, hexane, toluene, R245ca, ammonia, R134a, ethanol and R227ea.

A number of recent studies allow for a comparison of modelled results with the regression model predictions. It is noted that the results found in these studies are not described as the maximum obtainable thermal efficiency which is what the regression models predict.

Dai et al. [209] compare the optimum performance of ten different working fluids in both the simple cycle and the recuperated cycle. With the parameters used; $T_{hs,i}$, $T_{hs,o}$, $\eta_{po,ex}$ equal to 145°C, 73°C, 85%, respectively; Dai et al. [209] find an efficiency of 12.27% and the regression model finds 14.8% for a simple ORC. For a recuperated process Dai et al. [209] finds with similar data an efficiency of 12.54%, while the model finds 15.5%. Dai et al. [209] uses a pinch point temperature difference of 8°C and the regression model assumes 5°C. Also, the expander efficiency is slightly above the valid area for the regression model; however, this does not account for the difference or the inherent regression model error; instead, this difference suggests that a more efficient working fluid and/or process conditions may be available.

Walraven et al. [210] present results which are in good agreement with the present regression model. The optimum efficiencies are 11.5 and 14.5% for a simple and a recuperated ORC, and the regression model predicts 11.7 and 16.4%, respectively. There is also good agreement when comparing the results of Trapp et al. [131]. The optimum efficiency in this study is 13.1%, and the regression model predicts a maximum of 12.8% under the given conditions. The discrepancy is within the error margin of the model.

Last, it is noted that the predicted efficiencies are well beyond what can be found in current ORC plants, particularly for smaller scale systems. Quoilin et al. [129] state that current thermal efficiencies for ORC plants do not exceed 24%.

3.4.3 System analysis and optimisation of a Kalina Split-cycle for waste heat recovery on large marine diesel engines

For large ships, the fuel expenses constitute about 30-55% of the total operational costs, depending on the type of vessel [24]. Hence, in times with high fuel prices, there are significant economic advantages associated with investing in a diesel engine exhaust WHR system [36]. The higher the fuel price, the larger investment in the WHR system can be allowed. Moreover, when considering very large ships, the large scale makes it feasible to consider relatively complex systems, compared to other WHR applications.

With a WHR system output of about 10-11% of the main engine power, the Kalina cycles perform at a very similar level as is found for other advanced types of WHR systems. An example is the cascade type system, consisting of a steam Rankine cycle combined with an ORC in a combined cycle for marine engine WHR, studied by Choi et al. [211]. As mentioned, MDT have presented studies of single- and dual-pressure steam WHR systems with an output of up to 11% of the engine power, when using an additional exhaust gas power turbine and also utilising the charge air and jacket water heat streams [18]. The Kalina cycle outputs are comparable, but the heat source inlet temperatures are significantly higher, because the engines in the case study are four-stroke engines. Compared to the ORC performance found by Bombarda et al. [169], the Kalina Split-cycles in the present work are shown to be superior at the same boundary conditions; however, the efficiency estimated using the regression models suggests that a recuperated ORC can achieve a higher efficiency than the Split-cycle with reheat.

In comparison with the working fluid of the steam cycle, the toxicity of ammonia-water mixtures prompts the use of additional safety measures in the machinery rooms on board ships. Even more so will the use of ORC working fluids, which can be seriously hazardous, especially the organic fluids. For the Kalina cycle, ammonia and their mixtures with water are already in use in marine refrigeration applications and for the reduction of NOx emissions using urea in selective catalytic reduction installations on board; however, the concentrations of the solutions may not be as strong as for the Kalina cycle. Ammonia-water mixtures are naturally occurring and have a relatively low environmental impact compared to the ORC refrigerant fluids which are investigated by Yang et al. [212], among others. Moreover, when considering only low hazard and environmentally friendly working fluids in ORCs, the efficiency is much lower than the thermodynamically optimum solution, as shown earlier (See Fig. 3.17).

The simplified cost analysis shows that the payback time is very short compared to the ship lifetime. MAN Diesel & Turbo [18] estimate a payback time of 4-6 years for steam cycle WHR systems of similar complexity, and this is likely to be more realistic than the 2-2.5 years found in the present study for the Kalina cycles. The dual-pressure steam cycle

presented by MAN Diesel & Turbo is as complex as the Kalina cycle, and this suggests that the Kalina cycles should not be rejected due to their complexity or for economical reasons.

The component cost figures used are based on past purchase orders and experienced professional estimations [194]. The pump and turbine costs could alternatively be estimated based partly on the working fluid properties as done by Zare et al. [213] for ORC systems. This would be useful, when considering the reheat option as the expander size and price is then affected; However, since the working fluid is ammonia-water and the process is not similar to a small scale ORC, and to keep the cost analysis coherent, values from Rodriguez et al. [194] are used.

A serious challenge for the application of the Kalina cycles may be the size of the boiler heat exchangers. The space inside a cargo ship is valuable; although it is difficult to estimate the exact value. Compared to Wang et al. [171], who analysed a simple ammonia-water Rankine cycle driven by exhaust gas, the $\overline{U}$A values found in the present study are 8-10 times larger for the Kalina cycle and even higher for the Split-cycle. Also the realisation of recuperator 2 and evaporator 1 in the Split-cycle may present challenges. The relatively high boiler pressures could also be mentioned as a drawback in terms of cost and safety.

A simulation using the same process and parameter values as used by Bombarda et al. [169], was the starting point for this work. When applying the genetic algorithm, the optimised output was about 100 kW or about 6% greater. This indicates the level of the challenge of optimising the Kalina process with its relatively large number of design parameters. The additional Split-cycle components further increase the complexity of the optimisation process, suggesting that applying a multi-variable optimisation algorithm is a useful strategy. With up to nine parameters, the algorithm is first used to find the near-optimum area and is then applied again with narrower ranges of parameter limits in an effort to find the true optimum. Still, several attempts of finding and verifying the optimum are needed, a drawback to this methodology.

An optimisation result found using the genetic algorithm is not guaranteed to be the true optimum. Intermediate results during the optimisations revealed that the algorithm pursued two strategies simultaneously in the effort to maximise the power output: i) reducing the turbine exhaust pressure by also reducing the working fluid concentration and turbine inlet pressure, and ii) increasing the turbine inlet pressure and working fluid concentration. Although Table 3.15 presents the optimum parameters, different combinations of parameters can result in almost equally high efficiencies. This explains to some degree why the trends of the optimised parameters are somewhat unclear.

In the application of WHR systems on large marine engines, the engine jacket cooling water and turbocharger charge air cooling streams may also be integrated into the Kalina Split-cycle; the following chapter treats this option. Based on the present analysis, it is

proposed to place these heat sources where they will enable the further dilution of the condensing stream. Depending on the temperature of the turbine exhaust, additional heat could successfully be supplied to the separator feed stream, before and/or after Recuperator 1 (see Fig. 3.10, p. 93).

Theoretically, using the Split-cycle boiler technique of changing the working fluid concentration during preheating and evaporation, is not limited to the Kalina process. ORCs operating with zeotropic mixtures may benefit from splitting the working fluid streams in a similar way, and further studies on this topic are recommended based on the present findings; however, the Kalina process in the form presented here, with a separator playing the significant role as described in the analysis, is designed specifically for the fluid properties of ammonia-water. Preliminary studies (made by the present author) of the process using other fluid mixtures did not lead to advantages compared to ammonia-water mixtures.

4 Comparison of waste heat recovery systems

This chapter presents two separate studies of the combined cycle, consisting of the two-stroke diesel engine and a WHR system. As opposed to the already presented studies, this chapter includes studies where the main engine parameters are tuned in order to improve the WHR system and the combined cycle performance. Firstly, the power turbine and the three previously presented WHR system alternatives are compared with regards to combined cycle power, SFOC and NOx. Secondly, a study of the simultaneous optimisation of the SFOC and the NOx emissions using the marine two-stroke engine and different configurations of turbocharger, power turbine and an ORC WHR system is presented.

4.1 Introduction

In this section brief outlines of the two mentioned studies are provided as well as the general introduction to each of the studies.

A comparison of advanced heat recovery power cycles in a combined cycle for large ships is a study that compares the performance parameters and important qualitative aspects of a dual-pressure steam Rankine cycle, an advanced Kalina cycle and an advanced organic Rankine cycle. All three cycles utilise the three major waste heat sources; i.e., the heat from the exhaust gas, the charge air cooler and the engine jacket water cooler. The aim is to compare the cycles on an even basis not only considering the thermodynamic performance.

Development of a model for the prediction of the fuel consumption and nitrogen oxides emission trade-off for large ships is a study which presents an approach suitable for the analysis of the part-load performance of the main engine, turbochargers and organic Rankine cycle WHR systems; five different system configurations are compared. The aim is to evaluate the SFOC-NOx trade-off for various WHR system configurations, including the effects of using an exhaust gas recirculation (EGR) system.

4.1.1 A comparison of advanced heat recovery power cycles in a combined cycle for large ships

Being among the most common types of vessels in the current world fleet, the case in focus in this study is a feeder class container ship which has a typical capacity of 2500 TEU

(twenty foot equivalent units) containers and a length of 200 meter. Widely used in this class, and used in this case study, is the previously described 7L70MC engine.

WHR systems are not yet standard in this class of vessels although solutions are currently available, namely either a steam Rankine plant or alternatively an exhaust gas power turbine. In the literature, the most often mentioned alternatives to the steam cycle are the ORC and the Kalina cycle. The ORC is proposed for WHR in maritime applications by MAN Diesel & Turbo [18] as a WHR solution for smaller engines. As mentioned, the literature provides studies [147, 162] suggesting that the Kalina cycle possess the potential to achieve higher conversion efficiencies for WHR in general, compared to both ORC and steam Rankine cycles; however, controversy exists and modelling efforts [169] show that the performance of ORC and Kalina may at best be similar, for the marine application.

The goal of the present study is thus to compare the three power cycles for the mentioned case study. The net power output of the cycles is the main parameter for comparison. It is assumed that a shaft motor is applied for the conversion of the WHR system power to propulsion power. Therefore the net power of the combined cycle determines the resulting SFOC and specific NOx emissions of the combined cycle. In addition, important qualitative implications are considered in the comparison of the three different power cycles.

Though the concepts of the mentioned combined cycle processes are well described in the literature e.g., by MDT [18], modelling efforts for the design and optimisation are not; however, one well described example is as mentioned Danov and Gupta [34, 35], who present a comprehensive mathematical model of a marine turbocharged diesel engine and a single-pressure level steam Rankine WHR system including the associated auxiliary components. Validation of the model is presented at varied engine loads and speeds and the resulting fuel consumption is analysed.

In contribution to previous studies, the present study includes the estimation of the NOx emissions and it includes the direct comparison of three power cycles; a dual-pressure steam Rankine cycle, a Kalina cycle and an ORC; all modified to integrate the three available heat sources. In addition, the ORC optimisation method is more comprehensive, compared to previous work described in the literature, because it includes the previously described methodology (Sec. 3.2.1) aiming at the simultaneous optimisation of the process layout, the working fluid and the operating parameters.

4.1.2 Development of a model for the prediction of the fuel consumption and nitrogen oxides emission trade-off for large ships

The modest reduction from IMO Tier I to Tier II (about 15%) imposed as of 2011, can be achieved in various ways, simplest by adjusting the engine parameters, e.g., the valve and injection timings; however, it is well known that such measures used to reduce the NOx often lead to increases in the SFOC and vice versa. Exhaust gas recirculation (EGR) is well known to strongly reduce NOx emissions, and EGR can therefore also affect this NOx-SFOC trade-off mechanism and lead to reduced SFOC while complying with NOx regulations [30].

As mentioned, the IMO NOx emission limits are defined as a weighted average at four engine loads, 100, 75, 50 and 25% (ISO 8178). Normally, ship engines run at part-loads a significant part of the time [214]; hence, the analysis of the part-load performance is important.

The design and optimisation procedure will likely result in superior combined cycle performance when considering the parameters of both the main engine and the WHR system simultaneously. However, the consequence is that a relatively large number of parameters is involved in the process and the cost of experimental tests at this scale is high. Motivation is therefore present for the detailed modelling of the combined cycle.

The novel academic contributions of the present work are summarised as follows. The present study builds upon previous results (see Sec. 2.3.3) by studying the potential of engine tuning to enhance the combined cycle performance. Thus, an investigation aiming at quantifying the part-load weighted SFOC-NOx trade-off is presented along with methodologies for the optimisation of the performance of five different system configurations based on the two-stroke marine diesel engine. The configurations include a power turbine, an EGR system, an ORC WHR system and a hybrid T/C and ORC system. The optimisation efforts include the main engine tuning parameters, namely, the injection and valve timings, air and fuel mass flow rates and the scavenging pressures, which are optimised simultaneously with the WHR system operating parameters. In the above mentioned studies, and in other studies that can be found in the open literature concerning marine two-stroke engine systems, the aspect of main engine tuning has not been considered from a system perspective to the detail presented in this work. Moreover, investigations of the SFOC and NOx trade-off, whilst considering the part-load behaviour of all system components, have, to the best knowledge of the author, not been presented for the mentioned type of combined cycle systems. Finally, studies that include the innovative combination of using a hybrid type turbocharger together with an ORC for WHR on the two-stroke engine have also not been presented before.

4.2 Methodology

This section describes aspects of the methodologies of the two studies, that are not already described in the previous sections.

4.2.1 A comparison of advanced heat recovery power cycles in a combined cycle for large ships

The engine model used in this study is the same as described earlier in the present work (see Ch. 2). An initial calibration attempt was done for the present study preceding the final validation shown in Sec. 2.3.2. The procedure is described as follows to match measured performance data from Goldsworthy [72]:

1. The end of injection timing was adjusted to obtain correct maximum cylinder pressure.
2. To obtain correct brake power output, the time of opening the exhaust valve was adjusted.
3. It was chosen to investigate a case of a mechanically controlled engine and therefore the best compromise for the exhaust valve opening time for both loads 75% and 100% was selected.

All the WHR models are made using Matlab 2010b in combination with the NIST Refprop fluid property database [107] and are otherwise similar to the already presented approaches.

An integrated steam cycle

As inspiration for the steam Rankine cycle process layout in this study, is the plant currently proposed by MDT [18]. The process flow diagram is shown in Fig. 4.1 and the process description is provided in Sec. 3.1.3 (p. 70).

An integrated Kalina cycle

The Kalina cycle is proposed in many different configurations and in the present comparison, the model is made with a configuration similar the one presented in Sec. 3.2.3 and

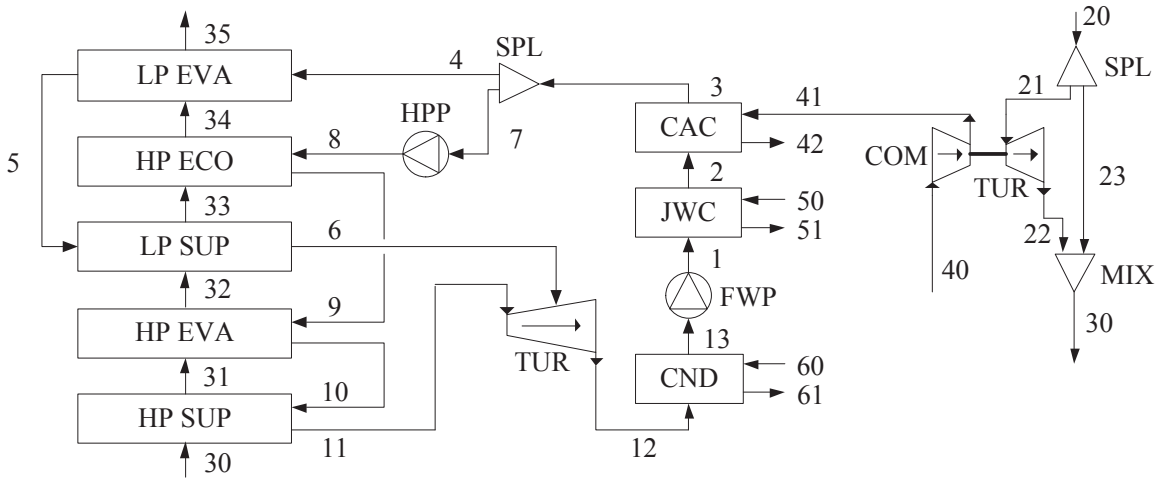

Figure 4.1: Steam cycle process flow diagram

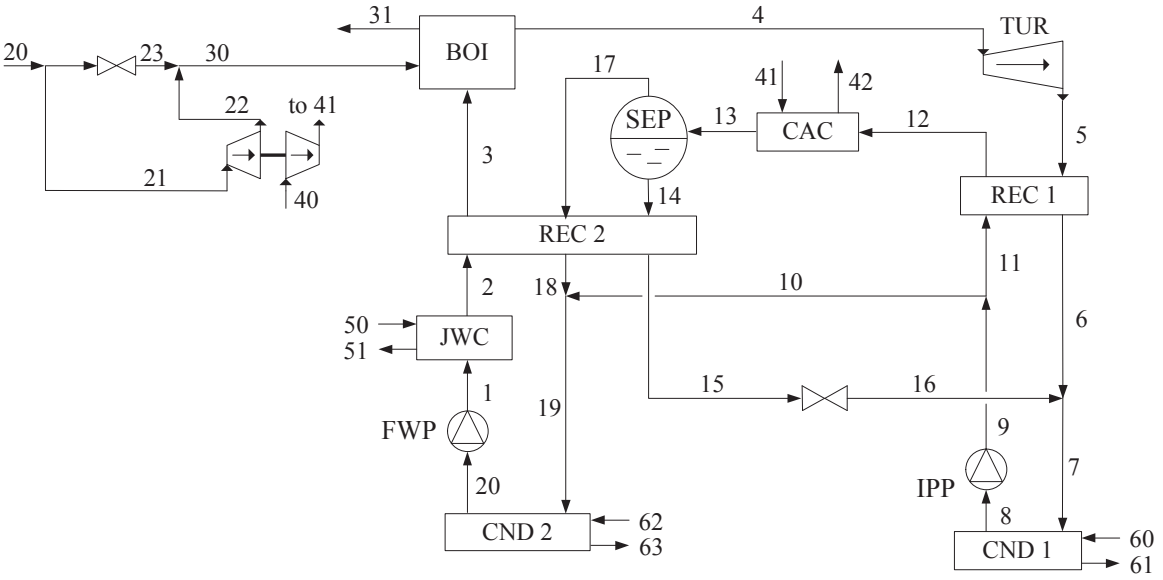

Figure 4.2: Kalina cycle process flow diagram

to those suggested in work by Jonsson et al. [148] and Bombarda et al. [169], which are there found suitable for the marine application.

Figure 4.2 illustrates the process flow diagram of the Kalina cycle and the T/C. Starting from the feed water pump (FWP), the working fluid (1) is preheated in the jacket water cooler (JWC) and further in a recuperator heat exchanger (REC 2). The fluid then enters the boiler (BOI) where the exhaust gas from the engine (30) rejects heat in order to preheat,

evaporate and superheat the working fluid. Power is extracted from the fluid in the turbine (TUR) where after the fluid give off heat in the recuperator (REC 1). The stream (6) is then mixed with another stream (16) before it is condensed. After the condenser, the stream (8) is pumped to an intermediate pressure before it is split into two streams (10) and (11). Stream (11) is heated via REC 1 and heated again via the CAC. The stream (13) then enters a separator which separates the stream into an ammonia lean liquid stream (14) and an ammonia rich vapour stream (17). Both of these streams give off heat in REC 2. The rich stream (18) is then mixed with stream (10) before it is condensed again.

As mentioned, to obtain maximum power, the stream running through the turbine (4), needs to be as ammonia rich as possible and at the same time the outlet pressure needs to be as low as possible. However, high ammonia concentrations require relatively high condensation pressures; therefore, the separator supplies a stream of fluid with a relatively low concentration of ammonia (14), which is mixed with the turbine outlet stream (6). The separator also has to supply an ammonia rich stream (17) to be mixed with the stream that is condensed (10), at a sufficient rate in order to restore the stream concentration which again will be running through the turbine.

For the separator to be able to deliver these concentrations and flow rates, the main concern is to ensure that the separator feed temperature is high enough and the feed pressure is low enough. The feed pressure is dictated by the need for condensation and thus depends also on the working fluid concentration and cooling water temperature and flow in condenser 2 (CND 2). Most important is the feed temperature which normally depends on the recuperation of energy from the turbine outlet stream; however, at low turbine outlet pressures there might not be enough heat to recuperate; hence, there is a motivation for inserting the heat source of the charge air cooler (CAC) at this point (12).

Alternatively the CAC can be placed to preheat and possibly evaporate the feed stream in points (2) and (3); however, by placing the CAC to heat the separator feed stream and then having a second recuperator (REC 2), it may be possible to recover most of the CAC heat for the feed stream anyway. Another alternative would be to place the CAC as a source for reheating of the fluid after the turbine. These options are merely suggestions and are not explored in the present study under the assumption that the present placement is the best alternative.

The turbocharger is integrated in the same way for the Kalina cycle and the ORC, as shown in Fig. 4.2 and as described in Sec. 3.1.3, p. 69.

An integrated organic Rankine cycle

Figure 4.3 illustrates the ORC process flow diagram. Working fluid enters the JWC at high pressure (1). The fluid is then heated further in a recuperator (REC) and in the CAC before entering the boiler. After the boiler, the fluid is expanded in a turbine before giving off heat in the recuperator (6). It is then condensed and pumped back to high pressure.

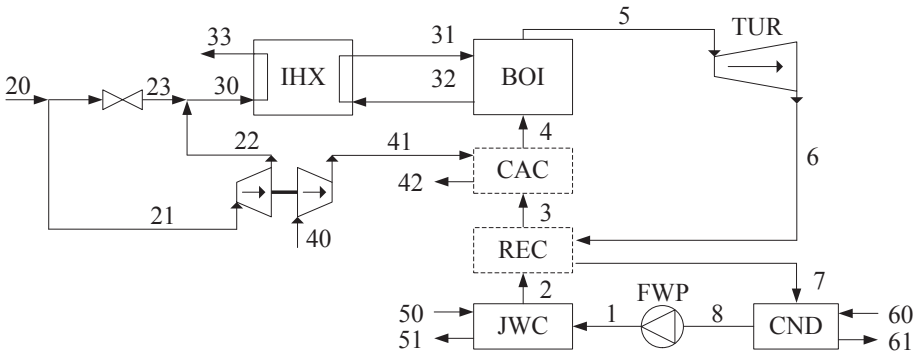

Figure 4.3: Organic Rankine cycle process flow diagram

In all other aspects the presently applied ORC model is identical to the one described in Sec. 3.2.1 and also in this case a total of 109 fluids from the Refprop fluid properties database are tested.

The great amount of heat possessed by the dry type of fluids after expansion may in this configuration 'compete' with the available heat from the jacket water and the charge air, in the sense that not all the heat be utilised in this cycle. Therefore an adaptable model is developed, such that the fluid properties, the different temperature levels and heat available can influence the process layout. Figure 4.3 shows dashed lines around the CAC and the recuperator (REC) to illustrate that these components are optional for the process. Also the superheater is optional but as before it is chosen to have the degree of superheating be an optimisation variable.

Moreover, to avoid a situation where a leakage results in the highly flammable organic working fluids coming into contact with the hot exhaust gasses, an intermediate loop of heat transfer fluid (IHX) is inserted to transfer the heat to the boiler. A fluid designed for this purpose is a heat transfer fluid called DOWthermQ from the DOW chemical company and it is modelled as suggested by Pierobon et al. [215].

Turbines

A trend in the recent literature about optimisation of organic Rankine cycles, is to include the consideration of component design and cost estimation. The total cost of an ORC plant seems to depend mainly on the costs of the heat exchangers and the expander. Toffolo et al. [216] provide examples of different studies which estimate the turbine costs to be up to 50% of the total equipment cost.

Angelino et al. [121] proposed already in 1984 to correlate the size and efficiency of a turbine with the working fluid properties using the size parameter (VH):

$$VH = \dot{V}_o^{0.5} \Delta h_s^{-0.25} \tag{4.1}$$

where the VH value is proportional with the turbine size. Moreover, the volumetric expansion ratio, i.e., the ratio of the outlet and inlet volumetric flow ratios, is considered to be similarly important; low volumetric expansion ratios enable high efficiencies [123].

Astolfi et al. [217] present a simplified procedure useful for the evaluation of axial turbine design and efficiency. Using the isentropic enthalpy drop over the turbine and the volumetric flow ratio, the number of turbine stages can be estimated. Astolfi et al. [217] state that a stage must be added for every 65 kJ/kg enthalpy drop, while the maximum volumetric flow ratio for each stage is 4. The cost can then be estimated using the number of stages and the size parameter.

Optimisation

Also in this study the Genetic algorithm is used to optimise the model parameters, which for all the WHR systems are the boiler pressure, and in the case of ORC and Kalina, the fluid and solution concentration, respectively. For the steam plant, the mass flow rate fraction in the high pressure circuit is optimised and for the ORC, the superheater approach and the process layout are optimised. The turbine outlet pressure is optimised for the Kalina cycle only. The optimisation variable limits are all kept sufficiently wide, such that the optimum solutions are not limited by the boundaries. An exception is the evaporation pressure of the ORC which is kept sub-critical, i.e., lower than 95% of the respective critical pressure of the working fluid.

Modelling parameters and conditions

Table 4.1 lists the design and operation parameters used for the WHR process models. The exhaust gas temperature at the boiler exit is again limited to 160°C for the prevention of sulphuric acid corrosion on heat exchanger surfaces. Since the turbocharger compressor and turbine operates at a limited pressure range and at the same conditions for all simulations, using an isentropic efficiency is assumed adequate. Efficiencies for the T/C are calculated from the calibration case presented by Goldsworthy [96] at loads 75% and 100%.

Table 4.1: Design and operation parameters

Minimum superheater approach (°C)	20
Exhaust gas temperature after boiler (°C)	160
Minimum evaporator pinch point temperature difference (°C)	10
Minimum turbine steam quality (%)	85
Condenser working fluid outlet temperature (°C)	40
WHR turbine polytropic efficiency (%)	80
Power turbine isentropic efficiency (%)	89
Pump isentropic efficiency (%)	80
T/C compressor isentropic efficiency (%)	84
T/C turbine isentropic efficiency (%)	89
Charge air cooler pinch point temperature difference (°C)	10
Jacket water cooler pinch point temperature difference (°C)	5
Recuperator pinch point temperature difference (°C)	10

4.2.2 Development of a model for the prediction of the fuel consumption and nitrogen oxides emission trade-off for large ships

In the following the studied system configurations are presented. Then follow descriptions of the models of the individual components and finally the optimisation methodology is outlined.

System configurations

Five system configurations are investigated individually with regards to the SFOC-NOx trade-off: 1) The baseline configuration is a diesel engine with three T/Cs and an auxiliary blower (AB), 2) an exhaust gas power turbine (PT) is added to the baseline system, 3) the baseline with an EGR system, 4) the baseline with an ORC exhaust WHR system, and 5) the diesel engine with three hybrid T/Cs and an ORC exhaust WHR system and no AB.

The simplified system layout of configurations 1-3 is outlined in Fig. 4.4. Each T/C consists of a radial flow compressor (C) and a single-stage axial-flow turbine (T). A throttle valve is used to bypass the amount of exhaust gas which is in excess in relation to powering of the T/Cs. An AB is used to provide the needed air flow and pressure at 25% load. Ambient air enters the compressors and is cooled in the air cooler before it enters the scavenge air receiver and finally the engine. The engine exhaust enters the exhaust receiver from where it can be directed to the EGR system, the power turbine, the T/Cs and the bypass. In the PT configuration (2), the mentioned excess exhaust gas is expanded to produce electrical power via a generator (G), which is then converted back into propulsion power using a propeller shaft motor (SM).

In the EGR configuration (3), 10% of the exhaust is recirculated through an EGR cooler (EC) and an EGR blower (EB) is used to provide the needed flow and pressure. This EGR arrangement is directly inspired by the work on marine EGR systems presented by Kaltoft et al. [30] and not all the components are depicted, most importantly the exhaust scrubbers, a water mist catcher, valves and mixing chambers, which are considered to be of minor influence to the results.

Figure 4.5 illustrates a configuration of the main engine fitted with hybrid turbochargers and an ORC for exhaust gas heat recovery. The hybrid T/C is a turbocharger with an electric motor and generator (G) on the same shaft as the compressor and turbine (see Sec. 4.2.2). Electrical power produced by the ORC and hybrid T/Cs is converted into shaft power using the shaft motor.

Figure 4.6 illustrates the ORC configuration where the working fluid first enters a pump

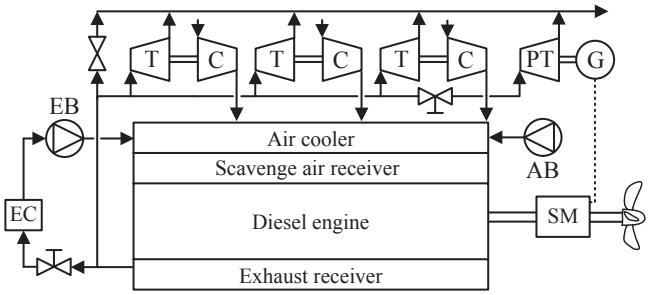

Figure 4.4: Sketch of configurations 1-3

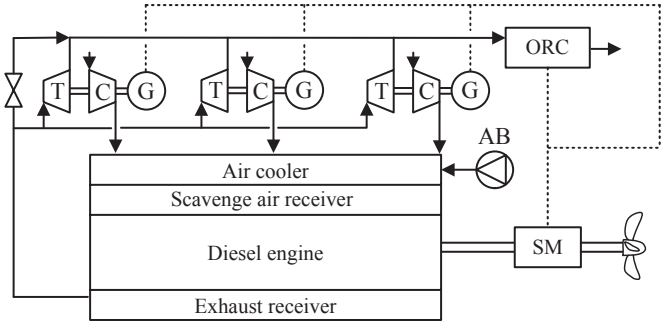

Figure 4.5: Sketch of configurations 4 and 5

and is then preheated in a recuperator. The fluid is then further preheated, evaporated and finally superheated using the exhaust gas. The fluid then expands in a turbine while producing power via a generator, before the remaining heat is transferred to the working fluid again and is finally condensed in the condenser.

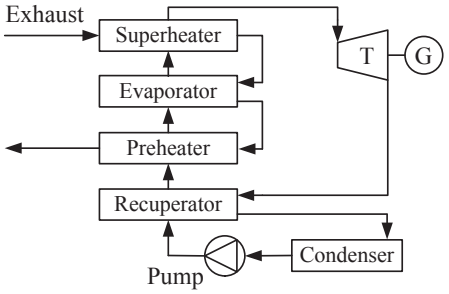

Figure 4.6: Sketch of the ORC process

Turbochargers and blowers

The T/Cs were modelled using compressor and turbine maps for a turbocharger model type (ABB A175) which is slightly smaller than the type A185, that is recommended by the manufacturer of the 12K98ME engine. The maps were provided by ABB and are kept confidential as to the request of ABB. The compressor and turbine maps were scaled by applying the methodology presented by Kurzke [218], with the volumetric flow at 100% load representing the reference point. A compressor operating line was drawn on the map to ensure maximum isentropic efficiencies for the loads 50-100%, while maintaining a surge safety margin of 15% [39] and an even larger choke margin. The relationship between mass flow rate ($\dot{m}$), pressure in and out (P_i and P_o) and inlet temperature (T_i) for the T/C turbine is governed by the Stodola [219] turbine constant (C_T):

$$C_T = \frac{\dot{m}\sqrt{T_i}}{\sqrt{P_i^2 - P_o^2}} \tag{4.2}$$

The compressor and turbine isentropic efficiencies were derived from the mentioned maps. Thermodynamic properties of the air and exhaust gas were obtained using Refprop version 9 [107]. The power turbine and the hybrid turbines were assumed to have the same characteristics as the T/C turbines. See also Sec. 2.2.10 (p. 47).

The power consumption of the auxiliary and EGR blowers were estimated by dividing the product of the averaged volumetric flow rate and the inlet and outlet pressure difference with a constant efficiency. A pressure drop of 0.02 bar over the EGR cooler was assumed [30].

The hybrid turbocharger

It is well known that the exhaust gas temperature from the low-speed two-stroke diesel engine is low compared to other engine types, especially at low loads. The T/C efficiency is therefore required to be relatively high in order to provide the required scavenging pressures and flows, using only the exhaust gas to drive the compressors. This has driven the development to the point where the T/C efficiency is higher than needed at high loads.

Mitsui [220], Mitsubishi [221] and others have proposed a hybrid type T/C (HTC) which consists of a turbine and a compressor directly coupled to a high-speed electric generator/motor (see Fig. 4.5). At high load conditions, additional electrical power can be produced and at low loads the motor can add needed power. With this system it is claimed that the auxiliary blower can be removed as well as the power turbine, thus simplifying the

system. Moreover, the hybrid T/C provides an additional degree of freedom in the engine tuning because the WHR system can provide power to assist the T/Cs at any point.

The organic Rankine cycle

The pump was modelled in a similar way as done by Quoilin et al. [222], but due to the larger scale of application, it was assumed to have a higher overall efficiency; the coefficients (a, b, c and d) were therefore adjusted to make the pump characteristics resemble those of commercially available centrifugal pumps [223]. The pump isentropic efficiency (η_p) at part-load relative to the design point efficiency ($\eta_{p,d}$) is thus defined as a function of the volumetric flows at part-load and design point ($\dot{V}$ and $\dot{V}_d$):

$$\frac{\eta_p}{\eta_{p,d}} = a\left(\frac{\dot{V}}{\dot{V}_d}\right)^3 + b\left(\frac{\dot{V}}{\dot{V}_d}\right)^2 + c\frac{\dot{V}}{\dot{V}_d} + d \tag{4.3}$$

with constants a, b, c and d equal to -0.168, -0.0336, 0.6317 and 0.5699. Estimation of the turbine isentropic efficiency was based on the work on axial steam turbines by Schobeiri [224]. Manente et al. [225] recently applied a very similar approach in a model of a large scale geothermal ORC power station. The relative isentropic efficiency at any load is defined as follows:

$$\frac{\eta_s}{\eta_{s,d}} = \frac{N}{N_d}\sqrt{\frac{\Delta h_{s,d}}{\Delta h_s}}\left(2 - \frac{N}{N_d}\sqrt{\frac{\Delta h_{s,d}}{\Delta h_s}}\right) \tag{4.4}$$

where h is enthalpy, and the subscripts s and d are short for isentropic and design point. Δ symbolises the difference between inlet and outlet. The relationship between expander pressures, temperatures and mass flow rates is governed by the law of the ellipse by Stodola [219] (Eq. 4.2).

The overall design point UA values ($\overline{U}A_d$) for each heat exchanger were determined by dividing the heat flow rate with the logarithmic mean temperature. At part-load conditions the UA values correlate with the mass flow rates as follows:

$$\overline{U}A = \overline{U}A_d\left(\frac{\dot{m}}{\dot{m}_d}\right)^m \tag{4.5}$$

Table 4.2: Weighting factors for NOx

Engine speed (%)	100	91	80	63
Brake power (%)	100	75	50	25
Weighting factor (-)	0.2	0.5	0.15	0.15

where $\overline{U}$ is the overall heat transfer coefficient and A is the heat transfer area. It was assumed that a once-through boiler is to be applied and that the heat transfer is dominated by the gas flow on the outside of the tubes. Therefore, a value of 0.6 was selected for the exponent m in reference to Incropera et al. [226].

Haglind [227] presented, for the application on board large ships, an expression for the generator part-load efficiency (η_e) as a function of the load (l), the design point efficiency ($\eta_{d,e}$) and the copper loss fraction (F_{cu}), which was adjusted to 0.43 to match manufacturer data:

$$\eta_e = \frac{l\eta_{d,e}}{l\eta_{d,e} + (1-\eta_{d,e})\Big[(1-F_{cu}) + F_{cu}l^2\Big]} \tag{4.6}$$

Based on the review of Bao et al. [123] and on the work previously presented (see Sec. 3.3.1), the selection of working fluids for investigation includes R245fa, R365mfc, R236ea, hexamethyldisiloxane, isohexane, cyclopentane, toluene and benzene.

4.2.3 Optimisation

To perform the optimisation a Genetic algorithm function (*gamultiobj*) from the Matlab [184] *optimtool* toolbox was used. The algorithm optimises both the NOx and the SFOC simultaneously forming a Pareto front, which is a line of optimum solutions, where at any point the value of one objective cannot be reduced without increasing the value of the other [44]. This algorithm was chosen because it is particularly suitable for optimisation in cases with many parameters and in cases where a global minimum might not be located due to the presence of local minima. The default parameters [184] were used for the *gamultiobj* function, except for the number of generations which was set to 50-100 and the number of individuals was set to 4,000-15,000 depending on how easily the algorithm seemed to be able to find the optima. These values were found to provide a reasonable compromise between repeatability of the optimisation results and computational cost, which is important considering the time consumption of the optimisations was between 3-21 days per result, using a machine with a 64-bit quad-core i7 3.2 Ghz processor.

Table 4.3 presents the optimisation parameters and their boundaries, which were chosen wide enough to ensure that the optima would not be limited by the parameter variation limits. The start of injection time (SOI), end of injection time, exhaust valve closing time (EVC), scavenge pressure (P_{sc}) and fuel mass flow rates ($\dot{m}_f$) were optimised independently for each load (25, 50, 75 and 100%). The air mass flow rates ($\dot{m}_a$) were optimised only at design point, i.e., 100% load and at 25% in cases with an auxiliary blower. The mass flow rates at 75 and 50% load were determined by the pressure and the compressor operating line. P_{cr} is short for the fluid critical pressure, and ΔT_{pp} is the minimum pinch point temperature difference.

Table 4.3: Optimisation parameters and limits

	Limits
Start of injection (CAD)	± 5
End of injection (CAD)	± 10
Exhaust valve closing (CAD)	± 10
Scavenge pressure (%)	± 10
Fuel mass flow rate (%)	± 10
Air mass flow rate (%)	± 10
ORC boiler ΔT_{pp} (°C)	10-100
ORC recuperator ΔT_{pp} (°C)	10-75
ORC evaporation pressure (bar)	3 - 0.95P_{cr}

The part-load performance of the ORC depends on the applied control strategy; in the present case a sliding-pressure mode was adopted. The part-load evaporation pressures are thus governed by the Stodola equation (Eq. 4.2), by the heat transfer processes and by the pump characteristic curve. The latter component is here equipped with a variable frequency motor. This feature allows to investigate different operational modes, for example, keeping the turbine inlet temperature constant; however, results suggested that keeping the boiler exhaust gas outlet temperature constant, at the minimum allowed temperature (160°C), lead to the highest combined cycle work outputs. In addition, an advantage of applying this strategy is that it ensures that sulphuric acid condensation in the heat exchangers is effectively prevented, particularly at low loads.

The optimisation algorithm was furthermore programmed to discard solutions which violate a minimum temperature approach of 10°C, between the outlet of the recuperator and the boiling temperature, to prevent evaporation in the preheater.

It was decided to disable the ORC at 25% load because it was found that the combined cycle plant could be optimised to perform better overall, when only operating at 50-100% loads. This is partly due to the required ORC boiler exhaust outlet temperature, creating a low temperature difference between the heat source inlet and outlet at low loads. Another reason is that the IMO weighting factors strongly favour the performance at 75% load (see Table 4.2).

For the type of system under study, the engine crank shaft is directly coupled to the propeller shaft, i.e., the engine turns at the same speed as the propeller. The IMO rules specify that for the evaluation of the SFOC and NOx, the engine has to operate under the constraint of the propeller law, which states that the engine brake power divided by the engine revolutions (rpm) to the power of three, must be constant [46]. This constant is related to the characteristics and working conditions of the propeller, and this relationship was respected at all loads, using the value of the constant calculated at standard tuning conditions. Hence, the propeller law poses an important constraint for the optimisation of the engine operational parameters. A one percent tolerance was allowed in order to facilitate the convergence of the optimisation, a value corresponding to the measurement inaccuracy allowed by the IMO [110].

The sequence of running the models during optimisation was as follows: first the engine with turbochargers was simulated at loads 100, 75, 50 and 25%. Then the ORC was simulated at design point to determine the design point power, UA values, turbine constant and other outputs. Then, the ORC was simulated at part-loads 75 and 50%. Finally, the propeller constant was calculated, and the deviation from the standard tuning value, was used as a factor to increase the values of the SFOC and the NOx. This way the optimisation algorithm simultaneously optimised the system parameters and minimised the deviation from the propeller law.

4.2.4 Modelling conditions

Table 4.4 lists the modelling boundary conditions. The pressure rise is the difference between the compression pressure and the maximum pressure, and a value corresponding to the reference tuning of the engine was selected, to have the same level of resulting mechanical stresses [228]. However, to enable the investigation of the optimum maximum cylinder pressures, no upper limit was specified.

4.3 Results and analyses

4.3.1 A comparison of advanced heat recovery power cycles in a combined cycle for large ships

First in this section, results from the main engine calibration and tuning are presented. Then the combined cycle performances are compared. Finally, a qualitative evaluation of other relevant aspects concerning each of the cycles is presented.

Table 4.4: Modelling conditions

Organic Rankine cycle	
Pump design point efficiency (%)	72
Turbine design point efficiency (%)	80
Generator design point efficiency (%)	98
Condenser outlet temperature (°C)	30
Diesel engine	
Ambient air temperature (°C)	25
Ambient pressure (bar)	1.013
Cooling water temperature (°C)	25
Minimum exhaust temperature (°C)	160
Allowed pressure rise (bar)	30
Blower efficiencies (-)	0.70

Engine model

Table 4.5 presents calculated outputs from both the calibration efforts and the engine tuning (designated *WHR engine*). Calibration data are shown in the parentheses for the 75% and 100% load cases, and these are obtained at ISO ambient reference conditions, i.e., 25°C and 1 bar pressure.

At 100% load, the model under-estimates the power output, while it is over-estimated at 75% load. Conversely, the SFOC is over-estimated at 100% load and under-estimated at 75%. The deviations are within 1% accuracy while NOx emissions are predicted with a 5-10% deviation.

Except for the jacket water heat, the overall energy balance of the engine seems to be predicted accurately. In the work of Goldsworthy [96], i.e., the source of the calibration values, it is not made clear whether lubrication oil heat from the engine is included in the stated amount of heat from the engine. If that is the case, then the calculated results are with an accuracy of 5-10% of the reference values. The uncertainties of the experimental data provided by Goldsworthy [96] are unfortunately not described.

The main engine parameters are tuned such that the exhaust gas temperature is suitable for WHR at a design point of 85% MCR; the effects of changes in injection timing, scavenging pressure, fuel and air mass flow rates and cylinder wall temperature were investigated. A targeted increase of the exhaust gas temperature of 50-65°C is set as is in accordance with what is stated by the engine manufacturer [18].

The exhaust gas temperature after the T/C for the standard tuning 85% load is 179°C and the application of a WHR system is assumed infeasible in this case. A combination of 10% lower charge pressure, 10% lower inlet air mass flow rate and an increase of 100°C of the averaged cylinder wall temperature, is found to be a fuel effective way to gain an

Table 4.5: Engine model outputs

Performance characteristics	Standard	Standard	Standard	WHR engine
Load (%)	100	85	75	85
Power (MW)	19.66 (19.81)	16.93	14.92 (14.86)	16.93
SFOC (g/kWh)	175.3 (174.0)	170.6	170.4 (171.1)	173.3
NOx (g/kWh)	14.5 (13.6)	15.8	16.3 (17.6)	17.3
Maximum pressure (bar)	141.0 (141.0)	135.5	126.0 (126.0)	128.3
Exhaust temperature before T/C (°C)	344 (333)	302	281 (284)	344
Exhaust temperature after T/C, (°C)	204	179	173	234
Charge air temperature after T/C (°C)	181	161	146	148
Fuel mass flow (kg/s)	0.90	0.81	0.70	0.82
Exhaust mass flow (kg/s)	52.1	46.2	41.9	42.1
Charge air mass flow (kg/s)	51.2	45.4	41.2	41.3
Jacket water heat (MW)	2.28 (3.00)	2.24	2.18 (2.40)	2.16

increase of 55°C. The increased wall temperature causes an additional thermal loading of the engine, which is however not considered in this work. It is seen in Table 4.5 how this tuning also causes reduced jacket water heat and a reduced temperature of the charge air.

Combined cycle performance

A comparison of the calculated performances of the combined cycles is shown in Table 4.6. The results suggest that the maximum obtainable net power production is highest for the ORC. The steam Rankine produces only about 75% of the power of the ORC and the Kalina process has a similar output. The SFOC and NOx emissions are reduced accordingly.

Table 4.6: Optimised performance

	Engine	Steam	ORC	Kalina	Power turbine
WHR power production (MW)	-	0.863	1.165	0.825	0.453
Total power production (MW)	16.93	17.80	18.10	17.76	17.39
SFOC (g/kWh)	170.6	164.9	162.2	165.3	168.8
NOx (g/kWh)	15.8	16.6	16.2	16.7	16.8
Combined thermal efficiency (%)	49.4	51.1	52.0	51.0	49.9
WHR system thermal efficiency (%)	-	21.4	16.0	13.0	-

The results indicate that by using the ORC WHR system, the SFOC can be reduced by 5% while the NOx increases slightly due to the tuning. The overall plant efficiency is 52.0% with the ORC, compared to 49.4% without a WHR system. Table 4.6 also shows the potential output of a stand-alone power turbine generator. Being much less complex, the power turbine produces a little more than half of the power produced by the Kalina cycle. In comparison, similar calculations suggests that a single-pressure steam cycle can produce up to 786 kW utilising the same heat sources under the same conditions.

Though the net power is comparable for all cycles, the WHR system thermal efficiency for the steam cycle is much higher than the Kalina and ORC systems. The reason is that the amount of heat added to the steam cycle is less, but hotter on average, compared to the others. The added exhaust gas heat is the same for all three cycles, but the charge air heat only constitute 9% of the total heat added for the steam cycle, while it constitutes 40% and 33% for the Kalina cycle and the ORC.

Table 4.7 presents the optimised parameters of each of the cycles. It is clear that the boiler pressure required to reach the maximum power output is relatively high for the Kalina cycle compared to the others and this may influence the overall cost and safety precautions of the plant negatively.

Table 4.7: Optimised parameters

Steam		ORC		Kalina	
Boiler pressure high (bar)	9.8	Fluid (-)	R245ca	Boiler pressure (bar)	86.6
Boiler pressure low (bar)	3.4	Boiler pressure (bar)	37.1	Turbine outlet pressure (bar)	5.1
High pressure mass flow (%)	65.7	Superheater approach (°C)	52.2	Boiler NH_3 concentration (%)	76.4

For the ORC process, the optimised pressure is just below the super-critical pressure. The optimised process layout of the ORC using R245ca as working fluid, has almost no superheating and this heat exchanger is therefore in theory not needed. The ORC layout includes heat exchangers for the utilisation of all three heat sources and the recuperator. R245ca is a HFC refrigerant fluid also known as penta-fluro-propane.

Figure 4.7 illustrates the optimised boiler heat transfer characteristics for comparison. The working fluid temperatures entering the boiler are similar for the steam cycle and the ORC and about 40°C lower for the Kalina process. This indicates that the Kalina cycle utilises the jacket water and charge air heat less efficiently. The ORC process uses the jacket water, recuperator and then the charge air cooler heat to preheat the working fluid to about 135°C, just as high as the steam cycle. Note that in the figure the ORC process heat source is the heat transfer fluid (DOW).

An alternative configuration of the ORC is considered; by using a non-flammable working fluid in the ORC, the process can be simplified by removing the intermediate heat transfer circuit. The maximum net power obtainable for this configuration is 1,060 kW resulting in a combined cycle power of 18.00 MW, with R236ea working fluid at the super-critical pressure of 68.3 bar. R236ea has a global warming potential of 1,200 (CO_2-equivalent 100 years horizon) compared to 560 for the R245ca fluid [229], and thus represents an increase in environmental impact.

The multiple regression model previously derived (see Sec. 3.3.2) is in the following used to estimate the maximum performance of a plant layout that uses two independent

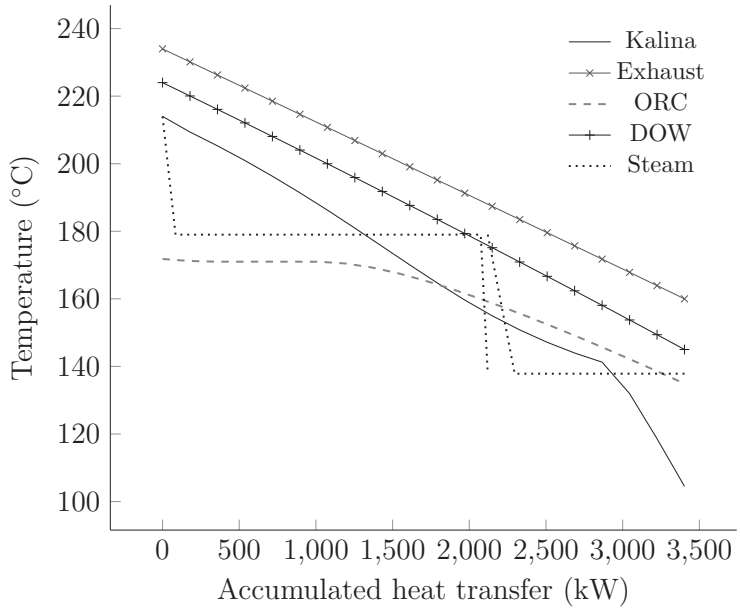

Figure 4.7: Boiler heat transfer diagram for the three power cycle alternatives

ORCs; one for the exhaust gas heat and one for the charge air heat. Hountalas et al. [230] present optimisations of an ORC utilising exhaust gas and charge air heat on a large two-stroke engine running at different loads. The study concludes that utilising the exhaust heat and the charge air heat in the same cycle with a single recuperated ORC, may not be the optimum solution in terms of thermal efficiency.

The maximum obtainable thermal efficiency estimated using the high-temperature regression model (Eq. 3.34) is 22.3% and with a heat input from the exhaust of 3,403 kW, the maximum potential net power is estimated to 759 kW. The low-temperature regression models are not valid for a 40°C condensing temperature; however, model optimisation results (using the previously described methodology) suggests that a simple non-recuperated ORC can at best produce about 363 kW from the charge air heat. In this case the combined WHR system power is then about 1,122 kW, while not utilising the jacket water heat. It can thus be concluded that the integrated ORC system presented first performs well in comparison, and considering that the integrated system is simpler, i.e., with only one turbine, one condenser etc., the integrated ORC system may be more cost-effective.

To investigate the relative performances of the three power cycles at a higher temperature, corresponding to the temperature found in a report from the engine manufacturer [18], the exhaust temperature is set artificially to 285°C, with no other parameter changes. The results suggest that the net power of the steam cycle, the ORC and the Kalina cycle, are 1,576 kW, 1,738 kW, and 1,457 kW, respectively.

Qualitative comparison

Other aspects are drawn into the comparison of the three power cycles for a wider evaluation. A comparison of the size parameters and volumetric flow ratios for the three cycles is provided in Fig. 4.8. The values are normalised with respect to the values of the low-pressure steam turbine. The results suggest that the Kalina cycle has advantageous working fluid properties for the turbine design and thereby the cost, given that it has the lowest volumetric flow ratio and size parameter. The main reason is the relatively high condensing pressures of the cycle.

Further investigations suggest that the ORC working fluid and operating parameters can be altered such that the volumetric flow ratio and size parameter are reduced; however, the consequence is a loss of potentially achievable power.

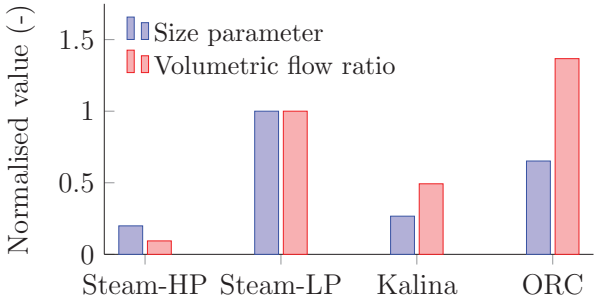

Figure 4.8: Size parameter and volumetric flow ratio relative to the steam LP turbine

Figure 4.9 presents the heat transfer-temperature profiles for the condensers. Note that for the Kalina cycle only the low-pressure condenser is shown, since the other condenser exhibits the same trend. The profiles are clearly not similar even though the same pinch point temperature difference of 2°C is applied. The resulting amount of cooling water is very different for each cycle with only about 45 kg/s for the Kalina cycle (for both condensers), 225 kg/s for the steam cycle and 400 kg/s for the ORC.

Table 4.8 presents an overview of important qualities for each power cycle. Each of the options are given a minus, zero or a plus to indicate a relative qualitative disadvantage, a neutral evaluation or an advantage, respectively.

Each of the aspects may be weighted subjectively according to particular needs and requirements. The comparison in Table 4.8 and the other results presented above, suggests that the Kalina cycle may only present advantages in terms of the condensers and of a simpler turbine design compared to the other cycles; however, the quite high pressure of the Kalina cycle may as mentioned affect the equipment cost and safety requirements negatively.

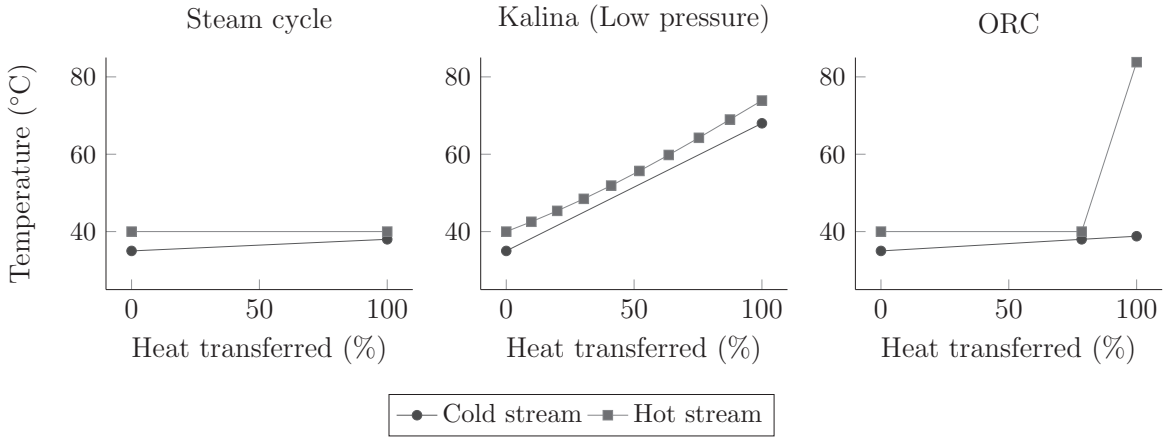

Figure 4.9: Comparison of the condenser heat transfer-temperature profile

Table 4.8: Comparative qualities

	Steam	Kalina	ORC
Net power output	0	-	+
Known technology	+	-	0
Process complexity	0	-	+
Toxic working fluid	+	-	-
Hazardous working fluid	+	-	-
Environmental concerns	+	0	-

The ORC fluid is flammable with a fire hazard level of 1 (HMIS) and additional safety measures are thus needed, in comparison with the other cycles, resulting in additional costs. Both ammonia-water and R245ca are toxic; R245ca has a HMIS health hazard level of 2 while the toxicity of the ammonia-water mixture depends on the mixture concentration.

The ORC presents advantages of being highly efficient with a relatively simple process layout. The steam cycle, being the industry standard, is clearly a desirable choice due to its high efficiency, proven technology and very good environmental profile. Moreover, the steam cycle can provide steam services which the other cycles can not. A remaining aspect is the equipment costs, but to be able to provide estimations on the costs of each plant type, further analyses are needed.

4.3.2 Development of a model for the prediction of the fuel consumption and nitrogen oxides emission trade-off for large ships

This section presents the results from the combined cycle multi-objective optimisation. Figure 4.10 presents optimised trade-off curves for the five mentioned cases. Compared to the baseline case, i.e., tuning of the main engine (ME), the results suggest that the use of a power turbine (ME, PT) can contribute to 3-4% SFOC and NOx reductions.

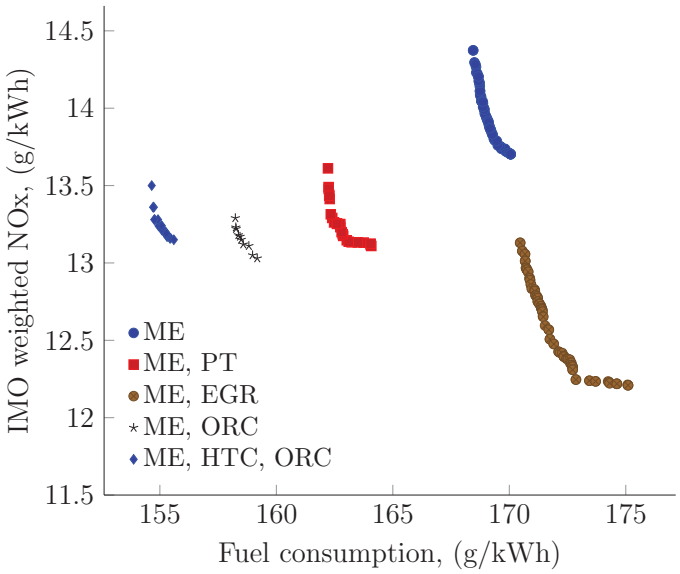

Figure 4.10: Fuel consumption and NOx trade-off

With the ORC WHR system (ME, ORC), the results suggest that an SFOC reduction of about 6% can be achieved, compared to the baseline case (ME), while the NOx emissions can be reduced to a lesser degree. The ORC and hybrid turbochargers layout (ME, HTC, ORC) may lead to SFOC reductions of around 8% compared to the baseline, while the NOx is generally higher compared to the layouts using a power turbine and an ORC.

The results for the system layouts with an ORC shown in Fig. 4.10 are based on an ORC utilising isohexane as the working fluid, with an evaporation pressure of about 17-18 bar, boiler pinch point temperature differences of about 15-25°C and recuperator pinch point temperature differences of 20-30°C (at design-point).

With the use of 10% EGR (ME, EGR) results suggest that the SFOC increases a few percent but the NOx is reduced by about 10%. The (ME, EGR) trade-off curve suggests that the use of 10% EGR can lead to NOx reductions, while maintaining the SFOC at the same level as the baseline case when it is tuned to the minimum NOx emissions.

Figures 4.11 and 4.12 present the optimised trade-off for six ORC working fluid options. The results suggest that using benzene, isohexane, cyclopentane and toluene as the working fluid may lead to the largest reductions. With the use of R245fa in the (ME, HTC, ORC) system, the SFOC-NOx trade-off is comparable to that of the (ME, PT) system. Simulations using R236ea provided no useful results in either system due to too low evaporation temperatures, leading to thermodynamic inconsistencies in the part-load calculations.

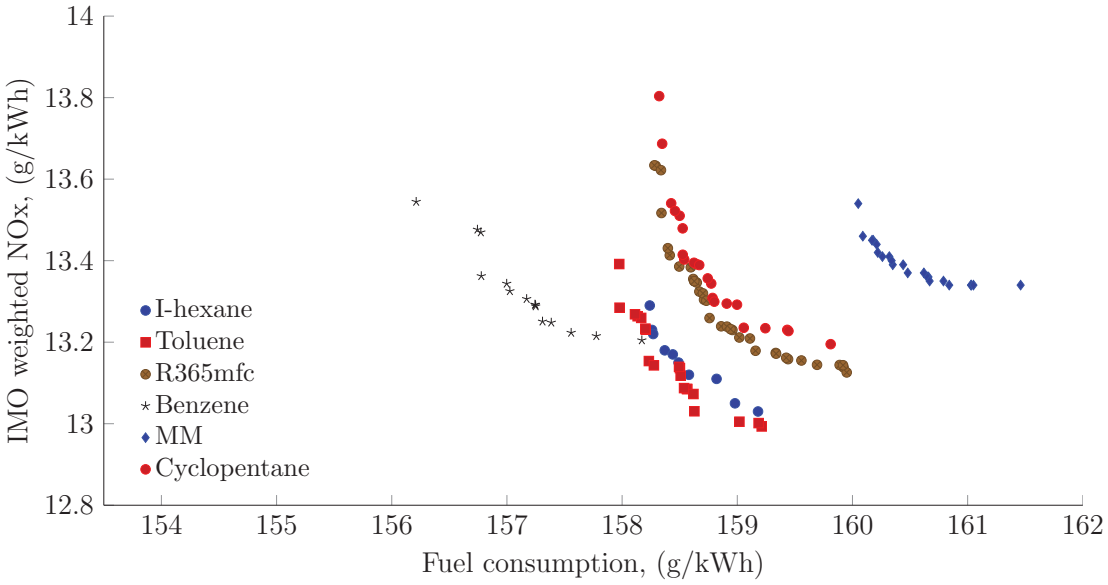

Figure 4.11: Fuel consumption and NOx trade-off using the main engine and ORC layout

Figure 4.13 presents the heat transfer-temperature diagrams of the optimised solution for the ME, HTC, ORC configuration using isohexane. It is seen how the exhaust gas inlet temperature increases with decreasing loads.

Table 4.9: Optimised main engine performance parameters relative to the reference (75% load)

	P_c (%)		P_m(%)		T_e(%)		$\dot{m}_e$(%)		T_{whr}(%)		NOx(%)		SFOC(%)	
Tuning	SFOC	NOx	SFOC	NOx	SFOC	NOx	SFOC	NOx	SFOC	NOx	SFOC	NOx	SFOC	NOx
ME	-7	-2	-2	1	-5	-7	14	14	-16	-19	-3	-10	-3	-2
PT	-8	-4	-6	-3	21	16	-9	-4	23	16	-2	-9	0	0
EGR	0	1	3	-6	-5	-4	8	10	-11	-10	-12	-20	-2	1
ORC	-11	-12	-13	-15	26	26	-10	-10	32	33	-1	-2	2	3
HTC, ORC	-11	-10	-13	-14	26	25	-10	-9	32	31	1	-3	2	2

Table 4.9 presents the optimised engine performance parameters at 75% load, relative to the reference, i.e., the parameters leading to the validation results (see Sec. 2.3.3). Relatively low compression pressures lead to the best performance, with the exception of the EGR case. With low compression pressures, less work is needed for the compression stroke [231]

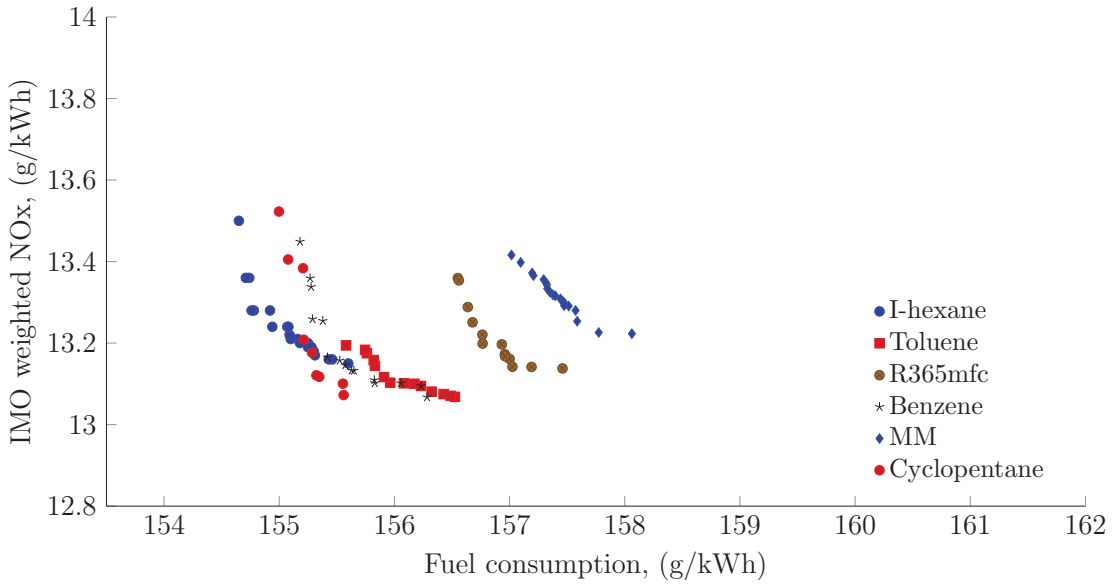

Figure 4.12: Fuel consumption and NOx trade-off using the main engine and HTC-ORC layout

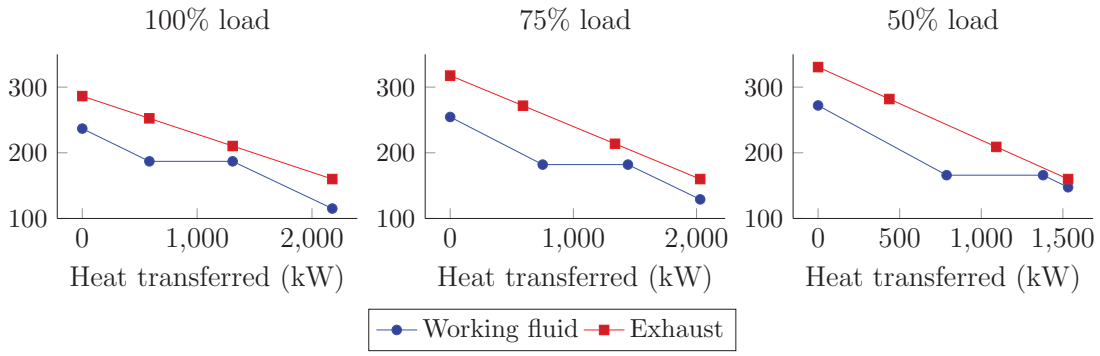

Figure 4.13: Heat transfer-temperature diagrams (ME, HTC, ORC with i-hexane)

which in this case contributes to the lower NOx and SFOC; however, the maximum pressure is not reduced as much in the (ME) case, and this illustrates the importance of the pressure rise ($P_m - P_c$) for the engine efficiency. In the cases with PT and ORCs, the maximum pressures are reduced. In the ORC cases this is the cause of the increase in the main engine SFOC and the reduction in NOx. However, reduced engine efficiencies contribute to increased exhaust temperatures (T_e) and thus WHR inlet temperatures (T_{whr}) thereby increasing the performance of the ORC systems. The same cases exhibit reductions in the exhaust mass flow rates ($\dot{m}_e$), which also result in higher exhaust WHR inlet temperatures.

Table 4.10 presents the optimised engine operating parameters relative to the standard

Table 4.10: Optimised main engine operating parameters relative to the standard tuning (75% load)

	SOI (CAD)		EOI (CAD)		EVC (CAD)		P_{scav} (%)		$\dot{m}_f$ (%)	
Objective	SFOC	NOx	SFOC	NOx	SFOC	NOx	SFOC	NOx	SFOC	NOx
ME	-0.4	-2.1	-1.0	6.5	8.3	6.0	4.0	5.3	-2.0	-1.6
PT	-0.1	-1.6	2.8	9.2	6.4	6.0	0.1	3.3	0.2	0.4
EGR	0.2	1.4	-5.8	3.2	5.0	4.6	6.8	6.2	-2.3	-0.1
ORC	1.2	1.3	4.6	6.8	7.0	6.3	-2.5	-4.5	2.0	3.2
HTC, ORC	1.7	1.5	3.1	6.4	7.1	7.1	-2.1	-0.8	1.9	1.8

tuning at 75% load. The lowering of the compression pressures is caused by delayed EVC timings and in the case with the ORCs also reduced scavenge pressures. The increased exhaust temperatures in the cases with ORC are also assisted by increased fuel flow rates. In the cases with ORC and PT the EOIs are retarded to reduce the maximum pressures. There is a clear trend in all cases towards retarding the EOI when the objective is to minimise the NOx.

Figure 4.14 presents the results of an optimisation with the main engine SFOC and the combined cycle SFOC as the two objectives. The results shown in the figure suggests that the main engine must be tuned in a way that results in a lower fuel efficiency, in order for the WHR system to perform better for the improvement of the combined cycle efficiency; here expressed as the SFOC.

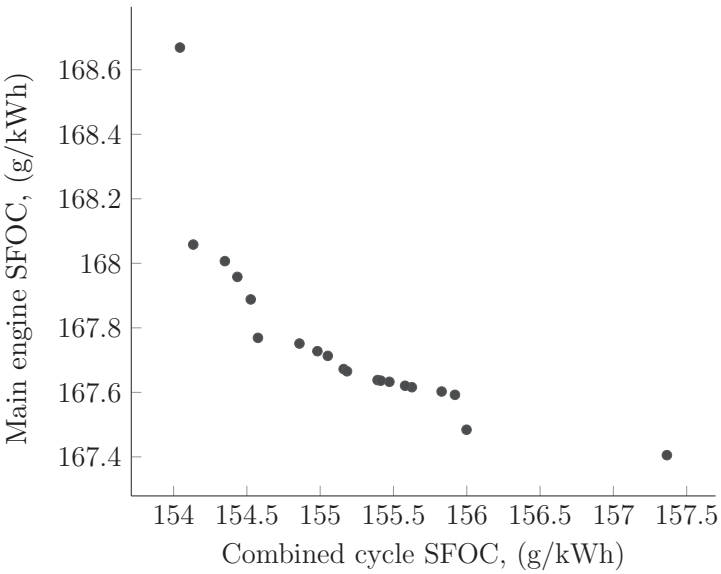

Figure 4.14: Fuel consumption for the main engine and HTC and ORC isohexane combined cycle

The ranges in the figure are not very wide and this is likely due to the constraints of the optimisation, i.e., the requirement to respect propeller law and limit the maximum pressure rise. Note that the SFOC of the combined cycle is slightly lower than what is shown in Fig. 4.12. This indicates that the genetic algorithm needs more iterations to find the global optima, when optimising the SFOC-NOx trade-off.

Economical comparison

For economical comparison, the component purchase costs for each WHR system were estimated and used to predict the net present values (NPV). The power turbine cost was estimated using a number provided by MAN Diesel & Turbo [18]; the ORC module costs were derived from Quillon et al. [129], and the generator costs from Lian et al. [232].

The estimated total purchase costs are 2.13, 8.25 and 8.64 million USD for the ME, PT, the ME, ORC and the ME, HTC, ORC systems. With a fuel price of 483 USD/ton [197] and optimised average fuel consumptions of 162.0, 158.5 and 155.0 g/kWh, for the same three systems, the yearly fuel savings amount to 0.94, 1.49 and 2.04 million USD/year. It is here assumed that the operation occurs as according to the IMO weighting factors (see Table 4.2) with an average operational time of 65% (an assumption which is based on discussions with colleagues in the industry).

Assuming an interest rate of 10%/year, the NPVs become positive after 2.5, 8.5 and 5.8 years for the ME, PT, the ME, ORC and the ME, HTC, ORC systems. The NPVs considering a 20 years ship life time [197] are 5.9, 4.5 and 8.8 million USD.

4.4 Discussion

4.4.1 A comparison of advanced heat recovery power cycles in a combined cycle for large ships

With the applied methodology the performance improvement of utilising either of the three power cycles as WHR for marine applications is quantified; however, the accuracy of the results relies on the reliability of the thermodynamic equations of state, residing in the Refprop database. Refprop is used for the modelling of various kinds of systems and is validated throughout the literature, one example is Colonna et al. [233]. Furthermore to the accuracy of the results; since the models in this study are made without any pressure and heat losses, the results should be interpreted as ideal, and thus smaller net power outputs can be realized in an actual plant.

While the investigations in this study are made for a single main engine load point, the decisions regarding WHR plant process layout and working fluid may rely on a range of load points. A combined optimisation of the main engine with T/C and WHR versus a typical voyage load profile is therefore a natural next step for the comparison.

According to a MAN Diesel & Turbo report [18], the same steam WHR system may produce about 10% extra power, but in the present study an increase of only 5% is found. The combined cycle efficiency in the report is stated to be 55% versus the 52% in the present study. The following reasons could be contributing to this discrepancy: firstly, in the MAN Diesel & Turbo report the WHR system includes both a Rankine cycle and a power turbine. Based on the results found for the power turbine in the present study, the resulting efficiency may be around 52.5%, at most, with a the steam cycle and power turbine. Secondly, the fuel consumption in the present study is increased by 2.7 g/kWh while in the mentioned report this number is 10 g/kWh. This indicates that the tuning involves a richer air fuel mixture in the main engine, compared to the tuning done in the present work. The additional fuel input increases the exhaust gas temperatures and mass flow rates which cause a significantly higher WHR system power output. In the previously mentioned report, the exhaust gas temperature entering the WHR system is 285°C compared to the 234°C shown in Table 4.5. Moreover, the engine type studied is not exactly the same as in the MAN Diesel & Turbo report [18]. Lastly, a contribution may be that the WHR turbine efficiency of 80% used in the present work is assumed too low, and thus the respective power outputs are consequently under-estimated.

4.4.2 Development of a model for the prediction of the fuel consumption and nitrogen oxides emission trade-off for large ships

As may be expected, the combined cycle fuel efficiencies of the investigated system layouts increase with increasing system complexity while the NOx generally decreases. The simple power turbine configuration shows a remarkable potential of about 4% SFOC and NOx reductions, which is similar to what is presented by the engine manufacturer [18]. The main reason is that the power turbine utilises the pressure component of the exhaust gas waste energy [119]. With a system layout consisting of the hybrid turbines and the ORC, significantly lower SFOC and NOx emissions can be achieved, comparable to what the manufacturer presents for a system layout with a power turbine and an advanced dual-pressure steam cycle, which utilises the heat from the engine jacket water cooler heat and the charge air cooler [18].

Choi et al. [211] investigate the potential of a steam and ORC dual-cycle exhaust gas WHR system for the mechanically controlled 12K98MC engine. While the methodology

applied is not similar to the present one, a similar potential of 6% SFOC reduction for a system without a power turbine is found.

The consideration of part-load performance influences the design and operating parameters of main engine and WHR system significantly. For example, when considering design point optimisation only, as done in Ch. 3, the ORC boiler temperature pinch points can be set relatively small, e.g., 10°C; however, the intermediate calculations in the investigations using the present methodology suggests that such small pinch points at design point generally lead to problems such as pinch point violations and infinitely small superheating approaches at part-load conditions. This emphasises the importance of considering part-load performance of the presently studied type of systems, especially since the ships operate at part-load most of the time [234].

The optimised main engine tuning is markedly influenced by the system layout (Tables 4.9 and 4.10). This suggests that the investigation of the combined cycle efficiency must include engine tuning; this is not often seen in the literature although Srinivasan et al. [38] is one example.

For the application on board ships it is, as mentioned, an advantage that the ORC working fluid is not very hazardous, because safety is a major concern in the machinery rooms. For this reason refrigerant fluids that have low hazard levels may be preferred. However, none of the tested refrigerants performed well (R245fa and R236ea), except R365mfc which is highly flammable.

The reference performance of the main engine alone using the parameters of the calibration case (see Fig. 2.10, Sec. 2.3.3, p. 56) results in an IMO weighted SFOC of 172.2 g/kWh and 14.9 g/kWh NOx. This result is not on the optimised trade-off curve (Fig. 4.10, p. 157) and there may be a number of reasons for this; the engine may have been tuned for another scenario and not for the IMO weighted best performance; considering the date of the tests, which is 2006 and thus before the financial crisis, the engine is most likely optimised for high loads. The engine may have been fitted with different T/Cs, and finally, other practical concerns which are not considered in the present study may influence the engine settings.

The economical comparison suggests that the ME, ORC system may, in a ship life time, not present a higher NPV than the simpler ME, PT configuration. Moreover, the ME, HTC, ORC configuration NPV becomes larger than the ME, PT system only after about 9.5 years. It is noted that these results are averaged estimates under assumptions that are uncertain, for example due to ever changing fuel prices or slow-steaming operation. Moreover, additional expenses related to installation and maintenance must be added. Still, the numbers are in good agreement with numbers presented by the industry for similar systems [197].

5 Conclusion

This chapter concludes the present thesis by addressing the posed research questions, summarising the thesis contributions to the current knowledge and describing the main limitations of the presented studies. Finally, recommendations for future research are proposed, and a set of recommendations about which WHR systems that are suitable for ships are also provided.

The main objective of the present thesis is to investigate alternative waste heat recovery systems that can lead to the reduction of the fuel consumption and NOx emission of large ships.

The magnitude of the merchandise ship transport and the significance of the resulting pollution are considerable, and are as mentioned not expected to decrease. Even the most efficient diesel engines utilise only 50% of the fuel energy and there is therefore a significant amount of low-grade energy wasted via the waste heat, if it is not utilised. Hence, the application of a waste heat recovery system presents a significant opportunity for the reduction of the global ship pollution.

Together the investigations presented in this thesis provide answers to the research questions; purely thermodynamic advantages and disadvantages of the ORC and Kalina cycles are identified and their potential performances are predicted and compared; suitable process layouts and working fluids are identified and useful methodologies for the design and optimisation of such WHR systems operated together with the low-speed two-stroke engine are presented.

5.1 Research questions

This section addresses the research questions posed in Sec. 1.2 (p. 8) based on the studies presented in the previous chapters.

Considering the thermodynamic performance only, the results indicate that both the Kalina Split-cycle and the ORC present significant advantages over the steam Rankine cycle, but they also a possess important disadvantages.

The results suggest that both cycles can achieve significantly higher power outputs compared to the steam cycle, even though both are single-pressure cycles and the steam cycle is a dual-pressure cycle. This advantage is more pronounced for the ORC than the Kalina

Split-cycle. It is however doubtful that reference Kalina cycle (Fig. 3.5, p. 78) can produce more power than the dual-pressure steam cycle in any case.

The direct comparison of the three relevant power cycles (see Sec. 4.1.1) involved a Kalina cycle layout which is quite similar to the reference cycle in the study concerning the Split-cycle (see Sec. 3.1.6). In the direct comparison the Kalina reference cycle performed not quite as well as the steam cycle with a 4.5% lower power output compared to the steam cycle. The Split-cycle produced a 6% higher power output compared to the reference layout and with reheat the Split-cycle produced 11.4% more power. Based on these results it seems likely that the Split-cycle can achieve higher efficiencies than the dual-pressure level steam cycle; based on the derived regression models the Split-cycle can however not outperform an optimised recuperated ORC, which is remarkable considering the difference in complexity of the two cycle types.

The simplified turbine analysis suggests that the working fluid properties and operational parameters can be chosen such that they are advantageous for both alternative cycles, in comparison with the steam cycle.

The disadvantages in terms of thermodynamic performance of the Kalina cycle and the ORC are related to the high evaporation pressures needed to achieve the superior efficiency; the Kalina cycle in particular; the results indicate that the working fluid of the ORC can be chosen such that the evaporation pressure is less than 20 bar with a small performance penalty.

The Kalina cycle requires a complex process layout to achieve the high efficiency. The opposite is the case for the ORC. The ORC process is claimed to be so simple that the control of it can be done automatically [207], however, this is likely not the case of the Kalina Split-cycle; although there is no available knowledge to verify this claim.

The results of the simplified heat exchanger analysis of the Kalina cycles suggests that the heat exchangers are required to have a very large heat transfer areas to achieve the high efficiencies; however, based on the simple investigation of the cooling water demand, large areas for the condensers may not be required.

It is not straightforward to provide an answer to the question of which WHR system process layouts and working fluids that are suitable for the application on board ships. Compared to the established steam Rankine cycle it can be argued that neither of the two alternatives, the ORC and the Kalina cycle, are suitable. Supporting this argument is the fact that the shipping industry is well known for having a conservative attitude towards new technologies.

Regarding the system layout, the Kalina cycles, and particularly the Split-cycle, are as mentioned a lot more complex than the ORCs; however, the Kalina cycles are not more

complex than the dual-pressure steam cycle currently in use.

On board large ships the WHR system can be relatively more complex and a relatively high investment can be allowed, due to the scale of the system and a typical operational profile with long steady voyages. The application of either the Kalina cycle or the ORC requires an additional steam boiler to supply steam services; such configurations are more likely to be feasible on board large vessels.

Smaller ships with shorter and more unsteady route patterns may find challenges with regards to the financing; the investment made for the WHR system is relatively larger due to the scale and the return on investment is therefore be expected to be lower, thus affecting the choice of WHR system. For these ships the power turbine seems to be a straightforward choice due to the reasonable efficiency, the low investment cost, the simplicity and the size. The same may be the case for ORCs which are developed for smaller scales than the steam cycle.

The relatively small difference in performance between the recuperated and the simple ORC makes the simple ORC an interesting option for smaller vessels. The multitude of fluids also points to the viability of the ORCs on board small ships because it is likely that a near-to optimum efficiency can be achieved for almost any given machinery room situation. The ORC can for example be driven by the cooling water or the charge air heat alone; an option which is hardly feasible for the steam cycle. Thus the ORC is uniquely efficient, flexible and simple; features all arguing for the feasibility on board smaller vessels.

The results suggest that system configurations including the hybrid T/C and an ORC is a very promising WHR system layout, for ships of different sizes.

The working fluid of the WHR system is as big an issue as the system layout. The steam cycle is far superior in this regard, both because it is non-hazardous and environmentally friendly and because the fluid can be used for multiple purposes, e.g., steam services.

Ammonia-water mixtures in the concentrations present in the Kalina cycle (up to 90% or more) are highly toxic. The health hazard level of pure ammonia is 3 (HMIS) and the fire hazard level is 1 (HMIS). The low environmental impact of this fluid is perhaps the strongest argument for the use compared to the ORC fluids.

The results suggest that the ORC working fluid can to some degree be selected to have a low hazard level for the application on board ships. R245ca is a good example which is shown to be able to provide the highest efficiencies in some of the studies in this thesis.

The use of hydrocarbon fluids lead to the highest efficiencies found in this thesis, both in the design point optimisations and when considering part-load behaviour. The large fire hazard is the biggest drawback to their use; however, considering that natural gas is a relatively well-known fuel on board ships, and is expected to be more widespread in the

near future, it can be argued that the use of the organic fluids is a matter of crossing a threshold and proving that the fluids can be handled safely using proper precautions. From the use on land, ORCs are well proven and they can be built hermetically sealed with leakage sensors and an automated shut-down in case of leakage [207, 235]. An advantage of using pure hydrocarbon fluids compared to for example refrigerants is that in case of accidental fire, the smoke is not nearly as toxic [207]

The results show that ethanol leads to superior performance in the simple ORC over a heat source temperature range between 240-360°C and over a large range of pressures. This, together with a benign environmental impact profile, makes it an interesting candidate for further investigation, possibly mixed with water to reduce the toxicity and fire hazard level.

The highly efficient Kalina cycle has a relatively complex layout, a thermodynamic process which may not easily be understood by the marine engineers operating it, a toxic and corrosive working fluid, the process is patented, not many plants exist to prove the reliability, and it is not markedly more efficient than a steam cycle of similar complexity. These points are all making the Kalina cycle a very hard sale in a conservative sector, which primary concerns are cost-effectiveness, reliability and safety; the presently made investigations do not present a convincing case for the Kalina cycle layouts and working fluid.

Due to the above mentioned reasons, the ORC presents a much more convincing case. The main arguments are a uniquely high efficiency, also at smaller scales, automated operation and a the range of working fluids that enables the process to be adapted to many scenarios.

Methodologies that are useful for the design and optimisation of the low-speed two-stroke diesel engine and WHR system combined cycle are presented in this thesis.

The main engine is undoubtedly the most important component of the considered systems, and the modelling and validation of it constitutes a significant part of the efforts made in the present work.

From one point of view, there is little novelty related to the applied sub-models and correlations used to build the engine model. The heat loss correlation, the heat release model, the working media correlations and the NOx formation mechanisms, are all well known and are validated, and documented in numerous studies in the literature; however, as explained, the low-speed two-stroke engine is not entirely similar to the much smaller scale automotive four-stroke engines, which most of the sub-models are derived and validated for.

For the purpose of the analyses in the present work, the engine model is required to be able to provide quantitative and qualitative predictions; the preliminary validation (Sec. 2.3.1) verified the ability of the model to qualitatively predict the NOx and SFOC trends.

The ability to make absolute predictions of the SFOC is verified in two cases using different model inputs; however, the NOx predictions rely on the local air-fuel ratio in the burn zone. It appears from the literature that using this ratio to calibrate the NOx emission is currently the preferred approach; in lack of better options. The phenomena involved in the combustion and NOx formation processes are of a complexity which is beyond the capabilities of zero-dimensional models, i.e., models useful for system analyses in general. The fact that the 12K98ME model predicts NOx at an quantitatively correct level, as far as can be determined, using the same local air-fuel ratio as calibrated in the 7L70MC model case, is a satisfactory results.

The results presented in the studies of Goldsworthy [72, 96] illustrate well the challenges related to NOx predictions with zero-dimensional models. The results Goldsworthy [96] obtained through model simulations are in agreement with the experimental data provided by the manufacturer; however, the present work have identified two points that are questionable: firstly, Kilpinen [92] made a subsequent revision of the NOx formation mechanisms that Goldsworthy [96] applied, and concluded that the equations are erroneous; secondly, the turbocharger efficiency required to match the operation and performance parameters provided, is excessive considering when the work was performed (2003) and the currently available turbocharger efficiencies.

In addition, the resulting predictions of the cooling water heat, or cylinder heat losses, using the present engine model raise questions; considering that the present model utilises an energy balance at all instants of the engine cycle, the first law of thermodynamics is certainly not violated in the model results. Still, in comparison with the figures provided by the engine manufacturer for this study (Sec. 2.3.3), and the data obtained from Goldsworthy [72], i.e., the data in two of the validation cases, the agreement between predictions and reference data is not satisfactory. It is unclear why these discrepancies exists and this question remains unanswered.

The three cases of validation presents together a strong argumentation towards the validity of the prediction ability of the model. There is a good response in terms of SFOC and NOx to the key engine operational parameters; the compression, maximum and scavenge pressures. The exhaust temperatures are predicted well at all loads which is of key importance in the present work. Importantly, the model performs well without extensive manipulation in terms of calibration. It is noted that the range of validity for the predictions is limited for this kind of model; the results suggest that the use of the propeller law to keep the engine power versus engine speed the same as in the calibrations case, is a useful approach to keep the parameter variations within a valid range.

The WHR system modelling methodology for the ORC represents a novel contribution to the scientific literature. The large range of ORC working fluids presents opportunities for obtaining several desirable qualities for the WHR system, but at the same time the

large range makes the optimisation process labourous, even though the process is rather simple.

The proposed methodology enables the estimation of the maximum potential of the ORC under different constraints which are relevant to consider for the application of ORCs on board ships (Sec. 3.3.1). Given the properties of the ORC working fluids, it is useful to be able to evaluate the potential gain, in terms of a high thermal efficiency, against the risks of having such hazardous fluids in the machinery rooms. Moreover, it is shown to be suitable for the presented study of comparison of the three integrated power cycles (Sec. 4.1.1).

Moreover, the methodology led to the presented regression models (Sec. 3.1.5) which are in themselves a useful tool for the evaluation of the implementation of an ORC WHR system for a given purpose. Using the regression models enable the immediate evaluation of key design parameters, i.e., turbine efficiency, condensing temperature, etc.

The methodologies used to optimise the part-load performance (Sec. 4.2.2) shows promise of being a strong tool that can address the very relevant issue of the optimisation of the machinery system for slow-steaming operational patterns. Moreover, the results of the efforts of simultaneously optimising the engine, T/C and WHR system strongly suggests that this approach is useful.

5.2 Contribution to current knowledge

The contribution of the work on the validation of the engine model is most importantly the validation of the qualitative response on SFOC and NOx due to changes in key operating parameters or engine tuning settings. This validation enables the study of a combined or simultaneous optimisation of the engine and the WHR system as presented in Sec. 4.1.2. The NOx-SFOC trade-off is as mentioned of key importance in the design and optimisation of marine machinery systems, and the presented simultaneous optimisation efforts (Sec. 4.1.2) constitute another contribution made in this thesis.

The literature about ORC fluid selection methodologies and the optimisation of ORCs has progressed significantly during the project period. A trend develops towards considering multiple aspects, such as economics, volume of the plant, life-cycle environmental impact and component design, besides the thermodynamic performance, examples of this are Pierobon et al. [8] or Astolfi et al. [217]. These factors are now included in some optimisation algorithms. On this background, the presented ORC optimisation methodology (Sec. 3.2.1) can be seen as only a foundation on which the other mentioned aspects can be built; however, the presented ORC methodology has shown its usefulness as already men-

tioned, not least with the resulting regression model study which is another contribution branching from this methodology.

The presented design and optimisation efforts concerning the Kalina Split-cycle (Sec. 3.1.6) constitutes a novel contribution, because the cycle is merely described qualitatively in the literature. The thermodynamic analysis quantifies the advantages claimed by the inventor (Kalina) and the simplified cost analysis evaluates the added cost against the increase in thermal efficiency for the different process layouts.

Finally, the comparison of the three power cycles that are integrated with the marine engine, contributes by quantifying both the NOx and SFOC resulting from using the different power cycles on an engine which is somewhat tuned for better WHR system performance.

5.3 Limitations

A general limitation in the thesis is that the operational profile of the ship is not properly considered, with the exception of the final study of the part-load weighted NOx-SFOC trade-off (Sec. 4.1.2). A comparison of the part-load performance of three power cycles, steam, Kalina and ORC would add important value to the analyses. The study of the comparison of the three power cycles 4.1.1 is furthermore limited by not including an economical evaluation of the three cycles.

Another general limitation is that the systems surrounding the main engine and WHR system are not considered.

The limitations related to the engine model are mainly related the need for a fast execution time and the need for more experimental data for validation (see Ch. 2). An important limitation is that it remains somewhat unclear whether the model can predict the effects of high exhaust gas recirculation rates (EGR) adequately. In order to be able to comply with IMO Tier III (3.4 g NOx/kWh) using only EGR, EGR rates up to 30 or 40% are needed. Experimental data needed to support further validation and possible development of the model was not obtained. Moreover, the results suggest that the model is inaccurate at high EGR rates and by examining the literature, it seems that significant efforts are needed to approach this problem. The validation of the NOx response to the different operating parameters (Sec. 2.3.1) or the examination of the low EGR rates (Sec. 2.3.3), do not provide enough validation to support such studies, while highly relevant as the implementation of Tier III limits approaches.

5.4 Recommendations for future research

The listed recommendations for further studies are based on what seems to be lacking in the literature, on the mentioned limitations and on perceived pathways for further improvements of marine machinery systems.

1. For the marine application the scope of study is rather challenging; ideally the design and optimisation of the main machinery systems should include considerations of the entire ship energy system and the operational pattern(s) intended. At the same time a very specific and narrow focus is required to study the individual components of the system, the mentioned problems related to EGR is an example. Another example is the turbocharger, which is a key component for both the main engine and the WHR system, and thus also the resulting pollution; in order to improve this interaction, close attention on the turbocharger as a component is required. Baldi [26] presents important results and discussions about the above mentioned aspects and his research stands out as an inspiration for future research in this direction. It is however recommended to incorporate a higher level of detail in the models of Baldi [26], to accommodate the ability to predict for example various innovative scenarios not yet existing.

2. Further development of the present engine model may enable more detailed studies of the NOx formation and techniques for the reduction of NOx; more detailed fuel injection and combustion models may enable a range of hereby recommended studies, e.g., of different injection strategies with multiple injections (as for example studied by Andreadis et al. [236]), which also include the WHR system for a more holistic system optimisation. Moreover, the modelling of other important pollutants, such as particulates and SOx, for the study of pollutants trade-off mechanisms, is recommended for further research.

3. It is also recommended to further develop the cooling system modelling of the engine model in order to improve the estimation of the states of the waste heat streams. Throughout the ship fleet in general, significant exergy destructions (destruction of energy quality) occur in the machinery cooling systems [26]. Such destruction ruins the possibilities of recovering energy because the temperatures are too low for it to be feasible. For example the lube oil system experiences relatively high temperatures, especially in the cooling of the pistons [237]. Therefore, more a detailed modelling can help to identify opportunities for additional heat recovery.

4. Detailed studies of different turbocharger configurations and their interaction with the engine and WHR system are also recommended. Variable geometry T/Cs, two-stage T/Cs, cut-out options, hybrid T/Cs are all technologies that can have a sig-

nificant impact on the system performance, including the NOx emissions (see for example Kaltoft et al. [30]).

5. It is recommended to further study the part-load behaviour and performance of the Kalina cycle. The additional degree of thermodynamic freedom, provided by the fact that the working fluid is a mixture, can possibly lead to superior part-load performance. A high average efficiency under varying operational patterns is a great advantage and may justify the use of the Kalina cycle WHR systems. No studies verifying this seems to exist.

6. Continuing the trend in the very recent ORC literature of including the components design in the system design and optimisation methodology (see for example in Pierobon et al. [8]), is recommended future research; such efforts not only enable a more realistic estimation of the costs and performance of the systems, but it also enable the inclusion of considerations regarding the physical plant layout. As Kaltoft et al. [30] point out, a given system design is advantageous if the physical design results in an installation that requires a minimum of changes to existing machinery room designs. The shipyard is likely to be more willing to accommodate such a system, and the price of doing so will likely be lower, because the shipyard will then not need to reconsider their own manufacturing process.

7. Further studies of integrated machinery system are also recommended. Depending on the vessel and its mission, there are possibilities to integrate different energy systems, possibly resulting in benefits such as fewer components overall, a more compact machinery system, better utilisation of waste from different processes; interesting concept studies of this sort is recommended for specific case studies.

8. The use of alternative fuels is evidently the only way to reach a markedly higher level of sustainability while using the studied type of machinery systems. Therefore it is recommended to further study the use of such fuels, which may be liquefied natural gas, methanol or dimethylether (DME) [238]; and the resulting interactions between the engine and different WHR systems. For example, with the use of fuels that are not containing sulphur, a much lower funnel temperature is expected to be acceptable; this parameter is a key parameter for the design and optimisation of the WHR system.

5.5 Recommendations for a suitable waste heat recovery system

This section presents recommendations for a suitable WHR system based on the vessel size. The recommendations are meant for WHR systems utilising heat from low-speed two-stroke engines.

Large vessels:

- Since large vessels operate on the long inter-continental routes the engine is running at steady loads for long periods at the time. Because of this and due to the large scale, the cost-effective investment in the WHR system can be expected to be relatively large, allowing for a relatively complex system.
- For this type of vessels the use of a power turbine is recommended in all cases.
- Based on the results in the previous chapters and on considerations of the toxicity of the working fluid, it is recommended to avoid the application of a Kalina cycle. This recommendation includes the all of the studied Kalina cycle process layouts.
- The dual-pressure steam Rankine cycle is, not surprisingly, recommended due to the high efficiency, environmentally benign working fluid; because the process is proven and well known, also to the operators, and because it can provide steam services.
- The integrated ORC treated in Sec. 4.1.1 is also recommended due to the superior net power output. The fuel efficiency is the main performance parameter in ship operations of this type, and the investments in the needed safety precautions and an additional steam boiler for steam services, is believed to be feasible, considering the ORC yields an output that is about 35% higher than the dual-pressure steam cycle. The investment in an additional steam boiler and an ORC plant may not even exceed the investment of the dual-pressure steam cycle; the reason is that the ORC system layout is much simpler and the number of component smaller. The simple turbine comparison also favoured the ORC with a much lower number of turbine stages, suggesting a lower cost. Further studies are as mentioned needed to verify this claim.
- The results of the investigation of the part-load performance of different system configurations (Sec. 4.1.2) indicate that the hybrid T/Cs combined with an ORC can lead to significantly reduced SFOC and NOx with a very simple process layout; hence, this WHR system layout is recommended for this application.

- Regarding the ORC working fluids it is recommended to accept the flammable fluids and therefore to design the machinery room to take into account the increased fire hazard. Important precautionary measures are the use of a heat transfer fluid, hermetically sealed ORC units and leakage sensors combined with automated shut-down mechanisms.

Feeder class vessels:

- The voyage pattern of these vessel can vary significantly over the life time of the ship. Therefore, the flexibility of the WHR system configuration may be an important parameter.
- For this type of vessels the use of a power turbine is recommended in all cases due to the cost-effectiveness.
- For the same reasons as mentioned above, it is recommended to avoid the Kalina cycles as a WHR system option.
- Based on the results in Sec. 4.3.1 it is recommended to consider the integrated ORC WHR system. The expected relatively low investment cost combined with a high power output suggests that this option is more desirable than the dual-pressure steam cycle. More detailed studies of the economics are required for verification of this claim.
- A recuperated ORC utilising only the exhaust gas heat is also recommended based on the high power output, simple design an because it can function independently without the need of an operator [207].
- Based on the literature studied in the present work [18], a single-pressure steam Rankine cycle produces significantly less power in comparison with the ORC; however due to the same reasons as mentioned above, such a WHR system is also recommended.
- The hybrid T/C and ORC system is recommended also for this class of vessels, due to the same reasons as mentioned above.

It is recommended that the ORC working fluid selection is based on the specific case of application; however, a number of suitable fluids are presented in the previous chapters. Among those are benzene, isohexane, MM, cyclopentane, MM, R245ca, R236ea in the recuperated ORCs; benzene, ethanol, cyclopropane, toluene, R245ca and R245fa are candidates for the simple ORC. The results suggests that the refrigerants are less suitable compared to the hydrocarbon fluids, when considering part-load operation of the ORC.

It is noted that the use of the mentioned fluids may require significant efforts with regards to certification and the like before implementation. Currently there is not much available documentation on ORCs installed on board ships; one example is a marine ORC WHR system (Opcon) [239] using R236fa for low-temperature heat recovery.

5.6 A final remark

The motivational background for the present investigation states that the ORC and the Kalina cycle may possibly be suitable for a WHR system on board ships. The results of the studies are quite clear; the Kalina cycle is not a suitable candidate while the ORC can be a very suitable worthwhile candidate, if the risks resulting from the hazards of the working fluid can be managed and accepted. The ORC offers unique opportunities; it can be automated, it can be adapted to different scenarios and it can be highly efficient even at small scales. At least in theory, the working fluid may even be replaced by a more suitable candidate if the ship voyage pattern changes for a longer period.

The difference between having a WHR system or not is certainly of greater importance than the marginal differences analysed in the present thesis. A very promising alternative to the steam cycle is identified through the present study. The high efficiency of the ORC compared to the advanced dual-pressure steam cycle, suggests an even greater advantage over the single-pressure steam cycle; an advantage that may well be the factor that makes the investment in a WHR system feasible for feeder class size ships, the largest group of container ships globally [240].

Bibliography

[1] Larsen U, Pierobon L, Haglind F, Gabrielii C. Design and optimisation of organic rankine cycles for waste heat recovery in marine applications using the principles of natural selection. Energy 2013;55:803–12. doi:10.1016/j.energy.2013.03.021.

[2] Larsen U, Pierobon L, Wronski J, Haglind F. Multiple regression models for the prediction of the maximum obtainable thermal efficiency of organic Rankine cycles. Energy 2013;doi:10.1016/j.energy.2013.10.026.

[3] Larsen U, Nguyen TV, Knudsen T, Haglind F. System analysis and optimisation of a Kalina Split-cycle for waste heat recovery on large marine diesel engines. Energy 2014;64:484–94. doi:10.1016/j.energy.2013.10.069.

[4] Larsen U, Sigthorsson O, Haglind F. A comparison of advanced heat recovery power cycles in a combined cycle for large ships. Energy 2014;74:260–8. doi:dx.doi.org/10.1016/j.energy.2014.06.096. International Conference on Efficiency, Cost, Optimization, Simulation and Environmental Impact of Energy Systems ECOS 2013.

[5] Larsen U, Pierobon L, Baldi F, Haglind F, Ivarsson A. Development of a model for the prediction of the fuel consumption and nitrogen oxides emission trade-off for large ships. Energy 2014;:1 –11doi:dx.doi.org/10.1016/j.energy.2014.12.009.

[6] Scappin F, Stefansson SH, Haglind F, Andreasen A, Larsen U. Validation of a zero-dimensional model for prediction of NOx and engine performance for electronically controlled marine two-stroke diesel engines. Applied Thermal Engineering 2012;37:344 –52. doi:10.1016/j.applthermaleng.2011.11.047.

[7] Pierobon L, Rokni M, Larsen U, Haglind F. Thermodynamic analysis of an integrated gasification solid oxide fuel cell plant combined with an organic Rankine cycle. Renewable Energy 2013;60:226 –34. doi:10.1016/j.renene.2013.05.021.

[8] Pierobon L, Nguyen TV, Larsen U, Haglind F, Elmegaard B. Multi-objective optimization of organic Rankine cycles for waste heat recovery: Application in an offshore platform. Energy 2013;58:538–49. doi:dx.doi.org/10.1016/j.energy.2013.05.039.

[9] Nielsen RF, Haglind F, Larsen U. Design and modeling of an advanced marine machinery system including waste heat recovery and removal of sulphur oxides. Energy Conversion and Management 2014;85:687–693. doi:dx.doi.org/10.1016/j.enconman.2014.03.038.

[10] Nguyen TV, Knudsen T, Larsen U, Haglind F, Elmegaard B. Thermodynamic evaluation of the Kalina Split-cycle concept for waste heat recovery applications. Energy 2014;71:277–288.

[11] Andreasen J, Larsen U, Knudsen T, Pierobon L, Haglind F. Selection and optimization of pure and mixed working fluids for low grade heat utilization using organic Rankine cycles. Energy 2014;73:204 –13. doi:dx.doi.org/10.1016/j.energy.2014.06.012.

[12] Larsen U, Nguyen TV, Haglind F. Development of a multi-level approach to model and optimise the Kalina Split cycle. In: Proceedings of the 53rd Scandinavian Conference on Simulation and Modeling. Orkustofnun National Energy Authority, Reykjavik, Iceland; 2012, p. 243–54. Accessed 2014/05/10; URL os.is/gogn/Skyrslur/OS-2012/OS-2012-06.pdf.

[13] Larsen U, Haglind F, Sigthorsson O. A comparison of advanced heat recovery power cycles in a combined cycle for large ships. In: Proceedings of ECOS 2013 - The 26th International Conference on Efficiency, Cost, Optimization, Simulation and Environmental Impact of Energy Systems, 2013. Chinese Society of Engineering Thermophysics, 11 Beisihuanxi Road, Beijing 100190, China; 2013, p. 1–13.

[14] Frimann Nielsen R, Haglind F, Larsen U. Design and modeling of an advanced marine machinery system including waste heat recovery and removal of sulphur oxides. In: Proceedings of ECOS 2013 - The 26th International Conference on Efficiency, Cost, Optimization, Simulation and Environmental Impact of Energy Systems. Chinese Society of Engineering Thermophysics; 2013, p. 1–13.

[15] Pierobon L, Larsen U, Nguyen TV, Haglind F. Optimization of Organic Rankine Cycles for Off-Shore Applications. American Society of Mechanical Engineers; 2013,2013; GT2013-94108.

[16] Pierobon L, Larsen U, Haglind F. Part-load performance of a combined gas turbine - organic Rankine cycle for off-shore applications. 2013.

[17] Baldi F, Larsen U, Gabrielii C, Andersson K. Analysis of the influence of the engine, propeller and auxiliary generation interaction on the energy efficiency of controllable pitch propeller ships. In: International Conference of Maritime Technology (ICMT). Glasgow, UK; 2014, p. 1–8.

[18] MAN Diesel and Turbo . Waste Heat Recovery System (WHRS) for Reduction of Fuel Consumption, Emissions and EEDI. Tech. Rep.; Copenhagen, Denmark; 2012.

[19] Chow A, Wyszynski ML. Thermodynamic modelling of complete engine systems - a review. Proceedings of the institution of mechanical engineers part d-journal of automobile engineering 1999;213(D4):403–15.

[20] Regina Asariotis and Hassiba Benamara and Jan Hoffmann and Azhar Jaimurzina and Anila Premti and Jose Maria Rubiato and Vincent Valentine and Frida Youssef . Review of Maritime Transport 2013. Tech. Rep.; UNCTAD; Geneva, Switzerland; 2013. Accessed 17/03/2014; URL unctad.org.

[21] Zabi Bazari and Tore Longva . Assessment Of IMO Mandated Energy Efficiency Measures for International Shipping. Tech. Rep.; The International Maritime Organisation; London, The United Kingdom; 2011. Accessed 20/03/2014; URL imo.org.

[22] The International Maritime Organisation . Nitrogen Oxides (NOx) Regulation 13. 2014. Accessed 20/03/2014; URL imo.org.

[23] DNV . First statement of compliance with IMO Tier II NOx emission limits issued. 2014. Accessed 20/03/2014; URL dnv.com.

[24] Kalli J, Karvonen T, Makkonen T. Sulphur content in ships bunker fuel in 2015. Tech. Rep.; Ministry of Transport and Communications; Helsinki, Finland; 2009. Accessed 08/09/2013; URL jernkontoret.se/energi_och_miljo/transporter/pdf/sulphur_content_in_ships_bunker_fuel_2015.pdf.

[25] Maersk . Triple E - the World's Largest Ship. 2014. Accessed 11/04/2014; URL worldslargestship.com.

[26] Baldi F. Improving Ship Energy Efficiency through a Systems Perspective. Chalmers University of Technology, Shipping and Marine Technology; 2013.

[27] The Hercules C project. 2014. Accessed 12/04/2014; URL hercules-c.com.

[28] Kyrtatos N, Hellberg L, Poensgen C. Ten Years After: Results from the Major Programme HERCULES A-B-C on Marine Engine R&D. In: CIMAC International Council on Combustion engines 2013. Shanghai: CIMAC; 2013, p. 1–8.

[29] Kjemtrup N, Aabo K, Knudsen TS. Developments on Exhaust Emission Modelling for Large Two-Stroke Diesel Engines Some Comparisons with Measured Data and an Update on the Latest Emission Reduction Techniques. In: CIMAC International Council on Combustion engines 2007. Vienna, Austria: CIMAC; 2007, p. 1–16.

[30] Kaltoft J, Preem M. Development of integrated EGR system for two-stroke diesel engines. In: CIMAC International Council on Combustion engines 2013. Shanghai, China: CIMAC; 2013, p. 1–14.

[31] Theotokatos G, Livanos G. Techno-economical analysis of single pressure exhaust gas waste heat recovery systems in marine propulsion plants. Proceedings of the Institution of Mechanical Engineers, Part M: Journal of Engineering for the Maritime Environment 2013;227(2):83–97. doi:10.1177/1475090212457894. Accessed 2014/05/10; URL pim.sagepub.com/content/227/2/83.abstract.

[32] Dimopoulos GG, Georgopoulou CA, Kakalis NM. Modelling and optimisation of an integrated marine combined cycle system. Novi sad, Serbia: Proceedings of ECOS; 2011, p. 1283–98.

[33] Dimopoulos GG, Georgopoulou CA, Kakalis NM. The introduction of exergy analysis to the thermo-economic modelling and optimisation of a marine combined cycle system. Perugia, Italia: Proceedings of ECOS; 2012, p. 611–6116.

[34] Danov SN, Gupta AK. Modeling the performance characteristics of diesel engine based combined-cycle power plants-part i: Mathematical model. Transactions- American Society Of Mechanical Engineers Journal Of Engineering For Gas Turbines And Power 2004;126(Part 1):28–34.

[35] Danov SN, Gupta AK. Modeling the performance characteristics of diesel engine based combined-cycle power plants - part ii: Results and applications. Journal of Engineering for Gas Turbines and Power 2004;126(1):35–9. doi:10.1115/1.1635397.

[36] Shu G, Liang Y, Wei H, Tian H, Zhao J, Liu L. A review of waste heat recovery on two-stroke IC engine aboard ships. Renewable and Sustainable Energy Reviews 2013;19:385 – 401. doi:dx.doi.org/10.1016/j.rser.2012.11.034.

[37] Teng H, Regner G, Cowland C. Achieving High Engine Efficiency for Heavy-Duty Diesel Engines by Waste Heat Recovery Using Supercritical Organic Fluid Rankine Cycle. SAE International; 2006,doi:10.4271/2006-01-3522.

[38] Srinivasan KK, Mago PJ, Krishnan SR. Analysis of exhaust waste heat recovery from a dual fuel low temperature combustion engine using an organic Rankine cycle. Energy 2010;35(6):2387 –99. doi:dx.doi.org/10.1016/j.energy.2010.02.018.

[39] Heim K. Existing and Future Demands on the Turbocharging of Modern Large Two-stroke Diesel Engines. Tech. Rep.; Wartsila, Switzerland; Winterthur, Switzerland; 2002.

[40] Kristensen HO. Energy Demand And Exhaust Gas Emissions Of Marine Engines. Tech. Rep.; Technical University of Denmark; Lyngby, Denmark; 2012. Accessed 18/12/2013; URL skibstekniskselskab.dk/.

[41] Hoffmann M. Literature review of state-of-the-art numerical optimisation. 2012. Accessed 11/04/2014; URL hercules-c.com.

[42] Chipperfield A, Fleming PJ, Pohlheim H, Fonseca CM. Genetic Algorithm Toolbox for use with Matlab. Tech. Rep.; Department of Automatic Control and Systems Engineering, University of Sheffield, United Kingdom; Sheffield; 1994.

[43] Zarei A, Ngatchou P, El-Sharkawi MA. Pareto multi objective optimization. Proceedings of the 13th International Conference on Intelligent Systems Application To Power Systems, ISAP'05 2005;2005:84–91. doi:10.1109/ISAP.2005.1599245.

[44] Econlib Resources. 2014. Accessed 11/01/2014; URL econlib.org.

[45] Woodyard DF. Pounders marine diesel engines and gas turbines. Elsevier/Butterworth-Heinemann; 2009. ISBN 0750689846, 9780750689847.

[46] MAN Diesel and Turbo . Basic principles of ship propulsion. 2013.

[47] Shaaban S. Experimental investigation and extended simulation of turbocharger non-adiabatic performance. Ph.D. thesis; Universitet Hannover, Germany; 2004. URL d-nb.info/974988219/34.

[48] Sinatov S. Turbocharging helps to diesel engine in cogeneration and combined cycles. In: CIMAC International Council on Combustion engines 1998. Copenhagen, Denmark: CIMAC; 1998, p. 1–12.

[49] Codan E, Mathey C, Rettig A. 2-Stage Turbocharging Flexibility for Engine Optimisation. In: CIMAC International Council on Combustion engines 2010. Bergen, Norway: CIMAC; 2010, p. 1–16.

[50] Schmuttermair H, Fernandez A, Witt M. Fuel Economy by Load Profile Optimized Charging Systems from MAN. In: CIMAC International Council on Combustion engines 2010. Bergen, Norway: CIMAC; 2010, p. 1–15.

[51] Haglind F. A review on the use of gas and steam turbine combined cycles as prime movers for large ships. part iii: Fuels and emissions. Energy Conversion And Management 2008;49(12):3476–82.

[52] EPA, United States . Learn the issues. 2009. Accessed 17/12/2013; URL epa.gov.

[53] van Aardenne J, Colette A, Degraeuwe B, Hammingh P, Viana M, de Vlieger I. The impact of international shipping on European air quality and climate forcing. Tech. Rep.; European Environmental Agency; Copenhagen, Denmark; 2013.

[54] Holtbecker R, Geist M. Exhaust emissions reduction technology for Sulzer marine diesel engines: General aspects. 1998.

[55] Shmid H, Weisser G. Marine technologies for reduced emissions. 2006.

[56] Kontoulis P, Chryssakis C, Kaiktsis L. Evaluation of pilot injections in a large two-stroke marine diesel engine, using CFD and t-f mapping. Proceedings of the 7th International Conference on Modeling and Diagnostics for Advanced Engine Systems, COMODIA 2008 2008;:181–8.

[57] Pedersen MF, Andreasen A, Mayer S. Two-stroke Engine Emission Reduction Technology: State-of-the-art. In: CIMAC International Council on Combustion engines 2010. Bergen, Norway: CIMAC; 2010, p. 1–15.

[58] MAN Diesel and Turbo . Exhaust Gas Emission Control Today and Tomorrow. 2010. Accessed 19/12/2013; URL mandieselturbo.com.

[59] Heywood J. Internal combustion engine fundamentals. McGraw-Hill series in mechanical engineering; McGraw-Hill; 1988. ISBN 9780070286375.

[60] Kumar S, Kumar Chauhan M, Varun . Numerical modeling of compression ignition engine: A review. Renewable and Sustainable Energy Reviews 2013;19:517–30. doi:10.1016/j.rser.2012.11.043.

[61] Lakshminarayanan PA, Aghav YV. Modelling Diesel Combustion. Springer Science+Business Media B.V; 2010. ISBN 904813885x, 9789048138852.

[62] Grimmelius H, Mesbahi E, Schulten P, Stapersma D. The use of Diesel engine simulation models in ship propulsion plant design and operation. In: CIMAC International Council on Combustion engines 2007. Vienna, Austria: CIMAC; 2007, p. 1–12.

[63] Mayer S, Elena TA, Andreasen A. Design of experiments analysis of the NOx-SFOC trade-off in two-stroke marine engine. In: CIMAC International Council on Combustion engines 2010. Bergen: CIMAC; 2010, p. 1–10.

[64] Seykens XLJ. Modelling of combustion and nitric oxide formation for medium-speed di diesel engines: A comparative evaluation of zero- and three-dimensional approaches. Ph.D. thesis; Swiss Federal Institute Of Technology Zurich, Switzerland; 2001. Accessed: 28/01/2014; URL lav.ethz.ch/publications/thesis/GW_thesis.pdf.

[65] Wimmer A, Pirker G, Engelmayer M, Gufler M, Chmela F, Hirschl G. Advances and Challenges in Simulating Combustion and Emission Formation in Large Diesel Engines. In: CIMAC International Council on Combustion engines 2013. Shanghai: CIMAC; 2013, p. 1–15.

[66] Grimmelius HT, Stapersma D. The Impact Of Propulsion Plant Control On Diesel Engine Thermal Loading. In: CIMAC International Council on Combustion engines 2001. Hamburg, Germany: CIMAC; 2001, p. 1–18.

[67] Yu D, Stapersma D, Grimmelius H. Cylinder process simulation with heat release analysis in diesel engine. In: Power and Energy Engineering Conference, 2009. APPEEC 2009. Asia-Pacific. 2009, p. 1–4. doi:10.1109/APPEEC.2009.4918248.

[68] Graphische Thermodynamik und Berechnen der Verbrennungs-Maschinen und Turbinen. J. Springer; 1922. URL books.google.com.my/books?id=PXDVAAAAMAAJ.

[69] Woschni G. A universally applicable equation for the instantaneous heat transfer coefficient in the internal combustion engine. SAE International 1967;doi:10.4271/670931.

[70] Chen SK, Flynn PF. Development of a single cylinder compression ignition research engine. 1965. doi:10.4271/650733.

[71] Gyftopoulos E, Beretta G. Thermodynamics: Foundations and Applications. Dover Civil and Mechanical Engineering; Dover Publications; 2012. ISBN 9780486135182.

[72] Goldsworthy L. Real time model for oxides of nitrogen emissions from a slow speed marine diesel. Proceedings of IMarEST - Part A - Journal of Marine Engineering and Technology 2003;2003(2):3–12. Accessed 2014/05/10; URL ingentaconnect.com/content/imarest/jmet/2003/00002003/00000002/art00001.

[73] Zevenhoven R. Non-ideal gases in diesel engine processes. Scandinavian Nordic Section Of The Combustion Institute Proceedings 2001;1:103–8.

[74] Lapuerta M, Ballesteros R, Agudelo JR. Effect of the gas state equation on the thermodynamic diagnostic of diesel combustion. Applied Thermal Engineering 2006;26(1415):1492 –9. doi:dx.doi.org/10.1016/j.applthermaleng.2006.01.001.

[75] Danov SN, Gupta AK. Influence of Imperfections in Working Media on Diesel Engine Indicator Process. Journal of Engineering for Gas Turbines and Power 2000;123(1):231–9. Accessed 2014/05/10; URL dx.doi.org/10.1115/1.1339986.

[76] Borman G, Nishiwaki K. Internal-combustion engine heat transfer. Progress in Energy and Combustion Science 1987;13(1):1 – 46. doi:dx.doi.org/10.1016/0360-1285(87)90005-0.

[77] Torregrossa AJ. Revising engine heat transfer. Annals Of The Faculty Of Engineering Hunedoara Journal Of Engineering 2008;3. Accessed 2014/05/10; URL annals.fih.upt.ro/pdf-full/2008/ANNALS-2008-3-45.pdf.

[78] Boulouchos K, Brunner D. Assessment of heat transfer models for larger , low-speed engines. In: CIMAC International Council on Combustion engines 1993. London: CIMAC; 1993, p. 1–15.

[79] Annand W. Heat transfer in cylinders of reciprocating internal combustion engines. Institution of Mechanical Engineers – Proceedings 1963;177(36):973–96.

[80] Merker G. Simulating Combustion: Simulation of Combustion and Pollutant Formation for Engine-development. Springer; 2006. ISBN 9783540251613. Accessed 2014/05/10; URL books.google.com.my/books?id=0IoPFDYMPGsC.

[81] Poulsen H. In-situ Investigations of the Combustion in Large, Two-stroke, Diesel Engines. Ph.D. thesis; Technical University of Denmark, Copenhagen Denmark; 2001.

[82] Digital M. Website of Marine Digital. 2014. Accessed 22/01/2012; URL marinedigital.com.

[83] Ghojel JI. Review of the development and applications of the Wiebe function: a tribute to the contribution of Ivan Wiebe to engine research. International Journal of Engine Research 2010;11(4):297–312.

[84] Miyamoto N, Chikahisa T, Murayama T, Sawyer R. Description And Analysis Of Diesel Engine Rate Of Combustion And Performance Using Wiebe's Functions. Proceedings - Society of Automotive Engineers 1985;:77–88.

[85] Egnell R. A simple approach to studying the relation between fuel rate heat release rate and NO formation in diesel engines. 1999. doi:10.4271/1999-01-3548.

[86] Ding Y, Stapersma D, Knoll H, Grimmelius H. Characterising Heat Release in a Diesel Engine: A comparison between Seiliger Process and Vibe Model. In: CIMAC International Council on Combustion engines 2010. Bergen, Norway: CIMAC; 2010, p. 1–13.

[87] Loganathan S, Manohar RM, Thamaraikannan R, Dhanasekaran R, Rameshbabu A, Krishnamoorthy V. Direct injection diesel engine rate of heat release prediction using universal load correction factor in double wiebe function for performance simulation. 2012. doi:10.4271/2011-01-2456.

[88] Egnell R. On zero-dimensional modelling of combustion and nox formation in diesel engines. Ph.D. thesis; Lund university, Sweden; 2001.

[89] Wilhelmsson C, Tunestl P, Widd BJA, Johansson R. A physical two-zone NOx model intended for embedded implementation. 2009. doi:10.4271/2009-01-1509.

[90] Rakopoulos C, Hountalas D, Tzanos E, Taklis G. A fast algorithm for calculating the composition of diesel combustion products using 11 species chemical equilibrium scheme. Advances in Engineering Software 1994;19(2):109 –19. doi:10.1016/0965-9978(94)90064-7.

[91] Tomeczek J, Gradon B. The role of nitrous oxide in the mechanism of thermal nitric oxide formation within flame temperature range. Combustion Science And Technology - New York Then Yverdon 1997;125(1/6):159–80.

[92] Kilpinen P. Optimization of a simplified sub-model for NO emission prediction by CFD in large 4-stroke marine diesel engines. Fuel Processing Technology 2010;91(2):218–28. doi:10.1016/j.fuproc.2009.10.001.

[93] Zabetta EC, Kilpinen P. Improved no x submodel for in-cylinder CFD simulation of low- and medium-speed compression ignition engines. Energy And Fuels 2001;15(PART 6):1425–33.

[94] Zabetta EC, Kilpinen P, Hupa M, Stahl K, Leppalahti J, Cannon M, et al. Kinetic modeling study on the potential of staged combustion in gas turbines for the reduction of nitrogen oxide emissions from biomass igcc plants. Energy And Fuels 2000;14(PART 4):751–61.

[95] Sorenson S. Engine principles and vehicles. Technical University of Denmark. Department of Mechanical Engineering; 2008. ISBN 9788770780391.

[96] Goldsworthy L. Reduced kinetics schemes for oxides of nitrogen emissions from a slow-speed marine diesel engine. Energy And Fuels 2003;17(2):450–6. doi:10.1021/ef020172c.

[97] Goldsworthy L. Predictive monitoring system for oxides of nitrogen emissions from marine diesel engines. In: CIMAC International Council on Combustion engines 2004. Kyoto, Japan: CIMAC; 2004, p. 1–12.

[98] Rao V, Honnery D. A comparison of two NOx prediction schemes for use in diesel engine thermodynamic modelling. Fuel 2013;107:662–70. doi:10.1016/j.fuel.2013.01.071.

[99] Seykens XLJ. Development and validation of a phenomenological diesel engine combustion model. Ph.D. thesis; Eindhoven University of Technology, The Netherlands; 2001.

[100] Voelund A, Felter C. Experimental Investigation of Lubrication Regimes on Piston Ring - Cylinder Liner Contacts for Large Two-stroke Engines. In: CIMAC International Council on Combustion engines 2010. Bergen, Norway: CIMAC; 2010, p. 1–10.

[101] Rakopoulos CD, Giakoumis EG. Prediction of friction development during transient diesel engine operation using a detailed model. International Journal Of Vehicle Design 2007;44(1-2):143–66.

[102] Burmeister & Wain, Copenhagen, Denmark . Instruction book operation edition 0002. Tech. Rep.; 2004.

[103] Livanos GA, Kyrtatos NP. Friction model of a marine diesel engine piston assembly. Tribology International 2007;40(10-12):1441–53. doi:10.1016/j.triboint.2007.01.020.

[104] Grimmelius H, Boonen EJ, Nicolai H, Stapersma D. The integration of mean value first principle diesel engine models in dynamic waste heat and cooling load analysis. In: CIMAC International Council on Combustion engines 2010. Bergen, Norway: CIMAC; 2010, p. 1–11.

[105] Yun KT, Cho H, Luck R, Mago PJ. Modeling of reciprocating internal combustion engines for power generation and heat recovery. Applied Energy Kidlington 2013;102:327–37.

[106] Payri F, Olmeda P, Martin J, Garcia A. A complete 0d thermodynamic predictive model for direct injection diesel engines. Applied Energy 2011;88(12):4632–41.

[107] Lemmon E, Huber M, McLinden M. National Institute of Standards and Technology, Maryland, United States, Standard Reference Database 23 Reference Fluid Thermodynamic and Transport Properties-REFPROP, Software version 9.0. 2010.

[108] MAN Diesel and Turbo, Copenhagen, Denmark . CEAS-ERD: Engine Room Dimensioning Software. 2013. Accessed 2013/08/01; URL `www.mandieselturbo.com/ceas/index.html`.

[109] MAN, Augsburg, Germany . Project Guide Exhaust Gas Turbocharger TCA-Series. Tech. Rep.; 2007.

[110] International Maritime Organization . IMO NOx technical code 2008. Tech. Rep.; IMO; London, United Kingdom; 2008. Accessed 21/01/2014; URL `imo.org`.

[111] Egeberg CE, Ostergaard A. The MC Engine And Its Future Development. In: CIMAC International Council on Combustion engines 2001. Hamburg, Germany: CIMAC; 2001, p. 1–10.

[112] Yamamoto S, Nagaoka M, Ueda R, Wakisaka Y, Noda S. Numerical simulation of diesel combustion with a high exhaust gas recirculation rate. International Journal Of Engine Research 2010;11(1):17–27. doi:10.1243/14680874JER05309.

[113] Kim SK, Wakisaka T, Aoyagi Y. A numerical study of the effects of boost pressure and exhaust gas recirculation ratio on the combustion process and exhaust emissions in a diesel engine. International Journal Of Engine Research 2007;8(2):147–62. doi:10.1243/14680874JER02606.

[114] Hountalas DT, Raptotasios SI, Zannis TC. Implications of exhaust gas, CO2, and N2 recirculation on heavy-duty diesel engine performance, soot, and NO emissions: A comparative study. Energy and Fuels 2013;27(8):204910–4929. doi:10.1021/ef400289w.

[115] Nanda S, Roskilly AP. Performance monitoring of slow speed diesel engines by dynamic exhaust gas temperature measurement and oxygen concentration measurement of blow down exhaust gas. In: CIMAC International Council on Combustion engines 2007. Vienna, Austria: CIMAC; 2007, p. 1–15.

[116] Payri F, Molina S, Martin J, Armas O. Influence of measurement errors and estimated parameters on combustion diagnosis. Applied Thermal Engineering 2006;26(2-3):226–36. doi:10.1016/j.applthermaleng.2005.05.006.

[117] Tsalapatis D, Schnohr O. Development and application capability of MAN B&W MCMCE engines. In: CIMAC International Council on Combustion engines 1987. Warsaw, Poland: CIMAC; 1987, p. 1–10.

[118] Hou Z, Vlaskos I, Fusstetter K, Kahi M, Neuenschwander P. New Application Fields for Marine Waste Heat Systems by Analysing the Main Design Parameters. In: CIMAC International Council on Combustion engines 2007. Vienna, Austria: CIMAC; 2007, p. 1–15.

[119] Woodward JB. Recovering The Energy In Diesel Exhaust: Some Thermodynamic Points. Marine Technology 1987;24(3):205–11.

[120] Invernizzi CM. Closed power cycles : thermodynamic fundamentals and applications. London New York: Springer; 2013. ISBN 9781447151401.

[121] Angelino G, Gaia M, Macchi E. Review Of Italian Activity In The Field Of Organic Rankine Cycles. VDI Berichte 1984;:465–82.

[122] Turboden . ORC, Advantages. 2013. Accessed November 2013; URL `turboden.eu/en/Rankine/Rankine-advantages.php`.

[123] Bao J, Zhao L. A review of working fluid and expander selections for organic Rankine cycle. Renewable and Sustainable Energy Reviews 2013;24:325 –42. doi:10.1016/j.rser.2013.03.040.

[124] ORC Power Systems committee of the ASME IGTI . Literature, Relevant publications. 2013. Accessed November 2013; URL `kcorc.org/en/literature/relevant-publications`.

[125] Wang Z, Zhou N, Guo J, Wang X. Fluid selection and parametric optimization of organic Rankine cycle using low temperature waste heat. Energy 2012;40(1):107–15. doi:10.1016/j.energy.2012.02.022.

[126] Wang E, Zhang H, Fan B, Ouyang M, Zhao Y, Mu Q. Study of working fluid selection of organic Rankine cycle (ORC) for engine waste heat recovery. Energy 2011;36(5):3406–18. doi:10.1016/j.energy.2011.03.041.

[127] Badr O, Probert S, O'Callaghan P. Selecting a working fluid for a Rankine-cycle engine. Applied Energy 1985;21(1):1–42. doi:10.1016/0306-2619(85)90072-8.

[128] Chen H, Goswami DY, Stefanakos EK. A review of thermodynamic cycles and working fluids for the conversion of low-grade heat. Renewable and Sustainable Energy Reviews 2010;14(9):3059–67. doi:10.1016/j.rser.2010.07.006.

[129] Quoilin S, Broek MVD, Declaye S, Dewallef P, Lemort V. Techno-economic survey of Organic Rankine Cycle (ORC) systems . Renewable and Sustainable Energy Reviews 2013;22:168 –86. doi:10.1016/j.rser.2013.01.028.

[130] Tchanche BF, Lambrinos G, Frangoudakis A, Papadakis G. Low-grade heat conversion into power using organic Rankine cycles A review of various applications. Renewable and Sustainable Energy Reviews 2011;15(8):3963–79. doi:10.1016/j.rser.2011.07.024.

[131] Trapp C. Efficiency Improvement in Precombustion CO2 Removal Units With a Waste Heat Recovery ORC Power Plant. Journal of Engineering for Gas Turbines and Power 2013;135(4):0423111–04231111. doi:10.1115/1.4023121.

[132] Siddiqi MA, Atakan B. Alkanes as fluids in Rankine cycles in comparison to water, benzene and toluene. Energy 2012;45(1):256 –63. doi:10.1016/j.energy.2012.06.005.

[133] Vaja I, Gambarotta A. Internal combustion engine (ICE) bottoming with Organic Rankine Cycles (ORCs). Energy 2010;35(2):1084 –93. doi:10.1016/j.energy.2009.06.001. ECOS 2008 21st International Conference, on Efficiency, Cost, Optimization, Simulation and Environmental Impact of Energy Systems.

[134] Mago PJ, Chamra LM, Somayaji C. Performance analysis of different working fluids for use in organic Rankine cycles. Proceedings of the Institution of Mechanical Engineers, Part A Journal of Power and Energy 2007;221(3):255–64.

[135] Karellas S, Schuster A. Supercritical Fluid Parameters in Organic Rankine Cycle Applications. Tech. Rep. 3; 2010. doi:10.5541/ijot.217.

[136] Drescher U, Brüggemann D. Fluid selection for the Organic Rankine Cycle (ORC) in biomass power and heat plants. Applied Thermal Engineering 2007;27(1):223–8. doi:10.1016/j.applthermaleng.2006.04.024.

[137] Saleh B, Koglbauer G, Wendland M, Fischer J. Working fluids for low-temperature organic Rankine cycles. Energy 2007;32(7):1210–21.

[138] Tchanche BF, Papadakis G, Lambrinos G, Frangoudakis A. Fluid selection for a low-temperature solar organic Rankine cycle. Applied Thermal Engineering 2009;29(11-12):2468–76. doi:10.1016/j.applthermaleng.2008.12.025.

[139] Dai Y, Wang J, Gao L. Parametric optimization and comparative study of organic Rankine cycle (ORC) for low grade waste heat recovery. Energy Conversion and Management 2009;50(3):576–82. doi:10.1016/j.enconman.2008.10.018.

[140] Papadopoulos AI, Stijepovic M, Linke P. On the systematic design and selection of optimal working fluids for Organic Rankine Cycles. Applied Thermal Engineering 2010;30(6-7):760–9. doi:10.1016/j.applthermaleng.2009.12.006.

[141] Liu BT, Chien KH, Wang CC. Effect of working fluids on organic Rankine cycle for waste heat recovery. Energy 2004;29(8):1207 –17. doi:10.1016/j.energy.2004.01.004.

[142] Teng H, Regner G, Cowland C. Waste heat recovery of heavy-duty diesel engines by organic Rankine cycle part ii: Working fluids for WHR-ORC. 2007. doi:10.4271/2007-01-0543.

[143] Wang E, Zhang H, Fan B, Ouyang M, Zhao Y, Mu Q. Study of working fluid selection of organic Rankine cycle (ORC) for engine waste heat recovery. Energy 2011;36(5):3406 –18. doi:10.1016/j.energy.2011.03.041.

[144] Kuo CR, Hsu SW, Chang KH, Wang CC. Analysis of a 50kW organic Rankine cycle system. Energy 2011;36(10):5877–85. doi:10.1016/j.energy.2011.08.035.

[145] Wang D, Ling X, Peng H, Liu L, Tao L. Efficiency and optimal performance evaluation of organic Rankine cycle for low grade waste heat power generation. Energy 2013;50:343 –52. doi:10.1016/j.energy.2012.11.010.

[146] Crook A, of Electrical Engineers I. Profiting from Low Grade Heat: Thermodynamic Cycles for Low-temperature Heat Sources. IEE energy series; Institution of Electrical Engineers; 1994. ISBN 9780852968352. Accessed 2014/05/10; URL books.google.dk/books?id=-hcGHMP89EYC.

[147] Kalina A. Combined cycle and waste heat recovery power systems based on a novel thermodynamic energy cycle utilizing low-temperature heat for power generation. Am Soc Mech Eng, (Pap); (United States) 1983;83-JPGC-GT.

[148] Jonnson M, Thorin E, Svedberg G. Gas Engine Bottoming Cycles With Ammonia-Water Mixtures as Working Fluid. ASME -Publications- PWR 1999;34(NO 2):55–66.

[149] Marston CH. Parametric Analysis of the Kalina Cycle. Journal of Engineering for Gas Turbines and Power 1990;112(1):107–.

[150] Kalina A, Leibowitz H, Lazzeri L, Diotti F. Recent development in the application of Kalina cycle for geothermal plants, geothermal-energy.org. 1995.

[151] Lazzeri L, Diotti F, Bruzzone M, Scala M. Application of Kalina Cycle to Geothermal Applications. Proceedings of the American Power Conference 1995;57(V1):370–3.

[152] Madhawa Hettiarachchi HD, Golubovic M, Worek WM, Ikegami Y. The Performance of the Kalina Cycle System 11(KCS-11) With Low-Temperature Heat Sources. Journal of Energy Resources Technology 2007;129(3):243–.

[153] Koroneos CJ, Rovas DC. Electricity from Geothermal Energy with the Kalina Cycle An Exergy Approach. In: International Conference on Clean Electrical Power, 2007. ICCEP '07. 2007, p. 423–8.

[154] Kalina AI. Application of recent developments in Kalina Cycle technology to the utilization of high temperature geothermal sources. Transactions - Geothermal Resources Council 2008;32:346–50.

[155] Nasruddin D, Usvika R, Rifaldi M, Noor A. Energy and exergy analysis of Kalina cycle system (KCS) 34 with mass fraction ammonia-water mixture variation. Journal of Mechanical Science and Technology 2009;23(7):1871–6.

[156] Ogriseck S. Integration of Kalina cycle in a combined heat and power plant, a case study. Applied Thermal Engineering 2009;29(14-15):2843–8.

[157] Valdimarsson P. Geothermal power plant cycles and main components. Tech. Rep.; University of Iceland; Reykjavik; 2011.

[158] Jonsson M, Yan J. Exergy and Pinch Analysis of Diesel Engine Bottoming Cycles with Ammonia-Water Mixtures as Working Fluid 2000;3(2):57–71.

[159] Jonsson M, Yan J. Ammonia-water bottoming cycles: a comparison between gas engines and gas diesel engines as prime movers. Energy 2001;26(1):31–44.

[160] Xia B, Tanaka S, Nakazawa T, Sugita H. Research on the application of the combined cycle used in the power plant for ship propelling systems. Proceedings of the International Conference on Power Engineering : ICOPE 2003;2003(3):3–162.

[161] He M, Zhang X, Zeng K, Gao K. A combined thermodynamic cycle used for waste heat recovery of internal combustion engine. Energy 2011;36(12):6821–9.

[162] Marston CH, Hyre M. Gas Turbine Bottoming Cycles: Triple-Pressure Steam Versus Kalina. Journal of Engineering for Gas Turbines and Power 1995;117(1):1–10.

[163] Nag P, Gupta A. Exergy analysis of the Kalina cycle. Applied Thermal Engineering 1998;18(6):427–39.

[164] Jonsson M, Yan J. Gas turbine with Kalina bottoming cycle versus evaporative gas turbine cycle. In: Proceedings of the International Joint Power Generation Conference. New Orleans: ISSN 1537-6753; 2001, p. 77–85.

[165] Zhang Y, He M, Jia Z, Liu X. First law-based thermodynamic analysis on Kalina cycle. Frontiers of Energy and Power Engineering in China 2008;2(2):145–51.

[166] Leibowitz HM, Zervos N. Installation and Early Test Results of a 3 MW Kalina Cycle Demonstration Plant. SAE International 1992;1992-08-03.

[167] Zervos NG, Leibowitz HM, Robinson K. Innovative Kalina cycle promises high efficiency [combined cycle power stations]. Power 1992;136(4):177–9.

[168] Zervos NG, Leibowitz HM, Robinson K. Startup and operating experience of the Kalina cycle demonstration plant. American Society of Mechanical Engineers, International Gas Turbine Institute (Publication) IGTI 1992;7.

[169] Bombarda P, Invernizzi CM, Pietra C. Heat recovery from Diesel engines: A thermodynamic comparison between Kalina and ORC cycles. Applied Thermal Engineering 2010;30(2-3):212 –9.

[170] Jonsson M, Yan J. Exergy and Pinch Analysis of Diesel Engine Bottoming Cycles with Ammonia-Water Mixtures as Working Fluid. International Journal of Thermodynamics 2010;3(2):57–71. doi:10.5541/ijot.34. Accessed 03/10/2013; URL ehakem.com/index.php/IJoT/article/view/34.

[171] Wang J, Yan Z, Wang M, Dai Y. Thermodynamic analysis and optimization of an ammonia-water power system with LNG (liquefied natural gas) as its heat sink. Energy 2013;50:513 –22. doi:dx.doi.org/10.1016/j.energy.2012.11.034.

[172] Li X, Zhang Q, Li X. A Kalina cycle with ejector . Energy 2013;54:212 –9. doi:dx.doi.org/10.1016/j.energy.2013.03.040.

[173] Tillner-Roth R, Friend D. A Helmholtz free energy formulation of the thermodynamic properties of the mixture {water+ammonia}. Journal of Physical and Chemical Reference Data 1998;27(1):63–96.

[174] Tillner-Roth R, Friend DG. Survey and Assessment of Available Measurements on Thermodynamic Properties of the Mixture {Water + Ammonia}. Journal of Physical and Chemical Reference Data 1998;27(1):45–62.

[175] Thorin E. Comparison of Correlations for Predicting Thermodynamic Properties of AmmoniaWater Mixtures. International Journal of Thermophysics 2000;21(4):853–70.

[176] Zhang X, He M, Zhang Y. A review of research on the Kalina cycle. Renewable and Sustainable Energy Reviews 2012;16(7):5309 –18. doi:10.1016/j.rser.2012.05.040.

[177] Bombarda P, Invernizzi CM, Pietra C. Heat recovery from Diesel engines: A thermodynamic comparison between Kalina and ORC cycles. Applied Thermal Engineering 2010;30(2-3):212–9.

[178] Mirolli MD. Kalina Cycle power systems in waste heat recovery applications. 2014. Accessed 29/03/2014; URL globalcement.com.

[179] Smidth FL. Waste Heat Recovery. 2014. Accessed 29/03/2014; URL flsmidth.com.

[180] T.Q. Nguyen J.D. Slawnwhite KB. Power generation from residual industrial heat. Energy Conversion and Management 2010;51(11):2220 –9. doi:10.1016/j.enconman.2010.03.016.

[181] Kalina A. A Kalina cycle technology and its applications. American Institute of Chemical Engineers, New York, NY United States of America; 1986,Accessed 30/08/2013; URL www.osti.gov.

[182] Kalina A. Website of Rex Research, US Patent # 4,548,043. 1985. Accessed 30/08/2013; URL www.rexresearch.com/kalina/kalina.htm.

[183] The Dow Chemical Company, Michigan, United States . DOWTHERM Q Heat Transfer Fluid. Tech. Rep.; 1997.

[184] Mathworks Massachusetts US. Matlab R2010b. 2010.

[185] American Coatings Association, Washington DC, United States . Hazardous Materials Identification System. 2012.

[186] Wang J, Yan Z, Wang M, Li M, Dai Y. Multi-objective optimization of an organic Rankine cycle (ORC) for low grade waste heat recovery using evolutionary algorithm. Energy Conversion and Management 2013;71:146 –58. doi:10.1016/j.enconman.2013.03.028.

[187] Larsen P. University of Southern Denmark website, Regression and analysis of variance. 2005. Last accessed July, 2013; URL statmaster.sdu.dk/courses/st111/index.html.

[188] Elmegaard B, Houbak N. DNA A General Energy System Simulation Tool. SIMS 2005 and Tapir Academic Press. ISBN 82-519-2093-0; 2005, p. 43–52.

[189] Aspen Tech Massachusetts, USA . Aspen Plus Software Version 7.2. 2010. Accessed 01/06/2013; URL aspentech.com.

[190] Westerberg A, Piela P. Equational-based process modeling. Tech. Rep.; Department of Chemical Engineering and the Engineering Design Research Center Carnegie Mellon University; Pittsburgh; 1994. Accessed 23/11/2013; URL www.cs.cmu.edu/~ascendFTP/pdffiles/ProcessModeling.pdf.

[191] Rodriguez CEC, Palacio JCE, Venturini OJ, Lora EES, Cobas VM, dos Santos DM, et al. Exergetic and economic comparison of ORC and Kalina cycle for low temperature enhanced geothermal system in Brazil. Applied Thermal Engineering 2013;52(1):109 –19. doi:dx.doi.org/10.1016/j.applthermaleng.2012.11.012.

[192] Thorin E. Thermophysical Properties of Ammonia-Water Mixtures for Prediction of Heat Transfer Areas in Power Cycles. International Journal Of Thermophysics 2001;22(Part 1):201–14.

[193] Roetzel W, Spang B. C3 typical values of overall heat transfer coefficients. In: VDI Heat Atlas. VDI-Buch; Springer Berlin Heidelberg. ISBN 978-3-540-77876-9; 2010, p. 75–8. doi:10.1007/978-3-540-77877-6_6.

[194] Rodriguez CEC, Palacio JCE, Venturini OJ, Lora EES, Cobas VM, dos Santos DM, et al. Exergetic and economic analysis of Kalina cycle for low temperature geothermal sources in Brazil . In: The 25th International Conference on Efficiency, Cost, Optimization, Simulation and Environmental Impact of Energy, ECOS 2012. 2012, p. 167 –79. Accessed 05/09/2013; URL www.fupress.com/archivio/pdf/5493.pdf.

[195] MAN Diesel and Turbo, Denmark . Thermo Efficiency System for Reduction of Fuel Consumption and CO2 Emission. 2009. Accessed 05/09/2013; URL www.mandieselturbo.de/files/news/filesof5055/5510-0030-01ppr.pdf.

[196] Wartsila, Helsinki, Finland . Wartsila 32, Technology Review. 2007. Accessed 05/09/2013; URL www.wartsila.com.

[197] MAN Diesel & Turbo, Denmark . Operation on Low-Sulphur Fuels. 2010. Accessed 05/09/2013; URL www.mandieselturbo.com.

[198] Lai NA, Wendland M, Fischer J. Working fluids for high-temperature organic Rankine cycles. Energy 2011;36(1):199–211. doi:10.1016/j.energy.2010.10.051.

[199] MAN Diesel & Turbo, Copenhagen and Denmark . K98MEC7 Engine project guide. 2013. Accessed 2014/05/10; URL www.mandieselturbo.com.

[200] United States Environmental Protection Agency, Washington United States . United States Environmental Protection Agency. 2012.

[201] Johnson RA, Wichern DW. Applied multivariate statistical analysis. Upper Saddle River,NJ: Pearson; 2007. ISBN 9780135143506.

[202] Kang SH. Design and experimental study of ORC (organic Rankine cycle) and radial turbine using R245fa working fluid. Energy 2012;41(1):514 –24. doi:10.1016/j.energy.2012.02.035. 23rd International Conference on Efficiency, Cost, Optimization, Simulation and Environmental Impact of Energy Systems, ECOS 2010.

[203] Colonna P, Harinck J, Rebay S, Guardone A. Real-Gas Effects in Organic Rankine Cycle Turbine Nozzles. Journal of Propulsion and Power 2008;24:282–94. doi:10.2514/1.29718.

[204] Montzka SA, Fraser PJ. Controlled substances and other source gases, Chapter 1 of the Scientific Assessment of Ozone Depletion: 2002, World Meteorological Organization Geneva, Switzerland. Tech. Rep.; 2003.

[205] Domingues A, Santos H, Costa M. Analysis of vehicle exhaust waste heat recovery potential using a Rankine cycle. Energy 2013;49:71 – 85. doi:10.1016/j.energy.2012.11.001.

[206] Vescovo R. ORC recovering industrial heat power generation from waste energy streams. Cogeneration and On-Site Power Production 2009;Accessed August 2013; URL www.cospp.com.

[207] van Buijtenen JP. The Tri-O-Gen Organic Rankine Cycle. Tech. Rep.; Power Engineer March 2009, Delft University, The Netherlands; 2009.

[208] Andersen WC, Bruno TJ. Rapid Screening of Fluids for Chemical Stability in Organic Rankine Cycle Applications. Industrial & Engineering Chemistry Research 2005;44(15):5560–6. doi:10.1021/ie050351s.

[209] Dai Y, Wang J, Gao L. Parametric optimization and comparative study of organic Rankine cycle (ORC) for low grade waste heat recovery. Energy Conversion and Management 2009;50(3):576 –82. doi:10.1016/j.enconman.2008.10.018.

[210] Walraven D, Laenen B, Dhaeseleer W. Comparison of thermodynamic cycles for power production from low-temperature geothermal heat sources. Energy Conversion and Management 2013;66:220 –33. doi:10.1016/j.enconman.2012.10.003.

[211] Choi BC, Kim YM. Thermodynamic analysis of a dual loop heat recovery system with trilateral cycle applied to exhaust gases of internal combustion engine for propulsion of the 6800 TEU container ship. Energy 2013;58:404 –16. doi:dx.doi.org/10.1016/j.energy.2013.05.017.

[212] Yang K, Zhang H, Wang Z, Zhang J, Yang F, Wang E, et al. Study of zeotropic mixtures of ORC (organic Rankine cycle) under engine various operating conditions. Energy 2013;58:494 – 510. doi:dx.doi.org/10.1016/j.energy.2013.04.074.

[213] Zare V, Mahmoudi S, Yari M, Amidpour M. Thermoeconomic analysis and optimization of an ammoniawater power/cooling cogeneration cycle. Energy 2012;47(1):271 –83. doi:dx.doi.org/10.1016/j.energy.2012.09.002. Asia-Pacific Forum on Renewable Energy 2011.

[214] Haglind F. Variable geometry gas turbines for improving the part-load performance of marine combined cycles combined cycle performance. Applied Thermal Engineering 2011;31(4):467 –76. doi:dx.doi.org/10.1016/j.applthermaleng.2010.09.029.

[215] Pierobon L, Kandepu R, Haglind F. Waste heat recovery for offshore applications; vol. 6. American Society of Mechanical Engineers. ISBN 9780791845226; 2012, p. 503–12. doi:10.1115/IMECE2012-86254.

[216] Toffolo A, Lazzaretto A, Manente G, Paci M. A multi-criteria approach for the optimal selection of working fluid and design parameters in Organic Rankine Cycle systems. Applied Energy - Kidlington 2014;121:219–32.

[217] Astolfi M, Romano MC, Bombarda P, Macchi E. Binary ORC (Organic Rankine Cycles) power plants for the exploitation of mediumlow temperature geothermal sources Part B Techno-economic optimization. Energy 2014;66:435–46.

[218] Kurzke J. How to create a performance model of a gas turbine from a limited amount of information. Proceedings of the ASME Turbo Expo 2005;1:145–53. doi:10.1115/GT2005-68536.

[219] Cooke DH. On Prediction Of Off-design Multistage Turbine Pressures By Stodola's Ellipse. Journal of Engineering for Gas Turbines and Power, Transactions of the ASME 1985;107(3):596–606.

[220] Tochio S, Kondo M, Kunimitsu M, Ide R. Development of Large-Scale Turbocharger Generator Unit. In: CIMAC International Council on Combustion engines 2010. Bergen: CIMAC; 2010, p. 1–15.

[221] Ono Y. Solutions for better engine performance at low load by Mitsubishi turbochargers. In: CIMAC International Council on Combustion engines 2013. Shanghai: CIMAC; 2013, p. 1–15.

[222] Quoilin S, Aumann R, Grill A, Schuster A, Lemort V, Spliethoff H. Dynamic modeling and optimal control strategy of waste heat recovery Organic Rankine Cycles. Applied Energy 2011;88(6):2183–90.

[223] Manolakos D, Papadakis G, Papantonis D, Kyritsis S. A simulation-optimisation programme for designing hybrid energy systems for supplying electricity and fresh water through desalination to remote areas: Case study: the Merssini village, Donoussa island, Aegean Sea, Greece. Energy 2001;26(7):679 – 704. doi:dx.doi.org/10.1016/S0360-5442(01)00026-3.

[224] Schobeiri M. Turbine aerodynamic design and off-design performance. In: Turbomachinery Flow Physics and Dynamic Performance. Springer Berlin Heidelberg. ISBN 978-3-540-22368-9; 2005, p. 409–37. doi:10.1007/978-3-540-26591-7_17.

[225] Manente G, Toffolo A, Lazzaretto A, Paci M. An Organic Rankine Cycle off-design model for the search of the optimal control strategy . Energy 2013;58:97 – 106. doi:dx.doi.org/10.1016/j.energy.2012.12.035.

[226] Incropera FP, DeWitt DP, Bergman TL, Lavine AS. Fundamentals of heat and mass transfer. Fundamentals of Heat and Mass Transfer; John Wiley; 2007. ISBN 9780471457282.

[227] Haglind F. Variable geometry gas turbines for improving the part-load performance of marine combined cycles gas turbine performance. Energy 2010;35(2):562 –70. doi:dx.doi.org/10.1016/j.energy.2009.10.026. ECOS 2008 21st International Conference, on Efficiency, Cost, Optimization, Simulation and Environmental Impact of Energy Systems.

[228] Taylor C. The Internal-combustion Engine in Theory and Practice: Thermodynamics, fluid flow, performance. The Internal-combustion Engine in Theory and Practice; MBI Publishing Company LLC; 1985. ISBN 9780262700269. Accessed 2014/05/10; URL books.google.dk/books?id=E_Tne3AKZVoC.

[229] Agency USEP. Global Warming Potentials of ODS Substitutes. 2014. Accessed 2014-03-13; URL epa.gov/ozone/geninfo/gwps.html.

[230] Hountalas DT, Mavropoulos GC, Katsanos C. Efficiency Optimization of a 2-Stroke Diesel Engine Power Plant Through the Recovery of Exhaust Gas Using a Rankine Cycle. Perugia, Italia: PROCEEDINGS OF ECOS 2012; 2012,.

[231] Stiesh G, Merker GP. A Phenomenological Heat Release Model for Direct Injection Diesel Engines. In: CIMAC International Council on Combustion engines 1998. Copenhagen, Denmark: CIMAC; 1998, p. 1–15. URL www.cimac.com.

[232] Lian Z, Chua K, Chou S. A thermoeconomic analysis of biomass energy for trigeneration. Applied Energy 2010;87(1):84 – 95. doi:dx.doi.org/10.1016/j.apenergy.2009.07.003.

[233] Colonna , van Putten . Dynamic modeling of steam power cycles. Applied Thermal Engineering 2007;27(2-3):467–80. doi:10.1016/j.applthermaleng.2006.06.011.

[234] Gurgenci H. Performance of power plants with organic Rankine cycles under part-load and off-design conditions. Solar energy 1986;36(1):45–51.

[235] Turboden . ORC, Advantages. 2014. Accessed May 2014; URL `triogen.nl/technology/triogen-high-speed-turbo-generator`.

[236] Andreadis P, Chryssakis C, Kaiktsis L. Optimization of injection characteristics in a large marine diesel engine using evolutionary algorithms. 2009. doi:10.4271/2009-01-1448.

[237] Knudsen TS, Egeberg CE. Design of the new two stroke engines from MAN Diesel A/S. In: CIMAC International Council on Combustion engines 2007. Vienna, Austria: CIMAC; 2007, p. 1–15.

[238] Brynolf S. Environmental assessment of present and future marine fuels. Chalmers University of Technology, Shipping and Marine Technology; 2014.

[239] Ohman H, Lundqvist P. Comparison and analysis of performance using low temperature power cycles. Applied Thermal Engineering 2013;52(1):160–9. doi:10.1016/j.applthermaleng.2012.11.024.

[240] MAN Diesel and Turbo, Copenhagen, Denmark . Propulsion trends in container vessels. 2009. Accessed 19/12/2013; URL `mandieselturbo.com`.

A Abstracts of co-authored journal publications

A.1 Validation of a zero-dimensional model for prediction of NOx and engine performance for electronically controlled marine two-stroke diesel engines

The aim of this paper is to derive a methodology suitable for energy system analysis for predicting the performance and NOx emissions of marine low speed diesel engines. The paper describes a zero-dimensional model, evaluating the engine performance by means of an energy balance and a two zone combustion model using ideal gas law equations over a complete crank cycle. The combustion process is divided into intervals, and the product composition and flame temperature are calculated in each interval. The NOx emissions are predicted using the extended Zeldovich mechanism. The model is validated using experimental data from two MAN B&W engines; one case being data subject to engine parameter changes corresponding to simulating an electronically controlled engine; the second case providing data covering almost all model input and output parameters. The first case of validation suggests that the model can predict specific fuel oil consumption and NOx emissions within the 95% confidence intervals given by the experimental measurements. The second validation confirms the capability of the model to match measured engine output parameters based on measured engine input parameters with a maximum 5% deviation.

A.2 Thermodynamic analysis of an integrated gasification solid oxide fuel cell plant combined with an organic Rankine cycle

A 100 kWe hybrid plant consisting of gasification system, solid oxide fuel cells and organic Rankine cycle is presented. The nominal power is selected based on cultivation area requirement. For the considered output a land of around 0.5 km^2 needs to be utilized. Woodchips are introduced into a fixed bed gasification plant to produce syngas which fuels the combined solid oxide fuel cells e organic Rankine cycle system to produce electricity. More than a hundred fluids are considered as possible alternative for the organic cycle using non-ideal equations of state (or state-of-the-art equations of state). A genetic al-

gorithm is employed to select the optimal working fluid and the maximum pressure for the bottoming cycle. Thermodynamic and physical properties, environmental impacts and hazard specifications are also considered in the screening process. The results suggest that efficiencies in the region of 54-56% can be achieved. The highest thermal efficiency (56.4%) is achieved with propylcyclohexane at 15.9 bar. A comparison with the available and future technologies for biomass to electricity conversion is carried out. It is shown that the proposed system presents twice the thermal efficiency achieved by simple and double stage organic Rankine cycle plants and around the same efficiency of a combined gasification, solid oxide fuel cells and micro gas turbine plant.

A.3 Multi-objective optimization of organic Rankine cycles for waste heat recovery: Application in an offshore platform

This paper aims at finding the optimal design of MW-size organic Rankine cycles by employing the multi-objective optimization with the genetic algorithm as the optimizer. We consider three objective functions: thermal efficiency, total volume of the system and net present value. The optimization variables are the working fluid, the turbine inlet pressure and temperature, the condensing temperature, the pinch points and the fluid velocities in the heat exchangers. The optimization process also includes the complete design of the shell and tube heat exchangers utilized in the organic Rankine cycle. The methodology is applied to recover the waste heat from the SGT-500 gas turbine installed on the Draugen off-shore oil and gas platform in the North Sea. Results suggest two optimal working fluids, i.e. acetone and cyclopentane. Thermal efficiency and net present value are higher for cyclopentane than for acetone. Other promising working fluids are cyclohexane, hexane and isohexane. The present methodology can be utilized in waste heat recovery applications where a compromise between performance, compactness and economic revenue is required.

A.4 Design and modeling of an advanced marine machinery system including waste heat recovery and removal of sulphur oxides

Stricter legislation on sulphur oxide emissions from ships will apply as of 2015 in emission control areas. Consequently, prices on low sulphur fuels are expected to increase drastically,

providing a strong incentive to find alternative ways of complying with the legislation and improving the efficiency of machinery systems. The wet sulphuric acid process is an effective way of removing flue gas sulphur oxides from land-based coal-fired power plants. Moreover, organic Rankine cycles (ORC) are suitable for heat to power conversion for low temperature heat sources. This paper describes the design and modelling of a highly efficient machinery system which includes the removal of exhaust gas sulphur oxides. The system consists of a two-stroke diesel engine, the wet sulphuric process for sulphur removal, a conventional steam Rankine cycle and an ORC. Results of numerical modelling efforts suggest that an ORC placed after the conventional waste heat recovery system is able to extract the sulphuric acid from the exhaust gas, while at the same time increase the combined cycle thermal efficiency by 2.6%. The findings indicate that the technology has potential in marine applications regarding both energy and the environment; however, further research and development efforts are needed.

A.5 Thermodynamic evaluation of the Kalina Split-cycle concepts for waste heat recovery applications

The Kalina split-cycle is a thermodynamic process for converting thermal energy into electrical power. It uses an ammonia-water mixture as working fluid (like a conventional Kalina cycle) and has a varying ammonia concentration during the preheating and evaporation steps. This second feature results in an improved match between the heat source and working fluid temperature profiles, decreasing the entropy generation in the heat recovery system. The present work compares the thermodynamic performance of this power cycle with the conventional Kalina process, and investigates the impact of varying boundary conditions by conducting an exergy analysis. The design parameters of each configuration were determined by performing a multi-variable optimisation. The results indicate that the Kalina split-cycle with reheat presents an exergetic efficiency higher by 2.8% points than a reference Kalina cycle with reheat, and by 4.3% points without reheat. The cycle performance varies by 14% points for a variation of the exhaust gas temperature of 100°C, and by 1% point for a cold water temperature variation of 30°C. This analysis also pinpoints the large irreversibilities in the low-pressure turbine and condenser, and indicates a reduction of the exergy destruction by about 23% in the heat recovery system compared to the baseline cycle.

A.6 Selection and optimization of pure and binary working fluids for low grade heat utilization using organic Rankine cycles

We present a generic methodology for organic Rankine cycle optimization, where the working fluid is included as an optimization parameter, in order to maximize the net power output of the cycle. The method is applied on two optimization cases with hot fluid inlet temperatures at 120°C and 90°C. Pure fluids and mixtures are compared to see how mixed working fluids affect performance and important design parameters. The results indicate that mixed working fluids can increase the net power output of the cycle, while reducing the pressure levels. The maximum net power output is obtained by fluids with a critical temperature close to half of the hot fluid inlet temperature. For some mixtures we find the maximum net power when the temperature glide of condensation matches the temperature increase of the cooling water, while for other mixtures there are large differences between these two parameters. Ethane is a fluid that obtains a large net power increase when used in mixtures. Compared to pure ethane, an optimized ethane/propane mixture attains a 12.9% net power increase when the hot fluid inlet temperature is 120°C and a 11.1% net power increase when the hot fluid inlet temperature is 90°C.

B Split-cycle state points

Table B.1: State points, Kalina cycle. *SUB* and *SH* are subcooled and superheated.

	$\dot{m}$(kg/s)	T(°C)	P(bar)	h(kJ/kg)	x	q
1	3.9	168.6	110.7	918	0.692	0
2	3.9	236	110.7	2100	0.692	1
3	3.9	330	110.7	2478	0.692	SH
4	3.9	99.9	3.3	1982	0.692	0.948
5	3.9	64.3	3.3	1170	0.692	0.61
6	9.9	54.5	3.3	487	0.473	0.217
7	9.9	30	3.3	46	0.473	0
8	9.9	30.1	7.6	46	0.473	SUB
9	7.8	30.1	7.6	46	0.473	SUB
10	7.8	58.9	7.6	216	0.473	0.026
11	7.8	83.6	7.6	621	0.473	0.227
12	6	83.6	7.6	266	0.332	0
13	1.8	83.6	7.6	1830	0.954	1
14	6	35.1	7.6	47	0.332	SUB
15	6	35.2	3.3	47	0.332	SUB
16	1.8	51.5	7.6	1591	0.954	0.917
17	2.1	30.1	7.6	46	0.473	SUB
18	3.9	51.2	7.6	749	0.692	0.379
19	3.9	30.2	7.6	173	0.692	0
20	3.9	32.8	110.7	193	0.692	SUB
21	3.9	55.4	110.7	302	0.692	SUB
22	35	346	2	815	-	-
23	35	308.8	2	773	-	-
24	35	190.5	2	643	-	-
25	35	127.7	2	574	-	-

Table B.2: State points, Kalina cycle, reheat

	$\dot{m}$(kg/s)	T(°C)	P(bar)	h(kJ/kg)	x	q
1	3.6	156	102.1	884	0.735	0
2	3.6	224.8	102.1	2072	0.735	1
3	3.6	330	102.1	2469	0.735	SH
3'	3.6	290.5	47.3	2338	0.735	SH
3"	3.6	330	47.3	2549	0.735	SH
4	3.6	134.6	3.8	2138	0.735	SH
5	3.6	63.3	3.8	1226	0.735	0.651
6	8.8	56.1	3.8	533	0.5	0.242
7	8.8	30.1	3.8	56	0.5	0
8	8.8	30.2	8.3	56	0.5	SUB
9	7.1	30.2	8.3	56	0.5	SUB
10	7.1	58	8.3	228	0.5	0.03
11	7.1	86.5	8.3	696	0.5	0.267
12	5.2	86.5	8.3	281	0.335	0
13	1.9	86.5	8.3	1836	0.953	1
14	5.2	35.2	8.3	47	0.335	SUB
15	5.2	35.3	3.8	47	0.335	SUB
16	1.9	53.1	8.3	1585	0.953	0.912
17	1.7	30.2	8.3	56	0.5	SUB
18	3.6	51.2	8.3	851	0.735	0.442
19	3.6	30.2	8.3	210	0.735	0
20	3.6	32.7	102.1	229	0.735	SUB
21	3.6	59.7	102.1	359	0.735	SUB
22	35	346	2	815	-	-
23	35	289.8	2	752	-	-
24	35	177.9	2	629	-	-
25	35	127.7	2	574	-	-

Table B.3: State points, Split-cycle

	$\dot{m}$(kg/s)	T(°C)	P(bar)	h(kJ/kg)	x	q
1	4.112	212	127.1	1499	0.683	0.535
2	4.112	242.9	127.1	2067	0.683	1
3	4.112	330	127.1	2454	0.683	SH
4	4.112	100.4	3.4	1955	0.683	0.932
5	4.112	67.6	3.4	1188	0.683	0.612
6	9.858	52.2	3.4	545	0.512	0.258
7	9.858	30	3.4	37	0.512	0
8	9.858	30.2	9.6	38	0.512	SUB
9	9.858	62.5	9.6	267	0.512	0.041
10	9.858	81.2	9.6	587	0.512	0.211
11	7.78	81.2	9.6	263	0.389	0
12	6.291	81.2	9.6	263	0.389	0
13	5.746	81.2	9.6	263	0.389	0
14	5.746	42.8	9.6	85	0.389	SUB
15	5.746	42.9	3.4	85	0.389	SUB
16	1.489	81.2	9.6	263	0.389	0
17	0.545	81.2	9.6	263	0.389	0
18	2.077	81.2	9.6	1803	0.971	1
19	1.653	81.2	9.6	1803	0.971	1
20	2.198	81.2	9.6	1421	0.827	0.752
21	2.198	61.7	9.6	1227	0.827	0.667
22	2.198	42.8	9.6	965	0.827	0.517
23	2.198	30.1	9.6	297	0.827	0
24	2.198	33.8	127.1	322	0.827	SUB
25	2.198	73.6	127.1	515	0.827	SUB
26	0.424	81.2	9.6	1803	0.971	1
27	1.914	81.2	9.6	604	0.518	0.222
28	1.914	72.6	9.6	470	0.518	0.154
29	1.914	42.8	9.6	123	0.518	SUB
30	1.914	45.3	127.1	144	0.518	SUB
31	1.914	73.6	127.1	278	0.518	SUB
32	1.914	212	127.1	1040	0.518	0
33	2.198	212	127.1	1899	0.827	1
34	35	346	2	815	-	-
35	35	305.6	2	770	-	-
36	35	245.5	2	703	-	-
37	35	127.7	2	574	-	-

Table B.4: State points, Split-cycle, reheat

	$\dot{m}$(kg/s)	T(°C)	P(bar)	h(kJ/kg)	x	q
1	3.6	194.8	101.7	1390	0.677	0.478
2	3.6	234.9	101.7	2134	0.677	1
3	3.6	330	101.7	2500	0.677	SH
3’	3.6	281	36.6	2331	0.677	SH
3”	3.6	330	36.6	2602	0.677	SH
4	3.6	133.1	2.9	2185	0.677	SH
5	3.6	73.4	2.9	1323	0.677	0.669
6	10.6	51.3	2.9	502	0.478	0.234
7	10.6	30	2.9	24	0.478	0
8	10.6	30.1	10.1	25	0.478	SUB
9	10.6	68.4	10.1	256	0.478	0.021
10	10.6	85.8	10.1	549	0.478	0.174
11	8.8	85.8	10.1	282	0.376	0
12	7.3	85.8	10.1	282	0.376	0
13	7	85.8	10.1	282	0.376	0
14	7	41.9	10.1	79	0.376	SUB
15	7	42	2.9	79	0.376	0
16	1.5	85.8	10.1	282	0.376	0
17	0.3	85.8	10.1	282	0.376	0
18	1.8	85.8	10.1	1817	0.965	1
19	1.4	85.8	10.1	1817	0.965	1
20	1.7	85.8	10.1	1559	0.867	0.832
21	1.7	60.3	10.1	1325	0.867	0.734
22	1.7	41.9	10.1	1087	0.867	0.597
23	1.7	30	10.1	337	0.867	0
24	1.7	33.1	101.7	357	0.867	SUB
25	1.7	80.8	101.7	591	0.867	SUB
26	0.4	85.8	10.1	1817	0.965	1
27	1.9	85.8	10.1	615	0.504	0.217
28	1.9	74.5	10.1	439	0.504	0.128
29	1.9	41.9	10.1	112	0.504	SUB
30	1.9	43.8	101.7	129	0.504	SUB
31	1.9	80.8	101.7	304	0.504	SUB
32	1.9	194.8	101.7	915	0.504	0
33	1.7	194.8	101.7	1909	0.867	1
34	35	346	2	815	-	-
35	35	287.3	2	749	-	-
36	35	217.7	2	672	-	-
37	35	127.7	2	574	-	-

C Fluids available in Refprop

Short name	Chemical name
acetone	propanone
ammonia	ammonia
argon	argon
benzene	benzene
butane	n-butane
butene	1-butene
carbon dioxide	carbon dioxide
carbon monoxide	carbon monoxide
carbonyl sulfide	carbon oxide sulfide
cis-butene	cis-2-butene
cyclohexane	cyclohexane
cyclopentane	cyclopentane
cyclopropane	cyclopropane
D4	octamethylcyclotetrasiloxane
D5	decamethylcyclopentasiloxane
D6	dodecamethylcyclohexasiloxane
decane	decane
deuterium	deuterium
dimethyl carbonate	dimethyl ester carbonic acid
dimethylether	methoxymethane
dodecane	dodecane
ethane	ethane
ethanol	ethyl alcohol
ethylene	ethene
fluorine	fluorine
heavy water	deuterium oxide
helium	helium-4
heptane	heptane
hexane	hexane
hydrogen (normal)	hydrogen (normal)
hydrogen sulfide	hydrogen sulfide
isobutane	2-methylpropane
isobutene	2-methyl-1-propene
isohexane	2-methylpentane
isopentane	2-methylbutane
krypton	krypton
md2m	decamethyltetrasiloxane
md3m	dodecamethylpentasiloxane
md4m	tetradecamethylhexasiloxane
mdm	octamethyltrisiloxane
methane	methane
methanol	methanol

Short name	Chemical name
methyl linoleate	methyl (Z,Z)-9,12-octadecadienoate
methyl linolenate	methyl (Z,Z,Z)-9,12,15-octadecatrienoate
methyl oleate	methyl cis-9-octadecenoate
methyl palmitate	methyl hexadecanoate
methyl stearate	methyl octadecanoate
methylcyclohexane	methylcyclohexane
MM	hexamethyldisiloxane
neon	neon
neopentane	2,2-dimethylpropane
nitrogen	nitrogen
nitrogen trifluoride	nitrogen trifluoride
nitrous oxide	dinitrogen monoxide
nonane	nonane
octane	octane
orthohydrogen	orthohydrogen
oxygen	oxygen
parahydrogen	parahydrogen
pentane	pentane
perfluorobutane	decafluorobutane
perfluoropentane	dodecafluoropentane
propane	propane
propylcyclohexane	n-propylcyclohexane
propylene	propene
propyne	propyne
sulfur dioxide	sulfur dioxide
sulfur hexafluoride	sulfur hexafluoride
toluene	methylbenzene
trans-butene	trans-2-butene
trifluoroiodomethane	trifluoroiodomethane
water	water
xenon	xenon
R11	trichlorofluoromethane
R12	dichlorodifluoromethane
R13	chlorotrifluoromethane
R14	tetrafluoromethane
R21	dichlorofluoromethane
R22	chlorodifluoromethane
R23	trifluoromethane
R32	difluoromethane
R41	fluoromethane
R113	1,1,2-trichloro-1,2,2-trifluoroethane
R114	1,2-dichloro-1,1,2,2-tetrafluoroethane

Short name	Chemical name
R115	chloropentafluoroethane
R116	hexafluoroethane
R123	2,2-dichloro-1,1,1-trifluoroethane
R1234yf	2,3,3,3-tetrafluoroprop-1-ene
R1234ze	trans-1,3,3,3-tetrafluoropropene
R124	1-chloro-1,2,2,2-tetrafluoroethane
R125	pentafluoroethane
R134a	1,1,1,2-tetrafluoroethane
R141b	1,1-dichloro-1-fluoroethane
R142b	1-chloro-1,1-difluoroethane
R143a	1,1,1-trifluoroethane
R152a	1,1-difluoroethane
R161	fluoroethane
R218	octafluoropropane
R227ea	1,1,1,2,3,3,3-heptafluoropropane
R236ea	1,1,1,2,3,3-hexafluoropropane
R236fa	1,1,1,3,3,3-hexafluoropropane
R245ca	1,1,2,2,3-pentafluoropropane
R245fa	1,1,1,3,3-pentafluoropropane
R365mfc	1,1,1,3,3-pentafluorobutane
RC318	octafluorocyclobutane

DTU Mechanical Engineering
Section of Thermal Energy
Technical University of Denmark

Nils Koppels Allé, Bld. 403
DK- 2800 Kgs. Lyngby
Denmark
Phone (+45) 4525 4131
Fax (+45) 4588 4325
www.mek.dtu.dk
ISBN: 978-87-7475-401-5